BioMed Research International

Advances in Endovascular Intervention Using Biomaterials

Lead Guest Editor: Xiangyu Cao
Guest Editors: Xing Chen, Ming Yang, and Weiluan Chen

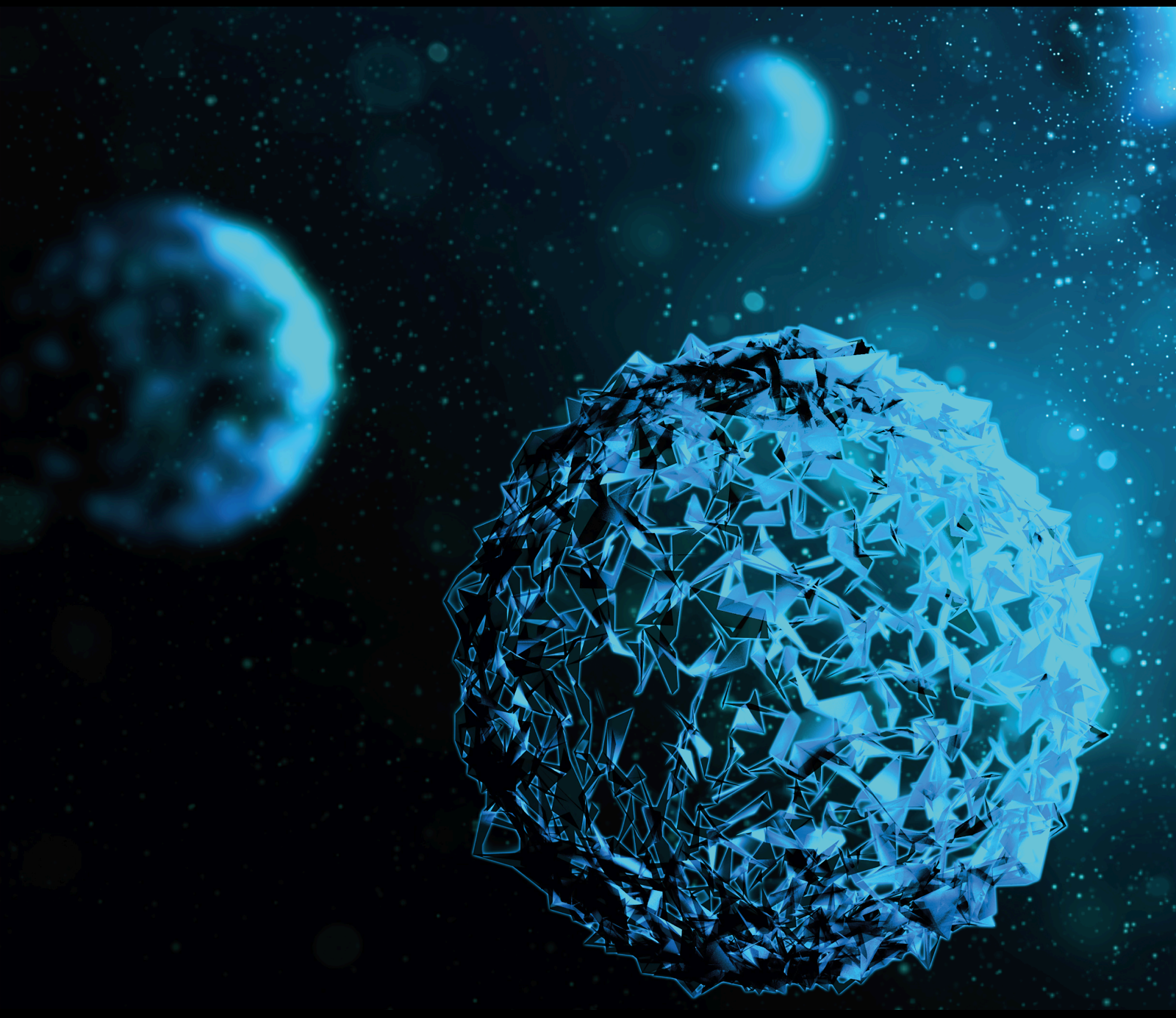

Advances in Endovascular Intervention Using Biomaterials

BioMed Research International

Advances in Endovascular Intervention Using Biomaterials

Lead Guest Editor: Xiangyu Cao
Guest Editors: Xing Chen, Ming Yang, and Weiluan Chen

Section Editors

Penny A. Asbell, USA
David Bernardo, Spain
Gerald Brandacher, USA
Kim Bridle, Australia
Laura Chronopoulou, Italy
Gerald A. Colvin, USA
Aaron S. Dumont, USA
Pierfrancesco Franco, Italy
Raj P. Kandpal, USA
Fabrizio Montecucco, Italy
Mangesh S. Pednekar, India
Letterio S. Politi, USA
Jinsong Ren, China
William B. Rodgers, USA
Harry W. Schroeder, USA
Andrea Scribante, Italy
Germán Vicente-Rodriguez, Spain
Momiao Xiong, USA
Hui Zhang, China

Academic Editors

Biomaterials

Contents

Hindawi
BioMed Research International
Volume 2021, Article ID 6657595, 7 pages
https://doi.org/10.1155/2021/6657595

Research Article

Safety Evaluation and Flow Modification in the Anterior Cerebral Artery after Pipeline Embolization Device Deployment across the Internal Carotid Artery Terminus

Chao Xu,[1] **Pei Wu**,[1] **Jianyi Han**,[2] **Bowen Sun**,[1] **Chunlei Wang**,[1] **Shancai Xu**,[1] **Bin Luo**,[3] **Xinjian Yang**,[4] **Qingchun Mu**,[5] **and Huaizhang Shi**[1]

[1]*Department of Neurosurgery, The First Affiliated Hospital of Harbin Medical University, Harbin, Heilongjiang Province, China*
[2]*Department of Neurosurgery, Binzhou People's Hospital, Binzhou, Shandong Province, China*
[3]*Beijing Neurosurgical Institute, Beijing Tiantan Hospital, Capital Medical University, Beijing, China*
[4]*Department of Interventional Neuroradiology, Beijing Neurosurgical Institute and Beijing Tiantan Hospital, Capital Medical University, Beijing, China*
[5]*Department of Neurosurgery, The People's Hospital of Gaozhou, Maoming, Guangdong Province, China*

Correspondence should be addressed to Huaizhang Shi; shihuaizhang@hrbmu.edu.cn

Received 25 December 2020; Revised 26 February 2021; Accepted 31 July 2021; Published 23 August 2021

Academic Editor: GuoXin Ni

Background and Objective. Whether anterior cerebral artery occlusion occurs after pipeline embolization devices (PEDs) are implanted to treat posterior communicating artery aneurysm is controversial. The purposes of this study were to explore the effect of a PED covering A1 on patients' clinical prognosis and to evaluate the factors related to vascular occlusion. *Method*. The clinical and imaging data of PEDs in the postmarket multicenter registry study (PLUS) in China were retrospectively analyzed, and patients were divided into two groups on the basis of the follow-up angiographic results: group 1 (no significant change in A1 blood flow) and group 2 (A1 occlusion or decreased blood flow). We collected patients' baseline data and evaluated the following imaging indicators: diameter and ratio of bilateral A1, M1, and internal carotid artery (ICA) vessels before stenting and the ratio of the PED size (sPED) to the ipsilateral ICA (I-ICA) diameter on the implantation side. *Results*. A total of 1171 patients were included, of whom 48 met the inclusion criteria (17 in group 1 and 31 in group 2). In group 2, three patients experienced neurological deterioration at follow-up. From the univariate analysis of outcomes, single PED without coils, incomplete aneurysm occlusion (IAO), maximum aneurysm diameter, aneurysms involving the ICA bifurcation (ICAb), and large sPED/I-ICA diameter ratio were included in the multivariate analysis ($P < 0.20$). The multivariate regression analysis results showed that the ratio of sPED/I-ICA diameter was the factor influencing A1 vessel occlusion. The area under the ROC curve was 73.2%. When the sPED/I-ICA diameter ratio was 1.14, sensitivity was 70.6%, and specificity was 77.4%. *Conclusion*. When an oversized PED is placed from M1 to the ICA, the higher porosity formed at the covered A1 orifice is conducive to maintaining stable A1 blood flow and reducing the risk of A1 vessel occlusion. This trial is registered with ClinicalTrials.gov identifier: NCT03831672.

1. Introduction

Pipeline embolization devices (PEDs) are an alternative treatment for complex intracranial aneurysms; however, there remains a risk of occlusion of jailed side branches, even in patients with good efficacy with antiplatelet drug therapy [1, 2]. Previous PED manufacturers' instructions suggested that these devices are suitable for large or giant wide-necked aneurysms from the petrous segment of the internal carotid artery (ICA) to the proximal superior hypophyseal artery in patients aged ≥22 years. Recently, the FDA incorporated ICA bifurcation into PED treatment coverage [3]. However, for carotid bifurcation aneurysms, it is often necessary to locate the distal end of the PED into the M1 segment

and to cover the origin of the ipsilateral A1 segment to ensure PED stability [3–6]. Previous studies have reported that this approach may affect A1 blood flow and that A1 segment occlusion can lead to neurological deficits [3–6].

To date, few studies have evaluated the long-term prognostic impact of covering the ipsilateral A1 segment origin and the related factors leading to occlusion. We retrospectively analyzed the clinical and imaging data from the postmarket multicenter registry study (PLUS) to investigate the long-term prognostic impact of A1 occlusion and factors associated with occlusion.

2. Method

2.1. Design and Process. We performed a retrospective review using the databases of the 14 participating Chinese institutions for aneurysms treated with PEDs between 2015 and 2019 in the PLUS. The study was a consecutive, real-world cohort registry study. Local institutional review boards or ethics committees approved the study and the use of the patients' data. All operations were performed with written informed consent. Inclusion criteria were as follows: (1) for intracranial aneurysms treated with a PED, a single PED was deployed from the M1 segment to the ICA and covered the orifice of A1 and (2) follow-up digital subtraction angiography (DSA) imaging data. Exclusion criteria were as follows: (1) multiple PEDs covering the beginning of A1, (2) loss of the A1 artery on the PED treated side, and (3) no follow-up DSA imaging data. Data on the patients' general information, aneurysms involving the ICA bifurcation, maximum aneurysmal diameter, intraoperative and postoperative complications, and the mRS scores before and at the last follow-up were collected. Patient selection for our study is summarized in Figure 1.

2.2. Angiographic Follow-Up. Aneurysm occlusion was classified using the O'Kelly-Marotta (OKM) grading scale [7, 8]. We described the flow modification in the ipsilateral A1 segment as follows: (1) no change in flow regarding patency and (2) occlusion or diminished flow [4]. To compare changes in A1 vessels, we divided patients into two groups. Group 1 comprised patients who showed no flow changes in the jailed artery at the last angiographic follow-up, and group 2 comprised patients in whom occlusion or diminished flow in the jailed artery had been observed at the last angiographic follow-up.

2.3. Perioperative Management. All patients received an antiplatelet regimen that included aspirin (100 or 300 mg daily) and clopidogrel (75 mg daily). Patients who were identified as clopidogrel nonresponders received aspirin (100 mg daily) and ticagrelor (90 mg twice daily). All patients demonstrated optimal platelet activity suppression before PED placement. Board-certified neuroendovascular surgeons performed all procedures. Intravenous heparin was administered intraprocedurally to achieve an activated clotting time of >250 seconds. Heparin was discontinued after completing the procedure. Dual antiplatelet therapy was continued for 6 months after PED placement. Patients received aspirin 100 mg/d for life.

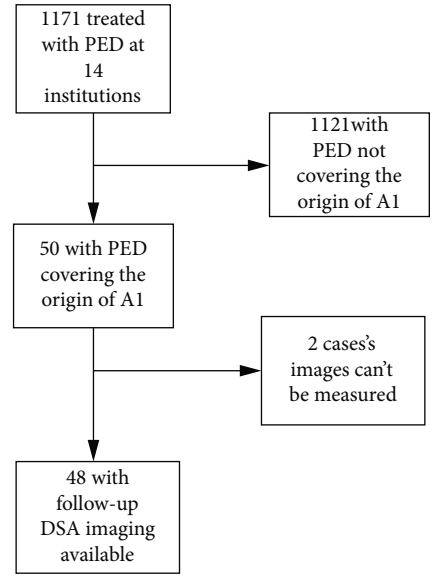

Figure 1: Patient selection for our study.

2.4. Parameter Measurement. All vessel measurements were obtained on the original calibrated DSA images using the Radiant DICOM Viewer 5.0.2 (https://www.radiantviewer.com/) by two experienced neurosurgeons. Measurements of the ipsilateral A1 segment and the M1 segment, supraclinoid ICA, and the contralateral A1 segment 3 mm from the ICAb were evaluated before PED deployment. For aneurysms at the ICA bifurcation (ICAb) site, a vessel diameter of 3 mm around the aneurysm was measured. The widest diameter on the calibrated images was recorded for each vessel of interest. The PED size/ipsilateral-ICA (sPED/I-ICA) ratio was defined as the ratio of the standard diameter of the PED to the average diameter of the proximal M1 segment and the landing area in the ICA. Other ratios, such as ipsilateral-A1/ipsilateral-M1 (I-A1/I-M1), ipsilateral-A1/ipsilateral internal carotid artery (A1/I-ICA), ipsilateral-M1/ipsilateral internal carotid artery (I-M1/ICA), and the odds ratio of ipsilateral-A1/contralateral-A1 (I-A1/C-A1), were obtained after the sPED/I-ICA measurement.

2.5. Statistical Analysis. Categorical variables are reported as proportions, and continuous variables are reported as the mean ± standard deviation or the median and interquartile range, as appropriate. Between the groups, the variables were compared using the chi-square test, Mann-Whitney U test, and t-test. Univariate analysis was used to test the following independent factors: age, sex, hypertension, smoking, aneurysm size, aneurysm occlusion status, aneurysms involving the ICAb, and the following ratios: I-A1/I-M1, I-A1/I-ICA, I-M1/ICA, and the odds ratios of I-A1/C-A1 and sPED/I-ICA. Factors that were predictive in the univariate analysis ($P < 0.20$) were entered into a multivariate logistic regression analysis. P values < 0.05 were considered statistically significant. We created a ROC curve to test the ability of the

sPED/I-ICA ratio to predict jailed A1 vessel patency. Statistical analysis was performed using SPSS 25 (IBM Corp., Armonk, NY, USA).

3. Results

3.1. General Data. A total of 48 patients were identified retrospectively in the present study; 31 (65%) patients were women, and 17 (35%) were men. The mean age was 54 ± 13.8 (range: 14–77) years. The average maximum diameter of the treated aneurysms was 9.2 ± 6.6 mm. Of the 48 patients, 12 (25%) had a history of hypertension, 14 (29.2%) had a history of tobacco smoking, and 4 (8.3%) had a history of diabetes (Table 1). Of the 51 aneurysms, 9 (30%) were fusiform. Aneurysms occurred at the following locations: 4 in the cavernous sinus segment, 13 in the ophthalmic artery segment, 16 in the posterior communicating segment, 2 in the anterior choroidal artery origin, and 12 in the ICAb; the remaining 4 aneurysms were middle cerebral artery (MCA) aneurysms. Of the 48 patients, 47 had 1 PED implanted, and 1 required 2 PEDs. The A1 origin ostium was covered by a single PED in all patients.

3.2. Clinical and Radiographic Outcomes. mRS scores in three patients changed, and one patient's right ICA became stenotic after PED treatment; the mRS score was 1 before operation and 3 at the last follow-up. The second patient with A1 occlusion had an mRS score of 1 before operation and 2 at the last follow-up (Figure 2). The third patient had in-stent restenosis and cerebral ischemia; the mRS score was 0 before operation and 2 at the last follow-up (Figure 3). Follow-up DSAs performed a median of 201 days (interquartile range: 168 to 276 days). The O'Kelly-Marotta (OKM) grading scale grades for the treated aneurysms were as follows: 31 were OKM-D (no filling), as complete obliteration; incomplete aneurysm occlusion (IAO) occurred in 20 aneurysms: 2 were OKM-C2 (entry remnant), 11 were OKM-B2/B3 (subtotal filling), and 7 were OKM-A1/A2 (total filling). Regarding the flow modification outcomes for A1, the last follow-up angiography showed that the covered A1 segment was occluded in 11 patients (22.9%), with diminished flow in 20 patients (41.7%). There was no flow change in 17 patients (35.4%) (Table 1).

3.3. Changes in the A1 Segment. Group 1 ($n = 17$) comprised patients who showed no flow changes in the jailed artery. Group 2 ($n = 31$) comprised patients who had occlusion or diminished flow in the jailed artery. The mean age in group 1 was 57.7 ± 14.5 years versus 53.0 ± 13.4 years in group 2. The mean aneurysm size in group 1 was 7.1 ± 3.8 mm versus 10.9 ± 7.5 mm in group 2. Complete obliteration was achieved in 6 (35.3%) patients in group 1 versus 25 (73.5%) in group 2. The sPED/I-ICA ratio in group 1 was 1.19 versus 1.06 in group 2. Other variables are summarized in Table 1 and Table S1.

In the univariate analysis, statistically significant factors associated with group 1 versus group 2 were single PED treatment (OR: 2.566, 95% CI: 0.693–9.502; $P = 0.158$), IAO (OR: 0.196, 95% CI: 0.056–0.687; $P = 0.011$), aneurysm size (OR: 1.099, 95% CI: 0.977–1.235; $P = 0.114$), aneurysms at the ICAb (OR: 3.048, 95% CI: 0.855–10.865; $P = 0.086$), and sPED/I-ICA (OR: 0.003, 95% CI: 0.0001–0.286; $P = 0.012$). Multivariate analysis demonstrated that sPED/I-ICA (OR: 0.0001, 95% CI: 0.0001–0.164; $P = 0.013$) was a statistically significant factor associated with jailed arteries with no flow change. Detailed information is shown in Table 2. The area under the ROC curve was 73.2%. When the sPED/I-ICA diameter ratio was 1.14, the sensitivity was 70.6% and the specificity was 77.4% (Figure 4).

4. Discussion

ICA bifurcation is an uncommon location for a PED. To avoid PED retraction after treatment, it is necessary to deploy the end of the PED in the M1 segment and cover the origin of A1 [6, 9–11]. Sufficient preoperative evaluation is required for this off-label use, and previous reports have shown that approximately 2/3 of arteries covered by a flow diverter will become stenotic or occluded during follow-up [2]. In a recent report of 10 patients with ICAb aneurysms, all PEDs covered the origin of A1, of whom 3 patients had asymptomatic occlusion of A1 [6]. We found that the blood flow reduction and occlusion rates in A1 were 41.7% and 22.9%, respectively. To the best of our knowledge, ours is the largest study to assess changes in jailed A1s in patients with PEDs deployed across the ICAb and covering the ostium of A1.

4.1. Prognosis of A1 Occlusion. Most researchers believe that PED placement has a significant effect on the blood flow of covered side branches. Currently, there is a consensus that if collateral circulation is inadequate to provide sufficient compensation, patency in the jailed branches is maintained by direct flow. Otherwise, if direct or pial collateral compensation is well preserved, the jailed branch will become progressively occluded or narrowed, usually without clinical consequences [2, 12]. One patient with A1 occlusion in our study had an mRS score of 1 before operation and 2 at the last follow-up, with symptoms associated with A1 occlusion. This indicates that there is a certain risk of covering A1 with a PED, and no A1 occlusion-related symptoms have been reported before, which may be related to the small number of cases. Therefore, it is necessary to fully evaluate the anterior communicating artery patency before the operation.

4.2. Influence of the Diameter Ratio of the Branch Vessels. Currently, it is believed that when a PED is placed in Y-shaped vessels, the blood flow changes in covered branches are related to the diameter ratio of the two branches: the thinner the branches, the greater the blood flow resistance [13]. The effect of side branch diameter on hemodynamics was quantitatively studied by Tang et al. [14]. After PED implantation, in the side branches with a diameter of 1 mm, the blood flow velocity and pressure decreased by 35% and 3.3%, respectively. For diameters of 2.0 mm, the velocity decrease was only 7.2%, but the pressure decreased by 4.3%. The reductions of the mean volume flow rates in the side branch vessel after PED deployment were 0.4% for $d = 1.0$ mm and 6.3% for $d = 2.0$ mm [14]. Narata and de Moura

Table 1: Baseline demographic data for all, group 1, and group 2 patients.

Characteristic	All	Group 1 ($n = 17$)	Group 2 ($n = 31$)	P value
Sex				0.52
M (%)	17 (35%)	5 (29.4%)	12 (38.7%)	
F (%)	31 (65%)	12 (71.0%)	19 (61.3%)	
Mean age in yrs	54 ± 13.8	57.7 ± 14.5	53.0 ± 13.4	0.26
Hypertension (%)	12 (25%)	6 (35.3%)	6 (19.4%)	0.30
Diabetes (%)	4 (8.3%)	2 (11.8%)	2 (6.5%)	0.52
Smoking (%)	14 (29.2%)	3 (17.6%)	11 (35.5%)	0.32
Aneurysm size (mm)	9.2 ± 6.6	7.1 ± 3.8	10.9 ± 7.5	0.08
Aneurysms at the ICAb (%)	15 (31.3%)	8 (47.0%)	7 (22.5%)	0.08
Treatment				0.15
PED (%)	32 (62.7%)	13 (76.5%)	19 (55.9%)	
PED+coil (%)	19 (37.3%)	4 (23.5%)	15 (44.1%)	
Aneurysm occlusion				0.008
Complete obliteration (%)	31 (60.8%)	6 (35.3%)	25 (73.5%)	
IAO (%)	20 (39.2%)	11 (64.7%)	9 (26.5%)	
Fate of A1				
Occlusion (%)	11 (22.9%)	—	11 (35.5%)	
Diminished flow (%)	20 (41.7%)	—	20 (64.5%)	
No flow change (%)	17 (35.4%)	17 (100%)	—	
I-A1/I-ICA (mean (SD))	0.50 (0.12)	0.49 (0.11)	0.51 (0.12)	0.74
I-M1/I-ICA (mean (SD))	0.76 (0.12)	0.77 (0.12)	0.76 (0.12)	0.78
I-A1/I-M1 (mean (SD))	0.67 (0.19)	0.67 (0.22)	0.68 (0.17)	0.88
OR I-A1/C-A1 (mean (SD))	0.92 (0.24)	0.91 (0.19)	0.93 (0.27)	0.81
sPED/I-ICA (mean (SD))	1.11 (0.16)	1.19 (0.18)	1.06 (0.12)	0.006

yrs: years; M: male; F: female; ICAb: the internal carotid artery bifurcation; PED: pipeline embolization device; IAO: incomplete aneurysm occlusion; I-A1: ipsilateral-A1; I-ICA: ipsilateral internal carotid artery; SD: standard deviation; I-M1: ipsilateral-M1; OR: the odds ratio; C-A1: contralateral-A1; sPED: the PED size.

[15] compared the ratios of the diameters of the two subbranches in 25 patients with bifurcation aneurysms without compensation from communicating branches, namely, 11 patients with no vessel caliber change and 14 patients with vascular occlusion or subacute occlusion. The mean value difference between the two groups was statistically significant when the ratio was <0.7 ($P < 0.001$). Further computational fluid dynamics analysis of the standard idealized model showed that a ratio of <0.65 had a statistically significantly greater effect on the wall shear area of the two branches before and after operations.

The first study evaluating occlusion following a PED covering the ipsilateral A1 segment was presented by Nossek et al. [4]; the authors found that six of seven patients who demonstrated occlusion of the A1 segment or reversal of flow from contralateral vessels manifested an average A1/M1 segment ratio of 0.58 (range: 0.29–0.76). Pujari et al. [3] reported 27 patients whose PEDs were positioned between the M1 and the supraclinoid segment of the ICA and covered the origin of A1. They found an average ratio of the patent covered A1 segments to the ipsilateral M1 of 0.71, compared with 0.50 for the occluded group. The difference using the t-test was statistically significant ($P = 0.0006$). In our study, the A1/M1 ratio was 0.68 in group 2 and 0.67 in group 1. Although the ratio was between 0.65 and 0.70, there was no significant difference using the t-test ($P = 0.87$). We believe that the current overall evaluation of A1/M1 ratios is based on a small sample of studies. With the increasing use of PEDs, we look forward to the results of larger studies.

4.3. Effect of PED Size. The porosity of a certain model of PED changes parabolically with increased artery diameter. Relative to the diameter of the landing artery, oversized PEDs increase in porosity and play an important role in the patency flow [16, 17]. As indicated in the in vitro study by Shapiro et al. [17], metal coverage falls rapidly with increasing device oversizing, with minimum coverage already observed when the artery is only 1 mm smaller than the nominal device diameter. Thus, even relatively modest degrees of oversizing translate into substantially lower metallic coverage. In actual treatment, the PED model chosen by neurointerventionists is slightly larger than the landing vessel diameter, but the ideal proportion is currently inconclusive, and it is worth exploring what proportion may preserve the flow in the covered vessel.

Our results showed that the sPED/I-ICA ratio in group 1 was 1.19 versus 1.06 in group 2. In the univariate analysis, sPED/I-ICA ratio (OR: 0.003, 95% CI: 0.0001–0.286; $P =$

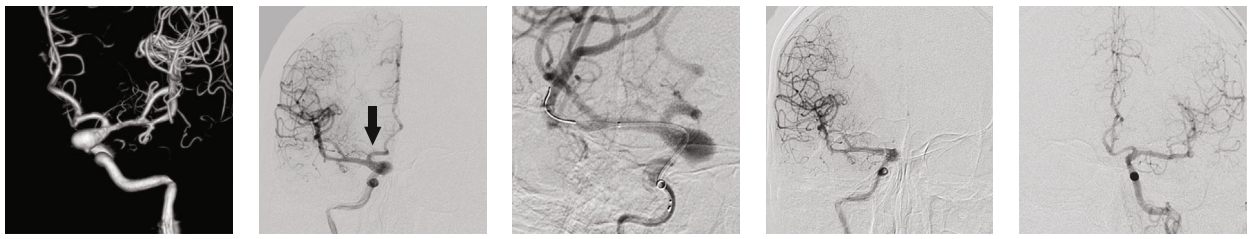

(a) (b) (c) (d) (e)

Figure 2: A 50-year-old male patient was treated with a single 4.25 mm × 25 mm pipeline embolization devices (PED) following the unexpected discovery of a C7 segment fusiform aneurysm by computed tomography angiography (CTA). The PED size/ipsilateral internal carotid artery (sPED/I-ICA) ratio was 1.05. The 2-year follow-up angiography (d) showed that the aneurysm still had a residual body, but A1 (b, black arrow) was occluded. The mRS score of the patient was 2. (a, b) Preoperative 3D reconstruction and orthographic angiography images showing patency of the ipsilateral A1 segment. (c) PED implantation. (d) Two-year angiography image showing the residual aneurysm with ipsilateral A1 occlusion. (e) Contralateral 2-year follow-up angiography showing that the right A2 blood supply area was compensated by the anterior communicating artery.

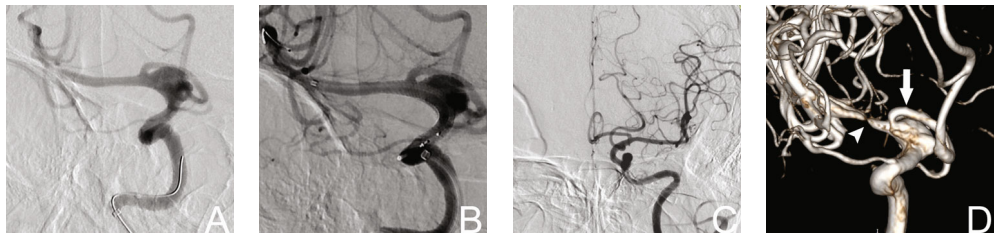

(a) (b) (c) (d)

Figure 3: Female patient, 56 years old. CTA images showing that a C7 segment aneurysm was treated with a single PED measuring 3 mm × 25 mm; the sPED/I-ICA ratio was 1.21. The 6-month follow-up angiography showed that a residual aneurysm was present with in-stent stenosis (indicated by the white arrowhead in d), and the patient's mRS score was 2. A1 (indicated by the white arrow in d) is intact. (a, b) The A1 origin was covered before and after PED implantation. (c) Contralateral ICA angiography. (d) Six-month follow-up angiography 3D reconstruction showing that most of the residual aneurysm and A1 remained intact, but M1 shows in-stent stenosis.

Table 2: Univariate and multivariate analyses of group 1 and group 2.

Characteristic	Univariate analysis*			Multivariate analysis		
	OR	95% CI	*P* value	OR	95% CI	*P* value
Single PED	2.566	0.693-9.502	0.158	0.717	0.098-5.263	0.744
IAO	0.196	0.056-0.687	0.011	0.228	0.028-1.840	0.165
Aneurysm size	1.099	0.977-1.235	0.114	1.143	0.990-1.320	0.068
Aneurysms at the ICAb	3.048	0.855-10.865	0.086	5.699	0.433-74.932	0.186
sPED/I-ICA	0.003	0.0001-0.286	0.012	0.0001	0.0001-0.164	0.013

PED: pipeline embolization device; IAO: incomplete aneurysm occlusion; ICAb: the internal carotid artery bifurcation; sPED: the PED size; I-ICA: ipsilateral internal carotid artery. *Also entered in the univariate analysis but not significant: I-A1/I-ICA, I-M1/I-ICA, and I-A1/I-M1.

0.012) was included in the multivariate analysis. The results of the multivariate analysis demonstrated that sPED/I-ICA (OR: 0.0001, 95% CI: 0.0001–0.164; $P = 0.013$) was a statistically significant factor predicting a jailed artery with no flow change. We believe that to match the diameter of the ICA of the landing zone, a relatively large diameter PED must be placed in the M1 segment, which has different diameters from the M1 segment to the ICA. Therefore, oversizing the PED will inevitably decrease the metal coverage where the diameter changes, with less impact on the flow into A1 [3, 4, 6].

PED porosity increases from the inner to the outer curves at each point along the vessel cross-section along a 180-degree curvature in vitro [17]. However, owing to the effects of vessel curvature and changes in diameter, the porosity at the ostium of A1 observed in vivo will be substantially more complex [18]. The sPED I-ICA ratio was statistically significantly different between our two groups, which may be related to the choice of PED model because this is based on the diameter of the ICA.

Our results are in accordance with the experimental results in swine reported by Berg et al. [19]. In their research, the authors implanted 5 × 20 mm PEDs into the carotid artery, which had diameters of 4.56 mm in case 1 and 5.32 mm in case 2, and covered the ascending pharyngeal artery, which had diameters of 2.18 mm and 2.42 mm, in

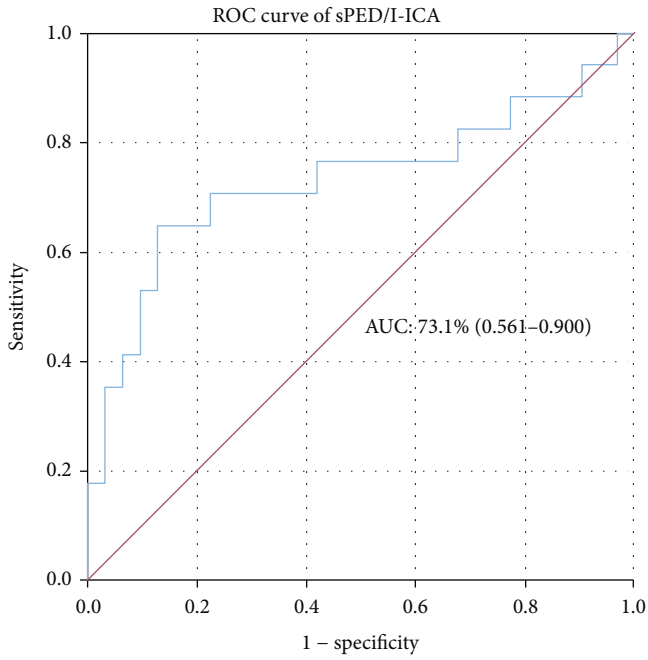

Figure 4: Ability of the sPED/I-ICA ratio to predict jailed A1 vessel patency. The area under the curve (AUC) for the sPED/I-ICA ratio was 73.1% (95% CI: 0.561–0.900). When the sPED/I-ICA ratio was 1.14, the sensitivity was 70.6%, and the specificity was 77.4%.

cases 1 and 2, respectively. Three-month postprocedure angiography showed that patency in the ascending pharyngeal artery (APhA) in case 1 was well preserved, while the ascending pharyngeal artery in case 2 was nearly occluded. Scanning electron microscopy further confirmed the structural basis of this phenomenon and evaluated the APhA ostium 3 months after procedure regarding the difference in acute stent strut angles. In case 1, the angle corresponded to 78° with a circulating surface of 359,208 μm^2. In case 2, the angle corresponded to 59.1°, with a circulating surface of 142,937 μm^2. This indicates that the oversized PED was stretched and that the metal coverage at the branch ostium was low. However, undersized PEDs are compressed, which results in high metal coverage and not only reduces the flow into the branch vessels but also provides more scaffolds for endothelial hyperplasia, which ultimately reduces the ostium area.

The mean flow rate reductions through the jailed branches are calculated using computational fluid dynamics. In the oversized case 1, mean flow rate decreases of 14.1% occurred. In comparison, the undersized case 2 showed a reduction of 25.5% [19]. In case 2, the low wall shear stress (WSS) along the strut region that covers the ostium enabled the proliferation of neointimal cells, which led to narrowing of the jailed arterial branch. Conversely, case 1 showed increased WSS at the ostium and shear load, especially across the distal area of the jailed side branch [19]. Similar results were confirmed in the study by Iosif et al., which compared the occlusive rate of jailed vessels by the PED between an anastomotic-type arterial configuration and a terminal-type. With higher occlusive rates of the anastomotic-type jailed vessels, the mean ostial shear stress on the struts was 6.7 Pa vs. 11.3 Pa for the terminal type [12]. These results are in accordance with a previous study investigating the effect of WSS on endothelial proliferation for an open-cell stent [20]. It appears that low WSS promotes endothelial proliferation not only on the stented parent artery but also on the free segments of the stent.

Clinically, in a regression analysis of 217 covered branches in 137 patients treated with a PED by Miller and Kole [21], a relatively undersized PED was associated with long-term covered vessel stenosis and occlusion. The authors suggested that relatively undersized PEDs result in higher metal coverage at the ostium of the covered vessel, which led to decreased blood flow and long-term vessel occlusion. Our results were similar. Kole et al. [22] performed regression analysis and showed that relatively undersized PEDs in 158 aneurysms treated with a single PED were associated with aneurysm resolution. Therefore, will the PED chosen to preserve A1 blood flow have an impact on the healing of aneurysms? Our results were significantly correlated with no change in A1 in the univariate analysis, but not in the multivariate analysis. This study provides a valuable reference for future treatment for considering the effect of PED size on blood flow when the PED needs to cover A1.

4.4. Limitations. (1) This was a retrospective study and the number of patients was relatively small. (2) Our data were derived from a multicenter study, and there were differences in the effect of the degree of PED pushing and pulling by the operators on the mesh during PED release. (3) Because some imaging data may be incomplete in a retrospective study, it is not certain that each patient's preoperative anterior communicating compensation status was evaluated preoperatively.

5. Conclusion

When relatively oversized PEDs are placed between M1 and the ICA, the higher porosity formed at the ostium of A1 is beneficial for maintaining stable A1 blood flow and reducing the risk of A1 artery occlusion.

Data Availability

All the data of this study can be obtained in the article and supplementary materials.

Conflicts of Interest

The authors declare that there is no conflict of interest regarding the publication of this paper.

Acknowledgments

We thank Edanz Group for the English revision. This study was funded by the National Nature Science Foundation of China (Grant no. 82071309), the National Natural Science Foundation of China (Grant no. 81901190), and the Natural Science Foundation of Heilongjiang Province of China (Grant no. YQ2019H015).

Supplementary Materials

Table S1: the size of the PED and the sPED/I-ICA ratio of the 48 patients. *(Supplementary Materials)*

References

[1] L. Rangel-Castilla, S. A. Munich, N. Jaleel et al., "Patency of anterior circulation branch vessels after pipeline embolization: longer-term results from 82 aneurysm cases," *Journal of Neurosurgery*, vol. 126, no. 4, pp. 1064–1069, 2017.

[2] N. Limbucci, G. Leone, L. Renieri et al., "Expanding indications for flow diverters: distal aneurysms, bifurcation aneurysms, small aneurysms, previously coiled aneurysms and clipped aneurysms, and carotid cavernous fistulas," *Neurosurgery*, vol. 86, Supplement_1, pp. S85–s94, 2020.

[3] A. Pujari, B. M. Howard, S. L. Skukalek et al., "Hemodynamic fate of the precommunicating anterior cerebral artery is predicted by vessel dominance after pipeline embolization device deployment across the internal carotid artery terminus," *World Neurosurgery*, vol. 128, pp. e688–e693, 2019.

[4] E. Nossek, D. J. Chalif, S. Chakraborty, and A. Setton, "Modifying flow in the ICA bifurcation: pipeline deployment from the supraclinoid ICA extending into the M1 segment-clinical and anatomic results," *AJNR. American Journal of Neuroradiology*, vol. 35, no. 11, pp. 2125–2129, 2014.

[5] G. Gascou, K. Lobotesis, H. Brunel et al., "Extra-aneurysmal flow modification following pipeline embolization device implantation: focus on regional branches, perforators, and the parent vessel," *AJNR. American Journal of Neuroradiology*, vol. 36, no. 4, pp. 725–731, 2015.

[6] A. Pujari, B. M. Howard, T. P. Madaelil et al., "Pipeline embolization device treatment of internal carotid artery terminus aneurysms," *Journal of neurointerventional surgery*, vol. 11, no. 5, pp. 485–488, 2019.

[7] C. J. O'kelly, T. Krings, D. Fiorella, and T. R. Marotta, "A novel grading scale for the angiographic assessment of intracranial aneurysms treated using flow diverting stents," *Interventional Neuroradiology*, vol. 16, no. 2, pp. 133–137, 2010.

[8] M. D. Joshi, C. J. O'Kelly, T. Krings, D. Fiorella, and T. R. Marotta, "Observer variability of an angiographic grading scale used for the assessment of intracranial aneurysms treated with flow-diverting stents," *AJNR. American Journal of Neuroradiology*, vol. 34, no. 8, pp. 1589–1592, 2013.

[9] N. Chalouhi, S. R. Satti, S. Tjoumakaris et al., "Delayed migration of a pipeline embolization device," *Neurosurgery*, vol. 72, 2013.

[10] N. Chalouhi, S. I. Tjoumakaris, L. F. Gonzalez et al., "Spontaneous delayed migration/shortening of the pipeline embolization device: report of 5 cases," *AJNR. American Journal of Neuroradiology*, vol. 34, no. 12, pp. 2326–2330, 2013.

[11] J. J. Heit, N. A. Telischak, H. M. Do, R. L. Dodd, G. K. Steinberg, and M. P. Marks, "Pipeline embolization device retraction and foreshortening after internal carotid artery blister aneurysm treatment," *Interventional Neuroradiology*, vol. 23, no. 6, pp. 614–619, 2017.

[12] C. Iosif, P. Berg, S. Ponsonnard et al., "Role of terminal and anastomotic circulation in the patency of arteries jailed by flow-diverting stents: from hemodynamic changes to ostia surface modifications," *Journal of Neurosurgery*, vol. 126, no. 5, pp. 1702–1713, 2017.

[13] P. Reymond, Y. Bohraus, F. Perren, F. Lazeyras, and N. Stergiopulos, "Validation of a patient-specific one-dimensional model of the systemic arterial tree," *American Journal of Physiology. Heart and Circulatory Physiology*, vol. 301, no. 3, pp. H1173–H1182, 2011.

[14] A. Y. Tang, W. C. Chung, E. T. Liu et al., "Computational fluid dynamics study of bifurcation aneurysms treated with pipeline embolization device: side branch diameter study," *Journal of medical and biological engineering*, vol. 35, no. 3, pp. 293–304, 2015.

[15] A. P. Narata and F. S. de Moura, "The role of hemodynamics in intracranial bifurcation arteries after aneurysm treatment with flow-diverter stents," *AJNR. American Journal of Neuroradiology*, vol. 39, no. 2, pp. 323–330, 2018.

[16] F. Mut and J. R. Cebral, "Effects of flow-diverting device oversizing on hemodynamics alteration in cerebral aneurysms," *AJNR. American Journal of Neuroradiology*, vol. 33, no. 10, pp. 2010–2016, 2012.

[17] M. Shapiro, E. Raz, T. Becske, and P. K. Nelson, "Variable porosity of the pipeline embolization device in straight and curved vessels: a guide for optimal deployment strategy," *AJNR. American Journal of Neuroradiology*, vol. 35, no. 4, pp. 727–733, 2014.

[18] R. Fahed, T. E. Darsaut, J. C. Gentric et al., "Flow diversion: what can clinicians learn from animal models?," *Neuroradiology*, vol. 59, no. 3, pp. 255–261, 2017.

[19] P. Berg, C. Iosif, S. Ponsonnard, C. Yardin, G. Janiga, and C. Mounayer, "Endothelialization of over- and undersized flow-diverter stents at covered vessel side branches: an in vivo and in silico study," *Journal of Biomechanics*, vol. 49, no. 1, pp. 4–12, 2016.

[20] N. Benard, D. Coisne, E. Donal, and R. Perrault, "Experimental study of laminar blood flow through an artery treated by a stent implantation: characterisation of intra-stent wall shear stress," *Journal of Biomechanics*, vol. 36, no. 7, pp. 991–998, 2003.

[21] T. R. Miller and M. J. Kole, "Pipeline diameter significantly impacts the long-term fate of jailed side branches during treatment of intracranial aneurysms," *AJNR. American Journal of Neuroradiology*, vol. 39, no. 12, pp. 2270–2277, 2018.

[22] M. J. Kole, T. R. Miller, G. Cannarsa et al., "Pipeline embolization device diameter is an important factor determining the efficacy of flow diversion treatment of small intracranial saccular aneurysms," *Journal of neurointerventional surgery*, vol. 11, no. 10, pp. 1004–1008, 2019.

Hindawi
BioMed Research International
Volume 2021, Article ID 5514608, 8 pages
https://doi.org/10.1155/2021/5514608

Research Article

AngioSuite-Assisted Volume Calculation and Coil Use Prediction in the Endovascular Treatment of Tiny Volume Intracranial Aneurysms

Zhihua Du, Bin Lv, Xiangyu Cao, Xinfeng Liu, Rongju Zhang, Hui Su, and Jun Wang

Department of Neurology, Chinese PLA General Hospital, The First Medical Center, Beijing, China

Correspondence should be addressed to Jun Wang; wangjun301@126.com

Received 8 January 2021; Revised 21 June 2021; Accepted 11 July 2021; Published 29 July 2021

Academic Editor: Silvia Todros

Background and Purpose. Ruptured tiny volume intracranial aneurysms (TVIAs) are associated with high risk of intraprocedural perforation. Aneurysm volume measuring is important for treatment planning and packing density calculation. We aim to assess the ability of the AngioSuite software in calculating TVIAs and guiding the selection of suitable coil. *Methods*. Thirty-three consecutive patients with 34 TVIAs were prospectively recruited and treated with endovascular techniques. The volume of TVIAs and the required length of coils were calculated by the AngioSuite software before embolization. The treatment efficacy of TVIAs was assessed using the Raymond scale (Rs) and the modified Rankin scale (mRs). *Results*. Of the 34 aneurysms with an average volume of 7.16 mm^3, 13 aneurysms were treated with sole coil embolization, 19 by stent-assisted embolization, and 2 by balloon-assisted embolization. The average coil length was 5.32 cm, and the average packing density was 41.21%. The immediate DSA showed that total occlusion (Rs = 1) was achieved in 15 aneurysms, subtotal (Rs = 2) in 9, and partial (Rs = 3) in 11. Total occlusion was achieved in 30 aneurysms and subtotal in the other 4 aneurysms at 6-month follow-up. Baseline volume and diameter of aneurysms were significantly correlated with the coil length ($r = 0.801$, $P < 0.001$; $r = 0.711$, $P < 0.001$). *Conclusions*. Coil embolization of TVIAs was easy to achieve high packing density. According to the data from AngioSuite, relative few coils can increase the safety in procedure and stenting may reduce risk of aneurysmal recurrence.

1. Introduction

Intracranial aneurysms (IAs) are commonly acquired cerebral lesions attacking about 2%~3% of the general population, which are associated with significant neurologic impairment and high mortality [1]. Unruptured IAs are more frequent and are being increasingly detected with the advancement of noninvasive imaging techniques with higher resolution [2]. The annual incidence of IA rupture is estimated to be 0.7%, which represents the leading cause of subarachnoid haemorrhage (SAH) [3]. A large cohort study involving 1993 patients with ruptured IAs showed that 83% of the aneurysms were found in anterior circulation locations and the median diameters of these aneurysms were 7 mm [4]. Besides, Grochowski et al. have concluded that rupture of small aneurysms (<5 mm) is a common cause of aneurysmal SAH [5].

Tiny volume intracranial aneurysms (TVIAs) are commonly defined as the aneurysms with size ≤ 3 mm in diameter. Currently, treatment of ruptured TVIAs is still technically challenging and associated with high risk of intraprocedural perforation due to their tiny volumes and thin fragile walls [6]. Endovascular treatments using coiling or stent-assisted coiling techniques emerge as important optional therapies for TVIAs because of their less invasive characteristics [7]. However, excessive coil introduction or insufficient packing will lead to coil compaction and recanalization after IA embolization [8]. The ability to assess the optimal packing density prior to endovascular treatment is fundamentally limited by the lack of accurate calculation of aneurysm volumes [9]. Aneurysm volume measuring is important for treatment planning and packing density calculation [10]. This is especially true for the exact volume calculation of TVIAs due to their extremely limited space for

stable coil deployment. Until recently, how TVIA volume should be measured and calculated reaches no consensus [11]. Therefore, based on the guiding role of TVIA volume measuring in endovascular treatment, we propose that the volume of TVIAs is a superior index over diameter in describing the characteristic of a cystic lesion, especially for those aneurysms with irregular appearance. The AngioSuite system is evaluated to be effective in accurate volume calculation of aneurysms based on two- or three-dimensional (2D or 3D) angiograms [9]. However, whether the AngioSuite software has comparable performance in assessing TVIA volume and packing density is currently unknown. Our study is aimed at assessing the ability of the AngioSuite software in calculating TVIA volume and then its role in prospectively selecting suitable coil, predicting packing density and the resultant clinical efficiency of endovascular treatment.

2. Materials and Methods

2.1. Definition of TVIAs. Tiny intracranial aneurysms are routinely defined as those aneurysms with a maximum diameter equal or less than 3 mm. However, it is not the case for those irregular aneurysm sacs with long and narrow appearances that their maximum diameter is above 3 mm, while the inner space of sacs is extremely small for further endovascular operations. Therefore, we proposed that the volume of TVIA could provide more details and assistance in predicting packing density and choosing suitable coils in real clinical practice. We assumed that the upper limit of TVIA volume could be calculated using the AngioSuite software by separately inputting 3 mm in length, width, and height, and the resultant TVIA volume was equal to $14.14\,mm^3$. Therefore, in this study, we defined any aneurysm with volume $\leq 14.14\,mm^3$ as TVIA.

2.2. Patients and Aneurysms. Thirty-three consecutive patients with 34 TVIAs (volume $\leq 14.14\,mm^3$) were prospectively recruited in our center from March 2016 to October2020. Thirty-two patients had ruptured aneurysms and presented acute SAH found by computed tomography (CT) scanning and CT angiography (CTA). They were admitted to our center within 24 h after the onset of SAH. Patient 17 carried an arteriovenous malformation- (AVM-) related unruptured TVIA, and it was embolized when treating the AVM. Patient 31 had 2 TVIAs; the ruptured one was located in the anterior communicating artery (AcoA) and treated at the first administration; the unruptured aneurysm in the middle cerebral artery (MCA) was embolized two weeks later (supplementary table (available here)). The Hunt-Hess grading system (0~V) was applied to evaluate the severity of the clinical symptoms of SAH. The institutional review board and ethics committee of our hospital approved the study protocol and informed consent form. Written informed consent was obtained from all patients.

2.3. Angiography and Volume Calculation. Digital subtraction angiography (DSA) and 3D rotational angiography were performed to observe the features of the aneurysms, including the location, diameter, and morphology as well as its anatomic relationship to the parent artery. The aneurysm volume was calculated using the AngioSuite software (Cascade Medical, Knoxville, TN, USA). As previously described, the AngioSuite system is a mathematical algorithm-dependent mobile phone application that uses the loaded biplane angiographic images or tomographic images to automatically calculate the volume of aneurysm only based on one aneurysm diameter [9, 10]. The packing density was also evaluated in this software by calculating the ratio of coil volume to aneurysm volume.

2.4. Embolization Procedure. All cases were assessed to be suitable for endovascular coil embolization by the consensus of the neurosurgeons and neurointerventionalists. Surgery was considered as an alternative option to coil embolization only after attempting endovascular treatment. Coiling alone or balloon/stent-assisted coiling treatment strategies were determined based on the parent vessel-aneurysm geometries and dome-to-neck ratio of the TVIAs. We decided to use a stent if the aneurysm was wide necked or had a complex morphology. Stent-assisted coiling was performed as a bail-out procedure in case of coil instability or after a failed attempt of simple coiling. For the embolization procedure, all embolization was performed under general anesthesia and the optimal projection was selected to fully expose the aneurysm neck and body and show the relationships to their parent artery and the major artery. A 6-French guiding catheter was delivered via a transfemoral approach with access through the femoral artery using a Siemen's biplane suite (Artis Q) with standard arteriographic and digital roadmap and SmartMask technique. A microcatheter for delivering stents was navigated to the location of aneurysm. Meanwhile, another steam-shaped microcatheter carrying the coil was directed into the aneurysm and partially inserted into the aneurysm cavity. The required length of the coil was calculated before embolization by the AngioSuite software when 30%-40% packing density was simulated. The calculated coil length was referred during coiling to ensure that the used length did not obviously exceed the calculated length in real practice. After one or more coils were released to fill the aneurysmal cavity, stent was partially released to prevent coil protrusion into the parent artery. Stent was completely released after the coil deployment was discontinued and the coil was isolated. Afterwards, the coil pusher was secured and the microcatheter containing the coil was slightly withdrawn. The coil delivery microcatheters used in this study included SL-10 (Stryker) and Echelon 10 (Covidien). The main coils used in this study were Axium coils (Covidien) and Target coils (Stryker Neurovascular, Freemont, CA). The type of stent was chosen depending on the surgeon's preference and the patient's vascular anatomy. Five types of stents were used in this study, including Neuroform EZ, Solitaire AB, Leo-Leo & Leo baby, Atlas, and Lvis Jr stents. Balloon-assisted coiling was performed in two patients to prevent prolapse of the coil loop, and the degree of balloon inflation varied during coil placement to allow for microcatheter movement. Detailed magnified view of angiography was performed at the end of each procedure to determine degree

Table 1: Baseline characteristics and aneurysmal features.

Clinical characteristics	Values
Gender (M/F)	13/21
Age (years)	60.24 ± 12.72
HH grade	
1	18
2	11
3	3
Unruptured	2
Aneurysmal location	
AcoA	13
PcoA	6
CPco	3
MCA	8
ACA	2
BA	2
Aneurysmal size	
Diameter (mm)	2.95 ± 0.74
Diameter ≤ 3 mm (cases)	21
Volumes (mm^3)	7.16 ± 3.74 (1.6~13.82)

Note: Emb: coil embolization; MCA: middle cerebral artery; BA: basilar artery; PcoA: posterior communicating artery; AcoA: anterior communicating artery; CPco: communicating segment of internal carotid artery; ACA: anterior cerebral artery.

of embolization and to identify possible complications such as rupture or thrombosis.

2.5. Anticoagulation and Antiplatelet Management. Heparin was intravenously administrated after placement of sheath at a dose of 0.6~0.8 mg/kg body weight, followed by hourly boluses (half of the dose of the baseline dose, but no less than 10 mg). The activated clotting time was maintained at 2~3 times the baseline throughout the procedure. If stent placement was scheduled for patients with ruptured aneurysm, a loading dose of 300 mg clopidogrel and 300 mg aspirin was administrated 2 hours before stenting; 100 mg aspirin and 75 mg clopidogrel were administered 24 hours after the procedure. For patients that underwent emergent stenting, tirofiban was intravenously injected at a dose of 0.005 mg/kg body weight before releasing the stent and this dose was maintained for 24 hours. Afterwards, tirofiban infusion was progressively decreased and changed to the regimens containing 100 mg aspirin and 75 mg clopidogrel. Aspirin (100 mg daily) and clopidogrel (75 mg daily) were maintained for 1~3 months after the operations based on the selection of stent type, followed by aspirin alone (100 mg daily) afterwards for 3~6months.

2.6. Outcome Evaluation and Follow-Up. A conventional follow-up using catheter angiography was performed 6 months after the embolization. The degree of aneurysm embolization was assessed using the Raymond scale (Rs) immediately after the embolization and 6 months postoperatively. Rs was classified as complete occlusion of the sac and neck of the aneurysm (Rs = 1), near-complete occlusion (the sac was occluded but a neck remnant was suspected or obviously present) (Rs = 2), and incomplete occlusion (there was persistent opacification of a sac remnant) (Rs = 3). Clinical outcome at follow-up was assessed using the modified Rankin scale (mRs) graded from 0 to 6.

Table 2: Embolization procedure and angiographic follow-up of the TVIAs.

Characteristics	Values
Embolization	
Single coil embolization	13
Stent-assisted	19
Balloon-assisted	2
Stent types	
Leo	7
Neuroform	4
Atlas	4
Solitaire AB	3
Lvis Jr	1
Coil types	
Target	29
Axium	4
Premier	1
Clinical outcomes	
Coil length (cm)	5.32 ± 3.18
Packing density (%)	41.31 ± 16.55
Immediate Rs	
1	15
2	9
3	10
Follow-up Rs	
1	30
2	4
Follow-up mRs	
0	32
1	2

Note: Emb: coil embolization; EZ: Neuroform stent; SAB: Solitaire AB stent; Leo: Leo & Leo baby stent; Ta: Target coil; Ax: Axium coil; Rs: Raymond scale; mRs: modified Rankin scale.

2.7. Data Analysis. All data analysis was performed in SPSS 26.0 software. Demographic and clinical characteristic data relating to continuous variables are expressed as means ± SD. Correlations between volume or diameter of aneurysms and coil length used or packing density were analyzed using Pearson analysis. A P value less than 0.05 is considered statistically significant.

3. Results and Discussion

3.1. Baseline Demographics and TVIA Characteristics. Thirty-four patients, consisting of 21 (61.8%) females and 13 (38.2%) males, were prospectively recruited in this study with

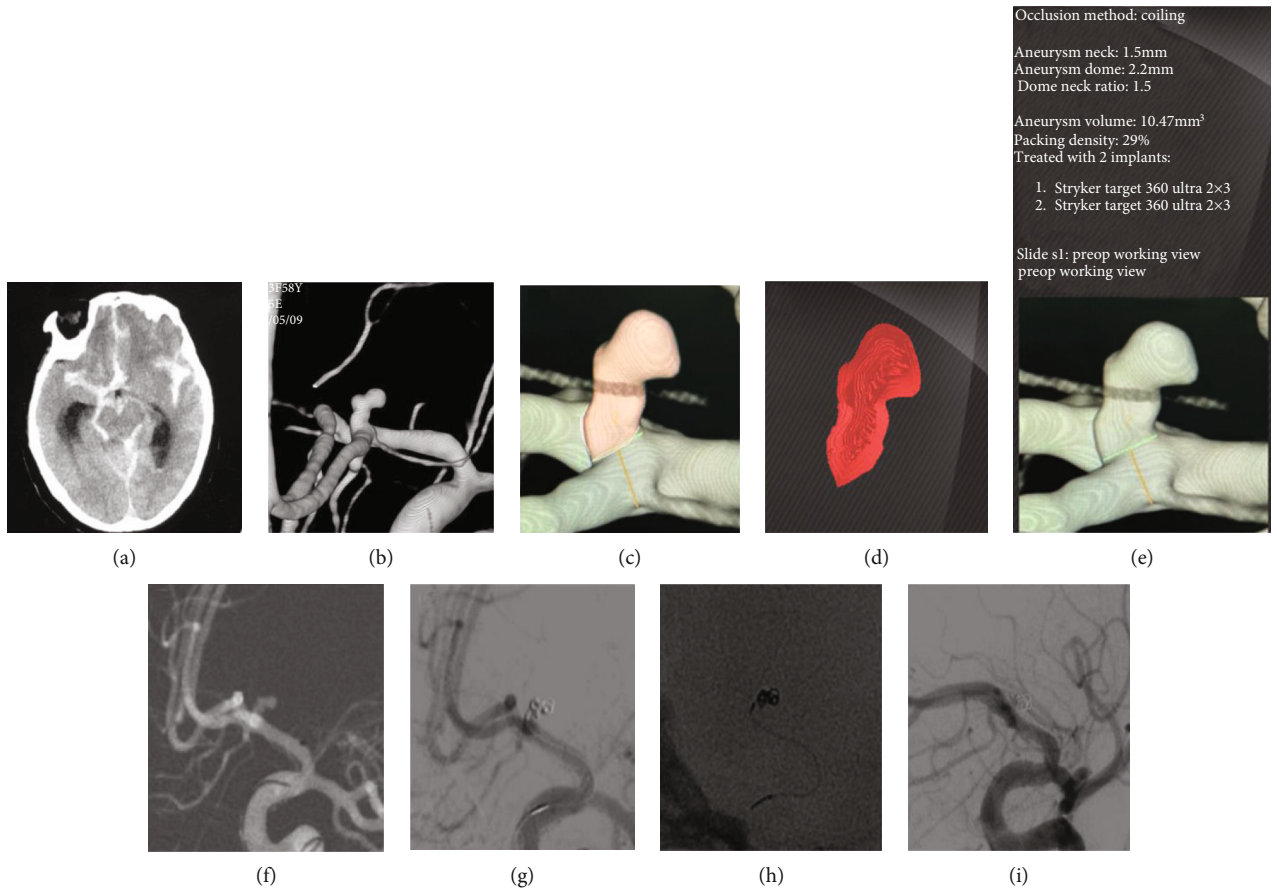

Figure 1: Case presentation of patient 6, female, 58 years old. She presented with (a) SAH on noncontrast head CT and (b) a ruptured irregular AcoA aneurysm on 3D reconstruction image of DSA. The AngioSuite software was used to configure and evaluate the volume of aneurysm before the embolization procedure (c–e). Based on the AngioSuite data, embolization with 2 coils (two targets 2-3 mm) could achieve sufficient immediate occlusion (Raymond 2) (f, g). Sparse coils showed on nonsubtracted image (h). Six-month follow-up showed a complete occlusion (Raymond 1) (i).

an average age of 60.24 ± 12.72 (ranging 32~85) years. These patients presented SAH due to tiny intracranial aneurysms with Hunt-Hess grade I in 18 cases, grade II in 11 cases, and grade III in 3 cases. These aneurysms were predominately located in AcoA (13 cases), MCA (8 cases), and posterior communicating artery (PcoA) (6 cases), accounting for 79.4% of the TVIAs. As calculated by the AngioSuite software, the average diameter and volume of the aneurysms were 2.95 mm (1.76~5.0 mm) and 7.16 mm^3 (1.6~13.82 mm^3), respectively. 21 (61.8%) aneurysms had diameter below 3 mm (Table 1).

3.2. Treatment Efficacy. For the treatment of intracranial aneurysms, 13 of them were managed with single coil embolization, 19 with stent-assisted embolization, and 2 with balloon-assisted embolization. The average length of coils was 5.12 ± 3.18 (1~12) cm, and packing density was 41.31 ± 16.55 (17~72) %. One case of stent thrombosis occurred during the procedures, and it was replaced with another Atlas stent. An aneurysm ruptured during the operation, and it was embolized with coil. All other aneurysms were treated successfully. Complete occlusion was achieved in 15 patients (46.2%), while 9 (30.8%) and 11 (23.1%) patients achieved near-complete occlusion and incomplete occlusion, respectively (Table 2).

3.3. Angiographic Follow-Up. All patients were followed up six months postoperatively; complete occlusion was achieved in 30 (88.2%) of 34 aneurysms and near-complete occlusion was achieved in 4 (11.8%) aneurysms. 33 of the aneurysms had decreased Rs grade compared to immediately postoperative outcome, and one aneurysm had no change in Rs grading. At six months of follow-up, 31 (93.9%) of the patients had no neurological complications as mRs scoring 0, and the remaining two patients (aged over 80 years) had mild symptoms but no functional deficiencies with mRs scoring 1 (Table 2). No migration of stents or coils occurred at follow-up compared with immediate position after embolization. None of the aneurysms showed recanalization requiring additional treatment. The case presentation of case 6 (supplementary table (available here)) is shown in Figure 1.

3.4. Roles of Aneurysm Volume Measurement in Guiding Coil Embolization. We further explored the correlation between volumes of aneurysms and coil length used during embolization by Pearson analysis. The results showed that baseline

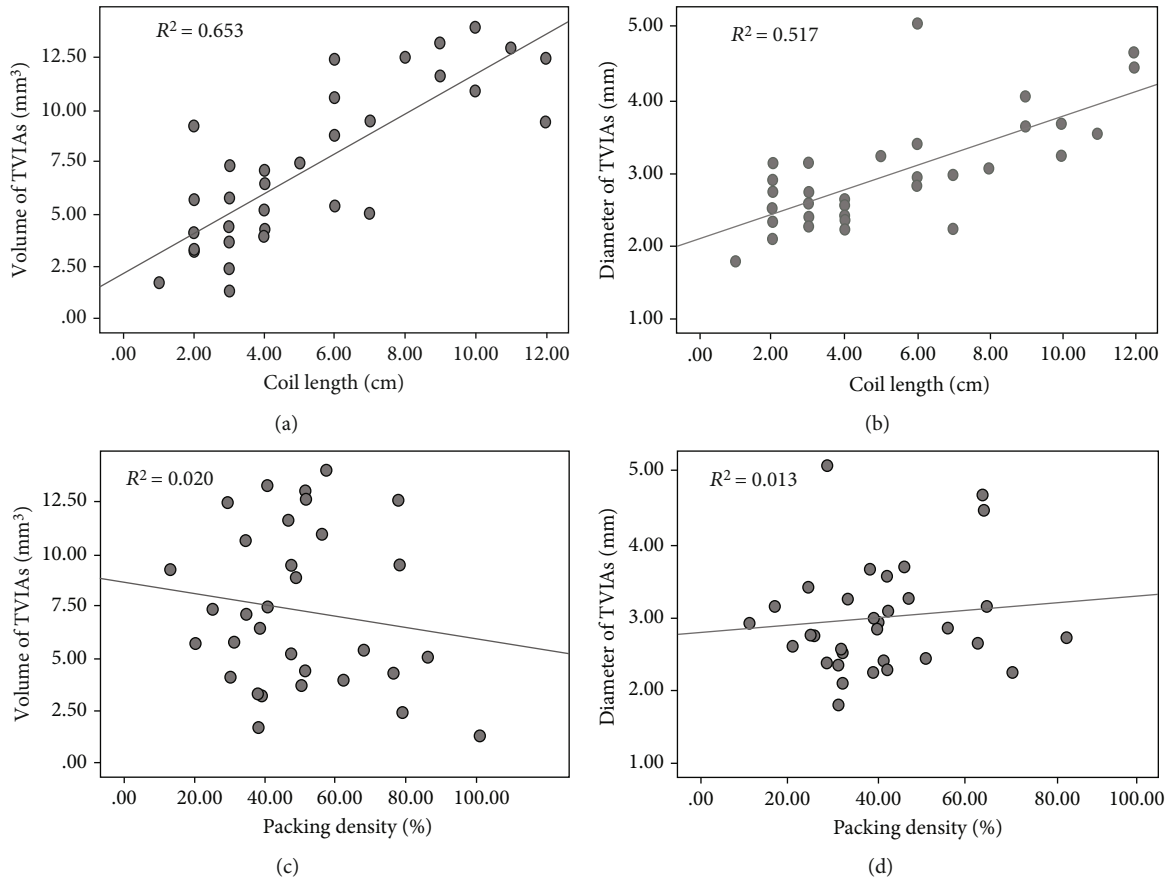

Figure 2: Correlation analyses between aneurysm volume or diameter and length of coils or packing density of coils during embolization. Scatter plots of (a) volume of TVIAs against coil length, (b) diameter of TVIAs *vs.* coil length, (c) volume of TVIAs *vs.* packing density, and (d) diameter of TVIAs *vs.* packing density.

volumes (calculated by the AngioSuite software) and diameters of TVIAs were significantly correlated with the coil length used during embolization ($r = 0.801$ and $P < 0.001$ and $r = 0.711$ and $P < 0.001$, respectively), indicating that aneurysmal volume as determined by AngioSuite was a preferable parameter in guiding the coil embolization procedure. In addition, no significant correlations were shown between volume or diameter and packing density of the aneurysms ($r = -0.163$, $P = 0.363$; $r = 0.099$, $P = 0.585$) (Figure 2).

4. Discussion

With the wide application of 3D rotational angiography, small and tiny aneurysms have been diagnosed more frequently. Tiny aneurysms have been expected to have a high rate of ruptures up to 15% [12, 13]. Unfortunately, no specific recommendations for treating TVIAs are available up to date [2]. In recent years, coil embolization with the assistance of stent or balloon offers a reliable and safe strategy for the treatment of tiny aneurysms with the advancement of endovascular techniques. However, TVIA embolization has higher risk of procedural complications than other intracranial aneurysms mainly due to excessive coils with limited space to obtain a stable microcatheter position for coil deployment [14]. Meanwhile, an optimal packing density during endovascular treatment is necessary for preventing coil compaction and improving prognosis of these patients. In this study, we used the AngioSuite software to calculate the TVIA volume and the required coil length to ensure sufficient packing density. The AngioSuite-based volume estimation provides efficient assistance for assessing the required coil length and packing density, in turn reducing the rupture during embolization and recurrence of TVIAs in the follow-up.

The volume of intracranial aneurysm is a very important parameter for endovascular treatment planning and embolization course, especially for those irregular cystic lesions. An inaccurate measurement in a millimeter level may cause higher risk of rupture of TVIAs and secondary misuse of expensive endovascular devices [10]. Currently, the accurate calculation of aneurysm volume remains a challenge. Woodward and Forsberg concluded that volume calculation based on 3D images was greatly affected by identification of threshold windows dependent on the operator, while 2D image-based volume calculations can be adversely influenced by lacking reliable markers, irregular aneurysm shapes, and overly simplistic spherical or elliptical geometric models [9]. Therefore, how to size the intracranial aneurysm has been disputed and discussed over the past years. A study by Behme et al. reported that the most exact aneurysm measurement can be achieved on a 2D DSA image with a short objective-to-detector distance adjusted according to a

previous 3D run [11]. Meanwhile, the AngioSuite software is proposed to be an accurate method to calculate aneurysm volumes in comparison with AngioCalc or other specialized software based on rotational angiography [9, 10]. The AngioSuite mathematical system runs based on bidimensional angiographic images. In this study, we used the AngioSuite software to calculate TVIAs' volume and the required length of coil that reached sufficient packing density. The coil length has more prominent influence on the packing density for TVIAs than for the large or giant IAs. Currently, most of the coil lengths are measured in centimeters, and an increase of 1 cm in coil length leads to obvious increase in packing density for TVIAs, while it may have no notable effect on an aneurysm with a diameter over 5 mm.

Most authors believe that increased packing densities result in lower compaction and decreased aneurysmal recurrence. Piotin et al. [15] noted a 44.4% recurrence rate in aneurysms with packing densities ≤ 25% and 29.8% in packing densities > 25%. Sluzewski et al. [16] showed that aneurysms packed to >24% did not show compaction at 6 months of follow-up. However, "the more the better" would not be always right in the embolization procedure. Intraprocedural rupture is a fearful complication in the endovascular treatment of TVIAs [17–19]. Nguyen et al. [17] found that endovascular coil embolization of very small (≤3 mm) ruptured cerebral aneurysms is 5 times more likely to result in procedure-related rupture compared with larger aneurysms. The smaller size of the aneurysm sac limits the movement of the microcatheter; thus, any unexpected movement during catheter positioning or coil deployment can result in rupture of the aneurysm sac [14]. Endovascular devices such as coils or stents may be oversized, which confer a higher rupture risk. Tiny volume is liable to reach sufficient packing density even when fewer coils are used. Chen et al. [20] found that aneurysmal size was an independent influencing factor for immediate angiographic outcome after embolization in patients with TVIAs. A study by Maeda et al. [21] suggested that the length of all coils should not be longer than 10 cm in the embolization of TVIAs in terms of safety. Lu et al. [22] believed that complete coil occlusion of the aneurysm sac was not necessary to achieve better long-term outcomes. We currently consider that >30% is a sufficient packing density for the embolization and approximate length of coils should be selected according to the data of AngioSuite. An acceptable immediate occlusion (Rs 1 and Rs 2) rate (70.6%) was obtained by a 5.32 cm average length of coils and 41.31% packing density in our series. We also found that there is a significant linear correlation between the length of coils and the volume of aneurysms.

In this study, we used the AngioSuite software before the procedure aiming to minimize the use of coils and increase the safety during the operations. Meanwhile, stent deployment enhanced the flow diverting and further reduced the use of coil. For case 11 (supplementary table (available here)), only 2 cm coil was used and the rupture risk of the aneurysm during embolization potentially decreased, while the resultant thrombotic complications could be efficiently treated with new antiplatelet drugs. Although fewer coils could reduce the risks of rupture during embolization, tiny volume is still an adverse factor for coil stabilization. Assistant devices such as high elasticity balloon and stent are needed sometimes. The placement of a balloon at the side of the aneurysm neck to stop haemorrhage has been advocated; however, the use of additional adjunctive devices during treatment of very small IAs has been proposed to associate with increased complication rates in some studies [23, 24]. Stent placement is helpful in packing coils and preventing coil escape, even playing a role in flow diverting. Stents across the neck of an aneurysm redirect the blood flow and decrease intra-aneurysmal flow velocity by disturbing the inflow. The reduced aneurysmal flow induces stasis and consequently thrombosis of the aneurysm [25]. Tateshima et al. [26] investigated the alterations in intra-aneurysmal hemodynamics following the placement of high-porosity open-cell stents across the necks of aneurysms and found that the placement of a single Neuroform stent reduced the intra-aneurysmal flow velocity by 22%-64%. In another study, the authors assessed the hemodynamic changes inside aneurysms induced by the implantation of conventional stents and found that the velocity of the jet flow entering the aneurysm and wall shear stresses on the aneurysm were significantly reduced by the deployment of a stent [27]. Even then, stent placement also associated with higher thrombosis complication in the endovascular treatment of TVIAs [28]. In our case series, more than half of the cases (19/34) underwent stent-assisted embolization procedure and one case of in-stent thrombosis was treated immediately. In our experience, intravenous transfusion of tirofiban (0.005 mg/kg/h) was prescribed before stent deployment and continued for 24 hours, and then, stepwise reduced doses were recommended until dual oral antiplatelet regimens (aspirin 100 mg and clopidogrel 75 mg per day) were given at least 3 times. In a study by Wu et al. [13], the patients with ruptured TVIAs were prescribed with dual antiplatelet therapy (aspirin 300 mg and clopidogrel 300 mg) 2 hours prior to the Lvis stent-assisted embolization, which also achieved safe outcomes. However, some cases with high grade of Fisher scale or with intracranial hematoma who had high possibility of surgery would not be indicated for stenting.

5. Conclusions

Embolization was reliable to achieve a high packing density and occlusion rate in treating TVIAs. According to the data from AngioSuite, relative few coils can increase the safety in procedure. For those patients with mild TVIAs, stent-assisted coil may be a helpful option to reduce the risk of aneurysm recurrence.

Data Availability

The datasets used during the present study are available from the corresponding author upon reasonable request.

Conflicts of Interest

The authors declare that there is no conflict of interest regarding the publication of this paper.

Authors' Contributions

Zhihua Du and Bin Lv contributed equally to this work.

Acknowledgments

We thank all the patients for their participation in this research.

Supplementary Materials

Supplementary Table: baseline characteristics and procedure/follow-up occlusion outcomes. *(Supplementary Materials)*

References

[1] R. D. Brown and J. P. Broderick, "Unruptured intracranial aneurysms: epidemiology, natural history, management options, and familial screening," *The Lancet Neurology*, vol. 13, no. 4, pp. 393–404, 2014.

[2] A. Malhotra, X. Wu, H. P. Forman, C. C. Matouk, D. Gandhi, and P. Sanelli, "Management of tiny unruptured intracranial aneurysms: a comparative effectiveness analysis," *JAMA Neurology*, vol. 75, no. 1, pp. 27–34, 2018.

[3] M. AlMatter, P. Bhogal, M. Aguilar Pérez et al., "The size of ruptured intracranial aneurysms: a 10-year series from a single center," *Clinical Neuroradiology*, vol. 29, no. 1, pp. 125–133, 2019.

[4] M. Korja, R. Kivisaari, B. Rezai Jahromi, and H. Lehto, "Size and location of ruptured intracranial aneurysms: consecutive series of 1993 hospital-admitted patients," *Journal of Neurosurgery*, vol. 127, no. 4, pp. 748–753, 2017.

[5] C. Grochowski, J. Litak, B. Kulesza et al., "Size and location correlations with higher rupture risk of intracranial aneurysms," *J Clin Neurosci*, vol. 48, pp. 181–184, 2018.

[6] M. C. Anokwute, J. A. Braca, B. Bohnstedt et al., "Endovascular treatment of ruptured tiny (⩽3 mm) intracranial aneurysms in the setting of subarachnoid hemorrhage: A case series of 20 patients and literature review," *Journal of Clinical Neuroscience*, vol. 40, pp. 52–56, 2017.

[7] Y. Zheng, Y. Song, D. Liu et al., "Stent-assisted coiling embolization of tiny, wide-necked intracranial aneurysms," *Acta Neurochirurgica*, vol. 159, no. 1, pp. 93–100, 2017.

[8] M. Tsutsumi, H. Aikawa, M. Onizuka et al., "Endovascular treatment of tiny ruptured anterior communicating artery aneurysms," *Neuroradiology*, vol. 50, no. 6, pp. 509–515, 2008.

[9] K. Woodward and D. A. Forsberg, "AngioSuite: an accurate method to calculate aneurysm volumes and packing densities," *Journal of NeuroInterventional Surgery*, vol. 5, Supplement 3, pp. iii28–iii32, 2013.

[10] V. H. Escobar-de la Garma, M. Zenteno, F. Padilla-Vázquez, D. San-Juan, and A. Cerón-Morales, "Comparative analysis of aneurysm volume by different methods based on angiography and computed tomography angiography," *Neurosurgical Review*, vol. 41, no. 4, pp. 1013–1019, 2018.

[11] D. Behme, N. Amelung, T. Khakzad, and M. N. Psychogios, "How to size intracranial aneurysms: a phantom study of invasive and noninvasive methods," *American Journal of Neuroradiology*, vol. 39, no. 12, pp. 2291–2296, 2018.

[12] M. Wei, H. Ren, and L. Yin, "The combinational use of dual microcatheter technique and new hypersoft helical coil for endovascular treatment of tiny intracranial aneurysm with difficult geometry," *Interventional Neuroradiology*, vol. 22, no. 1, pp. 18–25, 2016.

[13] P. Wu, P. E. Ocak, D. Wang et al., "Endovascular Treatment of Ruptured Tiny Intracranial Aneurysms with Low- Profile Visualized Intraluminal Support Device," *Journal of Stroke and Cerebrovascular Diseases*, vol. 28, no. 2, pp. 330–337, 2019.

[14] V. N. Yamaki, W. Brinjikji, M. H. Murad, and G. Lanzino, "Endovascular treatment of very small intracranial aneurysms: meta-analysis," *American Journal of Neuroradiology*, vol. 37, no. 5, pp. 862–867, 2016.

[15] M. Piotin, L. Spelle, C. Mounayer et al., "Intracranial aneurysms: treatment with bare platinum coils–aneurysm packing, complex coils, and angiographic recurrence," *Radiology*, vol. 243, no. 2, pp. 500–508, 2007.

[16] M. Sluzewski, W. J. van Rooij, M. J. Slob, J. O. Bescós, C. H. Slump, and D. Wijnalda, "Relation between aneurysm volume, packing, and compaction in 145 cerebral aneurysms treated with coils," *Radiology*, vol. 231, no. 3, pp. 653–658, 2004.

[17] T. N. Nguyen, J. Raymond, F. Guilbert et al., "Association of endovascular therapy of very small ruptured aneurysms with higher rates of procedure-related rupture," *Journal of Neurosurgery*, vol. 108, no. 6, pp. 1088–1092, 2008.

[18] W. Brinjikji, G. Lanzino, H. J. Cloft, A. Rabinstein, and D. F. Kallmes, "Endovascular treatment of very small (3 mm or smaller) intracranial aneurysms: report of a consecutive series and a meta-analysis," *Stroke*, vol. 41, no. 1, pp. 116–121, 2010.

[19] M. Sluzewski, J. A. Bosch, W. J. van Rooij, P. C. G. Nijssen, and D. Wijnalda, "Rupture of intracranial aneurysms during treatment with Guglielmi detachable coils: incidence, outcome, and risk factors," *Journal of Neurosurgery*, vol. 94, no. 2, pp. 238–240, 2001.

[20] J. X. Chen, L. F. Lai, K. Zheng et al., "Influencing factors of immediate angiographic results in intracranial aneurysms patients after endovascular treatment," *J Neurol*, vol. 262, no. 9, pp. 2115–2123, 2015.

[21] K. Maeda, R. Motoie, S. Karashima et al., "Coil embolization for very small intracranial aneurysms with diameter less than 3 mm: a case series of 14 patients and literature review," *No Shinkei Geka*, vol. 46, no. 4, pp. 303–312, 2018.

[22] J. Lu, J. C. Liu, L. J. Wang, P. Qi, and D. M. Wang, "Tiny intracranial aneurysms: endovascular treatment by coil embolisation or sole stent deployment," *European Journal of Radiology*, vol. 81, no. 6, pp. 1276–1281, 2012.

[23] G. Lanzino and D. F. Kallmes, "Endovascular treatment of very small ruptured intracranial aneurysms," *Journal of Neurosurgery*, vol. 108, no. 6, p. 1087, 2008.

[24] W. J. van Rooij, G. J. Keeren, J. P. P. Peluso, and M. Sluzewski, "Clinical and Angiographic Results of Coiling of 196 Very Small (≤ 3 mm) Intracranial Aneurysms," *American Journal of Neuroradiology*, vol. 30, no. 4, pp. 835–839, 2009.

[25] G. Cantón, D. I. Levy, and J. C. Lasheras, "Hemodynamic changes due to stent placement in bifurcating intracranial aneurysms," *Journal of Neurosurgery*, vol. 103, no. 1, pp. 146–155, 2005.

[26] S. Tateshima, K. Tanishita, Y. Hakata, S. Y. Tanoue, and F. Viñuela, "Alteration of intraaneurysmal hemodynamics by placement of a self-expandable stent. Laboratory investigation," *Journal of Neurosurgery*, vol. 111, no. 1, pp. 22–27, 2009.

[27] C. Wang, Z. Tian, J. Liu et al., "Flow diverter effect of LVIS stent on cerebral aneurysm hemodynamics: a comparison with Enterprise stents and the Pipeline device," *Journal of Translational Medicine*, vol. 14, no. 1, p. 199, 2016.

[28] J. Dalfino, A. K. Nair, D. Drazin, E. Gifford, N. Moores, and A. S. Boulos, "Strategies and outcomes for coiling very small aneurysms," *World Neurosurgery*, vol. 81, no. 5-6, pp. 765–772, 2014.

Hindawi
BioMed Research International
Volume 2021, Article ID 9976541, 8 pages
https://doi.org/10.1155/2021/9976541

Research Article

The Application of "Stilted Building" Technique in the Embolization of Aneurysms with Secondary Branches

Yi Qi,[1] **Yongquan Sun**,[1] **Yang Wang**,[1] **Jianwen Jia**,[1] **Hongliang Zhong**,[1] **Hongchao Yang**,[1] **Ming Lv**,[2] **and He Liu**[1]

[1]*Department of Neurosurgery, Beijing Chaoyang Hospital, Capital Medical University, Beijing, China*
[2]*Department of Interventional Neuroradiology, Tiantan Hospital, Capital Medical University, Beijing, China*

Correspondence should be addressed to Ming Lv; dragontiger@163.com and He Liu; 1515812733@qq.com

Received 28 March 2021; Revised 17 May 2021; Accepted 1 June 2021; Published 21 June 2021

Academic Editor: Xiangyu Cao

Objective. Many intracranial aneurysms often have branch arteries, and it is especially important to protect them during embolization. The purpose of the present study was to evaluate the curative effect and safety of the "stilted building" technique. *Methods*. 25 patients with intracranial aneurysms with branch arteries that have been treated by coil embolization with the "stilted building" technique were retrospectively reviewed. Clinical follow-up was performed after endovascular treatment. *Results*. All 25 patients successfully underwent aneurysm embolization. During the operation, the ruptured sac and most of the body of the aneurysm were embolized using the "stilted building" technique. Immediate imaging showed that the blood flow to the branch arteries from the neck or sidewall of the aneurysm was unobstructed. The mRS scores of the 25 patients during the follow-up period were mRS 0 for twenty-one patients, mRS 1 for three patients, and mRS 6 for one patient. No aneurysms recurred among the patients who completed the follow-up. *Conclusions*. In an aneurysm with a branch artery, when a balloon or stent cannot be effectively used to protect the branch artery, the use of "stilted building" embolization can achieve good therapeutic effects, and the short-term follow-up results are satisfactory; the technique can effectively protect branch arteries originating from aneurysms.

1. Introduction

Endovascular therapy is one of the main treatment methods for intracranial aneurysms. Coil embolization is widely used for ruptured and unruptured aneurysms and is capable of relatively high efficacy and safety [1–3]. Many aneurysms often have branch arteries, [4] and it is especially important to protect them during embolization. However, the protection of these arteries during aneurysm embolization is difficult [4–6] when the branch artery originates from the neck or the sidewall of the aneurysm and cannot be effectively protected by the balloon or stent. From June 2010 to June 2020, Beijing Chaoyang Hospital and Beijing Tiantan Hospital Affiliated with Capital Medical University received 25 patients with intracranial aneurysms involving branch arteries that were treated by embolization using the "stilted building" technique. The curative effect was satisfactory. The stilted buildings of the Chinese Tujia people feature a bamboo or wooden structure suspended above the ground and raised on timber stilts. The principle of the embolization technology is similar to that of stilted buildings, so it is named the "stilted building" technique and which was partial embolization [7]. A retrospective report and our technical experience are described below.

2. Materials and Methods

This is a retrospective study. From June 2010 to June 2020, a total of 25 patients with intracranial aneurysms with branch arteries were treated by coil embolization with the "stilted building" technique. The patient cohort included 7 males and 18 females aged 35 to 84 years, with a mean age of 63.5 ± 11.1 years. Eighteen patients had a spontaneous subarachnoid hemorrhage, nine with Hunt & Hess grade I, four with grade II, and five with grade III; the remaining 7 patients had no obvious symptoms, and their aneurysms were found

during physical examination. The diagnosis was confirmed by plain head CT scan and digital subtraction angiography (DSA). Twelve patients were embolized with the "stilted building" technique alone, 11 with the "stilted building" technique combined with stent-assisted embolization, and 2 with the "stilted building" technique combined with balloon-assisted embolization.

2.1. Technical Details of the "Stilted Building" Technique. All aneurysm embolization procedures were performed by two interventional neurosurgeons and one interventional neuroradiologist. For patients with ruptured aneurysms undergoing emergency surgery, if stent-assisted embolization was required, tirofiban was administered by intravenous infusion before the stent was released. The initial dose was 10 μg/kg, which was completely delivered within 3 minutes. Then, tirofiban was infused intravenously at a rate of 0.15 μg/kg/min. After the operation, tirofiban was instilled at a maintenance dose for 24 hours. Patients with indwelling stents were routinely given aspirin 100 mg/day and clopidogrel 75 mg/day after surgery for 3 months. Patients undergoing elective surgery were prescribed aspirin 100 mg/day and clopidogrel 75 mg/day at least 5 days before their operation. After the operation, they continued to receive dual antiplatelet therapy (aspirin 100 mg/day and clopidogrel 75 mg/day) for 3 months and long-term administration of aspirin after 3 months. If a stent was not used, the patients were given aspirin 100 mg/day for 1 month. All treatments were performed under general anesthesia and systemic heparinization, with an activated clotting time of approximately 250-300 seconds. An arterial sheath was inserted into the femoral artery using Seldinger's technique, and a 6F or 8F guiding catheter (Envoy, Codman Neurovascular, USA) was positioned into the extracranial segment of the internal carotid artery. A microcatheter, such as a Headway 17 (MicroVention-Terumo, Tustin, CA, USA) or an Echelon 10 (Medtronic, Minneapolis, MN, USA), was placed in an appropriate position relative to the aneurysm through the guiding catheter. The aneurysm was embolized by using the "stilted building" technique alone or after placement of a Hyperglide occluded balloon catheter (Medtronic) or Rebar stent catheter (Medtronic) into the target artery as required. The principle of this technique is similar to that of the Tujia stilted buildings supported by timber stilts (Figure 1(a)). First, a larger diameter coil that is slightly larger than the diameter of the aneurysm was chosen to form a stable internal frame to support the sidewall of the aneurysm and the wall of the branch artery, resembling the pillars of the "stilted building" and providing a strong support point for the aneurysm to later be filled with coils (Figure 1(d)). After completing the preliminary frame which still contained substantial coil-free dead space due to the use of large-diameter coils, leaving much of the aneurysmal space unembolized, the aneurysm was then filled with additional smaller coils (Figure 1(e)). By changing the position of the microcatheter tube head and selecting coils of different properties and diameters, the distribution of the coils can be adjusted to form the building body of the "stilted building", avoiding the area where the branch artery originates from the aneurysm (Figure 1). In addition, according to the type of aneurysm neck, an appropriate balloon or stent can be selected to form a more stable frame structure or to protect other branches.

2.2. Angiographic Evaluation. The location of the aneurysm was defined at the origin of the neck. The angiographic outcome was evaluated according to the Raymond classification [8, 9] immediately after the operation and at follow-up. Angiographic recurrence was defined as any worsening of the Raymond classification or enlargement of the residual aneurysm. By comparing the follow-up and intraoperative blood flow in the relevant arteries, the protective effects on the branches were evaluated. The follow-up period was defined as the number of postoperative months to recurrence or the latest angiogram. When performing DSA during the operation and the postoperative follow-up, a PHILIPS Allura Xper FD20 (Philips Healthcare, Best, the Netherlands) was used. The size of the aneurysm was measured with reconstructed 3D images by using an Allura 3D-RA workstation (Philips Healthcare, Best, the Netherlands).

2.3. Clinical Assessment. Clinical outpatient follow-up was performed at approximately six months and annually after treatment, and each patient was evaluated by the modified Rankin Scale (mRS) [10]. If possible, follow-up imaging with DSA, MRA, or CTA was performed. Perioperative complications were defined as any new neurologic deficits, serious adverse events extending hospitalization, or death occurring within 30 days after the operation.

3. Results

All 25 patients successfully underwent aneurysm embolization (Table 1). Of these, 9 aneurysms were located on the posterior communicating segment of the internal carotid artery (ICA), 11 aneurysms were located on the middle cerebral artery (MCA), 4 aneurysms were located on the anterior communication artery (AcomA), and 1 aneurysm was located on the basilar artery (BA). Furthermore, 12 aneurysms were located on the sidewall of the parent artery, and 13 were located at the artery bifurcation. During the operation, the ruptured sac and most of the body of the aneurysm were embolized using the "stilted building" technique. Immediate imaging showed that the blood flow to the branch arteries from the neck or sidewall of the aneurysm was unobstructed. The mRS scores of the 25 patients during the follow-up period were mRS 0 for twenty-one patients, mRS 1 for three patients, and mRS 6 for one patient. The DSA follow-up time was 0.5-12 months, with an average of 6.4 ± 3.0 months, and the follow-up rate was 36%. No aneurysms recurred among the patients who completed the follow-up. The branch arteries of 24 patients had normal blood flow and demonstrated no significant changes, while 1 patient showed related arterial blood flow restriction. Three patients (12%) were considered to have perioperative complications, all of which were related to ischemic perforator arteries. One patient, with an aneurysm at the bifurcation of the right MCA, developed right-sided facial paralysis and left limb weakness two weeks after surgery. MRI-DWI showed fresh

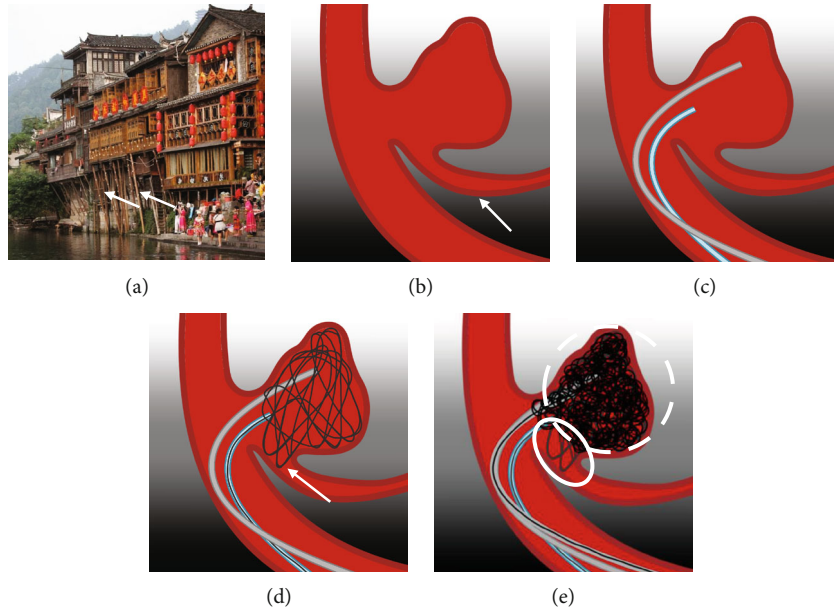

Figure 1: Technical details of the "stilted building" technique. (a) The stilted buildings of the Chinese Tujia people feature a bamboo or wooden structure suspended above the ground and raised on timber stilts (arrow). (b) A branch originates from the neck of the aneurysm (arrow), and its blood flow direction is at an acute angle with the parent artery. It is difficult to protect it with a balloon or stent during the embolization of the aneurysm. (c) The aneurysm is embolized by using the "stilted building" technique; first, a double microcatheter is placed in the appropriate part of the aneurysm. (d) A coil with a diameter slightly larger than the aneurysm is used to form a support frame within the aneurysm, allowing several rings to enter the branch artery to play a supporting role (arrow). (e) The ruptured sac and body continue to be embolized with the supporting frame, avoiding the branch artery. The presence of the supporting frame allows subsequent coils to be held in a suitable position without entering the branch artery. The pillars of the "stilted building" are indicated by the solid ellipse, and the body of the "stilted building" is shown by the dotted ellipse.

infarction of the hind limb of the right internal capsule, no clear arterial occlusion, and blood flow restriction on DSA review. A second patient, with a left posterior communicating aneurysm, showed decreased right limb muscle strength and reduced consciousness on the first postoperative day. Emergency reexamination of the brain CT showed no significant increase in hemorrhage or new infarcts. The patient's state gradually recovered after enhanced fluid perfusion. Considering possible small embolus shedding and vasospasm, the patient's consciousness was clear at the time of discharge, and the right limb muscle strength was grade 4. The last patient, with a left posterior communicating aneurysm, developed blurred vision and hemianopia on the right side but had normal limb movement 2 weeks after surgery. Reexamination of the brain CT showed left occipital lobe infarction, and DSA showed that the blood flow of the left posterior communicating artery was restricted. Additionally, two patients had nonsurgery-related complications. One patient, with an aneurysm of the sidewall of the M1 segment of the right MCA, developed communicating hydrocephalus 12 months after surgery and underwent a lumbar cisternal-abdominal shunting. The second patient, with a right posterior communicating aneurysm, died of postoperative ventricular fibrillation.

3.1. Illustrative Cases

3.1.1. Patient 1. A 66-year-old woman presented with a symptomatic aneurysm of the posterior communicating segment of the right ICA. Head CT showed subarachnoid and intraventricular hemorrhage. DSA examination revealed that a right posterior communicating ruptured aneurysm measuring approximately 10 mm × 7 mm, with a neck width measuring approximately 7 mm, and the embryonic posterior cerebral artery originated from the neck of the aneurysm (Figures 2(a)–2(c)). The patient underwent intracranial aneurysm embolization under general anesthesia. First, assisted by a supersmooth guidewire, a 6F guiding catheter was indwelled into the extracranial segment of the ICA; the Headway 17 microcatheter and the Echelon 10 microcatheter were placed within the aneurysm with assistance from the microguidewire through the guiding catheter. The microguidewire was withdrawn. Then, the first coil, with a slightly larger diameter (9 mm × 24 cm) than the aneurysm, was fed through the Headway 17 microcatheter. A few rings were inserted into the posterior communicating artery to form a stable support frame (Figure 2(d)). Angiography showed that the lumen of the ICA and the posterior communicating artery was unobstructed. The coil was then released. Finally, a 4 mm × 10 cm MicroPlex Coil System (MicroVention-Terumo, Tustin, CA, USA) and 4 mm × 12 cm and 4 mm × 10 cm Jasper coils (Peijia Medical, Suzhou, Jiangsu, China) were continuously fed through the Echelon 10 microcatheter. Angiography showed that the ruptured sac was embolized (Figure 2(e)). The aneurysm continued to be filled with 6 mm × 15 cm, 4 mm × 6 cm, 4 mm × 6 cm, 5 mm × 15 cm, and 4 mm × 10 cm Jasper coils (Peijia Medical) through the Headway 17 microcatheter (Figure 2(f)). Immediate angiography showed that the ruptured sac of the aneurysm and the

Table 1: Patient, aneurysm, procedure, and follow-up data.

	Stilted building technique	Stilted building technique +SAC	Stilted building technique +BAC	Total
General				
Sex				
Men	3	3	1	7
Women	9	8	1	18
Age (years)	66.2 ± 10.5	62.2 ± 8.2	55 ± 20	64 ± 11
Aneurysm characteristics				
Aneurysm location				
AcomA	4	0	0	4
MCA	3	7	1	11
PcomA	5	3	1	9
BA	0	1	0	1
Relationship with the parent artery				
Sidewall	6	5	1	12
Bifurcation	6	6	1	13
Aneurysm size (mm)	5.4 × 4.9	6.9 × 5.9	10.1 × 8.8	6.6 × 5.8
Rupture status				
Ruptured	9	7	2	18
Unruptured	3	4	0	7
Branch/origin				
A2/aneurysm neck	4	0	0	4
/aneurysm sidewall	0	0	0	0
M2/aneurysm neck	2	5	1	8
/aneurysm sidewall	0	2	0	2
PcomA/aneurysm neck	2	2	1	5
/aneurysm sidewall	3	1	0	4
Others				
Subsidiary MCA	1			1
Pericallosal artery	1			1
PCA, SCA		1		1
Central sulcus artery		1		1
Follow-up				
Perioperative complications				
Hemorrhage	0	0	0	0
Ischemia	1	2	0	3
Others	0	0	0	0
DSA				
Follow-up rate	8%	64%	100%	36%
Average time (month)	7	7.1	6.5	6.4
Outcome	One patient had limited blood flow in the left posterior communicating artery; the remaining patients had no recurrence and the branches were unobstructed	No recurrence and the branches were unobstructed	No recurrence and the branches were unobstructed	
mRS				
0	11	8	2	21
1	1	2	0	3

Table 1: Continued.

	Stilted building technique	Stilted building technique +SAC	Stilted building technique +BAC	Total
2	0	0	0	0
3	0	0	0	0
4	0	0	0	0
5	0	0	0	0
6	0	1(death from ventricular fibrillation)	0	1
Total	12	11	2	25

*AcomA: anterior communication artery; MCA: middle cerebral artery; PcomA: posterior communication artery; BA: basilar artery; PCA: posterior cerebral artery; SCA: superior cerebellar artery.

aneurysm body were embolized. The lumen of the communicating artery was unobstructed (Figure 2(g)). Head CT was reviewed after the operation, and no new bleeding was seen. Seven months after discharge, the mRS score was 0. Follow-up DSA showed no recurrence of the aneurysm, and the lumen of the posterior communicating artery was unobstructed (Figures 2(h) and 2(i)).

3.1.2. Patient 2. A 55-year-old man presented with a symptomatic aneurysm of the M1 segment of the right MCA. Head CT showed subarachnoid hemorrhage. DSA examination revealed a ruptured aneurysm of the M1 segment of the right MCA measuring 7.5 mm × 5.4 mm, with a neck width measuring approximately 5.7 mm, branch arteries originating from the body of the aneurysm supplying blood to the cortex, and the ruptured sac located at the bottom of the aneurysm. The other branch artery originated from the opposite wall of the parent artery. First, after placing the stent microcatheter and embolization microcatheter, multiple smaller coils were inserted through the Headway 17 catheter to embolize the ruptured sac (Figure 3(a)), and then, the distal half of the aneurysm was embolized. Then, a larger coil was selected to embolize approximately all of the remaining half to form a frame to support the sidewall of the aneurysm, and a few rings were entered into the branch artery from the aneurysm body to form the stable support (Figure 3(b), arrow). A 4 × 20 mm Solitaire stent (Medtronic) was placed to protect the neck and the large branch arteries from the opposite wall of the parent artery. With the support of the frame formed by the larger coil, the aneurysm continued to be filled with the coil, avoiding the branch from the body of the aneurysm (Figure 3(c)). Immediate DSA showed that the ruptured sac and body of the aneurysm were embolized, and the lumen of the branch artery from the body of the aneurysm was unobstructed (Figure 3(d)). The patient was reexamined 5 months after the operation. The mRS score was 0. Follow-up DSA showed that the aneurysm had not recurred, and the branch lumen from the sidewall of the aneurysm was unobstructed (Figure 3(e)). The patient had no complications.

4. Discussion

Endovascular aneurysm treatment includes coil embolization, balloon-assisted coil embolization, stent-assisted coil embolization, flow diverters, and intrasaccular flow disrupters. [11–14] In recent years, the technology for performing endovascular treatment of intracranial aneurysms has made great progress. The wider application of occlusion balloon- and stent-assisted embolization technology has greatly improved success in protecting branching arteries when embolizing aneurysms [15–19]. When the branch artery originates from the sidewall of the aneurysm and is very close to the aneurysm neck, an occlusion balloon or stent can protect the branch artery. However, when the angle between the branch artery of the aneurysm and the parent artery is less than 90° or when the diameter of the branch artery is small (<1 mm), it is difficult to release a stent and to ensure that the stent is completely inserted and fully open. In these cases, the use of the "stilted building" technique is very effective.

In the "stilted building" technique, the first set of larger coils form a frame in the aneurysm cavity, and one or two rings from the coils protrude into the branch artery to protect it and act as a support structure. The first set of coils can refer to the first coil alone or a group of coils; for aneurysms with necks that are too wide or extremely irregular in shape, the formation of a stable and uniform frame may require multiple coils with the help of multimicrocatheter technology. The main purpose of the "stilted building" technique is to palliatively or radically embolize the aneurysm while protecting the branch arteries adjacent to the aneurysm. The first set of slightly larger coils supports the wall of the branch artery and the wall of the aneurysm to stabilize the overall structure and form the pillars of the "stilted building." The subsequent coils focus on embolizing any ruptured sacs and the aneurysm body while avoiding the branch arteries, that is, the "body" of the "stilted building." The main points of the "stilted building" technique are as follows: First, the formation of a support frame, that is, from the frame attached to the wall of the aneurysm cavity, one or two rings from the coils (the pillars of the "stilted building") are allowed to enter the branch artery to protect it and provide support. The support point is located at the bifurcation of the artery at the neck of the aneurysm or within the branch itself. The idea of "support" means that the rings of the coil protruding into the branch artery should have a sufficient area to adhere to the artery wall rather than float within the artery cavity; then, given the support and restrictiveness of the frame coil, subsequent coils can be held within the aneurysm cavity (the body

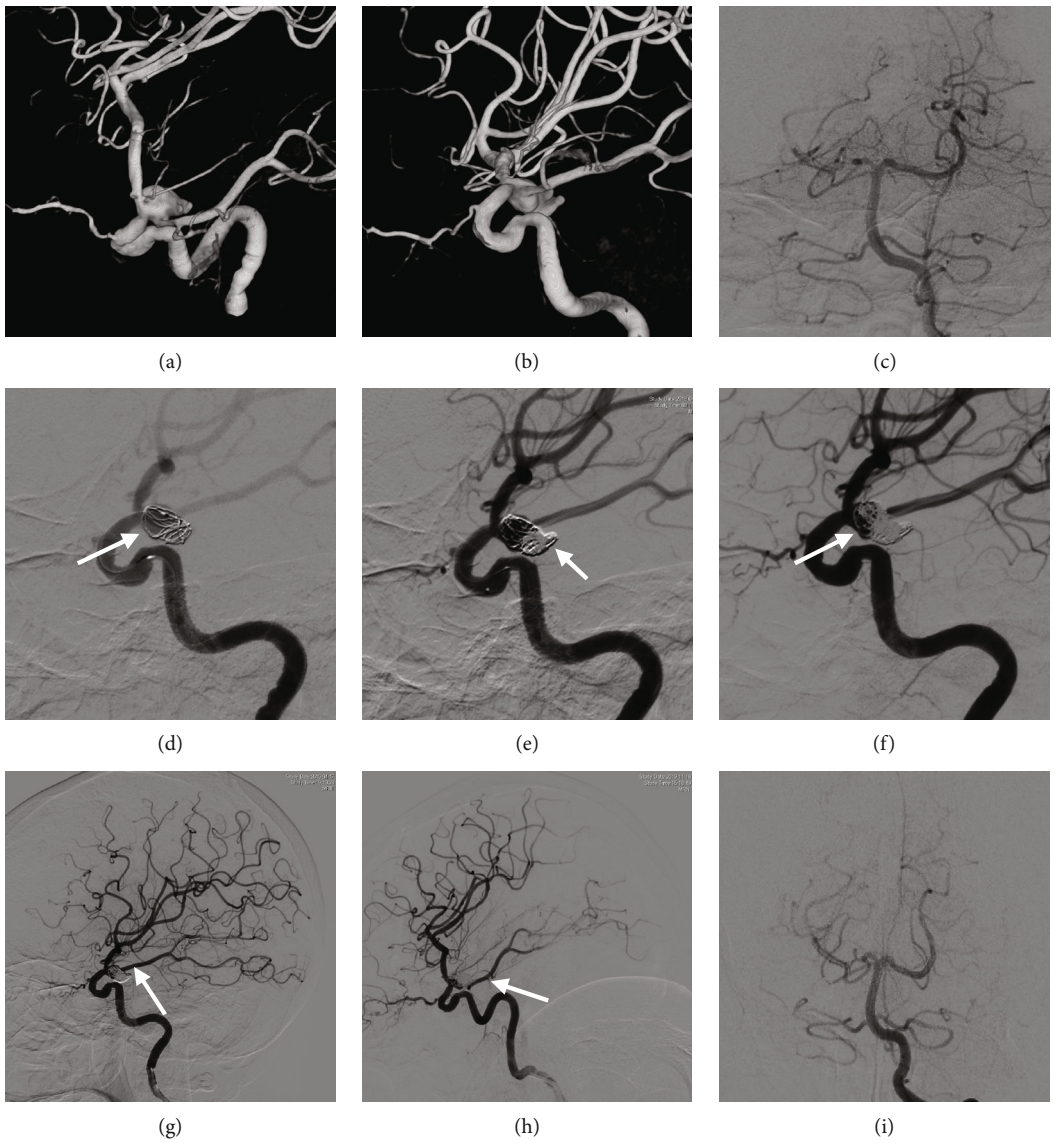

Figure 2: Cerebral angiography of the patient 1. (a–c) DSA examination revealed that a right posterior communicating ruptured aneurysm and the embryonic posterior cerebral artery originated from the neck of the aneurysm. (d) The first coil forms a stable support frame, and a few rings entered the posterior communicating artery to provide support (the pillars of the "stilted building") (arrow). (e) The aneurysm continues to be embolized, and angiography shows that the ruptured sac is densely embolized (arrow). (f) To embolize the aneurysm body, the detaining effect of the frame was leveraged to adjust the position of the coils and avoiding the branch artery (body of the "stilted building") (arrow). (g) Immediate angiography shows that the ruptured sac and body of the aneurysm are embolized. The lumen of the communicating artery is unobstructed (arrow). (h, i) Seven months after interventional surgery, follow-up DSA shows no recurrence of the aneurysm, and the lumen of the posterior communicating artery is unobstructed (arrow).

of the "stilted building") and are in no danger of entering into the supported artery. In most cases, the "stilted building" technique requires a combination of dual microcatheter, balloon, or stent assistive technology. When using dual microcatheter technology, one microcatheter is mainly used to form the supporting frame, and the other is mainly used to fill the aneurysm cavity. Balloons or stents are generally used to protect the main trunk or a branch of the parent artery, and an additional branch is protected by the "stilted building" technique.

A total of 12 patients in this group had aneurysms located on the sidewall of the parent artery. It was difficult for the microcatheter to enter the branch artery due to the angle. Furthermore, the diameter of some of the branch arteries was very small, making it difficult to release the stent and for balloons to protect the branch arteries. In this way, the first set of coils, which were relatively larger than the diameter of the aneurysm, were leveraged to support the branch artery wall and the aneurysm wall to form a frame, and the distribution of the subsequent coils was then adjusted to continue embolizing the aneurysm body. In some cases, the aneurysm embolization procedures were Class III according to the Raymond classification [8, 9]. However, since the residual aneurysm has a branch artery, a shunting effect for

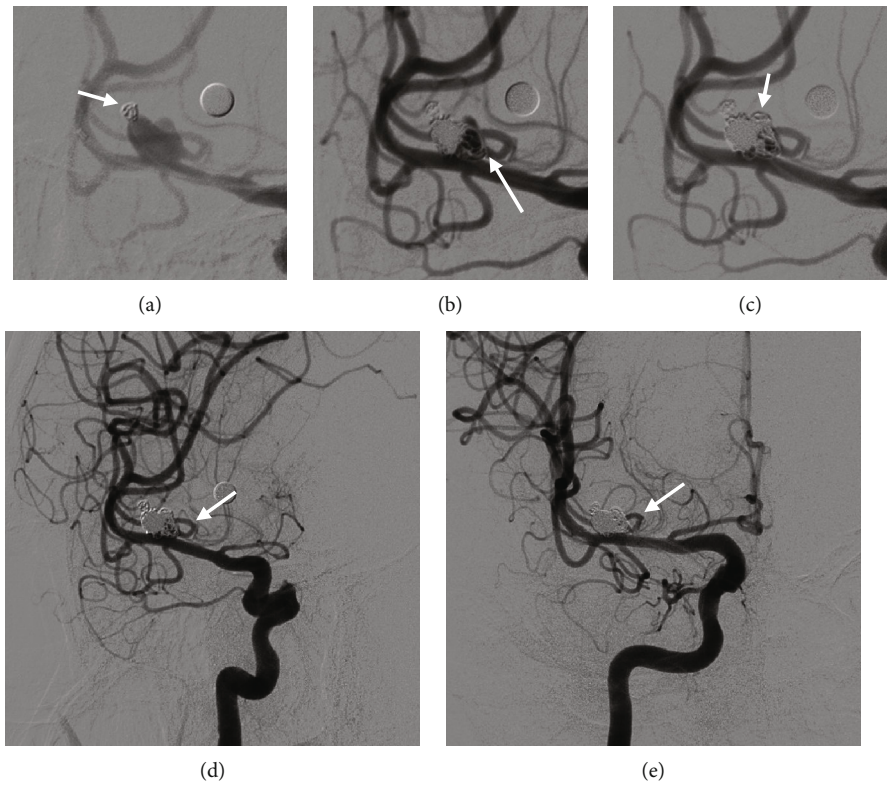

Figure 3: Cerebral angiography of the patient 2. (a) Embolization of the ruptured sac (arrow). (b) A few rings enter the branch artery to form stable support (pillars of the "stilted building") (arrow). (c) The aneurysm continues to be filled with the coil, avoiding the branch from the body of the aneurysm (body of the "stilted building") (arrow). (d) Immediate angiography shows that the ruptured sac and body of the aneurysm are embolized (Class IIIa [9]), and the lumen of the branch artery from the body of the aneurysm is unobstructed (arrow). (e) Five months after interventional surgery, follow-up DSA shows that the aneurysm had not recurred, and the branch lumen from the body of the aneurysm is unobstructed (arrow).

the blood flow was generated that could reduce the impact of the pressure of the blood flow on the remaining wall of the aneurysm, reducing the possibility of aneurysm recurrence in the residual. There does remain a possibility of recurrence; however, so closer angiographic follow-up is required. The short-term follow-up results in this group were satisfactory, but the DSA follow-up rate was relatively low. In the remaining 13 patients in this group, the aneurysm was located at the bifurcation of the parent artery, and most branch arteries originated from the neck of the aneurysm. There are many treatment methods for this type of aneurysm, including clipping, stent-assisted embolization, and balloon protection embolization; if the diameter of the artery lumen is sufficiently large, the branch artery can also be protected by inserting a single stent or a "Y" stent [20–22]. However, because these patients were older and in the acute stage of aneurysm rupture, we chose the "stilted building" technique to embolize the aneurysm. DSA follow-up showed that the embolization structure was very stable, and the branch arteries involved in the aneurysm had good patency.

When using the "stilted building" technique, a small part of the coils will be distributed near the beginning of the branch artery, which may affect the blood flow to that artery. However, the coverage of the metal coils is theoretically lower than that of the stent. The probability of the stent affecting the blood flow of the branch arteries that it covers is very low, and even LVIS stents, with their greater metal coverage, are relatively safe [23, 24]. Therefore, we can infer that the "stilted building" technique has only a limited effect on the blood flow of the branch artery. Additionally, the DSA follow-up results in this group also confirmed that the coil structure was stable and that the blood flow of the branch arteries did not change significantly. Furthermore, if the aneurysm was wide necked, the "stilted building" technique had to be combined with stent-assisted embolization. Considering that the stent may affect the blood flow of the branch arteries, we used the Solitaire stent with a larger mesh; even if the blood flow to the branch arteries is affected later, it would buy time for vascular compensation. Eleven patients underwent stent-assisted embolization for their aneurysms using the "stilted building" technique. Among the patients followed up by DSA, these aneurysms did not recur. When using this technique, thromboembolic complications may occur. Routine heparinization during surgery and the use of dual antiplatelet drugs after surgery reduced the risk of thrombosis. Because the ruptured sac of the aneurysm and most of the aneurysm body were embolized, the probability of rebleeding from the aneurysm was theoretically very low. In this group of 25 patients, no rebleeding occurred in the short-term outpatient follow-up after the operation. However, the sample size was small, and the follow-up rate for DSA was relatively low. Further follow-up is needed to assess the long-term efficacy.

5. Conclusions

In an aneurysm with a branch artery, when a balloon or stent cannot be effectively used to protect the branch artery, the use of "stilted building" embolization can achieve good therapeutic effects, and the short-term follow-up results are satisfactory; the technique can effectively protect branch arteries originating from aneurysms.

Data Availability

The datasets used and/or analyzed during the current study are available from the corresponding author on reasonable request.

Conflicts of Interest

The authors declare that there is no conflict of interest regarding the publication of this paper.

References

[1] A. J. Molyneux, J. Birks, A. Clarke, M. Sneade, and R. S. C. Kerr, "The durability of endovascular coiling versus neurosurgical clipping of ruptured cerebral aneurysms: 18 year follow-up of the UK cohort of the International Subarachnoid Aneurysm Trial (ISAT)," *The Lancet*, vol. 385, no. 9969, pp. 691–697, 2015.

[2] A. Lindgren, M. D. I. Vergouwen, I. van der Schaaf et al., "Endovascular coiling versus neurosurgical clipping for people with aneurysmal subarachnoid haemorrhage," *The Cochrane Database of Systematic Reviews*, vol. 8, article CD003085, 2018.

[3] M. Koyanagi, A. Ishii, H. Imamura et al., "Long-term outcomes of coil embolization of unruptured intracranial aneurysms," *Journal of Neurosurgery*, vol. 129, no. 6, pp. 1492–1498, 2018.

[4] M. B. Pritz, "Perforator and secondary branch origin in relation to the neck of saccular, cerebral bifurcation aneurysms," *World Neurosurgery*, vol. 82, no. 5, pp. 726–732, 2014.

[5] D. Simonato, S. Gargalas, P. J. Cox et al., "Aneurysms of the communicating segment of the internal carotid artery with posterior communicating artery agenesis are associated with perforator infarction after embolization," *Journal of neurointerventional surgery*, vol. 13, no. 4, pp. 347–352, 2021.

[6] B. M. Kim, S. I. Park, D. J. Kim et al., "Endovascular coil embolization of aneurysms with a branch incorporated into the sac," *AJNR American journal of neuroradiology*, vol. 31, no. 1, pp. 145–151, 2010.

[7] R. J. Damiano, V. M. Tutino, N. Paliwal et al., "Aneurysm characteristics, coil packing, and post-coiling hemodynamics affect long-term treatment outcome," *Journal of neurointerventional surgery*, vol. 12, no. 7, pp. 706–713, 2020.

[8] D. Roy, G. Milot, and J. Raymond, "Endovascular treatment of unruptured aneurysms," *Stroke*, vol. 32, no. 9, pp. 1998–2004, 2001.

[9] J. R. Mascitelli, H. Moyle, E. K. Oermann et al., "An update to the Raymond-Roy occlusion classification of intracranial aneurysms treated with coil embolization," *Journal of NeuroInterventional Surgery*, vol. 7, pp. 496–502, 2015.

[10] J. L. Banks and C. A. Marotta, "Outcomes validity and reliability of the modified Rankin scale: implications for stroke clinical trials: a literature review and synthesis," *Stroke*, vol. 38, no. 3, pp. 1091–1096, 2007.

[11] L. Pierot, J. Klisch, C. Cognard et al., "Endovascular WEB flow disruption in middle cerebral artery aneurysms: preliminary feasibility, clinical, and anatomical results in a multicenter study," *Neurosurgery*, vol. 73, no. 1, pp. 27–35, 2013.

[12] S. Asnafi, A. Rouchaud, L. Pierot, W. Brinjikji, M. H. Murad, and D. F. Kallmes, "Efficacy and safety of the Woven EndoBridge (WEB) device for the treatment of intracranial aneurysms: a systematic review and meta-analysis," *AJNR American journal of neuroradiology*, vol. 37, no. 12, pp. 2287–2292, 2016.

[13] D. F. Kallmes, R. Hanel, D. Lopes et al., "International retrospective study of the pipeline embolization device: a multicenter aneurysm treatment study," *AJNR American journal of neuroradiology*, vol. 36, no. 1, pp. 108–115, 2015.

[14] F. Wang, X. Chen, Y. Wang et al., "Stent-assisted coiling and balloon-assisted coiling in the management of intracranial aneurysms: a systematic review & meta-analysis," *Journal of the Neurological Sciences*, vol. 364, pp. 160–166, 2016.

[15] S. Oushy, L. Rinaldo, W. Brinjikji, H. Cloft, and G. Lanzino, "Recent advances in stent-assisted coiling of cerebral aneurysms," *Expert Review of Medical Devices*, vol. 17, no. 6, pp. 519–532, 2020.

[16] M. Mokin, C. T. Primiani, Z. Ren et al., "Stent-assisted coiling of cerebral aneurysms: multi-center analysis of radiographic and clinical outcomes in 659 patients," *J Neurointerv Surg*, vol. 12, no. 3, pp. 289–297, 2020.

[17] A. Consoli, C. Vignoli, L. Renieri et al., "Assisted coiling of saccular wide-necked unruptured intracranial aneurysms: stent versus balloon," *Journal of neurointerventional surgery*, vol. 8, no. 1, pp. 52–57, 2016.

[18] S.-M. Lee, Y.-J. Kim, and J. H. Ko, "The effectiveness of the waffle-cone technique in treating complex intracranial aneurysms," *Interventional neuroradiology : journal of peritherapeutic neuroradiology, surgical procedures and related neurosciences*, vol. 21, no. 4, pp. 470–478, 2015.

[19] Y. Hong, Y.-J. Wang, Z. Deng, Q. Wu, and J. M. Zhang, "Stent-assisted coiling versus coiling in treatment of intracranial aneurysm: a systematic review and meta-analysis," *PLoS One*, vol. 9, no. 1, article e82311, 2014.

[20] M. F. Granja, G. M. Cortez, P. Aguilar-Salinas et al., "Stent-assisted coiling of cerebral aneurysms using the Y-stenting technique: a systematic review and meta-analysis," *Journal of neurointerventional surgery*, vol. 11, no. 7, pp. 683–689, 2019.

[21] M. A. Mooney, E. D. Simon, S. Brigeman et al., "Long-term results of middle cerebral artery aneurysm clipping in the Barrow Ruptured Aneurysm Trial," *Journal of Neurosurgery*, vol. 130, pp. 895–901, 2019.

[22] F. Cagnazzo, N. Limbucci, S. Nappini et al., "Y-stent-assisted coiling of wide-neck bifurcation intracranial aneurysms: a meta-analysis," *AJNR American journal of neuroradiology*, vol. 40, no. 1, pp. 122–128, 2019.

[23] C. Iosif, M. Piotin, S. Saleme et al., "Safety and effectiveness of the Low Profile Visualized Intraluminal Support (LVIS and LVIS Jr) devices in the endovascular treatment of intracranial aneurysms: results of the TRAIL multicenter observational study," *Journal of neurointerventional surgery*, vol. 10, no. 7, pp. 675–681, 2018.

[24] Z. Feng, Q. Li, R. Zhao et al., "Endovascular treatment of middle cerebral artery aneurysm with the LVIS junior stent," *Journal of Stroke and Cerebrovascular Diseases : The Official Journal of National Stroke Association*, vol. 24, no. 6, pp. 1357–1362, 2015.

Hindawi
BioMed Research International
Volume 2021, Article ID 9951393, 13 pages
https://doi.org/10.1155/2021/9951393

Research Article

Efficacy and Safety of Surgical Ligation versus Endovascular Embolization for Type II Congenital Extrahepatic Portosystemic Shunt

Jinlong Zhang[1], **Weidong Duan**[2], **Zhuting Fang**[3,4], **Maoqiang Wang**[1], **Li Cui**[1], **Yanhua Bai**[1], **Xiaohui Li**[1], **Qicong Du**[5], **Mengqiu Shen**[1], **and Feng Duan**[1]

[1]*Institution of Oncology, Chinese PLA General Hospital, Beijing 100853, China*
[2]*Department of Hepatobiliary Surgery, First Medical Center of Chinese PLA General Hospital, Beijing 100853, China*
[3]*Shengli Clinical Medical College of Fujian Medical University, Fuzhou 350122, China*
[4]*Department of Interventional Radiology, Fujian Provincial Hospital, Fuzhou 350001, China*
[5]*Department of Radiology, First Medical Center of Chinese PLA General Hospital, Beijing 100853, China*

Correspondence should be addressed to Feng Duan; duanfeng@vip.sina.com

Received 22 March 2021; Accepted 20 May 2021; Published 1 June 2021

Academic Editor: Xing Chen

Objective. To evaluate the safety and efficacy of surgical ligation and endovascular embolization for the treatment of type II congenital extrahepatic portosystemic shunt (CEPS). *Methods*. In this retrospective study, 23 patients diagnosed with type II CEPS between March 2011 and April 2019 were divided into either a surgical group ($n = 13$; 41.5 ± 19.9 years) or the interventional group ($n = 10$; 44.9 ± 19.7 years). The surgical group underwent laparoscopic surgical ligation of the shunt alone or ligation of the shunt and splenic artery and/or vein. The interventional group underwent endovascular embolization using microcoils, detachable coils, and vascular plug. *Results*. All 23 patients received a one-step shunt closure, and their clinical symptoms were significantly improved within 3-month postprocedure and without recurrence during follow-up. The serum ammonia levels in both groups decreased after the procedure and dropped to normal level at 6- to 12-month postprocedure. Compared with baseline, the portal vein diameter in interventional group increased significantly at 3-, 6-, 12-, and 36-month postocclusion ($P = 0.01$ for all). The procedure time was shorter in the interventional group (127.0 ± 43.2 minutes) than the surgical group (219.8 ± 56.7 minutes; $P < 0.001$). The intraoperative blood loss in the interventional group (32.0 ± 62.5 mL) was less than that in the surgical group (238.5 ± 396.9 mL; $P = 0.001$). *Conclusion*. Both surgical ligation and endovascular embolization are effective in the treatment of type II CEPS. Endovascular embolization has the advantages of shorter procedure time and less intraoperative blood loss. The ligation of the portosystemic shunt and splenic artery and vein is feasible with apparent safety, and it could avoid a second surgical treatment.

1. Introduction

A congenital extrahepatic portosystemic shunt (CEPS), also known as an Abernethy malformation, is classified based on the extent of intact hypoplastic portal veins. Type I CEPS is characterized by an end-to-side portocaval shunt and the absence of intrahepatic portal vein branches, while type II CEPS has some hypoplastic intrahepatic portal veins preserved with a side-to-side portocaval shunt diverting the portal vein blood to the inferior vena cava (IVC) [1–3]. Although CEPS is a rare clinical disease with less than 400 cases reported, it may develop severe complications, such as hepatic encephalopathy, pulmonary arterial hypertension, hepatopulmonary syndrome, or nodular liver lesions, among others [4].

To date, most of the published articles regarding CEPS are case reports, with a few small-sample clinical studies. Therefore, no consensus is achieved in the treatment of CEPS [4]. The recommended strategies for asymptomatic patients with CEPS are keeping them under careful observation or

Table 1: Baseline characteristics of patients in both groups.

Characteristic	Surgical group ($n = 13$)	Interventional group ($n = 10$)	P value
Age	40.7 ± 20.4	44.9 ± 19.7	0.68
Male	5 (38.5)	8 (80.0)	
Female	8 (61.5	2 (20.0)	
CEPS symptoms			
Hepatic encephalopathy	6 (46.2)	5 (50.0)	>0.99
Gastrointestinal bleeding	4 (30.8)	2 (20.0)	0.66
Dyspnea	1 (7.7)	0 (0)	>0.99
Abdominal pain	1 (7.7)	1 (10.0)	>0.99
Hepatic myelopathy	1 (7.7)	1 (10.0)	>0.99
Hemoptysis	0 (0)	1 (10.0)	>0.99
Fatigue	2 (15.4)	1 (10.0)	>0.99
Comorbidity			
Hepatic cirrhosis	10 (76.9)	5 (50.0)	0.22
Hepatic adenoma	2 (15.4)	0 (0)	0.49
Pulmonary hypertension	1 (7.7)	1 (10.0)	>0.99
Hypersplenism	1 (7.7)	1 (10.0)	>0.99
Location of shunt vessels			
Splenorenal shunt	5 (38.5)	3 (30.0)	>0.99
SMV-IVC shunt	3 (23.1)	1 (10.0)	0.60
Portal vein-IVC shunt	3 (23.1)	2 (20.0)	>0.99
SMV-renal vein shunt	1 (7.7)	1 (10.0)	>0.99
Portal vein-renal vein shunt	1 (7.7)	1 (10.0)	>0.99
Portal vein-iliac vein shunt	0 (0)	2 (20.0)	0.18

Data are numbers of patients, with percentages in parentheses. SMV: superior mesenteric vein; IVC: inferior vena cava.

prophylactic interventional therapy [4]. Medical treatment is primarily used to improve symptoms caused by CEPS or its complications. While liver transplantation is the only curative treatment for type I CEPS, shunt occlusion by surgical ligation or endovascular embolization is the most common treatment for type II CEPS. The use of shunt occlusion depends on the expertise of local surgeons and the length and caliber of the shunts; however, a comparison of the two occlusion modalities in the management of type II CEPS has not been reported. We therefore retrospectively compared the safety and efficacy of surgical ligation and endovascular embolization in the treatment of type II CEPS from two medical centers.

2. Materials and Methods

2.1. Study Design and Patient Population. This was a retrospective clinical study performed at two medical centers in accordance with the Declaration of Helsinki and approved by the respective institutional review boards. All patients provided written informed consent prior to treatment. All patients in this study have not been reported.

This retrospective study included consecutive patients diagnosed with CEPS through abdominal ultrasound, computed tomographic angiography (CTA), and/or magnetic resonance imaging (MRI) between March 2011 and April 2019 in two hospitals. Study patient selection was performed in conjunction with radiologists, hepatobiliary surgeons, and interventional radiologists. Patients diagnosed with type II CEPS who presented with one malformation and at least one apparent CEPS manifestation or complication, including hepatic encephalopathy, gastrointestinal bleeding, pulmonary hypertension, hepatic myelopathy, hepatopulmonary syndrome, hepatic cirrhosis, or hepatic adenoma, were included in the study. Patients with type I CEPS, asymptomatic patients, and patients with multiple malformations, hepatocellular carcinoma, coagulopathies, active infection, chronic renal failure, or contraindications to angiography and surgery were excluded.

Initially, portal venography by way of systemic venous access and traversal of the portosystemic shunt and a 15 min shunt balloon occlusion test were performed. Patients with a large and short shunt, which may have a high risk of embolic material migration or portal venous pressure (PVP) > 25 mmHg after occlusion, underwent surgical ligation (surgical group), with all others undergoing endovascular embolization (interventional group).

2.2. Portography and Shunt Balloon Occlusion Test. To evaluate hemodynamics, measure PVP, and assess whether the shunt vessel could be closed, portal venography and shunt balloon occlusion test were conducted.

In general, the right femoral artery and femoral vein were cannulated using the Seldinger technique under local

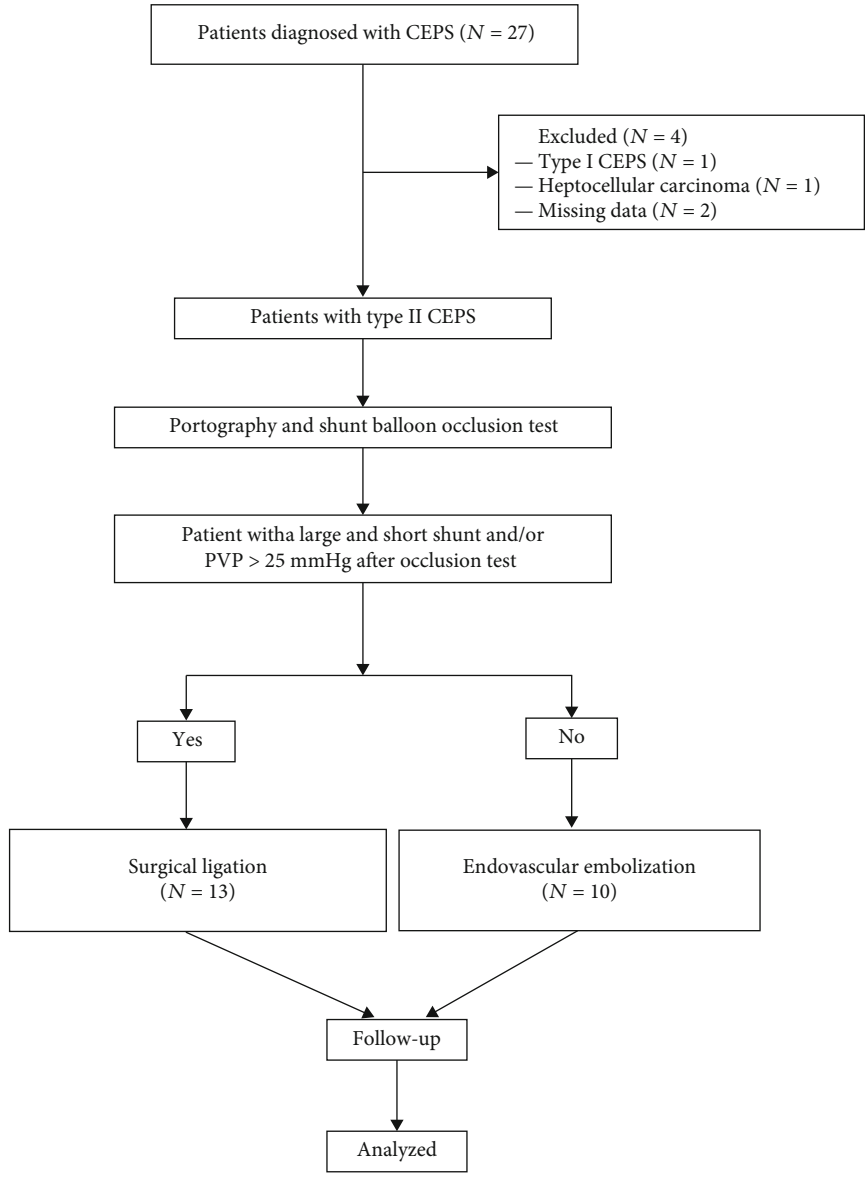

Figure 1: The flowchart shows the study population and groups. CEPS: congenital extrahepatic portosystemic shunt; PVP: portal venous pressure.

anesthesia or a transjugular or percutaneous transhepatic approach if the transfemoral vein approach failed. An indirect portal venography was then performed via selective angiography of the celiac artery, splenic artery, and superior mesenteric artery. Next, direct venography of the inferior mesenteric vein, splenic vein, and portal vein was performed. Lastly, a balloon occlusion test was performed (Fogarty, Thru Embolectomy Catheter, Edwards Lifesciences LLC, Irvine, CA, USA; Boston Scientific, Watertown, Mass) in the infrahepatic segment of IVC or shunt to detect the intrahepatic portal branches and measure PVP before and 15 min after balloon occlusion. If the shunt was suitable for endovascular embolization and endovascular occlusion, endovascular embolization and endovascular occlusion of the shunt were performed at the same time.

2.3. Laparoscopic Surgical Ligation. Under general anesthesia, a catheter was placed in the portal vein via the shunt through the femoral vein to monitor PVP. A 12 mm port for optics was placed in the umbilical area, and three 5 mm working ports were placed in the upper abdomen, right lower abdomen, and right lateral abdomen, respectively.

If PVP was <25 mmHg after 15 min of occlusion and without signs of intestinal wall edema and redness, the shunt was ligated alone. If PVP was >25 mmHg and/or there were signs of intestinal wall edema and redness, the splenic artery or splenic artery combined with splenic vein was dissected and ligated; if PVP was <25 mmHg without signs of intestinal wall edema and redness after 15 min, the splenic artery alone or splenic artery combined with splenic vein was taped. Otherwise, partial occlusion of the shunt was performed and the

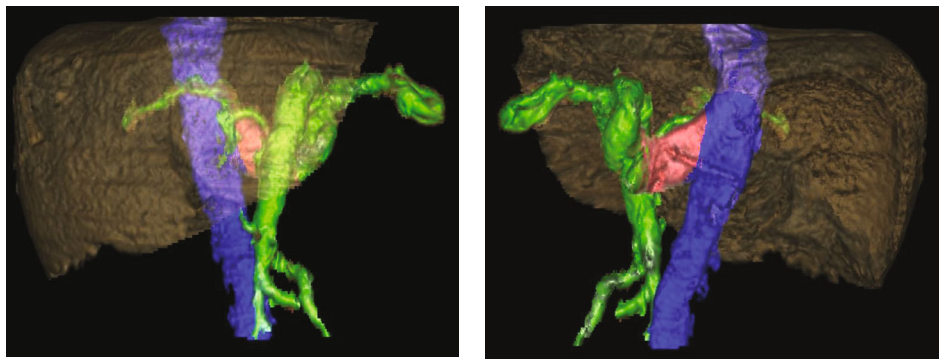

(a) (b)

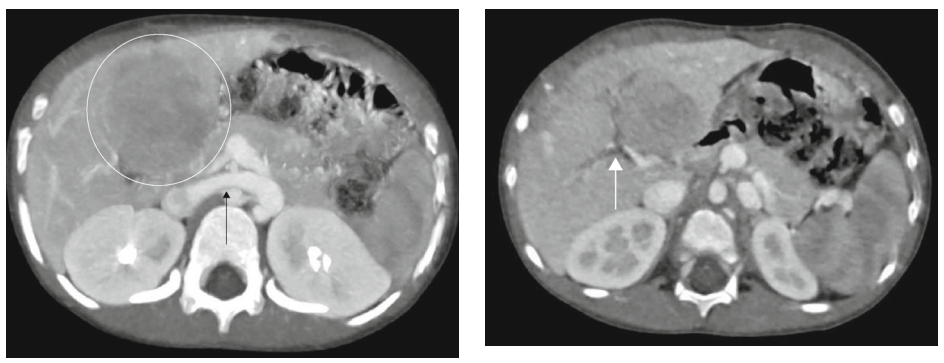

(c) (d)

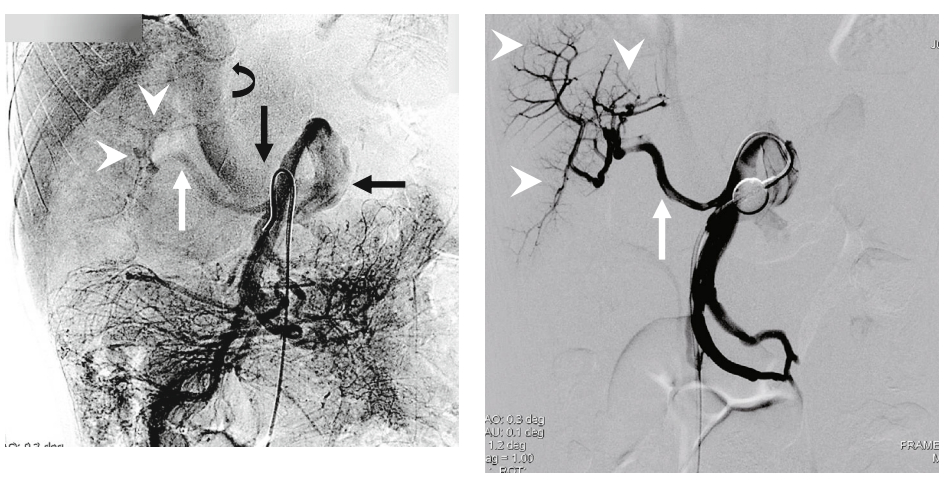

(e) (f)

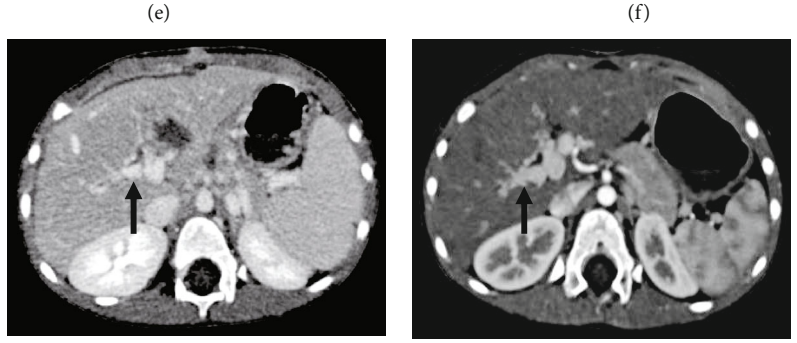

2014-8-25 2015-9-25

(g) (h)

Figure 2: Continued.

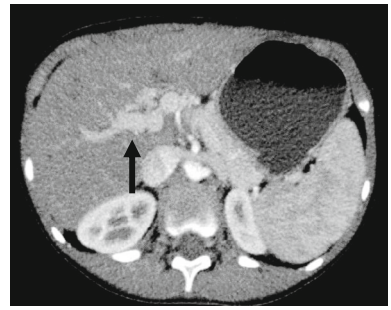

(i)

Figure 2: Images in a 3-year-old girl diagnosed with type II CEPS with hepatic encephalopathy (HE) who underwent surgical ligation due to large portal vein-IVC shunt. (a) Virtual reality (VR) images reconstructed from computed tomographic angiography (CTA) data prior to ligation. Anteroposterior view shows the portal vein and its branches (green), inferior vena cava (IVC) (blue), and the patent shunt communicating portal vein and IVC (red). (b) Posteroanterior VR image shows the portal vein and its branches (green), IVC (blue), and the portocaval shunt (red). (c) Axial CT image shows the large portal vein-IVC shunt (black arrow) and hepatic adenoma (circle) diagnosed by biopsy. (d) Axial contrast-enhanced CT image shows hypoplastic intrahepatic portal veins (white arrow) preoperative. (e) Indirect portal venography via the superior mesenteric artery (SMA) demonstrates venous outflow of the superior mesenteric vein (SMV) through the shunt (black arrow) drained into IVC (curved arrow), main portal vein (white arrow), and hypoplastic intrahepatic portal vein branches (arrowhead) which are visible. (f) Portal venography with balloon occlusion shows fine main portal vein (white arrow) and hypoplastic intrahepatic portal vein branches (arrowhead). The portal venous pressure (PVP) is 14.7 and 16.5 mmHg before and 15 min after balloon occlusion, respectively. (g) Contrast-enhanced CT images demonstrate the intrahepatic portal veins at 1 month after surgical ligation. (h) CT scan shows the intrahepatic portal veins at 12 months after surgical ligation. (i) CT scan shows the intrahepatic portal veins at 60 months after surgical ligation; the portal vein grows well over time.

shunt was completely occluded during the follow-up which was called "two-step closure."

2.4. Endovascular Shunt Occlusion. The selection of the embolic materials were dependent on the length and diameter of the shunt vessels. The embolization materials used were either one or a combination of 0.018-inch pushable microcoils (MicroNester; Cook Medical, Bloomington, USA), a 0.018-inch detachable coil (Interlock; Boston Scientific, Marlborough, Massachusetts, USA), and an Amplatzer vascular plug (16 mm, 18 mm, 20 mm, or 22 mm AVP IIA; Abbott Park, Illinois USA). After selective shunt catheterization, the microcoils and interlock coil were inserted through a coaxial 2.7 F microcatheter (Progreat; Terumo, Tokyo, Japan); the plug was inserted through a 6 to 10 F long sheath (Cook medical, USA). Indirect portography through SMA was performed to detect whether there were residual shunts.

2.5. Postprocedural Treatment. To prevent portal and mesenteric thrombosis, 30 mg of subcutaneous enoxaparin was administered every 12 h, beginning 12 h after the procedure and throughout 7 days of in-hospital observation. Patients were then discharged if no complications occurred, and 10 mg of oral rivaroxaban was administered once daily for 30 days.

Abdominal ultrasound and contrast-enhanced CT performed at 1 week and 1 month after the procedure determined whether portal vein system thrombosis had occurred. If there was an absence of thrombosis 1 month after the procedure, rivaroxaban was stopped.

2.6. Follow-Up and Clinical Assessment. Follow-up at 3, 6, and 12 months after the procedure and every 12 months thereafter included clinical status, routine blood tests, serum ammonia, liver function, coagulation, and abdominal contrast-enhanced CT. The diameter of the main portal vein was measured by two radiologists independently, with the mean value used as the final result.

The primary outcomes were defined as the improvement of the clinical symptoms, including hepatic encephalopathy, gastrointestinal bleeding, hepatic myelopathy, hemoptysis, and fatigue. The secondary outcomes were defined as the increase of portal vein diameter and the improvement of hemoglobin, serum ammonia, and Child-Pugh scores.

2.7. Statistical Analysis. Continuous variables were recorded as means ± standard deviations, and categorical data as numbers and percentages. All data were tested for normality using a Shapiro-Wilk test. Differences in PVP, hemoglobin, serum ammonia, portal vein diameter, and Child-Pugh score pre- and postprocedure within each group were compared with paired Student's t-test (normally distributed) or paired Wilcoxon rank-sum test (not normally distributed). Differences between groups were tested using a Student t-test or Wilcoxon rank-sum test. Differences in the main symptoms, comorbidities, and location of shunt vessels between groups were tested using the two-tailed Fisher exact test. $P < 0.05$ indicated a statistically significant difference (SPSS Statistics for Windows, version 20.0; IBM, Armonk, NY).

3. Results

3.1. Patient Characteristics. Baseline demographic and clinical data of the study patients are presented in Table 1. A total of 27 patients were recruited; four cases were excluded due to type I CEPS ($n = 1$), hepatocellular carcinoma ($n = 1$), and

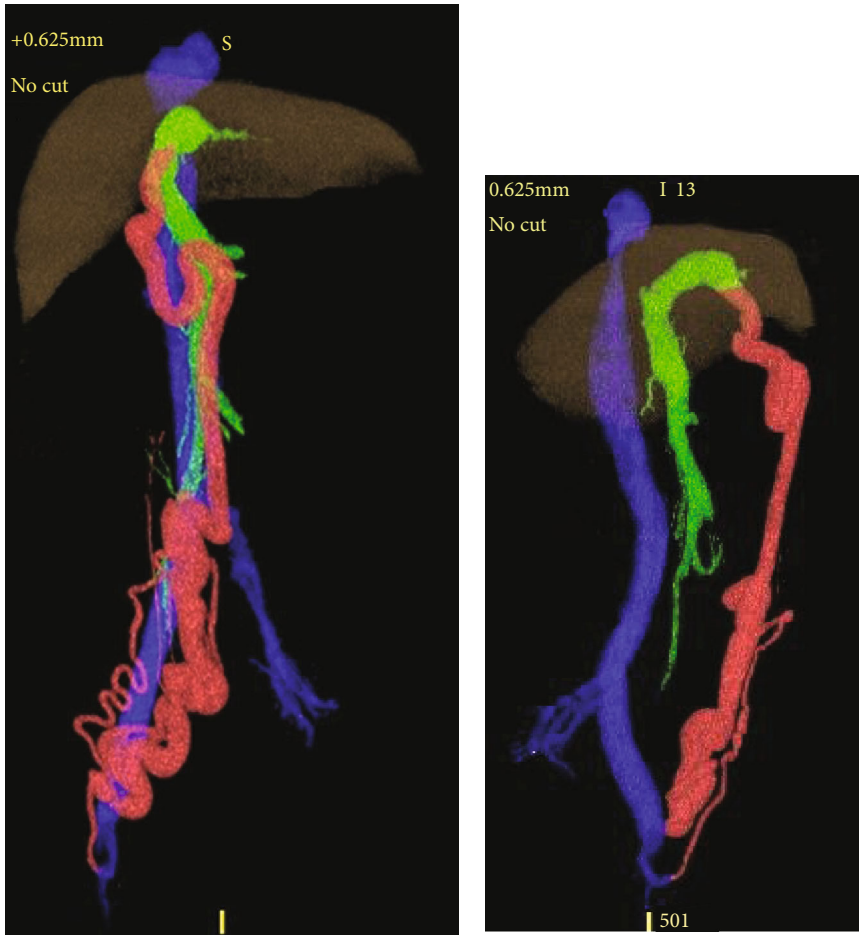

(a) (b)

Figure 3: Continued.

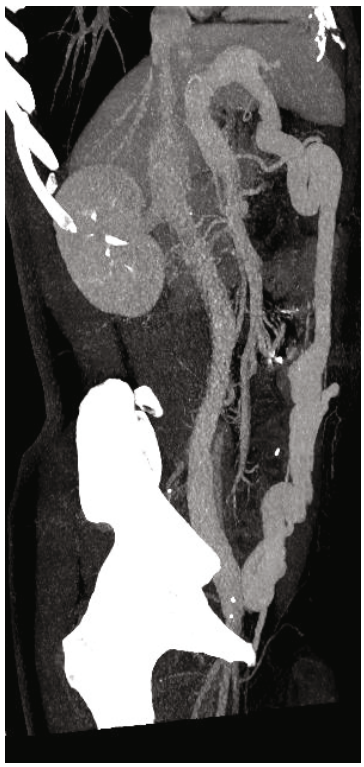

(c)

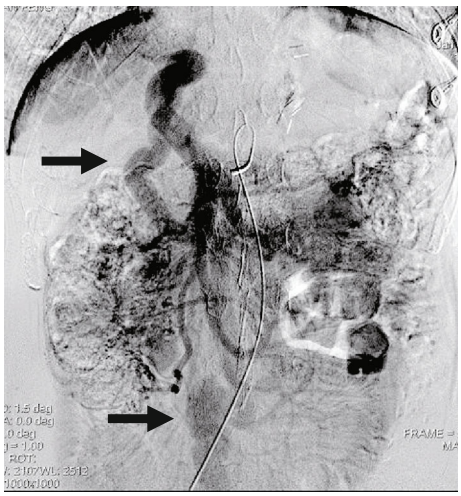

(d)

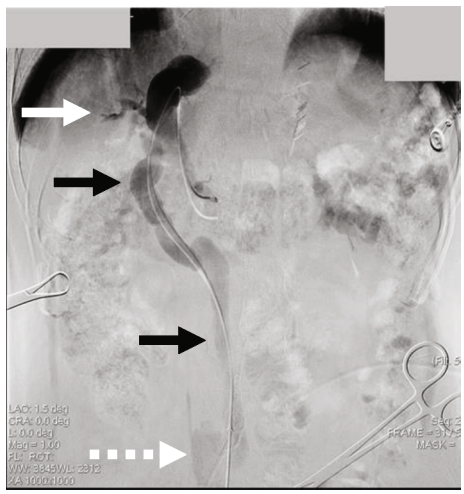

(e)

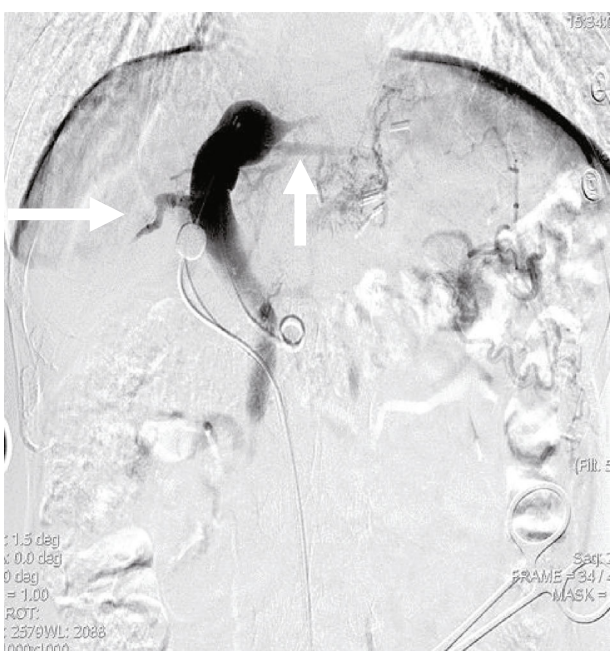

(f)

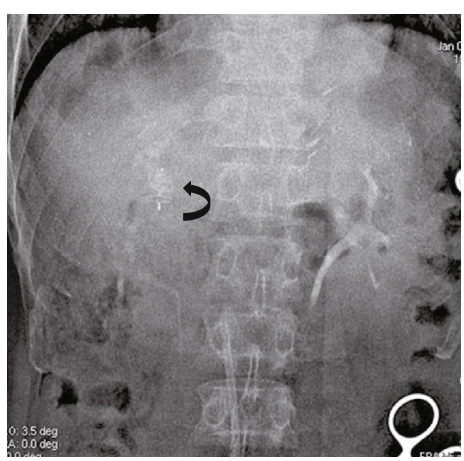

(g)

Figure 3: Continued.

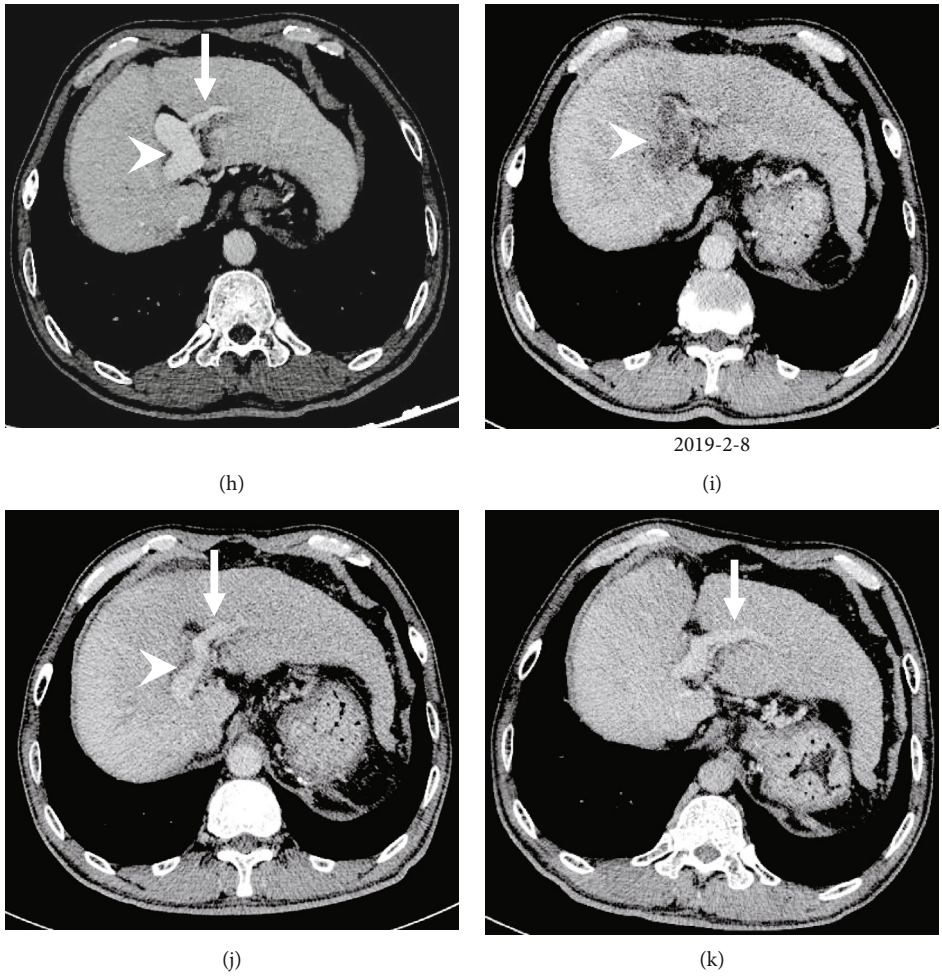

Figure 3: Images in a 54-year-old male diagnosed with type II CEPS with HE who underwent endovascular embolization. (a) Anteroposterior VR image reconstructed from CTA data prior to occlusion shows portal vein and its fine intrahepatic branches (green), IVC (blue), and tortuous and dilated portal vein-iliac vein shunt via the paraumbilical vein (red). (b) Sagittal VR image shows portal vein and its branches (green) IVC (blue) and the shunt (red). (c) Sagittal maximum intensity projection at the portal venous phase demonstrates the portal vein, IVC, and the shunt, in accordance with the VR findings. (d) Indirect portal venography via SMA demonstrates portal venous outflow drained into a tortuous and dilated shunt (black arrow). (e) Portal venography demonstrates partial hypoplastic intrahepatic portal venous veins (white arrow) and the communication between the portal vein and right iliac vein (dotted arrow) via the shunt (black arrow). (f) Portal venography with balloon occlusion shows hypoplastic intrahepatic portal veins (white arrow). The PVP is 21.7 and 24.3 mmHg before and 15 min after balloon occlusion, respectively. (g) The shunt was embolized with Amplatzer plug (curved arrow). (h) Preoperative contrast-enhanced CT image demonstrates the dilated main portal vein (arrowhead) and the hypoplastic intrahepatic portal vein branches (white arrow). (i) CT scan shows portal vein thrombosis (arrowhead) at 1 month after the procedure which disappeared after seven-day anticoagulation therapy. (j) Contrast-enhanced CT images demonstrate the main portal vein shrinking into normal level (arrowhead), and the intrahepatic portal veins (white arrow) grow well at 12 months after interventional occlusion. (k) CT scan demonstrates that the intrahepatic portal veins (white arrow) grow well at 36 months after the procedure.

incomplete data ($n = 2$). Twenty-three patients were included in the final analysis, 13 patients (five male, eight female; mean age, 40.7 years ± 20.4; age range, 3-67 years) in the surgical group and 10 patients (eight males, two females; mean age, 44.9 years ± 19.7; age range, 17-69 years) in the interventional group (Figure 1).

The main manifestations of CEPS in this cohort were hepatic encephalopathy (six in the surgical group and five in the interventional group) and gastrointestinal bleeding (four in the surgical group and two in the interventional group) with no significant difference between the groups ($P > 0.99$ and $P = 0.66$, respectively). Other manifestations included dyspnea, abdominal pain, hepatic myelopathy, hemoptysis, and fatigue, with no significant differences between groups ($P > 0.99$ for all).

Of the 13 patients in the surgical group, 10 experienced hepatic cirrhosis, two experienced hepatic adenoma, one experienced pulmonary hypertension, and one experienced hypersplenism. Similarly, of the 10 patients in the interventional group, five experienced hepatic cirrhosis, one experienced pulmonary hypertension, and one experienced hypersplenism.

Table 2: Comparison of portal vein pressure in the surgical and interventional group pre- and postprocedure.

Variable	Surgical group ($n = 13$)	Interventional group ($n = 10$)	P value
Portal vein pressure (mmHg)			
Preprocedure	12.9 ± 3.7	15.9 ± 4.7	0.18
Postprocedure	17.5 ± 3.8	17.1 ± 4.8	0.86
P value	<0.001	0.22	

3.2. Location of Shunt Vessels. In the surgical group, the types of shunt observed were splenorenal shunt ($n = 5$), superior mesenteric vein-inferior vena cava shunt (SMV-IVC; $n = 3$), portal vein-IVC shunt ($n = 3$), SMV-renal vein shunt ($n = 1$), and portal vein-renal vein shunt ($n = 1$), while in the interventional group, splenorenal shunt ($n = 3$), SMV-IVC ($n = 1$), portal vein-IVC shunt ($n = 2$), SMV-renal vein shunt ($n = 1$), portal vein-renal vein shunt ($n = 1$), and portal vein-iliac vein shunt ($n = 2$) were observed (Table 1; Figures 2 and 3).

3.3. Intraoperative Parameters. All 23 patients received a one-step closure. For patients in the surgical group, three underwent shunt ligation alone, six underwent shunt and splenic artery ligation, and four patients underwent ligation of the shunt and splenic artery and vein. The postprocedure PVP (17.5 ± 3.8 mmHg; range: 8.1-22.1 mmHg) was significantly greater than the preprocedure PVP (12.9 ± 3.7 mmHg; range: 5.9-17.6 mmHg; $P < 0.001$) in the surgical group, but it was lower than 25 mmHg. In the interventional group, the shunts were embolized using an Amplatzer vascular plug in four patients, with the remaining six cases using a combination of detachable and pushable coils (Figures 2 and 3). The PVP were not significantly different pre- and postocclusion (pre: 15.9 ± 4.7 mmHg; range: 11.4-21.7 mmHg; post: 17.1 ± 4.8 mmHg; range: 13.2-24.3 mmHg; $P = 0.22$) (Table 2).

The procedure time was significantly shorter in the interventional group (127.0 ± 43.2 min) than that in the surgical group (219.8 ± 56.7 min; $P < 0.001$). The intraoperative blood loss in the interventional group (32.0 ± 62.5 mL) was significantly less than that of the surgical group (238.5 ± 396.9 mL; $P = 0.001$). Additionally, the treatment expense of the interventional group (46331.5 ± 18839.1 yuan) was lower than that of the surgical group (59561.3 ± 21450.1 yuan) but without statistical significance ($P = 0.20$) (Table 3).

3.4. Clinical Outcomes. The mean follow-up period was 26.1 ± 17.6 months (range, 6-60 months). Clinical symptoms of all patients significantly improved within 3 months of their procedure without recurrence during follow-up. Serum ammonia levels decreased after both procedures to normal levels (9-30 μmol/L) at 6- to 12-month postprocedure. The symptoms of hepatic encephalopathy and hepatic myelopathy associated with hyperammonemia were improved within 1 month of the procedure and remained improved during the follow-up period (Table 4).

Patients with gastrointestinal bleeding (four in the surgical group and two in the interventional group) stopped bleeding after their procedure. One patient in the surgical group suffered hematemesis 6 months after occlusion. Gastroscopy revealed hemorrhage of a gastric ulcer, and bleeding stopped after endoscopic and acid suppression therapy. One patient with hemoptysis and one with dyspnea related to pulmonary hypertension achieved symptomatic relief at 1 week and 3 weeks after the procedure, respectively. Finally, one patient with hepatic adenoma underwent simultaneous resection.

Compared with baseline, the portal vein diameter in the interventional group increased significantly at 3-, 6-, 12-, and 36-month postocclusion ($P = 0.01$ for all), but there was no significant difference in the surgical group ($P > 0.05$ for all) (Table 4; Figure 4).

Portal vein thrombosis was detected in one patient in the interventional group using contrast-enhanced CT scan at 1 month after the procedure. Rivaroxaban was discontinued; intravenous heparin sodium (40 U/kg to control the activated partial thromboplastin time between 40 and 60 s) and urokinase (4000 U/kg, twice daily) were administered. Seven days later, the portal vein thrombosis disappeared. Once daily oral rivaroxaban (10 mg) was resumed for 4 months without thrombosis (Figure 3).

3.5. Complications. No signs of portal hypertension and splenic abscess have been observed, and no other complications occurred.

4. Discussion

CEPS is a congenital malformation created by an abnormal shunt between the portal vein and vena cava or azygos/hemiazygos system due to abnormal development of the umbilical vein and yolk vein during the embryonic period. In combination with other congenital malformations, patients with CEPS present with hypergalactosemia, high bile acid, high serum ammonia, and hepatic encephalopathy caused by the portal and vena cava shunt. It has been reported that 66-100% of patients with CEPS have hyperammonemia and 17-30% have hepatic encephalopathy [5–7].

Currently, liver transplantation is the only curative treatment for type I CEPS. Surgical ligation and endovascular embolization have been recommended to treat symptomatic type II CEPS; however, no consensus has been achieved and no comparison between the two procedures has been reported. Except for patients who are not suitable for endovascular occlusion due to shunt anatomy, no research has compared the more advantageous modalities for patients suitable for both treatment procedures so far. Our study found that both procedures were safe and effective in patients with type II CEPS. However, compared with laparoscopic surgical ligation, the endovascular approach has the advantages of shorter procedure time, less intraoperative blood loss, and lower treatment expense.

Angiography is the gold standard for diagnosing CEPS and identifying the type of CEPS present [8, 9]. While shunt anatomy and flow dynamics can be determined by

Table 3: Differences in intraoperative parameters between surgical and interventional groups.

Parameters	Surgical group ($n = 13$)	Interventional group ($n = 10$)	P value
Procedure time (min)	219.8 ± 56.7	127.0 ± 43.2	<0.001
Intraoperative blood loss (mL)	238.5 ± 396.9	32.0 ± 62.5	0.001
Treatment expense (yuan)	59561.3 ± 21450.1	46331.5 ± 18839.1	0.20

Table 4: Clinical outcomes in the surgical and interventional group pre- and postprocedure.

Variable	Surgical group ($n = 13$)	Interventional group ($n = 10$)	P value
Hemoglobin (g/L)			
Preprocedure	109.4 ± 26.2	102.0 ± 25.2	0.46
3 months	104.0 ± 27.0	112.4 ± 21.1	0.08
6 months	114.0 ± 8.5	125.0 ± 18.4	<0.001
12 months	104.3 ± 19.8	118.8 ± 18.9	<0.001
36 months	125.5 ± 24.7	127.7 ± 22.5	0.03
Serum ammonia (μmol/L)			
Preprocedure	83.6 ± 32.5	75.1 ± 30.5	0.12
3 months	56.4 ± 20.8	47.8 ± 46.4	0.003
6 months	41.0 ± 1.4	51.4 ± 49.8	0.01
12 months	19.2 ± 6.8	13.5 ± 6.4	<0.001
36 months	24.0 ± 6.4	16.7 ± 6.2	<0.001
Portal vein diameter (mm)			
Preprocedure	8.5 ± 4.9	9.3 ± 4.0	0.25
3 months	9.6 ± 3.4	10.7 ± 2.7	0.34
6 months	9.7 ± 3.0	10.8 ± 2.6	0.22
12 months	10.0 ± 3.0	11.2 ± 2.9	0.09
36 months	10.2 ± 2.9	11.6 ± 2.3	0.046
Child-Pugh score			
Preprocedure	7.8 ± 1.7	7.3 ± 2.4	0.36
3 months	6.7 ± 1.9	5.8 ± 1.3	0.01
6 months	5.5 ± 0.7	6.0 ± 1.4	0.001
12 months	6.0 ± 1.4	5.2 ± 0.4	<0.001
36 months	5.5 ± 0.7	5.3 ± 0.6	0.001

angiography and/or direct venography, balloon shunt occlusion venography is critical for detecting intrahepatic portal vein branches. This branch identification could also determine the type of CEPS and the pressure gradient pre- and postocclusion that is crucial for assessing the risk of portal hypertension after shunt occlusion [9–12].

In previous reports, 25 mmHg was used as a threshold to monitor PVP. If PVP was less than 25 mmHg after 15-20 min of occlusion, it indicated that the risk of portal hypertension was insignificant after shunt occlusion. Otherwise, a two-step closure is recommended with partial occlusion to initially acclimatize the intrahepatic portal system to increase flow and then completely occlude in 6 to 12 months [9, 13–16].

To avoid portal hypertension postocclusion for patients with PVP of more than 25 mmHg, we performed surgical ligation of the shunt combined with the splenic artery and/or vein and thereby avoided two surgical procedures for shunt closing, because the ligation of splenic artery and/or vein could reduce the PVP by reducing portal blood flow. Based on the abundant communication between the splenic artery, splenic vein, and splanchnic vessels, ligation of the splenic artery and splenic vein will not typically cause splenic necrosis or abscess. In this cohort, six patients underwent shunt and splenic artery ligation and four underwent additional splenic vein ligation. No portal hypertension or splenic abscess occurred, and a second surgical treatment was avoided. Therefore, surgical ligation could be used for these patients.

Portal vein and mesenteric venous thrombosis is a common complication after shunt ligation that can lead to portal hypertension; therefore, postprocedural anticoagulation therapy is very essential [4, 8]. Heparin and warfarin have been used to prevent thrombosis in previous studies; however, the activated partial thromboplastin time and international normalized ratio should be closely monitored to adjust drug dosage [14, 17]. In our practice, enoxaparin and rivaroxaban have been used sequentially for anticoagulation after occlusion and do not require monitoring indicators of coagulation and are more convenient to use. In the follow-up period, only one patient (1/23) suffered portal vein thrombosis, which disappeared after 7 days of conservative treatment.

Theoretically, the hypoplastic intrahepatic portal vein should dilate after the perfusion of portal vein blood increased due to shunt ligation. In this cohort, patients after endovascular embolization achieved a significant increase in portal vein diameter; however, there was no significant difference in surgical ligation. This may be attributed to the well-grown intrahepatic portal vein branches in several patients before occlusion and the limited number of cases. Additionally, during the follow-up, surgical candidates did a little worse than interventional group; this may be associated with these patients with worse-grade disease preprocedure.

Our study had some limitations. First, this study included only a small number of patients primarily due to the low incidence of CEPS. Second, the follow-up period was short, and due to the retrospective characteristics of the study, the follow-up intervals were not completely consistent and partial follow-up data was missing. Thirdly, the portosystemic gradient was not measured. Lastly, the patients of the two groups were divided according to the length and diameter of the shunt, so it might led to patient selection bias between the groups.

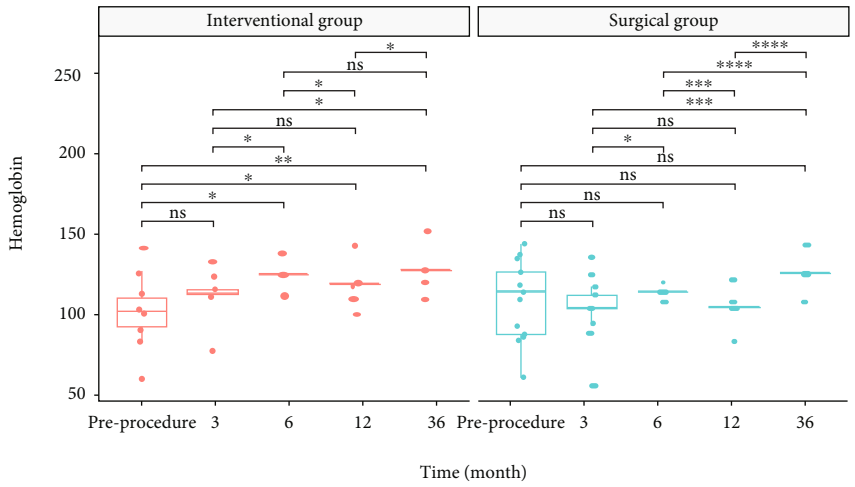

(a)

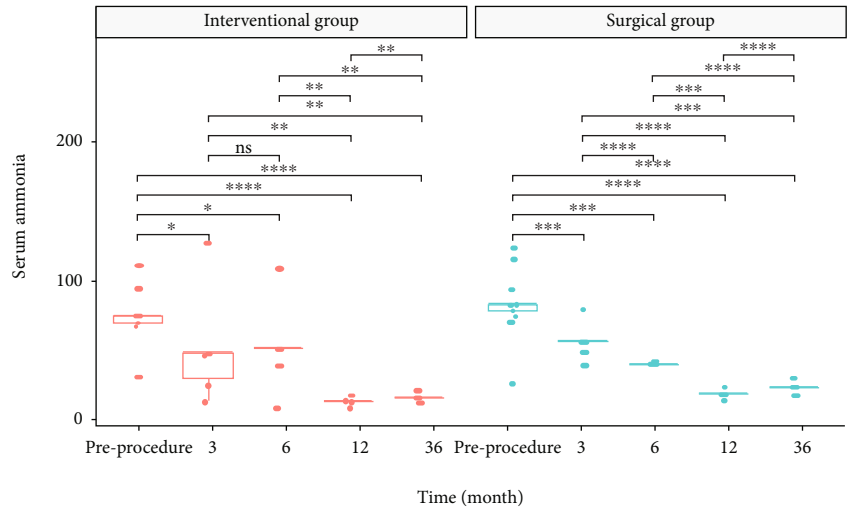

(b)

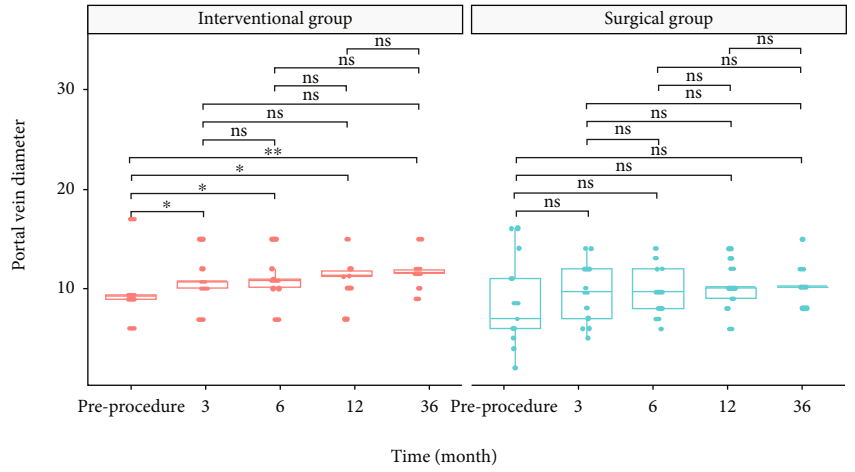

(c)

Figure 4: Continued.

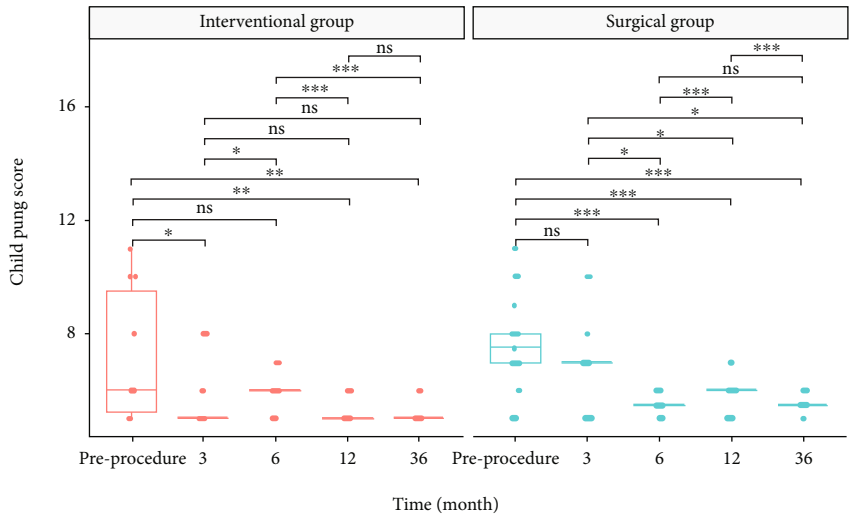

(d)

Figure 4: (a) Within-group comparison of hemoglobin in the interventional and surgical group pre- and postprocedure. (b) Within-group comparison of serum ammonia in the interventional and surgical group pre- and postprocedure. (c) Within-group comparison of portal vein pressure in the interventional and surgical group pre- and postprocedure. (d) Within-group comparison of Child-Pugh score in the interventional and surgical group pre- and postprocedure. Note: 0 "***"; 0.001 "**"; 0.01 "*"; 0.05 "."; 0.1 " " 1.

5. Conclusions

Both surgical ligation and endovascular embolization are effective in the treatment of type II CEPS. The endovascular approach has the advantages of shorter procedure time, less intraoperative blood loss, and lower treatment expense. Surgical ligation is recommended for patients with a high risk of embolic material migration due to short and large extrahepatic portosystemic shunts and patients with PVP more than 25 mmHg after occlusion, which could lead to portal hypertension. Ligation of the portosystemic shunt and the splenic artery and vein is feasible with apparent safety, and it could avoid a second surgical treatment.

Data Availability

The data used to support the findings of this study are included within the article.

Conflicts of Interest

The authors declare that they have no conflicts of interest.

Authors' Contributions

Jinlong Zhang, Weidong Duan, and Zhuting Fang contributed equally to this work and joined as first authors.

Acknowledgments

The manuscript is in the preprint. This study was supported by grants from the Major National Science and Technology Projects (2020ZX1001010), the Beijing Talents Fund (2016000021223ZK25), the China Postdoctoral Science Foundation (2019M664006), Fujian Province Natural Science Fund Project (2020J011096), and the Special Research Foundation of Fujian Provincial Department of Finance (No. [2020]822), China.

References

[1] G. Morgan and R. Superina, "Congenital absence of the portal vein: two cases and a proposed classification system for portasystemic vascular anomalies," *Journal of Pediatric Surgery*, vol. 29, no. 9, pp. 1239–1241, 1994.

[2] M. Passalacqua, K. T. Lie, and H. Yarmohammadi, "Congenital extrahepatic portosystemic shunt (Abernethy malformation) treated endovascularly with vascular plug shunt closure," *Pediatric Surgery International*, vol. 28, no. 1, pp. 79–83, 2012.

[3] A. David Jr., J. Meyer, I. Archambeaud, É. Frampas, C. Perret, and F. Douane, "Endovascular closure of a large congenital extrahepatic portosystemic shunt (Abernethy malformation) using vena cava filter and AMPLATZER vascular plugs," *Journal of vascular and interventional radiology : JVIR*, vol. 29, no. 11, pp. 1631–1633, 2018.

[4] A. Baiges, F. Turon, M. Simón-Talero et al., "Congenital extrahepatic portosystemic shunts (Abernethy malformation): an international observational study," *Hepatology*, vol. 71, no. 2, pp. 658–669, 2020.

[5] T. B. Lautz, N. Tantemsapya, E. Rowell, and R. A. Superina, "Management and classification of type II congenital portosystemic shunts," *Journal of Pediatric Surgery*, vol. 46, no. 2, pp. 308–314, 2011.

[6] S. Franchi-Abella, S. Branchereau, V. Lambert et al., "Complications of congenital portosystemic shunts in children: therapeutic options and outcomes," *Journal of Pediatric Gastroenterology and Nutrition*, vol. 51, no. 3, pp. 322–330, 2010.

[7] M. J. Kim, J. S. Ko, J. K. Seo et al., "Clinical features of congenital portosystemic shunt in children," *European Journal of Pediatrics*, vol. 171, no. 2, pp. 395–400, 2012.

[8] B. Zhang, K. T. Wu, L. Li, and H. Y. Lai, "Catheter embolization of type II congenital extrahepatic portosystemic shunt with hematochezia: a case series and review of the literature," *Cardiovascular and Interventional Radiology*, vol. 41, no. 7, pp. 1121–1127, 2018.

[9] S. V. Mathai, V. Kondray, E. Salloum, K. Kukreja, and S. Tavri, "Role of interventional radiology in the diagnosis and management of congenital extrahepatic portosystemic shunts: two case reports," *The Indian Journal of Radiology & Imaging*, vol. 29, no. 2, pp. 219–222, 2019.

[10] O. Bernard, S. Franchi-Abella, S. Branchereau, D. Pariente, F. Gauthier, and E. Jacquemin, "Congenital portosystemic shunts in children: recognition, evaluation, and management," *Seminars in Liver Disease*, vol. 32, no. 4, pp. 273–287, 2012.

[11] A. Shah, A. Aziz, A. Awwad, G. Ramjas, and Y. Higashi, "Incidental radiological diagnosis of asymptomatic Abernethy malformations-two case reports," *BJR Case Reports*, vol. 3, no. 1, article 20150496, 2017.

[12] T. Timpanaro, S. Passanisi, A. Sauna et al., "Congenital portosystemic shunt: our experience," *Case Reports in Pediatrics*, vol. 2015, Article ID 691618, 5 pages, 2015.

[13] Y. Takama, T. Ueno, S. Umeda, R. Saka, Y. Tazuke, and H. Okuyama, "Laparoscopic ligation of a congenital extrahepatic portosystemic shunt for children with hyperammonemia: a single-institution experience," *Surgery Today*, vol. 49, no. 4, pp. 323–327, 2019.

[14] T. Mori, Y. Yamada, K. Abe et al., "Laparoscopic partial closure for congenital portosystemic shunt-indications, postoperative management, and subsequent complete closure," *Journal of Laparoendoscopic & Advanced Surgical Techniques. Part A*, vol. 29, no. 4, pp. 573–578, 2019.

[15] T. Matsuura, Y. Takahashi, Y. Yanagi et al., "Surgical strategy according to the anatomical types of congenital portosystemic shunts in children," *Journal of Pediatric Surgery*, vol. 51, no. 12, pp. 2099–2104, 2016.

[16] W. Knirsch, D. C. Benz, P. Bühr et al., "Catheter interventional treatment of congenital portosystemic venous shunts in childhood," *Catheterization and Cardiovascular Interventions : official journal of the Society for Cardiac Angiography & Interventions*, vol. 87, no. 7, pp. 1281–1292, 2016.

[17] G. Chocarro, M. V. Amesty, J. L. Encinas et al., "Congenital portosystemic shunts: clinic heterogeneity requires an individual management of the patient," *European Journal of Pediatric Surgery*, vol. 26, no. 1, pp. 74–80, 2016.

Hindawi
BioMed Research International
Volume 2021, Article ID 5572395, 6 pages
https://doi.org/10.1155/2021/5572395

Research Article

The Effect of Preoperative Biliary Drainage with or without Pancreatic Stenting on Complications after Pancreatoduodenectomy: A Retrospective Cohort Study

Jiangtao Chu,[1] Shun He,[1] Yan Ke,[1] Xudong Liu,[1] Peng Wang,[2] Wei Zhang,[2] Guotong Qiu,[2] Chengfeng Wang,[2] Jianwei Zhang,[2] and Guiqi Wang[1]

[1]*The Department of Endoscopy, National Cancer Center/National clinical research center for Cancer/Cancer Hospital, Chinese Academy of Medical Sciences and Peking Union Medical College, Beijing 100021, China*
[2]*The Department of Pancreatic and Gastric Surgery, National Cancer Center/National clinical research center for Cancer/Cancer Hospital, Chinese Academy of Medical Sciences and Peking Union Medical College, Beijing 100021, China*

Correspondence should be addressed to Jianwei Zhang; panchutong@163.com and Guiqi Wang; wangguiq@126.com

Received 23 February 2021; Revised 10 April 2021; Accepted 16 April 2021; Published 30 April 2021

Academic Editor: Xing Chen

Background. The necessity of preoperative biliary drainage (PBD) prior to pancreaticoduodenectomy (PD) is still controversial. However, in some settings, PBD with endoscopic retrograde cholangiopancreatography (ERCP) procedure is recommended as a preferred management. Meanwhile, pancreatic duct stenting in the drainage procedure is rarely performed for selected indications, and its associated complications after PD remain quite unknown. *Methods*. A retrospective observational longitudinal cohort study was performed on patients who underwent PBD and PD from a prospectively maintained database at the National Cancer Center from March of 2015 to July of 2019. Patients who underwent biliary stenting alone, biliary and pancreatic stenting, were distributed into two study cohort groups, and their records were scrutinized for the incidence of postoperative complications. *Results*. A total of 83 patients who underwent successful PD after biliary drainage were identified. 29 patients underwent nasobiliary drainage (ENBD)/plastic or metal bile duct stenting (BS) and pancreatic duct stenting (PS group), and 54 patients underwent only ENBD/BS, without pancreatic duct stenting (NPS group). No differences were found between the two groups with respect to in-hospital time, overall complication rate, respective rate of serious (grade 3 or higher) complication rate, bile anastomotic leakage, bleeding, abdominal infection, surgical wound infection, organ dysfunction, and pancreatic anastomotic leakage. Postoperative gastrointestinal dysfunction rates differed significantly, which occurred in 3 (5.56%) cases in the NPS group, compared with 6 (20.7%) cases in the PS group ($P = 0.06$). In the univariate and multivariate regression model analysis, pancreatic duct stenting was correlated with higher rates of gastrointestinal dysfunction [odds ratio (OR) = 4.25, $P = 0.0472$]. *Conclusion*. Our data suggested that PBD and pancreatic duct stenting prior to pancreatoduodenectomy would increase the risk of postoperative delayed gastric emptying, while the overall incidence of postoperative complications and other complications, such as pancreatic leakage and bile duct leakage, showed no statistical difference.

1. Introduction

Biliary obstruction is a common problem in patients undergoing pancreaticoduodenectomy (PD). However, the necessity for preoperative biliary drainage (PBD) remains controversial [1]. A recent well-published study suggests that routine PBD is not recommended because it is associated with increased complications when PD is conducted [2]. However, if the bilirubin is markedly elevated in the symptomatic patient, or surgery needs to be delayed to optimize medical comorbidities or to

manage neoadjuvant therapy, PBD is still required [1]. Transpupillary endoscopic biliary drainage (EBD) with endoscopic retrograde cholangiopancreatography (ERCP) is recognized as the gold standard procedure for malignant biliary obstruction (MBO) prior to PD [3].

However, the ERCP procedure can cause complications such as pancreatitis, cholangitis, bleeding, and perforation, which delays the subsequent pancreaticoduodenectomy, and may cause postoperative complication [4].

Postoperative pancreatitis is a common complication after ERCP, especially for patients with difficult cannulation. Many studies have reported that pancreatic duct stenting can reduce the occurrence of pancreatitis after ERCP [5]. A cost-effective analysis showed that restricting preventive pancreatic stenting to high-risk patients is the most cost-effective strategy [6]. The European Society of Gastrointestinal Endoscopy strongly recommends that patients at high risk of postoperative pancreatitis, such as inadvertent guidewire insertion, opacification of the pancreatic duct, double-guidewire cannulation, could select pancreatic stenting [7].

Therefore, the correlation between pancreatic duct stenting and its resultant complications after pancreaticoduodenectomy needs to be evaluated. The purpose of our study was to analyze and assess the effect of pancreatic duct stenting on the complication of pancreaticoduodenectomy. This study compared the complication incidence of pancreaticoduodenectomy in patients with PBD and plastic pancreatic duct stenting (PS group) and patients with PBD alone (NPS group).

2. Methods

2.1. Patients Selection. From March 2015 to July 2019, the data of patients who underwent successful PD after biliary drainage with or without pancreatic stenting were extracted from the National Cancer Center database, and a retrospective observational cohort study was conducted. This study was approved by the institutional review board and ethics committee. Patients enrolled in the study met all the following requirements: (1) age $\geqq$ 18 years old, (2) with low malignant biliary obstruction, (3) successful PBD, or with/without pancreatic duct stenting, and (4) successful pancreaticoduodenectomy. Those who have undergone short-circuit surgery, percutaneous biliary drainage, or intraoperative tumor metastasis or unable to undergo radical resection were excluded.

A total of 83 patients who underwent successful PD after biliary drainage were identified. 31 patients had periampullary carcinoma, 16 had a tumor located in the head of the pancreas, 22 had cholangiocarcinoma, and 14 had duodenal adenocarcinomas, respectively. Among the 83 who had successful PD, 29 patients underwent biliary drainage and pancreatic duct stenting (PS group), and 54 patients underwent only biliary drainage without pancreatic duct stenting (NPS group).

2.2. Biliary Drainage and Pancreaticoduodenectomy. PBD procedure was performed with nasobiliary drainage, metal stent, or plastic stenting. When the double-guidewire method was selected for difficult bile duct canulation or the guidewire was accidentally inserted into the pancreatic duct, a 5-Fr plastic pancreatic duct stent with flanks on the inside was routinely implanted.

The standard surgical procedure for resectable tumors was the pylorus-preserving pancreaticoduodenectomy, including removal of all lymph nodes on the right side of the portal vein and mesenteric artery [8]. If metastasis into the proximal duodenum or pylorus was suspected, a classic Whipple procedure was performed, with resection of the distal stomach. If limited metastasis into the portal or superior mesenteric vein was found, a wedge resection of these vessels was included in the procedure [8, 9]. No specific modifications of the surgical technique were expected for patients with jaundice, particularly with respect to creating the hepaticojejunostomy.

2.3. Data Collection and Definition. Demographic characteristics of the included patients were evaluated, including pancreaticoduodenectomy, operation time, intraoperative blood transfusion, perioperative complications, clinical pathological results, margin conditions, and other indicators. The length of hospital stay was defined from the day of surgery to the day of discharge.

The severity of perioperative complications (i.e., perioperative bleeding, abdominal infection, delayed gastric emptying, bile anastomotic leakage, and pancreatic anastomotic leakage) was divided into 5 grades as described in Table 1 [10, 11]. Grade 1-2 was defined as the mild complication, and grade 3 or higher was defined as the severe complication.

2.4. Primary Outcome. The main outcome measure is the incidence of complications after pancreaticoduodenectomy of the enrolled patients.

2.5. Secondary Outcome. The secondary outcome included hospital stay time, operative time, and intraoperative blood transfusion volume.

2.6. Statistical Analysis. Continuous variables were described by median and range, while categorical variables were described by frequency and percentage. To analyze the differences between the two groups (pancreatic duct stent group and nonpancreatic duct stent group), categorical variables were analyzed using Fisher's exact test, and continuous variables were tested using ANOVA. The length of hospital stay and intraoperative blood transfusion was transformed into a normal distribution through logarithmic transformation, and ANOVA test was performed. R language was used to analyze the risk factors of surgical complications in univariate and multivariate analysis. Factors with a P value of <0.20 in univariate analysis were included in the multivariate analysis. Patients with missing values were excluded from the analysis.

3. Results

Between the two groups (Table 2), there have been no statistically significant differences in all demographic data including hospital stay time, operative time, and intraoperative blood transfusion volume, except the tumor location.

The overall complication rate of the study was 68.7%, including perioperative complications, severity of (grade 3 or higher) complications, delayed gastric emptying, biliary

Table 1: Complication criteria.

Grade definition
0: no complications
1: Oral medications or supportive care
2: IV medical therapy with resolution or antibiotics or specialized nutritional support
3: interventional radiology, endoscopic, or operative intervention
4: chronic deficit or disability associated with sequelae of this event
5: death associated with sequelae of this event

anastomotic leakage, pancreatic anastomotic leakage, abdominal infection, and wound infection as listed in Table 3. No significant differences were found between the two groups in overall complications. While postoperative gastrointestinal dysfunction rates differed with delayed gastric emptying occurring in 3 (5.56%) in the NPS group, compared to 6 (20.7%) in the PS group (NPS vs. PS $P = 0.06$).

In the univariate regression model analysis about postoperative gastrointestinal dysfunction, pancreatic duct stenting was correlated with higher rates of gastrointestinal dysfunction [odds ratio (OR) = 4.25, $P = 0.0472$]. In the multivariate regression model, PS had more delayed gastric emptying complication than the NPS group when adjusting for age. Table 4 shows that no other covariate was found significantly associated with the complications.

4. Discussion

The necessity of preoperative biliary drainage (PBD) prior to pancreaticoduodenectomy (PD) remained unclear because some studies showed that PBD procedure may be related to the complications of PD [4, 10, 12–16]. However, the PBD would be the recommended bridge management to resolve jaundice in some situations, such as acute cholangitis, obstruction with bilirubin levels exceeding 250 μmol/L, severe pruritus, jaundice associated with renal failure or comorbidities, or need of neoadjuvant chemotherapy for borderline resectable lesions [3]. Meanwhile, ERCP procedure with biliary stent or nasobiliary tube for PBD was preferred because of higher safety and better oncological outcomes [17, 18].

Postoperative pancreatitis was the most common complication of ERCP. According to reports, the incidence of postoperative pancreatitis was 2-10% for all patients, 2-4% for low-risk groups, and 8-40% for high-risk groups [19]. Pancreatic duct stent implantation was recommended to prevent postoperative pancreatitis [20], especially when the guidewire was accidentally inserted into the pancreatic duct, or the double-guidewire method was adopted.

There were few studies to evaluate the influence of pancreatic duct stenting during PBD on the complications of pancreaticoduodenectomy. A retrospective study by John et al. in 2018 showed that simultaneous cholangiopancreatic duct drainage increased the incidence of postoperative pancreatic leakage [21]. This study enrolled only 5 cases of simultaneous cholangiopancreatic duct drainage, which was regarded as a rare event during data analysis and Firth logistic regression. An opposite result was presented in our study, showing no significant difference between the two groups regarding the incidence of postoperative pancreatic leakage or bile duct leakage. The different results may be contributed to the method of pancreaticointestinal anastomosis and the proficiency of pancreatic duct stenting.

When analyzing each postoperative complication separately, there has been no statistical difference in terms of operation time, hospital stay, intraoperative blood transfusion, postoperative bleeding, pancreatic leakage, bile leakage, wound infection, abdominal infection, and organ dysfunction between the two groups. However, the incidence of delayed gastric emptying in the pancreatic duct stenting group was higher than that in the NPS group ($P = 0.06$). The multivariate and univariate adjusted analysis showed that pancreatic duct stenting was an independent risk factor for delayed gastric emptying (OR = 4.25, $P = 0.0472$), which was considered as one of the most common complications after pancreatic surgery, with about 19%-57% incidence [22].

The potential mechanisms for delayed gastric emptying after PD have been unclear. Some studies have reported that other postoperative complications, such as pancreatic leakage, accumulation of peripancreatic fluid, or abdominal abscess, could increase the incidence of gastric emptying disorders [23]. However, many patients develop delayed gastric emptying in the absence of pancreatic leakage or other abdominal infections, which may represent a distinct pathology [24]. The study is the first to report that the PBD and pancreatic duct stenting prior to pancreatoduodenectomy would increase the risk of postoperative delayed gastric emptying. The potential pancreatic inflammation after pancreatic duct stenting may play an important role in delayed gastric emptying. To most patients, although delayed gastric emptying was generally not life-threatened, patients could suffer abdominal discomfort, longer hospitalization time, increased hospitalization costs, and reduction of postoperative life quality.

The results suggest a hard choice in the PBD procedure when considering post-ERCP pancreatitis and outcomes of pancreaticoduodenectomy. Therefore, a PBD procedure without influence on the pancreatic duct would be preferred, such as endoscopic ultrasonography- (EUS-) guided biliary drainage method which can avoid contacting the pancreatic bile duct segmental in accessing the bile duct [25].

Several limitations in our study cannot be neglected. First, pancreaticoduodenectomy was not performed by the same surgeon. The difference in surgery proficiency may be one uncertainty, which affected the incidence of postoperative delayed gastric emptying. Second, our study did not find a significant difference in the incidence of other complications between the two groups, which may be attributed to the small number of cases of preoperative simultaneous cholangiopancreatic duct drainage. We cannot exactly exclude the possibility that pancreatic duct stent implantation may increase the incidence of other complications, such as surgical wound infection and abdominal infection. Also, the increase of the incidence of delayed gastric emptying needs to be clarified by a multicenter study.

Table 2: Demographic and clinical characteristics of patients NPS group and PS group.

	[ALL] $N = 83$	NPS* $N = 54$	PS* $N = 29$	P value
Sex (female)	42 (50.6%)	24 (44.4%)	18 (62.1%)	0.193
Age	58.0 [51.5; 63.0]	57.0 [51.0; 62.8]	59.0 [53.0; 63.0]	0.436
#BMI				0.684
Fat	35 (42.2%)	24 (44.4%)	11 (37.9%)	
Low	4 (4.82%)	2 (3.70%)	2 (6.90%)	
Normal	44 (53.0%)	28 (51.9%)	16 (55.2%)	
Biliary drainage				1.000
ENBD	66 (79.5%)	43 (79.6%)	23 (79.3%)	
Metal biliary stent	1 (1.20%)	1 (1.85%)	0 (0.00%)	
Plastic bile duct stent	16 (19.3%)	10 (18.5%)	6 (20.7%)	
Tumor location				0.024
Ampulla	31 (37.3%)	26 (48.1%)	5 (17.2%)	
Bile duct	22 (26.5%)	12 (22.2%)	10 (34.5%)	
Duodenum	14 (16.9%)	9 (16.7%)	5 (17.2%)	
Pancreas	16 (19.3%)	7 (13.0%)	9 (31.0%)	
Stay time	18.0 [14.0; 22.5]	20.0 [14.0; 23.0]	17.0 [15.0; 22.0]	0.681
Blood transfusion	300 [0.00; 750]	0.00 [0.00; 675]	500 [0.00; 800]	0.070
Operation duration	366 [306; 454]	359 [314; 466]	369 [300; 432]	0.909

Table 3: Outcomes of patients' PS group and NPS group.

	[all] $N = 83$	NPS* $N = 54$	PS* $N = 29$	P value
Complication criteria				0.57
None	26 (31.3%)	15 (27.8%)	11 (37.9%)	
Mild	42 (50.6%)	28 (51.9%)	14 (48.3%)	
Severe	15 (18.1%)	11 (20.4%)	4 (13.8%)	
Bile anastomotic leakage	7 (8.43%)	4 (7.41%)	3 (10.3%)	0.691
Bleeding				0.846
Blood transfusion	11 (13.3%)	8 (14.8%)	3 (10.3%)	
Dead	2 (2.41%)	2 (3.70%)	0 (0.00%)	
Hemostasis	3 (3.61%)	2 (3.70%)	1 (3.45%)	
None	67 (80.7%)	42 (77.8%)	25 (86.2%)	
Abdominal infection				0.670
Interventional therapy	10 (12.0%)	8 (14.8%)	2 (6.90%)	
Medication	24 (28.9%)	15 (27.8%)	9 (31.0%)	
None	49 (59.0%)	31 (57.4%)	18 (62.1%)	
Surgical wound infection	13 (15.7%)	8 (14.8%)	5 (17.2%)	0.761
Gastrointestinal dysfunction	9 (10.8%)	3 (5.56%)	6 (20.7%)	0.060
Organ dysfunction	6 (7.23%)	5 (9.26%)	1 (3.45%)	0.660
Pancreatic anastomotic leakage				0.380
None	58 (69.9%)	36 (66.7%)	22 (75.9%)	
A	8 (9.64%)	7 (13.0%)	1 (3.45%)	
B	17 (20.5%)	11 (20.4%)	6 (20.7%)	

Table 4: The univariate and multivariate analysis of predictive factors for postoperative delayed gastric emptying.

	[ALL]	Univariate analysis		Multivariate analysis	
	$N = 83$	OR	P value	OR	P value
Sex (male)	41 (49.4%)	2.16 [0.51;11.5]	0.313		
Age	58.0 [51.5; 63.0]	1.07 [0.98; 1.18]	0.085	1.07 [0.97; 1.17]	0.146
BMI			0.310		
Fat	35 (42.2%)	Ref.			
Low	4 (4.82%)	NA			
Normal	44 (53.0%)	NA			
Stay time	18.0 [14.0; 22.5]	0.99 [0.93; 1.06]	0.924		
Tumor location			0.522		
Ampulla	31 (37.3%)	Ref.			
Bile duct	22 (26.5%)	3.05 [0.51; 26.7]			
Duodenum	14 (16.9%)	2.36 [0.22; 25.0]			
Pancreas	16 (19.3%)	1.02 [0.03; 13.6]			
Blood transfusion	414 (490)	1.00 [1.00; 1.00]	0.145		
Operation duration	366 [306; 454]	1.00 [1.00; 1.01]	0.524		
Biliary drainage			1.000		
ENBD	66 (79.5%)	Ref.			
Metal biliary stent	1 (1.20%)	NA			
Plastic bile duct stent	16 (19.3%)	NA			
PDS	29 (34.9%)	4.25 [0.99; 22.9]	0.0472	4.36 [0.97; 19.42]	0.053
Bile leakage	7 (8.43%)		1.000		
Bleeding			0.636		
Blood transfusion	11 (13.3%)	Ref.			
Dead	2 (2.41%)	NA			
Hemostasis	3 (3.61%)	NA			
None	67 (80.7%)	NA			
Abdominal infection			1.000		
Interventional therapy	10 (12.0%)	Ref.			
Medication	24 (28.9%)	0.78 [0.06; 26.7]			
None	49 (59.0%)	1.14 [0.16; 32.2]			
Surgical wound infection	13 (15.7%)	0.72 [0.03; 4.63]	1.000		
Organ dysfunction	6 (7.23%)		1.000		
Pancreatic leakage			0.866		
0	58 (69.9%)	Ref.			
A	8 (9.64%)	NA			
B	17 (20.5%)	NA			

5. Conclusion

This study has shown that preoperative biliary drainage and pancreatic duct stenting prior to pancreaticoduodenectomy would increase the risk of postoperative delayed gastric emptying, while with no significant difference to the overall incidence of postoperative complications. More studies, especially RCTs, are preferred to verify the results in the future study.

Data Availability

From March 2015 to July 2019, the data of patients who underwent successful PD after biliary drainage with or without pancreatic stenting were extracted from the National Cancer Center database.

Conflicts of Interest

The authors declare that they have no conflicts of interest.

References

[1] M. Costa Santos, C. Cunha, S. Velho et al., "Preoperative biliary drainage in patients performing pancreaticoduodenectomy: guidelines and real-life practice," *Acta Gastro-Enterologica Belgica*, vol. 82, no. 3, pp. 389–395, 2019.

[2] Y. Shaib, M. A. Rahal, M. O. Rammal, A. Mailhac, and H. Tamim, "Preoperative biliary drainage for malignant biliary obstruction: results from a national database," *Journal of Hepato-Biliary-Pancreatic Sciences*, vol. 24, no. 11, pp. 637–642, 2017.

[3] A. Zarzavadjian le Bian, D. Fuks, R. Dalla Valle, M. Cesaretti, V. Violi, and R. Costi, "Effectiveness and risk of biliary drainage prior to pancreatoduodenectomy: review of current status," *Surgery Today*, vol. 48, no. 4, pp. 371–379, 2018.

[4] H. Moole, M. Bechtold, and S. R. Puli, "Efficacy of preoperative biliary drainage in malignant obstructive jaundice: a meta-analysis and systematic review," *World Journal of Surgical Oncology*, vol. 14, no. 1, p. 182, 2016.

[5] V. Phillip, A. Pukitis, A. Epstein et al., "Pancreatic stenting to prevent post-ERCP pancreatitis: a randomized multicenter trial," *Endoscopy International Open*, vol. 7, no. 7, pp. E860–E868, 2019.

[6] H. J. Hwang, M. A. Guidi, C. Curvale, J. Lasa, and R. Matano, "Post-ERCP pancreatitis: early precut or pancreatic duct stent? A multicenter, randomized-controlled trial and cost-effectiveness analysis," *Revista Española de Enfermedades Digestivas*, vol. 109, no. 3, pp. 174–179, 2017.

[7] J. M. Dumonceau, A. Andriulli, B. J. Elmunzer et al., "Prophylaxis of post-ERCP pancreatitis: European Society of Gastrointestinal Endoscopy (ESGE) Guideline - updated June 2014," *Endoscopy*, vol. 46, no. 9, pp. 799–815, 2014.

[8] D. J. Gouma, E. J. M. Nieveen van Dijkum, and H. Obertop, "The standard diagnostic work-up and surgical treatment of pancreatic head tumours," *European Journal of Surgical Oncology (EJSO)*, vol. 25, no. 2, pp. 113–123, 1999.

[9] R. C. van Geenen, F. J. ten Kate, L. T. de Wit, T. M. van Gulik, H. Obertop, and D. J. Gouma, "Segmental resection and wedge excision of the portal or superior mesenteric vein during pancreatoduodenectomy," *Surgery*, vol. 129, no. 2, pp. 158–163, 2001.

[10] C. Liu, J. W. Lu, Z. Q. du, X. M. Liu, Y. Lv, and X. F. Zhang, "Association of preoperative biliary drainage with postoperative morbidity after pancreaticoduodenectomy," *Gastroenterology Research and Practice*, vol. 2015, Article ID 796893, 8 pages, 2015.

[11] A. Schaible, P. Schemmer, T. Hackert et al., "Location of a biliary leak after liver resection determines success of endoscopic treatment," *Surgical Endoscopy*, vol. 31, no. 4, pp. 1814–1820, 2017.

[12] S. P. Povoski, M. S. Karpeh Jr., K. C. Conlon, L. H. Blumgart, and M. F. Brennan, "Association of preoperative biliary drainage with postoperative outcome following pancreaticoduodenectomy," *Annals of Surgery*, vol. 230, no. 2, pp. 131–142, 1999.

[13] T. A. Sohn, C. J. Yeo, J. L. Cameron, H. A. Pitt, and K. D. Lillemoe, "Do preoperative biliary stents increase postpancreaticoduodenectomy complications?," *Journal of Gastrointestinal Surgery: Official Journal of the Society for Surgery of the Alimentary Tract*, vol. 4, no. 3, pp. 258–268, 2000.

[14] P. W. Pisters, W. A. Hudec, K. R. Hess et al., "Effect of preoperative biliary decompression on pancreaticoduodenectomy-associated morbidity in 300 consecutive patients," *Annals of Surgery*, vol. 234, no. 1, pp. 47–55, 2001.

[15] N. Arkadopoulos, M. A. Kyriazi, I. S. Papanikolaou et al., "Preoperative biliary drainage of severely jaundiced patients increases morbidity of pancreaticoduodenectomy: results of a case-control study," *World Journal of Surgery*, vol. 38, no. 11, pp. 2967–2972, 2014.

[16] E. C. H. Lai, S. H. Y. Lau, and W. Y. Lau, "The current status of preoperative biliary drainage for patients who receive pancreaticoduodenectomy for periampullary carcinoma: a comprehensive review," *The Surgeon*, vol. 12, no. 5, pp. 290–296, 2014.

[17] Y. Murakami, K. Uemura, Y. Hashimoto et al., "Does preoperative biliary drainage compromise the long-term survival of patients with pancreatic head carcinoma?," *Journal of Surgical Oncology*, vol. 111, no. 3, pp. 270–276, 2015.

[18] K. Uemura, Y. Murakami, S. Satoi et al., "Impact of preoperative biliary drainage on long-term survival in resected pancreatic ductal adenocarcinoma: a multicenter observational study," *Annals of Surgical Oncology*, vol. 22, Supplement 3, pp. 1238–1246, 2015.

[19] G. Z. Li, F. Wang, J. Fang, H. L. Zha, and Q. Zhao, "Risk factors for post-endoscopic retrograde cholangiopancreatography pancreatitis: evidence from 1786 cases," *Medical Science Monitor*, vol. 24, pp. 8544–8552, 2018.

[20] M. L. Freeman, "Preventing post-ERCP pancreatitis: update 2016," *Current Treatment Options in Gastroenterology*, vol. 14, no. 3, pp. 340–347, 2016.

[21] J. M. Manipadam, S. Mahesh, J. M. Kadamapuzha, and H. Ramesh, "The effect of preoperative biliary and pancreatic drainage on postoperative pancreatic fistula: a retrospective cohort study," *The Surgery Journal*, vol. 4, no. 1, pp. e37–e42, 2018.

[22] M. N. Wente, S. V. Shrikhande, J. Kleeff et al., "Management of early hemorrhage from pancreatic anastomoses after pancreaticoduodenectomy," *Digestive Surgery*, vol. 23, no. 4, pp. 203–208, 2006.

[23] S. Räty, J. Sand, E. Lantto, and I. Nordback, "Postoperative acute pancreatitis as a major determinant of postoperative delayed gastric emptying after pancreaticoduodenectomy," *Journal of Gastrointestinal Surgery: Official Journal of the Society for Surgery of the Alimentary Tract*, vol. 10, no. 8, pp. 1131–1139, 2006.

[24] R. J. Ellis, A. R. Gupta, D. B. Hewitt et al., "Risk factors for post-pancreaticoduodenectomy delayed gastric emptying in the absence of pancreatic fistula or intra-abdominal infection," *Journal of Surgical Oncology*, vol. 119, no. 7, pp. 925–931, 2019.

[25] F. I. Téllez-Ávila, M. A. Figueredo-Zacarías, E. Muñoz-Anaya et al., "EUS-guided biliary drainage in patients with distal malignant biliary obstruction requires fewer interventions and has a lower cost compared to ERCP biliary drainage," *Surgical Endoscopy*, 2020.

Hindawi
BioMed Research International
Volume 2021, Article ID 5527988, 6 pages
https://doi.org/10.1155/2021/5527988

Research Article

Effects of the Vertebral Artery Ostium/Subclavian Artery Angle on In-Stent Restenosis after Vertebral Artery Ostium Stenting

Hui Su, Shengyuan Yu, Chenglin Tian, Zhihua Du, Xinfeng Liu, Jun Wang, and Xiangyu Cao

Department of Neurology, Chinese PLA General Hospital, First Medical Center, Beijing, China

Correspondence should be addressed to Xiangyu Cao; caoxiangyu301@126.com

Received 8 January 2021; Revised 10 April 2021; Accepted 22 April 2021; Published 28 April 2021

Academic Editor: Dorota Formanowicz

Background and Purpose. The cause of in-stent restenosis (ISR) after vertebral artery ostium (VAO) stenting remains unclear. We evaluated factors associated with ISR in patients who underwent VAO stenting. We also assessed the feasibility of stenting for treating VAO stenosis (VAOS). *Methods*. Between January 2016 and October 2018, sixty-four consecutive patients who underwent a total of 66 stenting procedures were screened for symptomatic and asymptomatic atherosclerotic VAOS. Of these patients, 57 had complete follow-up data. The baseline patient demographics and morphological features of the VAO were recorded. Potential factors influencing ISR, including conventional cerebrovascular disease risk factors, were assessed, together with outcome events including recurrent transient ischemic attack (TIA), stroke, and vascular-related mortality. *Results*. The average follow-up period was 13.2 ± 4.6 months. Technical success was achieved in all interventions. The degree of stenosis was reduced from 77.2 ± 6.1% to 13.7 ± 8.9% after the procedure. ISR was detected in eight treated vessels (14.0%) and occlusion in two (5.3%) arteries. Of the 57 patients, one had an ischemic stroke and 5 had TIAs. The angle of the VAO at the subclavian artery was associated with the risk of restenosis (preoperative, $P = 0.04$; postoperative, $P = 0.02$). *Conclusions*. Stenting is a feasible and effective treatment for VAOS. The angle of the VAO at the subclavian artery may contribute to the development of ISR.

1. Introduction

Atherosclerotic stenosis of the vertebral artery ostium (VAO), a recognized cause of ischemic stroke, accounts for 5.2–9% of posterior circulation ischemic strokes [1, 2]. Recent autopsy [3] and angiographic [4] studies have revealed VAO stenosis (VAOS) prevalence rates of 12.7% and 5.4%, respectively. Studies by The New England Medical Center Posterior Circulation Registry and Borgess Medical Center Vertebral Artery Ostium Stenting Registry found that atherosclerotic VAOS alone could explain posterior circulation ischemic stroke [5–7].

Currently, antiplatelet therapy is the first-line treatment for most posterior circulation strokes caused by VAOS or occlusion [8]. However, posterior circulation strokes are often refractory to medical treatment, which increases stroke recurrence [9]. Stent implantation for VAOS is a safe option for reducing the long-term risk of stroke [9, 10]; however, in-stent restenosis (ISR) is more common for stents placed at the origin of an artery than in those placed in the intracranial vertebral artery (VA) [11]. Moreover, the ISR rate of VAO stents is higher than that following carotid angioplasty and stenting [10, 12, 13]. Previous investigations have identified factors associated with ISR, including arterial anatomy, vessel diameter, coexisting carotid vascular occlusions, and medical management and stent type [14–17]. However, the effect of the VAO/subclavian artery angle in VAOS stent patients is seldom mentioned. This prospective, single-center study evaluated the incidence of and factors associated with ISR in 57 consecutive patients who underwent VAO stent placement.

2. Materials and Methods

2.1. Patient Characteristics. The study enrolled 64 consecutive patients treated with angioplasty and stenting for VAOS

at our hospital between January 2016 and October 2018. Of these patients, 57 (53 males, 4 females; average age, 63.1 years; range: 44–81 years) had available follow-up data. All patients met the following inclusion criteria: symptomatic VAOS, defined as VAOS ≥ 50% with transient ischemic attack (TIA) or stroke in the region of the vertebral artery (VA); asymptomatic VAOS (≥70% with hypoplasia of the contralateral VA); satisfactory neurological function, defined by a modified Rankin Scale score ≤ 2 (if a minor stroke occurred, the procedure was performed at least 2 weeks after the onset of the most recent ischemic symptoms); and complete imaging and clinical data. Patients with nonatherosclerotic diseases, those with tandem or extensive lesions requiring the placement of more than one stent, and those who had undergone previous vertebral ostium interventions were excluded from the study. The degree of stenosis was measured on digital subtraction angiography using the North American Symptomatic Carotid Endarterectomy Trial method [18] and classified as <50%, 50–69%, or 70–99% stenosis, or occlusion.

The angiography and stent procedures were explained fully, and all patients provided informed consent.

2.2. Clinical and Angiographic Follow-Up. All patients were discharged the day after the procedure and prescribed aspirin (100 mg/day) and clopidogrel (75 mg/day) for at least 6 months. To minimize the risk of atherosclerosis, the patients were treated for atherosclerotic risk factors, including hypertension, hyperlipidemia, and diabetes. Follow-up involved telephone interviews and clinical visits 1, 3, 6, and 12 months after the procedure and yearly thereafter. Outcome events included TIA, stroke (affecting the anterior and posterior circulation), myocardial infarction, and death. There were no periprocedural complications. Cervical Doppler ultrasound was performed at 3, 6, and 12 months postprocedure. If ISR was suspected on Doppler examination according to the vertebral stenosis criteria (ostium site peak systolic velocity (PSV) ≥ 140 cm/s and PSV ratio (vertebral ostium stenosis PSV divided by intervertebral segment PSV) ≥ 2.1) [19], computed tomography angiography (CTA) or digital subtraction angiography was performed to detect ISR, which we defined as recurrent in − stent stenosis > 50%.

The mean follow-up duration was 13.2 ± 4.6 months. Of the eight patients with ISR, six (75.0%) had clinical events (cerebral infarction, $n = 1$; TIA, $n = 5$).

2.3. Stenting and Digital Subtraction Angiography Procedures. All procedures were performed by experienced interventional neurosurgeons. All patients received aspirin (100 mg) and clopidogrel (75 mg) daily for at least 5 days before the procedure. The procedures were performed under local anesthesia, and the patients were heparinized to achieve an activated clotting time of 150–200 s. A 6F guide catheter was placed into the subclavian artery at the VAO. Under roadmap guidance, a steerable 0.014-inch microwire was directed into the VAO through the stenotic lesion and placed in the distal cervical VA allowing adequate purchase for the stent to pass to the site of the stenosis. Care was taken to avoid plaque dislodgement. A balloon-expandable stent was selected according to the lesion length and diameter of the nondiseased distal segment of the VA. Then, the stent was carefully advanced into the stenosed segment under fluoroscopic guidance using an 11 cm image-intensifier diameter and X-ray pulse rate of 30 frames per second. The stent was deployed first by manual inflation of the balloon to achieve better controllability and then by controlled inflation to 13 atm using a manometer and deployed to protrude 1 to 2 mm into the subclavian artery to guarantee complete coverage of the stenotic lesion.

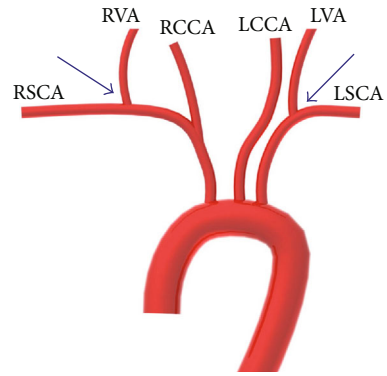

Figure 1: RVA: right vertebral artery; RCCA: right common carotid artery; LVA: left vertebral artery; LCCA: left common carotid artery; RSCA: right subclavian artery; LSCA: left subclavian artery. Vertebral artery ostium/subclavian artery angle (blue arrows).

The stent type was selected according to the preference and experience of the neurosurgeon and the characteristics of the stenotic lesion. Three types of stents were used: an Express Vascular SD stent (Boston Scientific Co., Natick, MA, USA) was used in 54 procedures (94.7%), an Apollo stent (Microport, Shanghai, China) was used in two procedures (3.5%), and a Blue stent (Cordis, Miami, FL, USA) was used in one procedure (1.8%).

The DSA images were imported into Digimizer Image Analysis Software V4.3.4 (MedCalc Software bvba, Ostend, Belgium) to obtain a 3D reconstruction of the prestent and poststent vertebral artery. The vertebral artery ostium/subclavian artery angle was defined the space between the vertibral artery and long axis of subclavian artery, and it was measured in degrees (Figure 1). The degrees were measured independently with the Digimizer Image Analysis Software V4.3.4 (MedCalc Software bvba, Ostend, Belgium) by two neuroradiologists.

2.4. Statistical Analyses. All statistical tests were performed using SPSS statistical software, version 25.0 (IBM Corp., Armonk, NY, USA). The one-sample Kolmogorov–Smirnov test was used to compare continuous variables. Normally distributed continuous variables are expressed as mean ± standard deviation. Differences between the ISR and non-ISR groups were assessed using Pearson's chi-squared test or Fisher's exact test for categorical data and Student's t-test for normally distributed continuous variables and the Mann–Whitney U-test for continuous skewed data. Kaplan–Meier curves and the log-rank test were used to show differences in ISR incidence between the groups. The hazard ratio (HR) and

Table 1: Demographic and clinical summary of vertebral artery ostium in patients with and without in-stent restenosis at follow-up.

Variable	ISR ≤ 50% ($n = 49$)	ISR > 50% ($n = 8$)	P	HR (95% CI)
Mean age (y)	63.2 ± 9.7	62.3 ± 9.8	0.54	0.64 (0.15-2.71)
Male (n (%))	46 (93.9)	7 (87.5)	0.64	0.58 (0.06-5.89)
Hypertension (n (%))	32 (65.3)	4 (50.0)	0.55	0.64 (0.14-2.84)
Diabetes (n (%))	15 (30.6)	2 (25.0)	0.78	1.30 (0.20-8.51)
Hyperlipidemia (n (%))	6 (12.2)	6 (75.0)	0.15	3.89 (0.60-25.13)
Coronary artery disease (n (%))	16 (32.7)	1 (12.5)	0.62	0.58 (0.07-5.10)
Smokers (n (%))	33 (67.3)	4 (50.0)	0.52	0.60 (0.12-2.92)
History of alcohol use (n (%))	26 (53.1)	3 (37.5)	0.38	0.51 (0.12-2.28)
Symptoms (n (%))				
TIA	34 (69.4)	5 (62.5)	0.45	0.37 (0.03-5.11)
Stroke	3 (6.1)	1 (12.5)	0.30	0.27 (0.02-3.20)
No symptoms	12 (24.5)	2 (25.0)	0.58	0.65 (0.16-3.10)
Contralateral vertebral				
Stenosis or occlusion (n (%))	13 (26.5)	2 (25.0)	0.50	0.50 (0.08-3.44)
Preoperative stenosis rate (%)	77.5 ± 6.0	75.0 ± 6.2	0.06	0.13 (0.01-1.08)
Residual stenosis (%)	13.7 ± 9.2	13.2 ± 7.1	0.34	0.15 (0.00-7.92)
Location of stenting (n (%))			0.84	1.22 (0.18-8.40)
LVAO	30 (61.2)	5 (62.5)		
RVAO	19 (38.8)	3 (37.5)		
Stent diameter (mm)	4.7 ± 0.8	4.8 ± 0.8	0.17	0.28 (0.05-1.72)
Stent length (mm)	15.7 ± 2.6	15.1 ± 1.4	0.57	3.11 (0.06-167.04)
Vessel tortuosity (n (%))	6 (12.2)	2 (25.0)	0.09	0.04 (0.00-1.80)
Preoperative angle (°)			0.04	0.19 (0.04-0.96)
≥70°	16 (72.7)	6 (27.3)		
<70°	33 (94.3)	2 (5.7)		
Postoperative angle (°)			0.02	12.11 (1.40-105.04)
≥70°	19 (76.0)	6 (24.0)		
<70°	30 (93.8)	2 (6.2)		

ISR: in-stent restenosis; TIA: transient ischaemic attack; LVAO: left vertebral artery origin; RVAO: right vertebral artery origin.

95% CI of the different occlusion groups were assessed by Cox regression. All statistical tests were two-sided, with P values < 0.05 indicating statistical significance.

3. Results

Of the 64 patients screened, 7 did not receive follow-up. The clinical, demographic, and procedure characteristics of the remaining 57 patients are shown in Table 1 according to ISR status. Twenty-two patients also had a stenosis of the internal carotid artery. The study included 43 patients (75.4%) with symptoms, including dizziness in 32 cases (74.4%), focal weakness or focal sensory disturbance in 12 (27.9%), visual symptoms (diplopia or visual field defect) in 8 (18.6%), vertigo in 6 (14.0%), ataxia in 4 (9.3%), dysarthria in 3 (7.0%), and drop attacks in 1 (2.3%).

The procedure was technically successful in all cases, and no adverse events occurred before discharge. There was no association between ISR after VAO stent implantation and age, sex, risk factors, rate of stenosis, location of stenting, stent diameter, stent length, or VAO tortuosity (Table 1). Stents were implanted in the left ($n = 35$, 61.4%) and right ($n = 22$, 38.6%) VAO. The degree of VAOS was reduced from 77.2 ± 6.1% to 13.7 ± 8.9%. Angiographic follow-up was conducted 13.2 ± 4.6 months (range: 6–24 months) after the procedure. Among the 43 symptomatic patients, complete resolution of symptoms was observed in 35 (81.4%); the remaining 8 (18.6%) patients showed marked clinical improvement.

The severity of stenosis on follow-up angiography exceeded 50% in eight cases (14%), two (3.5%) of which were shown by CTA to be occluded at 6 and 10 months (Figure 2). Six of the restenosis events were symptomatic: five patients had recurrent TIAs after a mean of 9.9 months (range: 6–12 months), and one patient had an acute cerebellar infarction at 12 months (Figure 2); he died of a heart attack 21 months after stent placement. The angle of the VAO at the subclavian artery exceeded 70° in six patients. Comparison of the ISR and non-ISR groups during follow-up revealed that the angle of the VAO at the subclavian artery (preprocedure, 63.8 ± 18.5°; postprocedure, 67.3 ± 15.7°) was associated with ISR (preoperative $P = 0.04$; postoperative $P = 0.02$) (Figure 3).

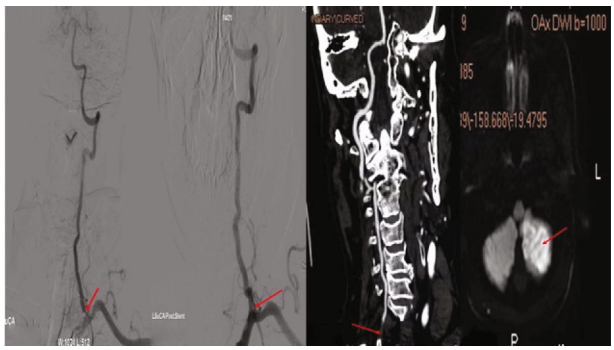

Figure 2: A 77-year-old male who presented with dizziness was admitted. His left subclavian arteriography shows severe stenosis of the vertebral artery ostium, and the vertebral artery ostium/subclavian artery angle was 93.9 degrees (a). After stenting of the left vertebral artery, ostium stenosis showed excellent dilatation of the lesion; then, the vertebral artery ostium/subclavian artery angle was 72.0 degrees (b). About ten months later, he was readmitted to the hospital because of dizziness reattack. His neck CTA showed left vertebral artery ostium occlusion (c). Brain MRI in DWI sequence showing left cerebellum restricted diffusion (d). Arrow in (a), stenosis site; arrow in (b), stent site; arrow in (c), occlusion site; arrow in (d), left cerebellum ischemic lesion.

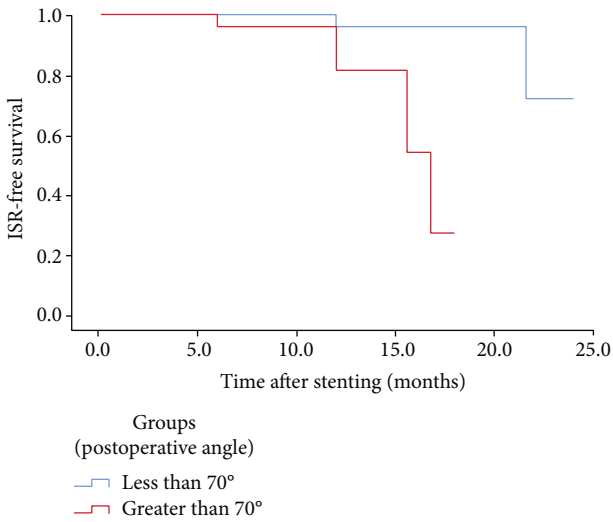

Figure 3: Kaplan-Meier estimates of cumulative ISR rate among patients with stenting in VAO.

There were no associations among mean age, sex, and risk factors (Table 1).

4. Discussion

We found that VAOS was more common in males than females. More than 50% ISR was found in 8 (14%) patients, most of whom were symptomatic. In contrast to other studies [20], no TIA, stroke, or death occurred within 30 days of the intervention in our series. To our knowledge, this is the first report that the angle of the VAO at the subclavian artery, both before and after stenting, can affect ISR.

Current treatments for VAOS include medical intervention, open surgery, percutaneous transluminal angioplasty, and stenting. All of the treatment options have advantages and drawbacks, which differ depending on the patient's race, the medications and stent types used, and the follow-up period. Motarjeme et al. performed the first VAO angioplasty in 1981 [21], and Storey et al. was the first to report VAO stent placement in 1996 [22]. The risk of extracranial VA stenting is lower than that of intracranial VA stenting [11, 15]. Moreover, despite a strict drug regimen after VAO stenting, ISR remains a frequent complication [23]. Although stenosis may be asymptomatic in patients with good collaterals, ISR is not always benign, and some patients who present with ischemic symptoms may ultimately require secondary stent placement.

In our study, ISR was observed in 14% of the patients after a mean follow-up of 13.2 ± 4.6 months. The reported rate of restenosis after endovascular treatment for VAOS can reach 67% [13, 24], which is higher than in our series. The risk factors for ISR remain unclear. Factors previously shown to contribute to ISR include age, diabetes mellitus, smoking, hyperlipidemia, small diameter stent (≤4 mm), longer stent length, tortuous V1 segment, long stenosis (>10 mm), contralateral VA hypoplasia, and contralateral VA occlusion at the time of stenting [17, 25–34]. The VAO has a high elastin concentration, which may increase the risk of stent recoil, kinking, and deformation, and contribute to ISR [35, 36].

Our findings confirm that the VAO/subclavian artery angle is associated with ISR after VAO stent placement. The angle of the VAO at the subclavian artery was 70–90° in 62.5% of the patients with ISR, which was significantly different from that of the non-ISR group. Local hemodynamic flow patterns change with vessel angle; the greater the angle, the higher the wall shear stress (WSS), which ultimately leads to ISR. A previous study found that high WSS at the junction of the VAO and subclavian artery markedly affected local blood flow [37]. A WSS of 2.0 Pa is sufficient to maintain the structure of arterial vessels. Low (<0.4 Pa) and high (>40 Pa) WSS contribute to ISR via different mechanisms [38, 39]. Moreover, flow velocity and pressure may influence the development of ISR. Several recent studies have investigated the effect of VAO stent location in an attempt to prevent ISR. One study found that implanting the stent 1 mm into the subclavian artery produced the smallest decrease in blood flow and WSS [34]. Although we successfully placed the proximal VA stent into the subclavian artery to a depth of 1–2 mm in all of our patients, ISR developed in several cases. Therefore, further investigation of stent type and placement in relation to the VAO/subclavian artery angle is warranted.

5. Study Limitations

The retrospective design, small sample size, and relatively high rate of loss to follow-up (10.9%) were the major study limitations of this study. Furthermore, the majority of the clinical follow-up data were obtained using noninvasive

imaging techniques, which may have affected the assessment of ISR.

6. Conclusion

Our findings suggest that the VAO/subclavian artery angle significantly affects the incidence of ISR. Future investigations of ISR prevention through intensive medical treatment should focus on fluid–structure interactions and appropriate stent selection. Furthermore, studies with larger sample sizes and longer follow-ups are needed.

Data Availability

If necessary, we can provide the crude data via the E-mail of corresponding author and data available in supplementary files.

Conflicts of Interest

The authors declare that they have no conflicts of interest.

Acknowledgments

This study was funded by the outstanding project of the Chinese people's liberation army (PLA) Medical Science and Technology Youth Cultivation Program (18QNP059).

Supplementary Materials

Supplementary 1. 57 patients' baseline characteristics at the time of the procedure.

Supplementary 2. Clinical characteristics of 57 patients (1).

Supplementary 3. Clinical characteristics of 57 patients (2).

Supplementary 4. Clinical characteristics of 57 patients (3).

References

[1] R. J. Wityk, H. M. Chang, A. Rosengart et al., "Proximal extracranial vertebral artery disease in the New England medical center posterior circulation registry," *Archives of Neurology*, vol. 55, no. 4, pp. 470–478, 1998.

[2] L. Gordon Perue Gillian, N. Ram, H. Zangiabadi Amir et al., "Prevalence of vertebral artery origin stenosis in a multiracethnic posterior circulation stroke cohort: Miami Stroke Registry (MIAMISR)," *International Journal of Stroke*, vol. 10, no. 2, pp. 185–187, 2015.

[3] M. Mazighi, J. Labreuche, F. Gongora-Rivera, C. Duyckaerts, H. Jean-Jacques, and P. Amarenco, "Autopsy prevalence of proximal extracranial atherosclerosis in patients with fatal stroke," *Stroke*, vol. 40, no. 3, pp. 713–718, 2009.

[4] S. Kumar Dundamadappa and K. Cauley, "Vertebral artery ostial stenosis: prevalence by digital subtraction angiography, MR angiography and CT angiography," *Journal of Neuroimaging*, vol. 23, no. 3, pp. 360–367, 2013.

[5] L. R. Caplan, R. J. Wityk, T. A. Glass et al., "New England medical center posterior circulation registry," *Annals of Neurology*, vol. 56, no. 3, pp. 389–398, 2004.

[6] A.-A. Firas, B. Tom, D. Li et al., "Vertebral artery ostium atherosclerotic plaque as a potential source of posterior circulation ischemic stroke: result from borgess medical center vertebral artery ostium stenting registry," *Stroke*, vol. 42, pp. 2544–2549, 2011.

[7] J. E. Cohen, R. R. Leker, J. M. Gomori et al., "Emergent revascularization of acute tandem vertebrobasilar occlusions: endovascular approaches and technical considerations—confirming the role of vertebral artery ostium stenosis as a cause of vertebrobasilar stroke," *Journal of Clinical Neuroscience*, vol. 34, pp. 70–76, 2016.

[8] A. Algra and J. van Gijn, "Cumulative meta-analysis of aspirin efficacy after cerebral ischaemia of arterial origin," *Journal of Neurology, Neurosurgery, and Psychiatry*, vol. 66, no. 2, p. 255, 1999.

[9] R. Mohammadian, A. Najaran, B. Sohrabi et al., "Vertebral artery orifice stenosis: a report of 43 cases from northwest iran treated with angioplasty and stenting," *The Neuroradiology Journal*, vol. 24, no. 5, pp. 749–757, 2011.

[10] A. M. Drazyk and H. S. Markus, "Recent advances in the management of symptomatic vertebral artery stenosis," *Current Opinion in Neurology*, vol. 31, no. 1, pp. 1–7, 2018.

[11] H. S. Markus, S. C. Larsson, W. Kuker et al., "Stenting for symptomatic vertebral artery stenosis," *Neurology*, vol. 89, no. 12, pp. 1229–1236, 2017.

[12] P. A. Lemos, A. Hoye, D. Goedhart et al., "Clinical, angiographic, and procedural predictors of angiographic restenosis after sirolimus-eluting stent implantation in complex patients: an evaluation from the Rapamycin-Eluting Stent Evaluated At Rotterdam Cardiology Hospital (RESEARCH) study," *Circulation*, vol. 109, no. 11, pp. 1366–1370, 2004.

[13] SSYLVIA Study Investigators, "Stenting of symptomatic atherosclerotic lesions in the vertebral or intracranial arteries (SSYLVIA)," *Stroke*, vol. 35, no. 6, pp. 1388–1392, 2004.

[14] K. Raghuram, C. Seynnaeve, and A. T. Rai, "Endovascular treatment of extracranial atherosclerotic disease involving the vertebral artery origins: a comparison of drugeluting and bare-metal stents," *Journal of Neurointerventional Surgery*, vol. 4, no. 3, pp. 206–210, 2012.

[15] A. N. Stayman, R. G. Nogueira, and R. Gupta, "A systematic review of stenting and angioplasty of symptomatic extracranial vertebral artery stenosis," *Stroke*, vol. 42, no. 8, pp. 2212–2216, 2011.

[16] Z. Zhou, Q. Yin, G. Xu et al., "Influence of vessel size and tortuosity on in-stent restenosis after stent implantation in the vertebral artery ostium," *Cardiovascular and Interventional Radiology*, vol. 34, no. 3, pp. 481–487, 2011.

[17] J. Li, Y. Hua, L. Needleman et al., "Arterial occlusions increase the risk of in-stent restenosis after vertebral artery ostium stenting," *Journal of Neurointerventional Surgery*, vol. 11, no. 6, pp. 574–578, 2019.

[18] H. J. Barnett, D. W. Taylor, M. Eliasziw et al., "Benefit of carotid endarterectomy in patients with symptomatic moderate or severe stenosis," *The New England Journal of Medicine*, vol. 339, no. 20, pp. 1415–1425, 1998.

[19] Y. Hua, X. F. Meng, L. Y. Jia et al., "Color Doppler imaging evaluation of proximal vertebral artery stenosis," *AJR. American Journal of Roentgenology*, vol. 193, no. 5, pp. 1434–1438, 2009.

[20] G. A. Antoniou, D. Murray, G. S. Georgiadis et al., "Percutaneous transluminal angioplasty and stenting in patients with proximal vertebral artery stenosis," *Journal of Vascular Surgery*, vol. 55, no. 4, pp. 1167–1177, 2012.

[21] A. Motarjeme, J. W. Keifer, and A. J. Zuska, "Percutaneous transluminal angioplasty of the vertebral arteries," *Radiology*, vol. 139, no. 3, pp. 715–717, 1981.

[22] G. S. Storey, M. P. Marks, M. Dake, A. M. Norbash, and G. K. Steinberg, "Vertebral artery stenting following percutaneous transluminal angioplasty. Technical note," *Journal of Neurosurgery*, vol. 84, no. 5, pp. 883–887, 1996.

[23] L. H. Bonati, J. Ederle, D. J. H. McCabe et al., "Long-term risk of carotid restenosis in patients randomly assigned to endovascular treatment or endarterectomy in the Carotid and Vertebral Artery Transluminal Angioplasty Study (CAVATAS): long-term follow-up of a randomised trial," *Lancet Neurology*, vol. 8, no. 10, pp. 908–917, 2009.

[24] K. Raghuram, C. Seynnaeve, and A. T. Rai, "Endovascular treatment of extracranial atherosclerotic disease involving the vertebral artery origins: a comparison of drug-eluting and bare-metal stents," *Journal of Neurointerventional Surgery*, vol. 4, no. 3, pp. 206–210, 2012.

[25] T. Hatano, T. Tsukahara, A. Miyakoshi, D. Arai, S. Yamaguchi, and M. Murakami, "Stent placement for atherosclerotic stenosis of the vertebral artery ostium: angiographic and clinical outcomes in 117 consecutive patients," *Neurosurgery*, vol. 68, no. 1, pp. 108–116, 2011.

[26] Y. H. Lin, Y. C. Liu, W. Y. Tseng et al., "The impact of lesion length on angiographic restenosis after vertebral artery origin stenting," *European Journal of Vascular and Endovascular Surgery*, vol. 32, no. 4, pp. 379–385, 2006.

[27] Y. J. Lin, J. W. Li, M. J. Zhang et al., "The association between CYP2C19 genotype and of in-stent restenosis among patients with vertebral artery stent treatment," *CNS Neuroscience & Therapeutics*, vol. 20, no. 2, pp. 125–130, 2014.

[28] R. C. Edgell, O. O. Zaidat, R. Gupta et al., "Multicenter study of safety in stenting for symptomatic vertebral artery origin stenosis: results from the Society of Vascular and Interventional Neurology Research Consortium," *Journal of Neuroimaging*, vol. 23, no. 2, pp. 170–174, 2013.

[29] V. Parkhutik, A. Lago, J. I. Tembl, F. Aparici, V. Vazquez, and E. Mainar, "Angioplasty and stenting of symptomatic and asymptomatic vertebral artery stenosis: to treat or not to treat," *European Journal of Neurology*, vol. 17, no. 2, pp. 267–272, 2010.

[30] R. A. Taylor, F. Siddiq, M. Z. Memon et al., "Vertebral artery ostial stent placement for atherosclerotic stenosis in 72 consecutive patients: clinical outcomes and follow-up results," *Neuroradiology*, vol. 51, no. 8, pp. 531–539, 2009.

[31] W. Chen, F. Huang, M. Li et al., "Incidence and predictors of the in-stent restenosis after vertebral artery ostium stenting," *Journal of Stroke and Cerebrovascular Diseases*, vol. 27, no. 11, pp. 3030–3035, 2018.

[32] C. Matula, S. Trattnig, M. Tschabitscher, J. D. Day, and W. T. Koos, "The course of the prevertebral segment of the vertebral artery: anatomy and clinical significance," *Surgical Neurology*, vol. 48, no. 2, pp. 125–131, 1997.

[33] X. Tang, F. Tang, C. Hu, Q. Wang, W. Long, and L. Li, "Dynamic respiratory tortuosity of the vertebral artery ostium," *Journal of Endovascular Therapy*, vol. 24, no. 1, pp. 124–129, 2017.

[34] A. Qiao, X. Dai, J. Niu, and L. Jiao, "Hemodynamics in stented vertebral artery ostial stenosis based on computational fluid dynamics simulations," *Computer Methods in Biomechanics and Biomedical Engineering*, vol. 19, no. 11, pp. 1190–1200, 2016.

[35] F. C. Albuquerque, D. Fiorella, P. Han, R. F. Spetzler, and C. G. McDougall, "A reappraisal of angioplasty and stenting for the treatment of vertebral origin stenosis," *Neurosurgery*, vol. 53, no. 3, pp. 607–616, 2003.

[36] J. Lu, J. Liu, D. Wang, and S. Wang, "Stent fracture and occlusion after treatment of symptomatic vertebral artery ostium stenosis with a self-expanding device. A case report," *Interventional Neuroradiology*, vol. 20, no. 6, pp. 755–760, 2014.

[37] B. Zhang, J. Gu, M. Qian, L. Niu, H. Zhou, and D. Ghista, "Correlation between quantitative analysis of wall shear stress and intima-media thickness in atherosclerosis development in carotid arteries," *Biomedical Engineering Online*, vol. 16, no. 1, p. 137, 2017.

[38] A. Dardik, L. Chen, J. Frattini et al., "Differential effects of orbital and laminar shear stress on endothelial cells," *Journal of Vascular Surgery*, vol. 41, no. 5, pp. 869–880, 2005.

[39] D. Martin, A. Zaman, J. Hacker, D. Mendelow, and D. Birchall, "Analysis of haemodynamic factors involved in carotid atherosclerosis using computational fluid dynamics," *The British Journal of Radiology*, vol. 82, no. special_issue_1, pp. S33–S38, 2009.

Hindawi
BioMed Research International
Volume 2021, Article ID 6626604, 8 pages
https://doi.org/10.1155/2021/6626604

Research Article

The Natural History and Reperfusion Therapy Outcomes of Acute Ischemic Stroke due to Isolated M2 Occlusions

Hongmin Gong,[1,2] Libo Zhao,[1,2] Ge Tang,[1,2] Yu Chen,[1,2] Deyu Yang,[1,2] and Shudong Liu [1,2]

[1]*Department of Neurology, Yongchuan Hospital of Chongqing Medical University, Chongqing 402160, China*
[2]*Chongqing Key Laboratory of Cerebrovascular Disease Research, Chongqing 402160, China*

Correspondence should be addressed to Shudong Liu; shudongliu@live.cn

Received 27 December 2020; Revised 1 April 2021; Accepted 16 April 2021; Published 27 April 2021

Academic Editor: Xiangyu Cao

Objective. Currently, the standard treatment modality for patients with acute ischemic stroke (AIS) presenting with isolated M2 occlusions is not specific. We therefore assessed the difference in treatment outcomes for patients with isolated M2 occlusions. *Methods*. We retrospectively analyzed consecutive patients with AIS presenting with isolated M2 occlusions from October 1, 2018, to June 30, 2020. Patients were divided into 3 groups based on the treatments they received: no reperfusion therapy (NRT), intravenous thrombolysis treatment (IVT), and endovascular intervention (EVT), which comprised IVT in conjunction with EVT or EVT alone. The primary outcomes were improvements in modified Rankin Scale (mRS) scores at 90 days and National Institutes of Health Stroke Scale (NIHSS) scores at 24 hours after treatment compared with the baseline. The secondary efficacy outcome comprised a good outcome rate defined as a 90 – day mRS score ≤ 2, final infarct volume (FIV), 90-day mortality rate, and successful recanalization rate, which was defined as a modified thrombolysis in cerebral infarction score ≥ 2b. Safety outcomes included symptomatic intracerebral hemorrhage and procedure-related complications. *Results*. Seventy patients were enrolled and divided into 3 groups: the NRT group ($n = 25$), IVT group ($n = 27$), and EVT group ($n = 18$). Twenty-four-hour posttreatment NIHSS scores were substantially decreased by EVT compared with NRT (adjusted β -4.01, 95% confidence interval [CI] -6.60 to -1.43; $P = 0.003$) or IVT (adjusted β, -3.61 [95% CI, -6.45 to -0.77]; $P = 0.013$). Compared with the outcomes observed after NRT, patients who received EVT were more likely to achieve lower 90-day mRS scores (adjusted β, -1.42 [95% CI, -2.66 to -0.63]; $P = 0.007$), higher good outcome rates (adjusted odds ratio, 8.73 [95% CI, 1.43-53.24]; $P = 0.019$), and smaller FIVs (adjusted β, -29.66 [95% CI, -59.73 to 0.42]; $P = 0.048$). The recanalization rate of EVT was high (88.89%), and procedure-related complications were rare (5.56%). *Conclusions*. For acute, isolated M2 occlusions, EVT could dramatically and rapidly improve neurological deficits with high safety and effectiveness. These changes were observed at 24 hours after treatment and were maintained over the long term.

1. Introduction

M2 occlusions are an important subgroup of anterior circulation vessel occlusions, accounting for 38.1% [1]. The outcome of patients with M2 occlusions is believed to be good and superior to that of patients with large vessel occlusions (LVOs) in the anterior circulation [2]. Actually, the outcome is much worse if no vascularization therapies are applied [1, 3].

Endovascular intervention (EVT) has become the standard first-line treatment for patients with acute ischemic stroke (AIS) presenting with LVO in the anterior circulation [4–9]. These studies mainly focused on proximal intracranial artery occlusions but largely ignored M2 occlusions. Thus, physicians questioned the efficacy and safety of EVT for patients with distal occlusions. Some analyses subsequently showed that patients with M2 occlusions might benefit from EVT if they met the EVT trial protocols. However, the studies were retrospective analysis and post hoc analysis rather than randomized controlled study, the evidence applied was insufficient [10, 11]. In addition, the treatment methods applied in the control group consisted of conventional medicinal treatment and intravenous tissue plasminogen activator (t-PA),

and the favorable response of distal occlusions to t-PA was neglected [12]. Confusion remains regarding the appropriate treatment for M2 occlusions.

We compared the comprehensive presentation, imaging, and clinical outcomes of patients who received no reperfusion therapy (NRT) as a control group with patients who received IVT alone and patients who received EVT, intending to provide evidence to clinical physicians that would enable them to choose an effective and safe treatment for isolated M2 occlusions.

2. Subjects and Methods

2.1. Subjects. After obtaining institutional review committee approval, we performed a retrospective cohort analysis of patients with AIS who presented with isolated M2 occlusions at the Yongchuan Hospital of Chongqing Medical University from October 1, 2018, to June 30, 2020. The inclusion criteria included time from last normal appearance to first computed tomographic angiography [CTA] of <24 hours, CTA-diagnosed isolated M2 occlusion, >18 years of age, National Institutes of Health Stroke Scale [NIHSS] score at admission ≥ 6 points, and available follow-up data within 90 days. Patients with a premorbid modified Rankin Scale (mRS) score of ≥3 points ($n = 2$), patients who lacked follow-up (within 2-7 days after admission) imaging data (including computed tomography [CT] or magnetic resonance imaging [MRI]) ($n = 8$), or patients whose previous intracranial lesions were affected when calculating the final infarct volume (FIV) due to this stroke ($n = 2$) were excluded. Finally, 70 patients with AIS presenting with isolated M2 occlusions were included and divided into 3 groups: the NRT group ($n = 25$), IVT group ($n = 27$), and EVT group ($n = 18$). Patients who neither met the intravenous thrombolysis criterion of the Chinese Guidelines for the Diagnosis and Treatment of Acute Ischemic Stroke 2018 nor met the indications for EVT in our study and those who met the criterion listed above but refused the two reperfusion treatments were enrolled in the NRT group. All patients in the IVT group met the criterion and agreed to receive IVT. Those who received IVT followed by EVT were included in the EVT group rather than the IVT group. Patients were eligible for EVT if the time from the last normal appearance to femoral artery puncture ≤ 24 hours, preoperative NIHSS score ≥ 6, and RAPID software (iSchemaView) estimated the following CT perfusion (CTP) data: initial infarct volume (ischemic core) < 70 ml, a ratio of the volume of ischemic tissue to initial infarct volume of ≥1.8, and an absolute volume of potentially reversible ischemia (penumbra) of ≥15 ml [8].

All enrolled patients received a head CT scan and CT angiography (CTA) of the head and neck at admission. Once CTA diagnosed M2 occlusions, CTP was essential to estimate the EVT criterion. Within the next 2-7 days after admission, a cranial MRI or CT scan was essential to calculate the final infarct volume (FIV). Information on baseline demographics, vascular risk factors (diabetes mellitus, hypertension, atrial fibrillation, hyperlipidemia, smoking, and congestive heart failure), current medications, including antiplatelet drugs and statins, blood glucose level at admission, time from symptom onset to treatment (the treatment referring to the initial antiplatelet drug treatment in the NRT group, venipuncture in the IVT group, and femoral artery puncture in the EVT group), and hospitalization days were collected from admission and discharge records.

The NIHSS score (range of 0-42 points, with higher scores indicating more serious stroke severity) at admission and at 24 hours posttreatment and the mRS score (range of 0-6 points, with higher scores indicating worse outcomes; a good outcome was defined as a mRS score of 0-2) at admission and at 90 days after symptom onset were assessed by a trained neurological physician who was blinded to the imaging data.

2.2. Study Treatment and Intervention. Patients in the NRT group received conservative medicinal treatment. In the IVT group, patients presenting within the first 4.5 hours from the last normal appearance were intravenously administered a full dose (0.9 mg per kilogram) of t-PA. In the EVT group, subjects who received IVT did not undergo heparinization, and a heparin infusion was administered at a dose of 70 U/kg at initiation of the procedure in those who had not received IVT. Before the thrombectomy procedure, three-dimensional digital subtraction angiography (3D-DSA) was performed under local anesthesia to identify the specific occlusion site and the morphology of the M2 segment. A direct first pass aspiration technique (ADAPT) was first considered during the thrombectomy procedure. If the M2 segment failed to be recanalized after three attempts, then a stent retriever was used as a rescue therapy. The devices used included Penumbra 3Max/4Max catheters and SOLITAIRE™ AB retrievers. 3D-DSA was performed again at the end of the operation to evaluate the recanalization status.

2.3. Neuroimaging Review. The occlusive site was defined by two authors based on the initial CTA. The beginning of the M2 segment was defined as the vertical segment lying within the mesial margin of the sylvian fissure at the CTA coronal position. Regional leptomeningeal scores (rLMCs, scores ranging from 0-20 points, with higher scores indicating better collateral circulation) were obtained at the coronal and horizontal planes of the initial CTA [13]. FIV was measured on follow-up (within the next 2-7 days after admission) MRI (diffusion-weighted [DWI] sequence) or CT images. We outlined the area of the infarct on each slice using the Mimics software and then summed the individual slice thicknesses of all outlined areas [13]. If the CT or MRI images completed within 7 days after treatment suggested cerebral hemorrhage, it was defined as symptomatic intracerebral hemorrhage (sICH) with an NIHSS score that increased by ≥4 points from baseline; otherwise, it was defined as asymptomatic intracerebral hemorrhage (aICH). For the EVT group, the rate of successful recanalization (defined as a modified thrombolysis in cerebral ischemia [mTICI] score ≥ 2b) and the occurrence of procedure-related complications was determined from postprocedure images of catheter-based angiograms [14]. Two neuroradiologists who were blinded to the group assignments, clinical data, and outcomes independently estimated all neuroimaging findings. The third experienced

Table 1: Baseline patient characteristics.

Characteristics	NRT ($n = 25$)	IVT ($n = 27$)	EVT ($n = 18$)	$F/Z/\chi 2$	P value
Age, mean ± SD, years	75.16 ± 7.60	79.41 ± 7.36	67.61 ± 11.43	12.42[a]	<0.01
Male (%)	13 (52)	12 (44.44)	11 (61.11)	1.21[b]	0.547
Left hemisphere (%)	17 (68)	15 (55.56)	13 (72.22)	1.54[b]	0.463
rLMCs, median (IQR)	15 (12, 17)	17 (14.7, 19)	16 (14, 18)	4.76[a]	0.105
Admission NIHSS score, median (IQR)	12 (7.5, 20.5)	11 (9, 15)	14 (9, 17.5)	2.42[a]	0.298
Admission NIHSS score stratification (%)					
<13	13 (52)	18 (66.67)	8 (44.44)		
13-19	5 (20)	9 (33.33)	9 (50)	4.70[c]	0.095
≥ 20	7 (28)	0	1 (5.56)		
Vascular risk factors					
Hypertension (%)	15 (60)	11 (40.74)	5 (27.78)	4.63[b]	0.099
Diabetes (%)	4 (16)	6 (22.22)	5 (27.78)	0.88[b]	0.644
Hyperlipidemia (%)	8 (32)	3 (11.11)	7 (38.89)	5.17[b]	0.076
Coronary heart disease (%)	3 (12)	8 (29.63)	4 (22.22)	2.41[b]	0.30
Congestive heart failure (%)	5 (20)	2 (7.41)	5 (27.78)	3.47[d]	0.171
Atrial fibrillation (%)	8 (32)	8 (29.63)	10 (55.56)	3.55[b]	0.186
History of ischemic stroke (%)	4 (16)	4 (14.81)	1 (5.56)	1.13[d]	0.668
Drinking (%)	1 (4)	2 (7.41)	3 (16.67)	2.08[d]	0.428
Smoking (%)	4 (16)	3 (11.11)	6 (33.33)	3.42[d]	0.166
Antiplatelet drugs are currently used (%)	1 (4)	0	3 (16.67)	4.62[d]	0.059
Statins are currently used (%)	1 (4)	0	3 (16.67)	4.62[d]	0.059
Admission serum glucose level, mean ± SD, mmol/l	8.06 ± 4.72	7.58 ± 2.39	7.71 ± 2.43	0.42[a]	0.81
Admission systolic blood pressure, mean ± SD, mmHg	156.8 ± 25.7	154 ± 22.06	142.67 ± 18.77	2.19[e]	0.12
Hospitalization days, mean ± SD	13.04 ± 4.95	11.70 ± 5.04	11.06 ± 4.54	0.95[e]	0.39
Time from onset to treatment, median (IQR), min	370 (230.5, 820.5)	154 (125.0, 238.0)	272.5 (183.8, 386.3)	20.80[a]	<0.01

Abbreviations: NRT: no reperfusion therapy; IVT: intravenous thrombolysis treatment; EVT: endovascular intervention; rLMCs: regional leptomeningeal score; NIHSS: National Institutes of Health Stroke Scale; SD: standard deviation; IQR: interquartile range. [a]Kruskal-Wallis test; [b]χ^2 test; [c]rank sum test; [d]Fisher's exact probability method; [e]ANOVA.

neuroradiologist was in charge of resolving cases in which a disagreement occurred.

2.4. Clinical and Radiological Variables. The delta NIHSS score (change in the NIHSS score from baseline at 24 h) and 90-day modified Rankin Scale score (mRS, range of 0 to 6 points, an excellent outcome was defined as an mRS score of 0-1, a good outcome was defined as an mRS score of 0-2, a bad outcome was defined as a mRS score of 3-5, and a mRS score of 6 referred to death) were the primary efficacy outcomes. The secondary efficacy outcomes included the 90-day good outcome rate (mRS score of 0-2), 90-day mortality rate, FIV, and successful recanalization rate. The safety outcomes included sICH and procedure-related complications.

2.5. Statistical Analysis. We compared baseline characteristics and clinical outcomes between the 3 groups. Continuous variables are presented as the means with standard deviations (SD) or medians and interquartile ranges (IQRs), and comparisons were performed using the Kruskal-Wallis test or analysis of variance (ANOVA). Categorical variables are reported as percentages [numbers (%)], and comparisons were performed using Fisher's exact probability method and χ^2 test, as appropriate. The rank sum test was used for grade data. The difference in the NIHSS score between baseline and 24 hours after treatment in each group was investigated using the Mann-Whitney U test. We performed two logistic regression analyses, linear regression, and binary logistic regression analyses, to determine the efficacy outcomes. The distributions of 90-day mRS scores, delta NIHSS scores, and FIVs were estimated using linear regression analyses. A 90-day mRS score of 0-2 was estimated using a binary logistic regression analysis. Adjusted estimates of outcome (common odds ratio and β) were calculated by considering the following variables: age, baseline NIHSS scores, and time

Table 2: Multiple comparisons based on age and time from onset to treatment.

Characteristics	NRT vs. IVT	NRT vs. EVT	IVT vs. EVT
Age, years	0.073*	0.065*	<0.001*
Time from onset to treatment, min	<0.001*	0.279*	<0.001*

*P value.

Table 3: Efficacy and safety outcomes according to treatment methods.

Characteristic	NRT	IVT	EVT	Unadjusted value (95% CI); *P* value	Adjusted value (95% CI)†: *P* value
Primary efficacy outcome					
Delta NIHSS score, median (IQR)	-1 (-2.5 to 0)	-3 (-6 to 0)	-5 (-10.25 to -3.75)	-0.98 (-3.18 to 1.22); $P = 0.38^{*}$	-0.40 (-2.89 to 2.09); $P = 0.750^{*}$
				-4.26 (-6.71 to -1.81); $P = 0.001^{\#}$	-4.01(-6.60 to -1.43); $P = 0.003^{\#}$
				-3.28 (-5.69 to -0.87); $P = 0.008^{\blacktriangle}$	-3.61 (-6.45 to -0.77); $P = 0.013^{\blacktriangle}$
90-day mRS score, median (IQR)	4 (1, 5)	2 (1, 3)	1 (1, 2)	-1.13 (-2.04 to -0.22); $P = 0.016^{*}$	-0.67 (-1.65 to 0.32); $P = 0.181^{*}$
				-1.64 (-2.66 to -0.63); $P = 0.002^{\#}$	-1.42 (-2.43 to -0.40); $P = 0.007^{\#}$
				-0.52 (-1.52 to 0.48); $P = 0.303^{\blacktriangle}$	-0.75 (-1.87 to 0.37); $P = 0.185^{\blacktriangle}$
Secondary efficacy outcomes					
90-day mRS score 0-2 (%)	11 (44.00)	20 (74.07)	16 (88.89)	3.64 (1.13-11.69); $P = 0.03^{*}$	2.23 (0.51-9.64); $P = 0.284^{*}$
				10.18 (1.92-54.02); $P = 0.006^{\#}$	8.73 (1.43-53.24); $P = 0.019^{\#}$
				2.80 (0.51-15.38); $P = 0.236^{\blacktriangle}$	6.38 (0.41-99.12); $P = 0.186^{\blacktriangle}$
FIV, median (IQR), ml	50.93 (8.55, 112.75)	30.77 (8.75, 55.270)	26.08 (6.78, 53.63)	-43.28 (-72.97 to -13.59); $P = 0.005^{*}$	-8.63 (-37.67 to 20.41); $P = 0.555^{*}$
				-37.24 (-70.32 to -4.17); $P = 0.028^{\#}$	-29.66 (-59.73 to 0.42); $P = 0.048^{\#}$
				6.04(-26.52 to 38.59); $P = 0.713^{\blacktriangle}$	-21.03 (-54.12 to 12.07); $P = 0.209^{\blacktriangle}$
90-day mortality rate (%)	6 (24)	2 (7.41)	0	NA	NA
mTICI ≥ 2b (%)	-	-	16 (88.89)	NA	NA
Safety outcomes					
sICH (%)	0	4 (14.81)	0	NA	NA
Procedure-related complications (%)	-	-	1 (5.56)	NA	NA

Abbreviations: NRT: no reperfusion therapy; IVT: intravenous thrombolysis treatment; EVT: endovascular intervention; NIHSS: National Institutes of Health Stroke Scale; IQR: interquartile range; mRS: modified Rankin Scale; sICH: symptomatic intracerebral hemorrhage; aICH: asymptomatic intracerebral hemorrhage; mTICI: modified thrombolysis in cerebral ischemia score; FIV: final infarct volume (within 2-7 days after symptom onset); NA: not applicable; delta NIHSS score: change in the NIHSS score from baseline to 24 h. †Model adjusted for age, admission NIHSS score, and time from onset to treatment. *A comparison was conducted between the NRT and IVT groups, and #comparison conducted between the NRT and EVT groups. ▲A comparison was conducted between the IVT and EVT groups.

from symptom onset to treatment. A *P* value <0.05 was considered significant. All analyses were conducted using the SPSS 23.0 software (IBM SPSS Statistics, Armonk, NY).

3. Results

3.1. Baseline Characteristics. Seventy patients (36 males [51.43%]; 34 females [48.57%]; mean [SD] age, 74.86 [9.72] years) were included in the analysis, of whom 25 received NRT, 27 received only IVT, and 18 received EVT. Of the 25 patients who did not receive IVT in the NRT group, 16 patients had a long interval from the last known normal appearance to treatment, 3 patients had a large FIV at admission, 1 patient achieved a significant improvement in neurological deficit as soon as the head CT was complete, and the remaining 3 patients met the indications but refused IVT. Of the 18 patients in the EVT group, 11 patients were treated with IVT in conjunction with EVT, as they did not achieve immediate and significant improvement in neurological deficit and the DSA suggested that the M2 segment was still occluded before the endovascular procedure. Another 7 patients were treated with EVT alone. Only 1 of 16 patients who received a direct first pass aspiration technique (ADAPT) failed to achieve successful recanalization after three attempts and then received stent retriever as a rescue therapy; 2 patients only received a stent retriever.

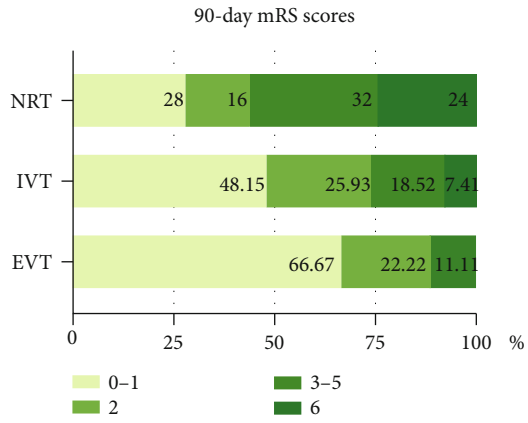

Figure 1: Distribution of mRS scores at 90 days in the three groups. Notes: proportion of mRS scores at 90 days in patients in the NRT, IVT, and EVT groups. NRT: no reperfusion therapy; IVT: intravenous thrombolysis treatment; EVT: endovascular intervention; mRS: modified Rankin Scale. A 90-day mRS score of 0-1 was defined as an excellent outcome, an mRS score of 0-2 was defined as a good outcome, an mRS score of 3-5 was defined as a bad outcome, and an mRS score of 6 referred to death.

Table 1 shows the baseline characteristics. Patients in the EVT group were younger (EVT vs. NRT, 67.61 [±11.43] vs. 75.16 [±7.60] years, $P = 0.065$; EVT vs. IVT, 67.61 [±11.43] vs. 79.41 [±7.36] years, $P < 0.001$). The time from symptom onset to treatment of patients in the IVT group (154 [125.0, 238.0], min) was shorter than that in the NRT group (370 [230.5, 820.5], min; $P < 0.001$) and the EVT group (272.5 [183.8, 386.3], min; $P < 0.001$) (Table 2). Otherwise, no significant differences were observed in sex, rLMCs, vascular risk factors, drugs currently used, admission serum glucose levels and systolic blood pressure, or hospitalization days.

3.2. Clinical Outcomes. Table 3 shows the efficacy and safety outcomes. The median 90-day mRS score was 4 (IQR, 1-5) in the NRT group, 2 (IQR, 1-3) in the IVT group, and 1 (IQR, 1-2) in the EVT group. A trend toward lower disability grades was observed in patients who received reperfusion treatments (unadjusted β values of -1.13 and -1.64, respectively; P values were all <0.05) (Table 3 and Figure 1). However, after adjustment for age, the NIHSS score at admission, and time from onset to treatment, we only showed a significant difference favoring EVT, with an adjusted β value of -1.42 (95% confidence interval [CI], -2.66 to -0.63; $P = 0.007$). The most dramatic difference in the NIHSS score at 24 hours after treatment from baseline was detected in the EVT group (median NIHSS score of 6 vs. 14; $P < 0.001$) (Figure 2). Compared with the NRT group (adjusted β -4.01 [95% CI, -6.60 to -1.43], $P = 0.003$) and the IVT group (adjusted β -3.61 [95% CI, -6.45 to -0.77], $P = 0.013$), the value was greater in the EVT group. Compared with the NRT group, the 90-day good outcome (mRS 0-2) rate (88.89% vs. 44.00%] adjusted OR 8.73 [95% CI, 1.43-53.24; $P = 0.019$]) was higher and the FIV within 7 days after treatment (50.93 [8.55, 112.75] vs. 26.08 [6.78, 53.63]; adjusted β -29.66 [95% CI, -59.73 to 0.42]; $P = 0.048$) was smaller in the EVT group. The recanalization rate in the EVT group was high (88.89%). The 90-day mortality rate in the NRT group was higher than that in the other 2 groups (NRT vs. IVT vs. EVT, 24% vs. 7.41% vs. 0%).

Regarding safety outcomes, patients in the IVT group were more vulnerable to sICH (NRT vs. IVT vs. EVT, 0% vs. 14.81% vs. 0%) (Table 3). Only 1 of the 18 patients who received EVT (5.56%) had a procedure-related complication, namely, vessel perforation. The M2 segment was perforated when the operator delivered the 3Max catheter to the terminus of the M1 segment and intended to move the catheter toward the occluded M2 segment. After stopping the superselection and starting digital subtraction angiography (DSA), contrast was extravasating from the perforated vessel, the operator terminated the operation immediately, and M2 therefore failed to be recanalized. The postprocedure CT of this patient showed minor subarachnoid hemorrhage, and the neurological deficit did not deteriorate, whereas the 90-day mRS score was 5.

4. Discussion

This retrospective, observational study analyzed consecutive patients who presented with acute symptomatic M2 occlusions. In our study, only 44% (11/25) of patients who received NRT achieved good outcomes at 90 days, and the mortality rate at 90 days reached 24% (6/25), similar to the results reported previously, where the 90-day good outcome rate ranged from 45.8 to 47.3% and the mortality rate at 6 months reached 20.8% [1, 3]. This finding revealed the severely poor natural history of patients with isolated M2 occlusions. Patients who received reperfusion treatment, either IVT or EVT, had a tendency toward achieving good functional outcomes at 90 days. In particular, patients treated with EVT were more likely to achieve an improvement in neurological deficits with high effectiveness and safety, which was observed at 24 hours after treatment and was maintained over the long term.

Our study suggested that the FIV of patients who received EVT was significantly smaller and that the 90-day functional outcomes were better than those of patients who received NRT. A smaller infarct volume was indicated to be associated with better functional outcomes [15]. Thus, the effect of EVT on functional outcome was possibly mediated by decreasing the FIV. However, the study was underpowered to draw the conclusion, as no causal mediation model was constructed in our study. As shown in the study by Compagne et al., preventing FIV progression only partially explains the beneficial effect of EVT on outcomes using mediation analysis [16]. The reperfusion of some key regions, such as the lateral fissure in the dominant hemisphere and the M3 and M6 regions in the Alberta Stroke Program Early CT Score, probably played a crucial role in favorable functional outcomes [17].

In our analysis, the change in NIHSS score from baseline to 24 hours after treatment in the IVT group was significant, and most patients (20/27, 74.07%) achieved good 90-day functional outcomes. Distal intracranial vessel occlusions responded well to t-PA with a high recanalization rate of

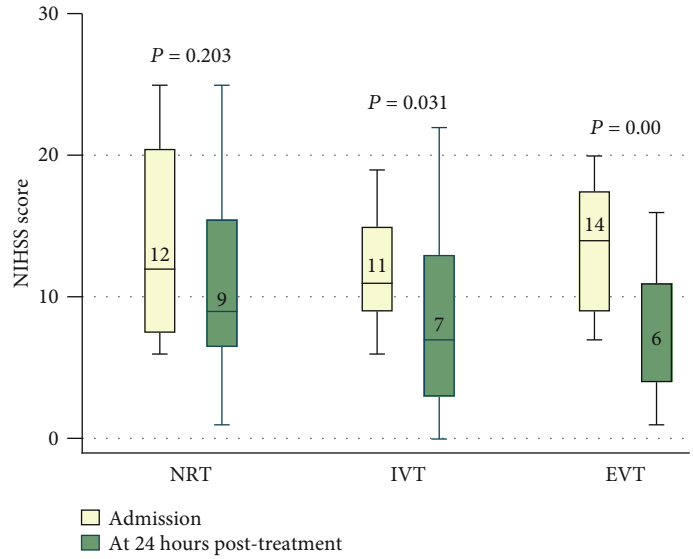

Figure 2: Comparison of NIHSS scores among the three groups. Notes: box and whisker plots comparing median NIHSS scores at admission and 24 hours after treatment in the no reperfusion therapy (NRT), intravenous thrombolysis treatment (IVT), and endovascular intervention (EVT) groups. The horizontal line in the middle of each box represents the median, and the upper and lower boundaries of the box represent the 75th percentile and 25th percentile, respectively. The whiskers above and below the box indicate the 90th and 10th percentiles, respectively.

30.8–68.4%, which is strongly associated with a 90-day good outcome, even when it occurs two hours after the t-PA bolus [18–22]. We therefore hypothesized that some patients who received only IVT had achieved successful recanalization after treatment. However, we were unable to determine whether the M2 segment recanalized due to the lack of follow-up vascular imaging. Furthermore, as the process of recanalization with intravenous t-PA was continuous over time, the time from t-PA bolus administration to recanalization assessment was associated with successful recanalization (odds ratio, 1.28 for every 30-minute increase in time [95% CI, 1.18-1.38]) [19]. This finding would raise concern about the time within which the follow-up vascular imaging should be completed after the administration of the t-PA bolus and the time at which the vessel recanalized would contribute to good outcomes.

Evidence has shown the benefit of EVT for M2 segment occlusions compared with the best medical treatment or M1 segment [11, 23]. Moreover, the 2 mechanical thrombectomy techniques most frequently utilized to treat M2 occlusions, ADAPT and stent retriever, did not differ in rates of 90-day good outcomes, sICH, successful recanalization, or mortality [24, 25]. In our study, the successful recanalization rate of patients who mainly received ADAPT reached 88.89% without sICH occurrence. In previous studies, the successful recanalization rate in the ADAPT group was lower (70.3-85.4%), and the sICH rate was higher (5.3-5.6%) [24, 25]. We hypothesized that the prioritization of effectiveness and safety in our study might be associated with the 3D-DSA used in the process of operation, which is often used in the diagnosis and treatment of cerebral aneurysms but is rarely mentioned in the process of EVT [26–28]. The M2 segment usually consists of 6-8 branches, and each branch has a different morphology and diameter, resulting in overlapping images on traditional two-dimensional digital subtraction angiography (2D-DSA), which would increase the operational difficulty and decrease the possibility of recanalization. 3D-DSA is helpful to observe the occluded M2 segment at some angles and planes that were missed using 2D-DSA. Further, random controlled trial to compare only EVT with EVT plus 3D-DSA in patients with acute M2 occlusions is probably a priority.

In our study, the 90-day good outcome rates in the IVT group and EVT group both were high (74.07% vs. 88.89%) and the difference between the two groups was not significant ($P = 0.186$). Patients received reperfusion treatment, either IVT or EVT, had a tendency toward achieving 90-day good functional outcomes. But on the other hand, the ability of EVT to decrease the NIHSS score at 24 hours after treatment from baseline was more significant than IVT (adjusted β -3.61 (-6.45 to -0.77); $P = 0.013$). Therefore, we recommend that EVT should be performed when a neurological improvement is not apparent after IVT.

Our study has several limitations. First, our study is a post hoc analysis and has all the limitations of a nonrandomized study. Second, we enrolled a relatively small number of patients, especially patients who received EVT, resulting in poorly balanced NIHSS score strata and the lack of stratification of patients in the EVT group for IVT. Third, follow-up vascular images captured after treatment were lacking in the NRT and IVT groups, thus leaving a gap in our understanding of the relationship between clinical recovery and successful reperfusion. Fourth, the outcomes of patients in different NIHSS score strata were not analyzed, and we were unable to recommend the NIHSS score strata within which IVT or EVT should be performed.

In summary, the natural history of patients with isolated M2 occlusions was very poor. The EVT modality dramatically and rapidly improved the clinical outcomes with higher safety and effectiveness, and the changes were present at 24 hours after treatment and maintained over the long term.

Data Availability

If necessary, we can provide the crude data via the E-mail of corresponding author.

Conflicts of Interest

The authors declare that the research was conducted in the absence of any commercial or financial relationships that could be construed as a potential conflict of interest.

Authors' Contributions

The study design and assignments were decided by the corresponding author, Dr. Shudong Liu. All neuroimagings were independently evaluated by two neuroradiologists, Ge Tang and Dr. Deyu Yang. And Dr. Libo Zhao was in charge of cases with disagreements. NIHSS scores and mRS scores were assessed by Dr. Yu Chen, who was blinded to the imaging result. After analyzing all of the data, Hongmin Gong wrote the manuscript. Dr. Shudong Liu took responsibility for critical revision of the manuscript.

Acknowledgments

This study was supported by the Chongqing Science and Health Joint Medical Research Project (grant no. 2019QNXM014) and Yongchuan District Jointly Funded Science and Technology Project (grant no. 2019nb0206).

References

[1] F. O. Lima, K. L. Furie, G. S. Silva et al., "Prognosis of untreated strokes due to anterior circulation proximal intracranial arterial occlusions detected by use of computed tomography angiography," *JAMA Neurology*, vol. 71, no. 2, pp. 151–157, 2014.

[2] S. A. Sheth, B. Yoo, J. L. Saver et al., "M2 occlusions as targets for endovascular therapy: comprehensive analysis of diffusion/perfusion MRI, angiography, and clinical outcomes," *Journal of NeuroInterventional Surgery*, vol. 7, no. 7, pp. 478–483, 2015.

[3] M. Hernández-Pérez, N. Pérez de la Ossa, A. Aleu et al., "Natural history of acute stroke due to occlusion of the middle cerebral artery and intracranial internal carotid artery," *Journal of Neuroimaging*, vol. 24, no. 4, pp. 354–358, 2014.

[4] B. C. Campbell, P. J. Mitchell, T. J. Kleinig et al., "Endovascular therapy for ischemic stroke with perfusion-imaging selection," *The New England Journal of Medicine*, vol. 372, no. 11, pp. 1009–1018, 2015.

[5] T. G. Jovin, A. Chamorro, E. Cobo et al., "Thrombectomy within 8 hours after symptom onset in ischemic stroke," *The New England Journal of Medicine*, vol. 372, no. 24, pp. 2296–2306, 2015.

[6] S. Bracard, X. Ducrocq, J. Mas et al., "Mechanical thrombectomy after intravenous alteplase versus alteplase alone after stroke (THRACE): a randomised controlled trial," *Lancet Neurology*, vol. 15, no. 11, pp. 1138–1147, 2016.

[7] R. G. Nogueira, A. P. Jadhav, D. C. Haussen et al., "Thrombectomy 6 to 24 hours after stroke with a mismatch between deficit and infarct," *The New England Journal of Medicine*, vol. 378, no. 1, pp. 11–21, 2018.

[8] G. W. Albers, M. P. Marks, S. Kemp et al., "Thrombectomy for stroke at 6 to 16 hours with selection by perfusion imaging," *The New England Journal of Medicine*, vol. 378, no. 8, pp. 708–718, 2018.

[9] M. Goyal, B. K. Menon, W. H. van Zwam et al., "Endovascular thrombectomy after large-vessel ischaemic stroke: a meta-analysis of individual patient data from five randomised trials," *Lancet*, vol. 387, no. 10029, pp. 1723–1731, 2016.

[10] A. Sarraj, N. Sangha, M. S. Hussain et al., "Endovascular therapy for acute ischemic stroke with occlusion of the middle cerebral artery M2 segment," *JAMA Neurology*, vol. 73, no. 11, pp. 1291–1296, 2016.

[11] B. K. Menon, M. D. Hill, A. Davalos et al., "Efficacy of endovascular thrombectomy in patients with M2 segment middle cerebral artery occlusions: meta-analysis of data from the HERMES Collaboration," *Journal of NeuroInterventional Surgery*, vol. 11, no. 11, pp. 1065–1069, 2019.

[12] A. I. Qureshi, M. A. Saleem, and E. Aytac, "Comparison of endovascular treatment with intravenous thrombolysis for isolated M2 segment of middle cerebral artery occlusion in acute ischemic stroke," *Journal of Vascular and Interventional Neurology*, vol. 9, no. 5, pp. 8–14, 2017.

[13] B. K. Menon, E. E. Smith, J. Modi et al., "Regional leptomeningeal score on CT angiography predicts clinical and imaging outcomes in patients with acute anterior circulation occlusions," *AJNR. American Journal of Neuroradiology*, vol. 32, no. 9, pp. 1640–1645, 2011.

[14] S. Rangaraju, K. Owada, A. R. Noorian et al., "Comparison of final infarct volumes in patients who received endovascular therapy or intravenous thrombolysis for acute intracranial large-vessel occlusions," *JAMA Neurology*, vol. 70, no. 7, pp. 831–836, 2013.

[15] M. Khan, R. P. Goddeau Jr, J. Zhang, M. Moonis, and N. Henninger, "Predictors of outcome following stroke due to isolated M2 occlusions," *Cerebrovascular Diseases Extra*, vol. 4, no. 1, pp. 52–60, 2014.

[16] for the MR CLEAN Investigators, K. C. J. Compagne, A. M. M. Boers et al., "Follow-up infarct volume as a mediator of endovascular treatment effect on functional outcome in ischaemic stroke," *European Radiology*, vol. 29, no. 2, pp. 736–744, 2019.

[17] M. Khan, G. L. Baird, R. P. Goddeau Jr., B. Silver, and N. Henninger, "Alberta stroke program early CT score infarct location predicts outcome following M2 occlusion," *Frontiers in Neurology*, vol. 8, p. 98, 2017.

[18] B. Campbell, P. J. Mitchell, L. Churilov et al., "Tenecteplase versus alteplase before thrombectomy for ischemic stroke," *The New England Journal of Medicine*, vol. 378, no. 17, pp. 1573–1582, 2018.

[19] B. K. Menon, F. S. al-Ajlan, M. Najm et al., "Association of clinical, imaging, and thrombus characteristics with recanalization of visible intracranial occlusion in patients with acute ischemic stroke," *Journal of the American Medical Association*, vol. 320, no. 10, pp. 1017–1026, 2018.

[20] R. Bhatia, M. D. Hill, N. Shobha et al., "Low rates of acute recanalization with intravenous recombinant tissue plasminogen

activator in ischemic stroke: real-world experience and a call for action," *Stroke*, vol. 41, no. 10, pp. 2254–2258, 2010.

[21] J. Aoki, K. Suzuki, T. Kanamaru et al., "Impact of complete recanalization on clinical recovery in cardioembolic stroke patients with M2 occlusion," *Journal of the Neurological Sciences*, vol. 415, p. 116873, 2020.

[22] M. Ribo, J́. Alvarez-Sabín, J. Montaner et al., "Temporal profile of recanalization after intravenous tissue plasminogen Activator," *Stroke*, vol. 37, no. 4, pp. 1000–1004, 2006.

[23] J. M. Coutinho, D. S. Liebeskind, L. A. Slater et al., "Mechanical thrombectomy for isolated M2 occlusions: a post hoc analysis of the STAR, SWIFT, and SWIFT PRIME studies," *AJNR. American Journal of Neuroradiology*, vol. 37, no. 4, pp. 667–672, 2016.

[24] K. Atchaneeyasakul, A. M. Malik, D. R. Yavagal et al., "Thrombectomy outcomes in acute ischemic stroke due to middle cerebral artery M2 occlusion with stent retriever versus aspiration: a multicenter experience," *Interventional Neurology*, vol. 8, no. 2-6, pp. 180–186, 2020.

[25] B. Lapergue, R. Blanc, B. Gory et al., "Effect of endovascular contact aspiration vs stent retriever on revascularization in patients with acute ischemic stroke and large vessel occlusion: the ASTER randomized clinical trial," *Journal of the American Medical Association*, vol. 318, no. 5, pp. 443–452, 2017.

[26] S. C. Wong, O. Nawawi, N. Ramli, and K. A. Abd Kadir, "Benefits of 3D rotational DSA compared with 2D DSA in the evaluation of intracranial aneurysm," *Academic Radiology*, vol. 19, no. 6, pp. 701–707, 2012.

[27] M. S. Pearl, C. Torok, Z. Katz et al., "Diagnostic quality and accuracy of low dose 3D-DSA protocols in the evaluation of intracranial aneurysms," *Journal of NeuroInterventional Surgery*, vol. 7, no. 5, pp. 386–390, 2015.

[28] S. Jiao, L. Gong, Z. Wu et al., "Assessment of the value of 3D-DSA combined with neurointerventional thrombolysis in the treatment of senile cerebrovascular occlusion," *Experimental and Therapeutic Medicine*, vol. 19, no. 2, pp. 891–896, 2020.

Hindawi
BioMed Research International
Volume 2021, Article ID 5564462, 4 pages
https://doi.org/10.1155/2021/5564462

Research Article

Renal Arteriography via Radial Artery Access with a 125 cm Long Angiographic Catheter

Ji-Xuan Liu,[1] **Zhi-Jun Sun**,[2] **and Jin-Da Wang**[2]

[1]*Department of Cardiology, Beijing Friendship Hospital, Capital Medical University, Beijing 100050, China*
[2]*Department of Cardiology, The Sixth Medical Centre of PLA General Hospital, Beijing 100853, China*

Correspondence should be addressed to Jin-Da Wang; wjd301@163.com

Received 9 February 2021; Revised 26 March 2021; Accepted 19 April 2021; Published 23 April 2021

Academic Editor: Xiangyu Cao

A 125 cm long catheter makes it possible to perform renal arteriography via radial artery, but its feasibility and safety remain unclear. Our study recruited 1,323 patients grouped by two different vascular accesses to renal arteriography, i.e., femoral artery access and radial artery access. The success rate of angiography was 100% in both groups. Differential analysis showed that the overall complication incidence of radial artery access group was significantly lower (2.5% for radial artery access vs. 4.8% for femoral artery access, $p = 0.03$). From this study, we suggest that using the 125 cm angiographic catheter to perform renal arteriography via radial artery access is feasible and safe.

1. Introduction

Atherosclerosis is the main cause of renal artery stenosis. Like other atherosclerotic diseases, the incidence of atherosclerotic renal artery stenosis (ARAS) rises with the progress of population aging [1, 2]. In fact, there exists a high rate of diagnostic omission errors for ARAS because asymptomatic patients usually cannot receive timely treatment until renal function deteriorates and cardiovascular injuries occur [3]. Therefore, early diagnosis becomes significantly important to the prognosis of patients with ARAS.

Renal arteriography (RAG) is the gold standard for diagnosing renal artery stenosis [4, 5]. The femoral artery is the traditional access of renal arteriography and is also preferred by most hospitals and interventional doctors. However, the femoral artery access (FAA) can cause strong discomfort, high incidence of complications such as hematoma and bleeding, and has been almost completely replaced by radial artery access (RAA) in the coronary intervention [6]. Moreover, 11.3 ~ 39% of coronary artery disease patients are complicated with ARAS [7]. It was reported that the 125 cm long angiographic catheter can make it easily accessible for the operation [8]. Therefore, this study is aimed at investigating the feasibility and safety of RAG via the RAA. The results would increase the diagnostic rate of ARAS.

2. Materials and Methods

2.1. Study Design. Our study was designed according to the reported standard of the observational study. We searched 1,323 consecutive patients admitted to the Department of Cardiology at the Chinese PLA General Hospital and extracted RAG from January 2016 to December 2020 in the PACS database. All subjects were grouped by different vascular access (decided by the experienced interventional cardiologists according to their own operation habit). The index related to RAG operation and the incidence of complications between the two groups were compared. This study was approved by the Ethics Committee of Chinese PLA General Hospital. All participants were called for verbal agreements.

2.2. Angiography Procedures. In the FAA group, either right or left femoral artery puncture was first performed; then, a 6F sheath was inserted. 2500 units of unfractionated heparin were injected into the artery to prevent catheter-related thrombosis. A 6F Judkins R angiography catheter was inserted through the femoral artery sheath to the level of

Table 1: Baseline characteristics of patients grouped by different vascular access.

Characteristics*	RAA ($N = 612$)	FAA ($N = 711$)	$p^{\dagger}$
Age, years	61.3 ± 17.7	62.1 ± 18.1	0.66
Male, no. (%)	385 (62.9)	422 (59.3)	0.18
Height, cm	166.3 ± 9.9	168.5 ± 9.7	0.42
Scr, ummol/L	87.6 ± 21.4	89.2 ± 22.3	0.42

*Categorical variables are shown as numbers (%) and continuous variables as means ± standard deviation. $^{\dagger}p$ values were calculated by comparing characteristics between two groups. RAA: radial artery access; FAA: femoral artery access; Scr: serum creatinine.

Table 2: Comparison of RAG-related index between different vascular access.

Item*	RAA ($N = 612$)	FAA ($N = 711$)	$p^{\dagger}$
Success rate, %	100	100	1
Operation time, min	8.96 ± 2.03	5.08 ± 1.75	0.01
X-ray exposure time, min	4.13 ± 0.23	2.11 ± 0.16	0.03
Contrast, mL	15.19 ± 3.38	14.38 ± 3.69	0.31
Change of Scr, ummol/L	9.32 ± 7.94	9.38 ± 8.09	0.82

*Categorical variables are shown as numbers (%) and continuous variables as means ± standard deviation. $^{\dagger}p$ values were calculated by comparing characteristics between two groups. RAG: renal arteriography; RAA: radial artery access; FAA: femoral artery access; Scr: serum creatinine.

Table 3: Comparison of complications between different vascular access.

Complications*	RAA ($N = 612$)	FAA ($N = 711$)	$p^{\dagger}$
Aortic artery dissection, no. (%)	0 (0)	0 (0)	1
Renal artery dissection, no. (%)	0 (0)	0 (0)	1
Retroperitoneal hematoma, no. (%)	0 (0)	0 (0)	1
Hematoma, no. (%)	11 (1.8)	25 (3.5)	0.06
Pseudoaneurysm, no. (%)	3 (0.5)	6 (0.8)	0.44
Arteriovenous fistula, no. (%)	1 (0.2)	3 (0.4)	0.39
Total, no. (%)	15 (2.5)	34 (4.8)	0.03

*Complications are shown as numbers (%). $^{\dagger}p$ values were calculated by comparing characteristics between two groups. RAG: renal arteriography; RAA: radial artery access; FAA: femoral artery access.

the first lumbar vertebra, and renal arteriography was implemented at the opening of the renal artery.

In the RAA group, after puncture was performed at the right or left radial artery, the 6F arterial sheath was inserted. 2500 units of heparin were injected into the artery to prevent catheter-related thrombosis and followed by 200 μg nitroglycerin to prevent vasospasm. Guided by the guidewire, a 6F and 125 cm long MP A1 angiography catheter (Cordis, USA) was put into the ascending aorta. The open end of the catheter was turned to the left of the patient at this time. At last, the guidewire was sent into the descending aorta, through which the catheter can be sent into the opening of the renal artery.

2.3. Data Collection. All demographic information was collected from the electronic medical record system in a standard report form, such as age, gender, height, and RAG-related data including X-ray irradiation time, contrast agent dosage, and complication incidence.

2.4. Data Analysis. SPSS version 20.0 was used to analyze all the data of our study. All statistics were two-sided tested at the 5% level of significance. All results were reported referring to STROBE statement. Continuous data with normal distribution and homogeneity of variance were compared by one-way ANOVA, otherwise by Mann–Whitney test. Categorical data were compared by χ^2 analysis.

3. Results

3.1. Baseline Characteristics. From 1,323 patients enrolled in our study, renal arteriography was performed in 612 patients (mean age of 61.3 ± 17.7, 62.9% male, mean height of 166.3 ± 9.9 cm, and mean serum creatinine 87.6 ± 21.4 ummol/L) via RAA and 711 patients (mean age of 62.1 ± 18.1, 59.3% male, mean height of 168.5 ± 9.7 cm, and mean serum creatinine 89.2 ± 22.3 ummol/L) via FAA. There presented no significant difference between the two groups in baseline characteristics (Table 1).

3.2. RAG Operation Related Index. In the RAA group, all 612 patients underwent angiography successfully via radial artery. The right radial artery was initially selected in 464 patients and the left radial artery for the others ($N = 148$). Among the patients who initially chose the right radial artery, 14 patients were taken another puncture of the left radial artery because the aortic arch was too tortuous so that the catheter could not be adjusted to the descending aorta to complete the RAG. In the FAA group, all 711 patients underwent angiography through femoral artery access without changing the punctured vessel. If the frequency of puncture is not considered, there is no difference of the success rate of angiography between the two vascular accesses (both 100%).

The differential analysis shows that operation time (5.08 ± 1.75 min for FAA vs. 8.96 ± 2.03 min for RAA, $p = 0.01$) and X-ray exposure time (2.11 ± 0.16 min for FAA vs. 4.13 ± 0.23 min for RAA, $p = 0.03$) of FAA were significantly shorter than that of the RAA group. However, there was no significant difference in the dosage of contrast (15.19 ± 3.38 mL for RAA vs. 14.38 ± 3.69 mL for FAA, $p = 0.31$) and the change of serum creatinine (9.32 ± 7.94 ummol/L for RAA vs. 9.38 ± 8.09 ummol/L for FAA, $p = 0.82$) between the two groups (Table 2).

3.3. Complications. χ^2 analysis showed that the incidence of complications in the RAA group was not higher than that in the FAA group. Although there was no significant difference in single complication (including aortic artery dissection, renal artery dissection, retroperitoneal hematoma,

hematoma, pseudoaneurysm, and arteriovenous fistula), the overall complication incidence of the radial artery group was significantly lower (2.5% for RAA vs. 4.8% for FAA, $p = 0.03$) (Table 3).

4. Discussion

In this retrospective cohort study, we found that the success rate of renal arteriography with the 125 cm long catheter via RAA was 100%. Despite slightly more operation and line exposure time, the complication rate of renal arteriography via radial artery was 48% less than that via the femoral artery.

Although previous studies have confirmed the possibility of renal arteriography via radial artery [8–10], few have compared the feasibility and safety between RAA and FAA [11]. Recently, a comparative study for noncoronary angiography with a small number of renal angiography cases has reported that radial artery is the feasible and safe access [12], which is consistent with our results.

The puncture point of the femoral artery approach is short from the opening of the renal artery, and the access is relatively straight. This anatomical feature makes the transfemoral artery approach easy to operate and keep the standard way of RAG. In our study, results related to RAG operation such as operation time and X-ray exposure time have reflected this feature. However, femoral artery access has inherent disadvantages as increased bleeding-related complications and patient discomfort [4, 5, 13]. The 125 cm long angiographic catheter enables enough distance for the RAG via RAA or even the right RAA. This study revealed that the success rate of renal arteriography via the right radial artery was up to 97% (464 in total, 450 patients succeeded, and 14 patients failed due to extreme distortion of the aortic arch).

It should be noted that in our study, a male with a height of 195 cm successfully received RAG via the right radial artery, but the 125 cm long catheter was completely inserted into the sheath of the radial artery. This case suggests that patients taller than a certain threshold should not receive RAG with the 125 cm long catheter, which should be further studied.

The limitations of our study included the recall bias and single-center study. More analysis should be conducted on data related to renal artery intervention and simultaneous coronary and renal angiography.

5. Conclusion

This study has shown that it is feasible and safe to use the 125 cm long angiographic catheter for renal arteriography via radial artery access. Radial artery vascular access can be the first choice for RAG in clinics.

Data Availability

The cohort study data used to support the findings of this study are restricted by the Ethics Committee of Chinese PLA General Hospital in order to protect patient privacy.

Conflicts of Interest

The authors declare that there is no conflict of interest regarding the publication of this paper.

Authors' Contributions

Jixuan Liu and Jinda Wang designed the study. Jinda Wang and Jixuan Liu collected the data. Jinda Wang and Jixuan Liu analyzed the data. Jinda Wang, Jixuan Liu, and Zhijun Sun analyzed and interpreted the results. Jixuan Liu and Jinda Wang drafted the article.

Acknowledgments

This study was supported by the National Key R&D Program of China (2017YFC0908700) and the Beijing Key Clinical Subject Program.

References

[1] M. Peng, X.-J. Jiang, H. Dong et al., "Etiology of renal artery stenosis in 2047 patients: a single-center retrospective analysis during a 15-year period in China," *Journal of Human Hypertension*, vol. 30, no. 2, pp. 124–128, 2016.

[2] S. C. Textor, "Renal arterial disease and hypertension," *The Medical Clinics of North America*, vol. 101, no. 1, pp. 65–79, 2017.

[3] S. H. Kwon and L. O. Lerman, "Atherosclerotic renal artery stenosis: current status," *Advances in Chronic Kidney Disease*, vol. 22, no. 3, pp. 224–231, 2015.

[4] J. L. Anderson, J. L. Halperin, N. M. Albert et al., "Management of patients with peripheral artery disease (compilation of 2005 and 2011 ACCF/AHA guideline recommendations): a report of the American College of Cardiology Foundation/American Heart Association Task Force on Practice Guidelines," *Circulation*, vol. 127, no. 13, pp. 1425–1443, 2013.

[5] A. J. Klein, M. R. Jaff, B. H. Gray et al., "SCAI appropriate use criteria for peripheral arterial interventions: an update," *Catheterization and Cardiovascular Interventions*, vol. 90, no. 4, pp. E90–E110, 2017.

[6] M. Lunardi, C. Gao, H. Hara et al., "Coronary interventions in 2020: the year in review," *EuroIntervention*, vol. 16, no. 15, pp. e1215–e1226, 2021.

[7] Q. de Mast and J. J. Beutler, "The prevalence of atherosclerotic renal artery stenosis in risk groups: a systematic literature review," *Journal of hypertension*, vol. 27, no. 7, pp. 1333–1340, 2009.

[8] D. Scheinert, S. Bräunlich, B. Nonnast-Daniel et al., "Transradial approach for renal artery stenting," *Catheterization and Cardiovascular Interventions*, vol. 54, no. 4, pp. 442–447, 2001.

[9] C. Trani, A. Tommasino, and F. Burzotta, "Transradial renal stenting: why and how," *Catheterization and Cardiovascular Interventions*, vol. 74, no. 6, pp. 951–956, 2009.

[10] D. O. Kessel, I. Robertson, E. J. Taylor, and J. V. Patel, "Renal stenting from the radial artery: a novel approach," *Cardiovascular and Interventional Radiology*, vol. 25, no. 2, pp. 146–149, 2002.

[11] O. Alli, V. Mathew, A. M. From, G. Barsness, S. Misra, and R. Gulati, "Transradial access for renal artery intervention is

feasible and safe," *Vascular and Endovascular Surgery*, vol. 45, no. 8, pp. 738–742, 2011.

[12] S. E. Park, S. B. Cho, H. J. Baek et al., "Clinical experience with distal transradial access for endovascular treatment of various noncoronary interventions in a multicenter study," *PLoS One*, vol. 15, no. 8, article e0237798, 2020.

[13] A. Y. Mousa, M. C. Bates, M. Broce, J. Bozzay, R. Morcos, and A. F. AbuRahma, "Issues related to renal artery angioplasty and stenting," *Vascular*, vol. 25, no. 6, pp. 618–628, 2017.

Hindawi
BioMed Research International
Volume 2021, Article ID 6693585, 7 pages
https://doi.org/10.1155/2021/6693585

Research Article

Application of Carbon Nanoparticles in Neck Dissection of Clinically Node-Negative Papillary Thyroid Carcinoma

Zhongyan Chen,[1] **Zhiming Zhong**,[2] **Guoqing Chen**,[3] **and Yun Feng**[1]

[1]*Department of Otolaryngology, China-Japan Friendship Hospital, Beijing 100029, China*
[2]*Department of Otolaryngology, Jianou Municipal Hospital, Fujian 353100, China*
[3]*Department of Otolaryngology, Jinnan Branch of Jinjiang Municipal Hospital, 362241 Fujian, China*

Correspondence should be addressed to Guoqing Chen; 2399650644@qq.com and Yun Feng; fjfengyun@sohu.com

Received 19 December 2020; Revised 9 February 2021; Accepted 29 March 2021; Published 22 April 2021

Academic Editor: Xiangyu Cao

Purpose. The purpose of this retrospective study was to evaluate the advantages of carbon nanoparticles in neck dissection and to conclude its application in the treatment of clinically node-negative papillary thyroid carcinoma (CN0PTC). *Methods*. As a retrospective cohort study, we divided the enrolled patients into two groups, the carbon nanoparticle (CN) group and the control group according to the usage of CN. In the CN group, CN was applied to reveal drainage lymph nodes and the picked LNs were sent for fast frozen testing. If metastasis exits, modified radical lateral lymph node dissection (LLND) was performed. For both groups, prophylactic central lymph node dissection was routinely done. Finally, the demographic information, tumor characteristics, postoperative pathological results, and laboratory data were collected for analysis. *Results*. A total of 61 CN0PTC were enrolled in this study, 33 in the CN group and 28 in the control group. The black-stained rate for CN was 29/40 (72.5%) with a positive prediction rate of 34.5%. The mainly black-stained region in the lateral neck was level III and possesses the highest lymph node ratio (17.5%). The metastasis that occurred in level VI was 30% and 11.8% in the CN and control groups, respectively ($p = 0.058$). During the available follow-up, no one showed recurrence. Statistical analysis showed that the CN suspension can significantly reduce the risk of damage to the parathyroid gland ($p = 0.001$ for hypocalcemia, <0.05; $p = 0.047$ for hypoparathyroidism, <0.05). *Conclusion*. The lateral neck metastasis in patients with papillary thyroid microcarcinoma in clinical stage cT1aN0 is not rare. CN can help surgeons to distinguish the real person who actually needs LLND. In prophylactic CLND, CN acts as a tracer which makes the parathyroid gland more identifiable and avoids risks of injuries to nerves and glands.

1. Introduction

With the development of ultrasonography, especially with the coming out of high-resolution machines, the incidence of thyroid cancer in China is dramatically increasing in recent years [1]. Over 90% of thyroid malignancies are differentiated thyroid cancer (DTC), most of which are papillary thyroid carcinoma (PTC) [2]. PTC is insensitive to either chemotherapy or radiotherapy and metastasis via mainly the lymphatic system. Up to now, surgery including thyroidectomy plus neck dissection is the best means of treatment. Importantly, the surgical strategy about lymph nodes is an essential issue that concerns every head and neck surgeon. In literature, a series of meta-analyses and clinical articles have discussed the outcomes of pCLND (prophylactic central lymph node dissection). A recently published retrospective study analyzing 399 patients to explore the role of prophylactic central lymph node dissection (pCLND) showed that pCLND can improve disease-free survival in patients with intermediate and high risk of disease recurrence [3]. Indeed, pCLND is believed to reduce locoregional recurrence rate and provide pathological evidence for the adjuvant radioiodine (RAI) treatment [4]. Nevertheless, some researchers thought that during the CLND, the protection of parathyroid glands and recurrent laryngeal nerve (RLN) injury plays a vital role due to its otherwise injury-causing poor life quality. Additionally, the role of lymph node metastases on prognosis and mortality is some kind doubtful. Gambardella et al. considered that pCLND has no positive influence on recurrence rate but brings higher postoperative complications [5].

Besides pCLND, there have been limited studies focusing on pLLND. Therefore, after a long period of academic discussion, prophylactic central (pCLND) and even lateral neck dissections (pLLND) in patients with clinically negative lymph nodes (CN0PTC) are still controversial. It is reported that the event of skip metastasis (lateral neck LN metastases without central LN metastasis) is not rare [6]. Considering all the above, we believed that importance should be attached to both pCLND and pLLND, and improving the safety and efficacy of pLLND is vital so that patients can get benefits from neck dissection while life quality will not be disturbed.

Since 2015, our center has been using carbon nanoparticle (CN) suspension to trace lymph nodes to reduce the occurrence of LND complications and lower the risk of disease recurrence. CN is made of particles with 150 nm diameter which allows CN to enter the lymphatic capillaries (the intercellular space of lymphatic capillary cells is 120–500 nm), but not the blood capillaries (the intercellular space of blood capillary cells is 20–50 nm). Taking use of those properties, CN can detect draining lymph nodes which are of importance in the surgical decision-making. Although certain articles about CN in thyroid cancer have been published, we wonder how the CN suspension was applied in PTC patients and the benefits it brings to the real-world condition. In order to conclude the five years' experience in the usage of CN, we conducted this retrospective cohort study based on the assumption that CN suspension can help the detection of occult lateral neck metastasis and significantly reduce the occurrence of associated complications. We hoped this work can uncover the application of CN in prophylactic neck dissection in CN0PTC patients and explore the influence of CN on the occurrence of hypocalcemia and hypoparathyroidism.

2. Method

A total of 61 patients diagnosed as CN0PTC from August 2015 to December 2019 at the Department of Otorhinolaryngology-Head and Neck Surgery of our center were collected retrospectively. The study was approved by the Institutional Review Board of the China-Japan Friendship Hospital, Beijing, China. Informed written consent was obtained from the enrolled patients.

2.1. Inclusion Criteria

(1) Patients with fine needle aspiration cytology- (FNAC-) proven PTC without suspicious lymph nodes in ultrasound (CN0PTC) were recruited. No history of head and neck surgery or radiation

(2) All patients had documentation of normal vocal cord mobility by preoperative laryngoscopy

(3) A preoperative neck ultrasound and neck CT scan showed no evidence of metastasis occurring in central and lateral cervical compartments (CN0PTC). Both ultrasound and neck CT scan were confirmed by two experienced specialists

(4) Patients were included in the CN group or control group according to the usage of CNs or not

2.2. Exclusion Criteria

(1) Patients in whom FNA had confirmed lateral neck lymph node metastases were excluded from this study

(2) Patients with aggressive histologic variants (columnar tall/tall cell, diffuse sclerosing, and insular types) were excluded

(3) Patients were also excluded if the frozen pathology examination during operation confirmed benign tumor or any other malignant tumor, such as medullary thyroid cancer and thyroid lymphoma

(4) Patients younger than 18 years, pregnant, breastfeeding, unable to participate in a postoperative follow-up, or unable to give informed consent were excluded

2.3. Procedure

2.3.1. Surgical Technique. All surgical procedures were performed by the same surgeon (Prof. Yun Feng) with high experience in thyroid surgery. General anesthesia was given to all patients. The patients were placed in the supine position. A cervical collar curved incision was made.

A 1 ml syringe was used for CN suspension injecting into the thyroid gland. Several injecting spots were randomized and uniformly distributed surrounding the tumor. For each spot, 0.05 ml-0.1 ml CN suspension was slowly injected after aspirate to ensure no flashback of blood. Then, manual pressure was given using a wet gauze sponge for 15 min to promote the diffusion of CN. We could see the CNs gradually diffused from the injecting spots to the surrounding area, until the entire thyroid lobe was uniformly stained black. Next, the region of level III was first investigated assisted by endoscopy to find black-stained LNs. Then, levels II, IV, and VI were explored in turn. Unilateral lobectomy plus isthmusectomy was performed for unilateral lesion, and a total thyroidectomy should be considered for patients with bilateral nodularity and other reasonable indication (such as combined with hyperthyroidism). The black-stained LNs in the lateral and center compartments were picked for the intraoperative frozen section. In the cases where metastasis was detected in black-stained LN upon frozen biopsy, an immediate modified radical LLND along the jugular and carotid vessels (including II, III, and IV regions) plus level VI should be done. If there is no evidence of LN metastasis in the lateral compartment, therapeutic lymph node dissection was only performed in level VI (central compartment). Due to the high occurrence of central compartment metastasis, we conducted prophylactic CLND for all 61 patients no matter if CN or control group (see Figure 1).

The boundaries of the central compartment of the neck (level VI) include the hyoid bone superiorly, right and left carotid arteries laterally, and the plane at the level of the innominate artery inferiorly. This includes the pretracheal, prelaryngeal, and paratracheal lymph nodes. Levels II, III,

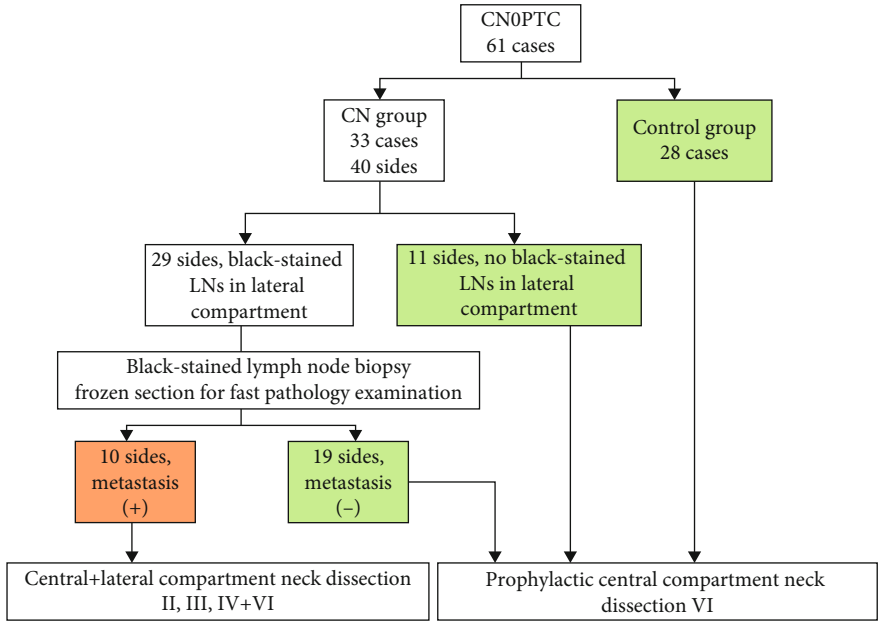

Figure 1: A flow diagram used to describe the therapeutic regimen for CN and control group, CN0PTC, and papillary thyroid carcinoma without suspicious lymph nodes in ultrasound. LN: lymph node.

and IV represent the lateral compartment, bordered inferiorly by the clavicle, superiorly by the digastric muscle, anteriorly by the sternohyoideus, and posteriorly by the sternocleidomastoid (SCM) muscle [7]. Level V which is referred to as the posterior triangle group includes the anterior border of the trapezius muscle laterally, the posterior border of the SCM medially, and the clavicle inferiorly and is divided into two sublevels, VA and VB using the horizontal plane that corresponds to the inferior border of the cricoid cartilage.

2.3.2. Data Collection. Demographic information about age, gender, history of abnormal thyroid function, cytological results, BRAF gene mutation, intraoperative bleeding, and surgery duration was collected. Preoperative FT3, FT4, TSH, Tg, and anti-Tg antibody levels were also evaluated. Levels of calcium and parathyroid hormone, along with any complications including hemorrhage, wound infection, seroma, hypocalcemia, and vocal cord palsy, were registered postoperatively and at the follow-up after one month, six months, and 12 months. Postoperative hypocalcemia is defined as lower than 2.0 mmol/l and 12 pg/ml for hypoparathyroidism. The lymph node yield was defined as the number of lymph nodes harvested after lymphadenectomy, and the lymph node ratio was defined as the ratio between metastatic lymph nodes and total lymph nodes retrieved, calculated only in patients with metastatic lymph nodes.

2.3.3. Statistical Analysis. SPSS 22.0 software (Chicago, IL, USA) was used for statistical analyses. The continuous variables were expressed as the means ± standard deviations (SD). Comparison between groups was done using *chi-square test* and *t test*. p values < 0.05 were considered statistically significant.

3. Results

A total of 61 CN0PTC were enrolled in this study, 33 in the CN group (8 were men and 25 were women) and 28 in the control group (4 were men and 24 were women). Age, sex, BRAF mutation results, primary tumor locations and size, tumor extent, number of tumors, thyroid procedures performed, black-stained LN location and numbers, LN pathological results, and other characteristics of these patients are shown in Table 1. There was no significant difference between the two groups in gender, age distribution, tumor size and location, laterality, multinodules, and BRAF mutation ($p < 0.05$). In both groups, no patients provided family history of malignant thyroid tumor, and 2 in the CN group had hyperthyroidism under stable control of drugs. No permanent hypocalcemia and hypoparathyroidism occurred in either the CN group or the control group. As for transient hypocalcemia and hypoparathyroidism, CN can significantly avoid parathyroid injuries ($p < 0.05$, see data in Table 1). Other complications including hemorrhage, wound infection, and seroma are listed in Table 1. Only 2 patients in the control group showed unilateral vocal cord palsy and recovered after three months of medical therapy. The occurrence of complications showed no significant difference between the two groups.

In the CN group, seven patients were confirmed to be suffering from bilateral thyroid cancer. Finally, a total of 40 sides were collected for analysis, in which 11 sides showed no black-stained LN in the lateral compartment after CN injection; as a result, the black-stained rate of this study was 29/40 (72.5%). Ten sides (10/29, 34.5%) in which lateral compartment metastasis was revealed on frozen sections underwent immediate LLND. Of these, five sides also suffered from central compartment metastasis. The central compartment (VI)

Table 1: General information and basic data of CN0PTC patients between CN group and control group.

	CN group 33 cases 40 sides	Control group 28 cases 34 sides	$\chi^2(t/Z)$ value	p value
Age, y (mean ± SD)	43.55 ± 11.56	42.89 ± 14.096	$t = 0.199$	0.338
Gender, M/F			$\chi^2 = 0.950$	0.330
Male	8	4		
Female	25	24		
Laterality			$\chi^2 = 0.000$	0.984
Bilateral	7	6		
Multinodules[1]			$\chi^2 = 0.728$	0.394
Single	27	26		
Multifoci	13	8		
Tumor size (n, %)[2]			$\chi^2 = 0.022$	0.883
$T \leq 1$ cm	30	26		
1 cm < $T \leq 2$ cm	10	8		
Tumor site			$\chi^2 = 1.774$	0.183
Upper pole	25	16		
Middle/lower portion	15	18		
BRAF mutation	26	21	$\chi^2 = 0.123$	0.726
LN metastasis/side				
Central	2	4	$\chi^2 = 3.606$	0.058
Lateral	5	—		
Central+lateral	5	—		
Complications				
Unilateral vocal cord palsy	0	2	$\chi^2 = 2.437$	0.118
Hemorrhage	0	0		—
Wound infection	0	0		—
Seroma	2	1	$\chi^2 = 0.201$	0.654
Transient hypocalcemia	6	17	$\chi^2 = 11.666$	0.001*
Transient hypoparathyroidism	9	14	$\chi^2 = 3.958$	0.047*

[1]Described by side. [2]Calculated by the maximum diameter if multifocal lesions existed. LN: lymph node. *$p < 0.05$.

LN metastatic rate was 30% (12/40). The black-stained LN distribution in different neck levels is shown in Figure 2. In conclusion, the positive prediction rate of CN suspension was 34.5% (10/29). Distribution of black-stained LNs in the lateral compartment was shown in Table 2. In the lateral neck area, 142 sentinel LNs detected by CN suspension in 33 patients were located in the ipsilateral lateral neck compartment. The most common location of lack of stained LNs was level III (Figure 2). Black-stained level VI LNs were observed in 5 sides with 3 persons was confirmed as positive for cancer metastasis.

As for the control group, 4 sides were proofed with central compartment metastasis (4/33, 11.8%). Parathyroid tissue was spotted in the dissected soft tissue from level VI in 3 patients. 17 patients show transient hypocalcemia while 14 patients suffered from hypoparathyroidism after surgery.

4. Discussion

This study investigated the application of CN suspension in CN0PTC by retrospectively analyzing two cohorts: the CN group and the control group. We found that the black-stained rate of CN is 72.5% with a positive prediction rate of 34.5%, that is, the occult lateral compartment LN metastasis possibility is 35%. The black-stained LNs were mainly located in level III, then levels II and IV. Cancer primarily influences the level III and II LNs in the lateral compartment. We compared the occurrence rate of hypocalcemia and hypoparathyroidism. It showed that CN promotes the identification of the parathyroid gland when the CLND was performed and mitigates injuries to the blood supply of the parathyroid gland. Moreover, with the application of CN, we can do pLLND via a form of picking berries then undergo

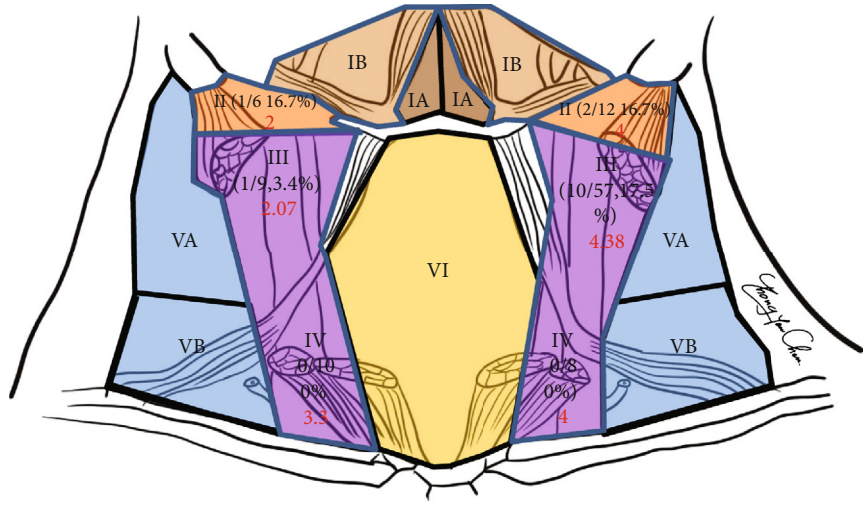

Figure 2: The distribution of the black-stained lymph nodes in different areas. Of these, level III has the highest possibility of detection of black-stained LN, while the metastasis in LN mostly occurs in levels VI, III, and II, and seldom involves levels V and I which is consistent with the literature. The mean lymph node yield in different areas was expressed in red.

Table 2: Distribution of black-stained LNs in the lateral compartment of CN0PTC patients.

	Number of sides	Positive for metastasis proof by intraoperative frozen section
No black-stained LN detected in lateral compartment	11	—
II level	1	0
III level	17	5
II, III level	6	5 (II: 1; III: 2; II+III: 2)
III, IV level	5	0
Total	40	10

PTC: papillary thyroid carcinoma; LN: lymph node.

modified radical LLND after positive frozen pathological feedback. Zhou et al. analyzed a total of 127 patients who were diagnosed with unilateral papillary thyroid microcarcinoma (clinical stage cT1aN0M0) who underwent primary thyroid surgery (hemi- or total thyroidectomy with ipsilateral central lymph node dissection (CLND) plus lateral lymph node dissection (LLND) including levels III and IV). They found that the total metastasis rate of the lateral lymph node was 21.26% (27/127), mainly located in level III [8]. Others also reported similar data [9].

The primary therapy for differentiated (papillary and follicular) thyroid cancer is surgery including total (or near-total) thyroidectomy and unilateral lobectomy and LND. For CN0PTC, LN metastasis occurs mostly in the central compartments while the lateral compartment LNs are also commonly involved. However, most research results primarily focused on the stained nodes in the central compartment so that the application of CN in CN0PTC lateral LND was rarely reported, and whether CN can improve the detection rate of metastatic lateral compartment nodes is still uncertain. It is believed that lateral LN metastasis was associated with tumor staging, postoperative therapy, distant metastases, prognosis, and survival [10]. Plenty of factors contribute to disease recurrence and metastasis, among which occult lateral compartment metastasis plays a vital role. So a complete neck LND is of great importance for preventing PTC recurrence and metastasis. If there is preoperative evidence (on exam or ultrasound and neck CT scan) of central or lateral node metastases, therapeutic lymph node dissection would be performed. However, it is still ambiguous whether prophylactic LLND should be performed in a situation in which neither ultrasound nor neck CT scan proves LN metastasis. Researchers are against prophylactic lateral LND due to the wide disturbed surgical field which may cause a series pre- and postoperative complications such as postoperative pain, worsening life quality of patient (wound pain, hoarseness), and injuries to vessels (Chyle leak, hemorrhage) and nerves (accessory, ramus mandibularis, sympathetic (Horner's syndrome), phrenic, brachial plexus, and cutaneous cervical plexus).

Therefore, finding a management which can balance the benefit of disease control by lateral LND and the loss of life quality greatly needs to be addressed. Lee et al. applied preoperative lymphoscintigraphy combined with a hand-held collimated gamma probe to search for "radioactive" lymph nodes to searching for the sentinel lymph node [11]. The tracer they used was a 99mTc-tin colloid which was intratumorally injected under ultrasound guidance. The radical lateral LND was performed if the picked SLN had metastasis proven by frozen pathology. They believed that sentinel

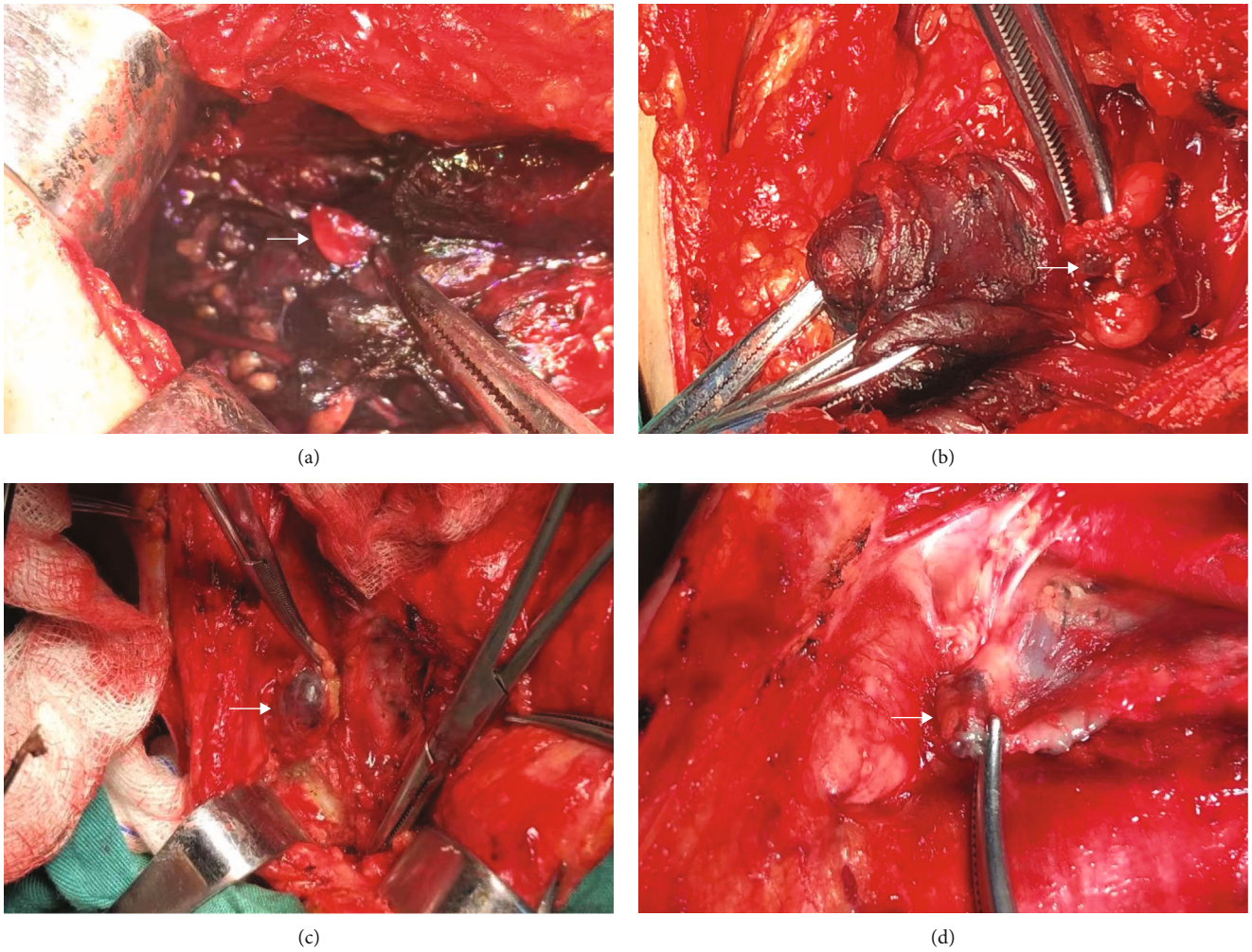

(a) (b) (c) (d)

Figure 3: The parathyroid glands were not stained because of sharing different lymphatic systems. Therefore, CN suspensions did help highlight parathyroid glands (a) (→ indicates the unstained parathyroid gland). (b–d) shows the staining of lymph nodes by CN in levels VI (b) and III (c, d). White arrows indicate the black-stained lymph nodes.

lymph node biopsy is a useful method for evaluating the occult lateral neck lymph node status in patients with PTC. This method of detecting SLN was reported by others. Besides radio-guided SLNB (rSLNB), the LN tracer also includes other kinds of dye techniques, such as CN, methylene blue and India ink, and indocyanine green (ICG).

Carbon nanoparticle suspension has good lymph tropism. After injection into the thyroid tissue, it will be absorbed by the lymph system quickly selectively blacking the lymph vessels and nodes, which will enter into the partial lymph pipe network and lymph gland without blood pipe absorption due to its 150 nm diameter which is bigger than the blood capillary gap (about 30-50 nm) and less than the lymphatic capillary gap (100-500 nm). Compared with the first generation of lymph tracers (methylene blue and India ink), CN suspension has the advantages of great dispersivity, with the parathyroid gland not stained and even dying [12]. In comparison with the radioactive tracer, CN is much easier to operate, requires no special equipment, is radiationless, and is safer for the human body. Carbon nanoparticle suspension has been widely employed for lymph node tracing in lots of malignant tumors such as gastric cancer, breast cancer, cervical cancer, oral cancer, colorectal cancer, and lung cancer. Recently, CN was applied in thyroid cancer as reported by several authors. Zhang et al. reported that carbon nanoparticle-assisted sentinel lymph node biopsy can detect incidental thyroid carcinoma which prevents the need for a second surgery [13].

Because carbon nanoparticles cannot stain the parathyroid gland, the parathyroid glands can be easily identified and protected to reduce the complications of transient hypoparathyroidism [14] (Figure 3(a)). This feature has great significance especially for those who unfortunately have bilateral thyroid cancer thus with a high risk of damage to the parathyroid gland or for patients who need a second neck surgery due to recurrence and other reasons. In this situation, CN can assist the surgeons to finish the bilateral central compartment dissection and protect the parathyroid gland to the maximum extent at the same time. In our study, none had permanent hypoparathyroidism which indicated that CN can effectively protect the parathyroid gland making CLND safer.

This study has some limitations. First, it showed that lateral neck nodal involvement is not uncommon, at 28%. However, it did not conduct long-term follow-up observations to illustrate the benefits of preventive LLND. Whether the use of CN suspension can improve the long-term prognosis and reduce the recurrence still needs to be explored in the future. Second, the conclusion in this study needs a greater sample clinical study for further confirmation.

In conclusion, this study indicated that lateral LN metastasis in CN0PTC is not uncommon. Thus, CN suspension-assisted identification of drainage LNs should be considered for facilitating the modified resection of lymph nodes at the central and lateral compartments of the neck, reducing neck dissection-associated complications, especially for the exploration and management of the lateral compartment in patients without definite evidence of lateral neck metastasis.

Data Availability

We can provide the underlying data if needed.

Ethical Approval

All procedures performed in studies involving human participants were in accordance with the ethical standards of the China-Japan Friendship Hospital Ethical Committee.

Consent

Informed consent was obtained from individual participants involved in the study.

Conflicts of Interest

The authors report no conflicts of interest and have received no payment in preparation of this manuscript.

Authors' Contributions

The authors alone are responsible for the content and writing of this paper.

References

[1] M. Li, L. Dal Maso, and S. Vaccarella, "Global trends in thyroid cancer incidence and the impact of overdiagnosis," *The lancet Diabetes & Endocrinology*, vol. 8, no. 6, pp. 468–470, 2020.

[2] M. Amin, S. Edge, and F. Greene, *AJCC Cancer Staging Manual*, Springer International Publishing, 2017.

[3] F. Medas, G. L. Canu, F. Cappellacci et al., "Prophylactic central lymph node dissection improves disease-free survival in patients with intermediate and high risk differentiated thyroid carcinoma: a retrospective analysis on 399 patients," *Cancers*, vol. 12, no. 6, p. 1658, 2020.

[4] D. E. Gyorki, B. Untch, R. M. Tuttle, and A. R. Shaha, "Prophylactic central neck dissection in differentiated thyroid cancer: an assessment of the evidence," *Annals of Surgical Oncology*, vol. 20, no. 7, pp. 2285–2289, 2013.

[5] C. Gambardella, R. Patrone, F. di Capua et al., "The role of prophylactic central compartment lymph node dissection in elderly patients with differentiated thyroid cancer: a multicentric study," *BMC Surgery*, vol. 18, no. S1, p. 110, 2019.

[6] Y. J. Ryu, S. J. Kang, J. S. Cho, J. H. Yoon, and M. H. Park, "Identifying risk factors of lateral lymph node recurrence in clinically node-negative papillary thyroid cancer," *Medicine*, vol. 97, no. 51, article e13435, 2018.

[7] T. S. Wang and J. A. Sosa, "Thyroid surgery for differentiated thyroid cancer - recent advances and future directions," *Nature Reviews Endocrinology*, vol. 14, no. 11, pp. 670–683, 2018.

[8] B. Zhou, L. Wei, and J. Qin, "The rate and risk factors for ipsilateral lateral neck lymph node metastasis in patients with papillary thyroid microcarcinoma (cT1aN0)," *Asian Journal of Surgery*, vol. 43, no. 9, pp. 959-960, 2020.

[9] N. Wada, Q. Y. Duh, K. Sugino et al., "Lymph node metastasis from 259 papillary thyroid microcarcinomas: frequency, pattern of occurrence and recurrence, and optimal strategy for neck dissection," *Annals of Surgery*, vol. 237, no. 3, pp. 399–407, 2003.

[10] S. Filetti, C. Durante, D. Hartl et al., "Thyroid cancer: ESMO Clinical Practice Guidelines for diagnosis, treatment and follow-up†," *Annals of Oncology*, vol. 30, no. 12, pp. 1856–1883, 2019.

[11] S. K. Lee, S. H. Kim, S. M. Hur, J. H. Choe, J. H. Kim, and J. S. Kim, "The efficacy of lateral neck sentinel lymph node biopsy in papillary thyroid carcinoma," *World Journal of Surgery*, vol. 35, no. 12, pp. 2675–2682, 2011.

[12] R. Wang, S. Mo, Q. Liu et al., "The safety and effectiveness of carbon nanoparticles suspension in tracking lymph node metastases of colorectal cancer: a prospective randomized controlled trial," *Japanese Journal of Clinical Oncology*, vol. 50, no. 5, pp. 535–542, 2020.

[13] C. Zhang, X. Li, Z. Zhang, S. Lei, P. Fan, and Q. X. Qiang Xiao, "The potential role of carbon nanoparticles-assisted biopsy for sentinel lymph nodes of incidental thyroid carcinoma," *Gland Surgery*, vol. 8, no. 4, pp. 370–377, 2019.

[14] Z. Chaojie, L. Shanshan, Z. Zhigong et al., "Evaluation of the clinical value of carbon nanoparticles as lymph node tracer in differentiated thyroid carcinoma requiring reoperation," *International Journal of Clinical Oncology*, vol. 21, no. 1, pp. 68–74, 2016.

Hindawi
BioMed Research International
Volume 2021, Article ID 6645500, 12 pages
https://doi.org/10.1155/2021/6645500

Research Article

Intracranial Angioplasty with Enterprise Stent for Intracranial Atherosclerotic Stenosis: A Single-Center Experience and a Systematic Review

Bowen Sun,[1] **Chao Xu**,[1] **Pei Wu**,[1] **Man Li**,[2] **Shancai Xu**,[1] **Chunlei Wang**,[1] **Xiangyu Liu**,[3] **Yeping Ling**,[1] **and Huaizhang Shi**[1]

[1]*Department of Neurosurgery, The First Affiliated Hospital of Harbin Medical University, Harbin, Heilongjiang Province, China*
[2]*Department of Neurology, The First Affiliated Hospital of Harbin Medical University, Harbin, Heilongjiang Province, China*
[3]*Department of Neurology, Shenzhen Longhua District Central Hospital, Shenzhen, Guangdong Province, China*

Correspondence should be addressed to Huaizhang Shi; shihuaizhang@hrbmu.edu.cn

Received 3 November 2020; Revised 16 March 2021; Accepted 26 March 2021; Published 19 April 2021

Academic Editor: Xing Chen

Background. The high rate of periprocedural complications for the endovascular stent procedure in the Stenting Versus Aggressive Medical Management Therapy for Intracranial Arterial Stenosis (SAMMPRIS) trial resulted in it being less recommended than medical therapy to treat intracranial atherosclerotic stenosis (ICAS). Because Enterprise stent use might reduce the incidence of complications in ICAS treatment compared to other frequently used stents, this paper evaluated the safety and effectiveness of the Enterprise stent for the treatment of ICAS. *Methods*. We performed a comprehensive literature search for reports on intracranial angioplasty using the Enterprise stent for ICAS treatment from the earliest date available from each database to May 2020 for PubMed, EMBASE, Web of Science, Cochrane, and Clinical Trials databases. We also reviewed the single-center experience of the First Affiliated Hospital of Harbin Medical University. We extracted information regarding periprocedural complications, procedure-related morbidity, mortality, immediate angiographic outcome, and long-term clinical and angiographic outcomes, among others. Event rates were pooled across studies using random-effects or fixed-effects models depending on the heterogeneity. *Results*. Five hundred fifty-seven patients with 588 lesions from seven studies, including the institutional series, were included in the analysis. The incidence of stroke or death within 30 days was 7.4% (95% confidence interval (CI), 5.5%–10.1%). The incidence of ischemic stroke or TIA in the territory of the qualifying artery beyond 30 days and during follow-up was 3.2% (95% CI, 1.1%–9.5%). The incidence of in-stent restenosis was 10.1% (95% CI, 4.6%–22.2%), and the incidence of symptomatic restenosis was 4.1% (95% CI, 1.7%–9.9%). *Conclusions*. Intracranial angioplasty utilizing the Enterprise stent for ICAS treatment was relatively safe and effective but required further verification using additional sources for evidence.

1. Introduction

For decades, intracranial atherosclerotic stenosis (ICAS) has been a major risk factor for ischemic stroke worldwide, especially in Asian populations [1, 2]. The Chinese Intracranial Atherosclerosis (CICAS) trial reported that, in China, 46.6% of patients with cerebral ischemia symptoms exhibited ICAS [3]. According to current guidelines, the primary treatment for ICAS is medical therapy [4]. However, for ICAS patients with severe stenosis and symptoms of cerebral ischemia (>70%), the stroke recurrence rate after receiving aggressive medical therapy (AMT) exceeds 20% annually [5]. Percutaneous transluminal angioplasty and stenting (PTAS) has been regarded as an effective alternative method to treat severe ICAS [6].

In the past decade, two large randomized controlled trials (RCTs), Stenting Versus Aggressive Medical Management Therapy for Intracranial Arterial Stenosis (SAMMPRIS) [7] and Vitesse Intracranial Stent Study for Ischemic Stroke Therapy (VISSIT) [8], indicated that AMT was the preferred

ICAS treatment relative to PTAS due to high rates of periprocedural complications associated with PTAS. In the SAMMPRIS trial, the 30-day incidence of stroke or death in the stent group was 14.7%, which was significantly higher than 5.8% for the AMT group and was partly due to the use of the Wingspan stent [9, 10]. The Wingspan stent is the only stent currently approved by the Food and Drug Administration for the treatment of ICAS [11]. However, concerns have been raised that its rigidity and open-cell design with high radial force could be related to the higher perioperative complication rate observed in previous trials [12].

Meanwhile, other stent varieties not originally designed to treat ICAS have been used for off-label treatment of ICAS. Some of these off-label stents have achieved satisfactory results, including other self-expanding stents such as the Enterprise stent (Codman Neurovascular, Raynham, Massachusetts, USA), balloon-expandable stents, and drug-eluting stents [9, 13–20]. Among these varieties, the Enterprise stent, which has a closed-cell design, special bearing system, and lower radial force, provides an attractive option to treat ICAS [9, 13–17]. This preference is supported by the fact that the Enterprise stent is associated with fewer perioperative complications, and it can reach many lesions that other stents cannot due to the inclusion of microcatheters [9, 13–17]. However, only a few case series with limited sample sizes have been published that assess the treatment of ICAS using the Enterprise stent [9, 13–17]. No systematic review has been conducted. Due to the advantages mentioned above, it is possible that the Enterprise stent might become one of the predominant devices used to treat ICAS. Therefore, it is necessary to further verify the safety and effectiveness of the Enterprise stent in the treatment of ICAS. Thus, we reported on the outcomes of using the Enterprise stent to treat ICAS in a high-volume center and systematically reviewed all relevant literature.

2. Materials and Methods

2.1. Institutional Series

2.1.1. Patient Population and Lesion Characteristics. We conducted a study of case series from a single center and reported the results according to the Preferred Reporting Of CasE Series in Surgery (PROCESS) guidelines [21]. We retrospectively collected data from consecutive patients who underwent PTAS using the Enterprise Stent to treat ICAS in our institution (First Affiliated Hospital of Harbin Medical University, Harbin, China) from June 13, 2017, to April 3, 2020. The First Affiliated Hospital of Harbin Medical University is located in Harbin, Heilongjiang Province, in northeastern China. The area is located at a high altitude, cold climate, and a high incidence of cerebrovascular diseases. The center sees more than 1,500 cases of cerebrovascular diseases each year, including PTAS, and treats approximately 200 ICAS patients per year.

Written informed consent was obtained from each patient, and all study procedures were approved by the institutional ethics review board (Ethical approval: number ID, 20D0051). The inclusion criteria included the following. (1) The patient received a diagnosis of ICAS with a degree > 70 %, which was confirmed by digital subtraction angiography (DSA), using the same methods as the Comparison of Warfarin and Aspirin for Symptomatic Intracranial Arterial Stenosis (WASID) trial [5]. (2) The patient exhibited recurrent transient ischemic attack (TIA) or ischemic stroke despite receiving AMT. (3) Hypoperfusion was present in the region surrounding the qualifying artery that was confirmed by computed tomography perfusion (CTP) and magnetic resonance imaging (MRI). The exclusion criteria included the presence of (1) complete occlusion of the cerebral artery; (2) stenosis caused by nonatherosclerotic factors; (3) ICAS combined with other intracranial diseases such as cerebral hemorrhage, malformation, aneurysm, moyamoya disease, and intracranial tumors; and (4) occurrence of a new ischemic stroke within two weeks before admission, as verified by diffusion-weighted imaging (DWI).

2.1.2. Procedures. All patients received dual antithrombotic therapy for a minimum of five days before stenting, as well as oral aspirin (100 mg/d) and clopidogrel (75 mg/d), and their platelet inhibition rate was assessed. Preoperative blood pressure was maintained 15% lower than the baseline blood pressure. Patients remained under general anesthesia during the stent procedure, and heparin was infused following induction of anesthesia. A 6F catheter was inserted into the common carotid or vertebral artery via the femoral artery using the Seldinger method. After femoral artery puncture, heparin was injected intravenously, and heparin saline was continuously infused during the procedure to ensure that the activated clotting time was between 150 and 250 seconds. Subsequently, angiography was performed to assess stenosis lesions and blood flow compensation.

We calculated the diameter and length of stenosis lesions utilizing both three-dimensional rotation and two-dimensional imaging. Under the guidance of the path map, a Traxcess 14 (Microvention, USA) microguidewire was used with the Excelsior SL-10 (Stryker, Kalamazoo, Michigan, USA) microcatheter to super select the distal end or branch of the blood vessel through the lesion area, and the microguidewire was withdrawn. After confirming the true lumen of the blood vessel, the Transcend 300 microguidewire (Stryker) was inserted to withdraw the microcatheter. Then, the Gateway balloon catheter (Boston Scientific, USA) was sent along the Transcend Floppy 300 guidewire to the distal end of the lesion area, such that the size of the balloon catheter reached 80% of the lesion stenosis and the balloon was expanded slowly. After satisfactory balloon expansion, it was withdrawn, and the Select Plus microcatheter (Stryker) was inserted along the exchange guidewire. The Enterprise stent (Codman) was delivered to the lesion area through the microcatheter. It was necessary that the stent completely cover the lesion, and the length needed to be greater than 3-5 mm at both ends of the lesion area. After stenting, angiography was performed to assess the procedure results and rule out thrombosis in the stent or distal thromboembolism. The patient's blood pressure was maintained at 120-140 mmHg after treatment, and the patient continued to receive dual antithrombotic therapy, including clopidogrel

(75 mg/d) for six weeks and aspirin (100 mg/d) for at least six months. Patients received follow-up telephone calls 30 days after the procedure.

2.1.3. Data Collection and Outcomes. We reviewed medical records and extracted basic information concerning the patients and lesions, including demographic data, lesion characteristics, clinical presentations, modified Rankin scale (mRS) scores, and the degree of arterial stenosis. Indicators related to stent placement were recorded, including the size of the balloon catheter and Enterprise stent, complications within 30 days after stenting, and postoperative angiography results.

The safety was assessed by noting the occurrence of adverse events within 30 days after stenting, including TIA, stroke, or death, based on the guidelines of the SAMMPRIS trial. Besides, we recorded the rate of technical success, which was defined as remaining stenosis of 50% or less as measured by immediate postoperative angiography, which indicated the precise release of the Enterprise stent into the lesion area.

2.2. Literature Review

2.2.1. Study Protocol and Search Strategy. We conducted a systematic review of relevant literature, following the Preferred Reporting Items for Systematic Reviews and Meta-Analyses (PRISMA) guidelines [22]. The study was registered in the International System of Review Prospective Register (PROSPERO, CRD42020183509). With the assistance of an experienced librarian, we searched PubMed, EMBASE, Web of Science, Cochrane, and Clinical Trials databases. Keywords, including "intracranial arteriosclerosis," "cerebral arterial diseases," "cerebral arteries," "internal carotid," "vertebrobasilar arteries," "middle cerebral artery," "stents," and "Enterprise" were used in both "AND" and "OR" combinations, as described in Table S1. The literature search period was from the earliest date available for each database to May 2020. All studies reporting ICAS patients treated with the Enterprise stent were selected.

2.2.2. Trial Selection. Studies reporting an ICAS case series treated with Enterprise stents with a sample size greater than five met the initial inclusion criteria. We reviewed all potentially qualified studies with results specifically related to safety or effectiveness. We excluded studies that did not provide perioperative complication rates and technical success rates. Duplicate studies were moved. Non-English articles, conference abstracts without full text, and case series combined with complete occlusion of the cerebral artery and moyamoya disease also were excluded.

2.2.3. Data Extraction. Two investigators (BWS and CX) independently extracted the following information from each eligible study: the total number of patients and lesions treated with the Enterprise stent, pretreated and posttreated mean stenosis degree, technical success rate, intraprocedural complications, frequency of stroke, TIA, or death within 30 days after implantation of the Enterprise stent, frequency and mean duration of clinical and imaging follow-ups, frequency of stroke, TIA or death in the territory of the qualifying artery beyond 30 days, and the in-stent restenosis (ISR) and symptomatic ISR rates. The presence of ISR was indicated by a greater than 50% residual stenosis in the stent after placement as assessed by follow-up DSA or computed tomographic angiography (CTA) examination.

2.2.4. Qualitative Assessment. Two investigators (BWS and CX) independently assessed the quality of the included literature, and a third investigator resolved any disagreements. Literature quality was assessed using a modified version of the Newcastle-Ottawa Quality Assessment Scale (NOS) [23], which was specifically designed to assess the quality of nonrandomized studies, such as case-control studies and cohort studies. We evaluated the quality of each study based on three aspects, including (1) selection of the study groups, (2) comparability of the study groups, and (3) achievement of the outcome of interest. Specific evaluation details are shown in Table S2.

2.3. Statistical Analysis. All statistical analyses were performed using R software (version 3.6.1, R Core Team, Vienna, Austria). Standard descriptive statistics were used for the institutional series. Continuous data were presented as means ± standard deviation. Categorical data were presented as percentages. Since all included studies were noncomparative studies, we calculated incidence rates rather than relative risks or mean differences. The cumulative incidence and 95% confidence interval (CI) for all events were recorded, and cumulative outcomes were calculated. Subgroup analyses were conducted based on the anterior circulation (AC) and posterior circulation (PC) of the cerebral arteries. For the pooled analysis, event rates were summarized using a random-effects model if heterogeneity was significant; otherwise, a fixed-effects model was used [24]. Study heterogeneity was evaluated using the I^2 statistic. I^2 values of 0-25%, 26-50%, 51-75%, and>75% indicated light, low, moderate, and high heterogeneity, respectively [25]. If any apparent heterogeneity was observed, a sensitivity analysis was used to explore the source of the heterogeneity. Visualization using a funnel plot was employed to assess publication bias when there were sufficient numbers of eligible studies to create the plot. Asymmetric funnel plots are suggestive of publication bias.

3. Results

3.1. Institutional Series

3.1.1. Patient Population and Lesion Characteristics. Three hundred twenty-one ICAS patients received PTAS treatment at our center from June 13, 2017, to April 3, 2020. After excluding ineligible participants, 104 patients (mean age, 58.61 ± 9.32 years) with 105 stenosis lesions were incorporated into the present study (60 male patients, 57.69%). The screening flowchart is seen in Figure S1. All relevant patient data are shown in Table 1. Forty-seven (44.76%) lesions were located in the AC (13 in the intracranial segment of the internal carotid artery, ICA (12.38%); and 34 in the middle cerebral artery, MCA (32.38%)). Fifty-eight (55.24%) lesions were located in the PC (15 in the

Table 1: The patient's demographic data, clinical and angiographic outcome.

Characteristic	Value
Age, years (mean ± SD)	58.61 ± 9.32
Sex, male/female (*n*)	60/44
Qualifying event (*n* (%))	
Transient ischemic attack	21 (20.19)
Cerebral infarction	83 (79.81)
Comorbidities (*n* (%))	
Hypertension	80 (76.92)
Diabetes	30 (28.85)
Coronary artery disease	18 (17.31)
Pretreated modified Rankin scale score (*n* (%))	
0	17 (16.35)
1	69 (66.35)
2	16 (15.38)
3	1 (0.96)
Location (*n* (%))	
Intracranial segment of internal carotid artery	13 (12.38)
Middle cerebral artery	34 (32.38)
Basilar artery	43 (40.95)
Intracranial segment of the vertebral artery	15 (14.28)
Lesion morphology (*n* (%))	
A	14 (13.33)
B	40 (38.10)
C	51 (48.57)
Complications (*n* (%))	
Any stroke or death within 30 d	7 (6.73)
Nonfatal ischemic stroke within 30 d	4 (3.85)
Nonfatal hemorrhage stroke within 30 d	2 (1.92)
Death within 30 d	1 (0.96)
Angiographic outcome	
Pretreated stenosis degree (%) (mean ± SD)	87.13 ± 7.80
Posttreated stenosis degree (%) (mean ± SD)	27.31 ± 8.89
Length of stenosis (mean ± SD)	10.68 ± 4.99
Enterprise stent length (mm) (mean ± SD)	25.12 ± 5.03
Balloon catheter length (mm) (mean ± SD)	13.22 ± 3.64

intracranial segment of the vertebral artery, VA (14.28%); and 43 in the basilar artery, BA (40.95%)). Twenty-one (20.19%) patients were admitted to the hospital for TIA and 83 (79.81%) for stroke. The frequency of preoperative mRS scores were as follows: 0, 17 (16.35%); 1, 69 (66.35%); 2, 16 (15.38%); and 3, 1 (0.96%). The preoperative degree of arterial stenosis was 87.13 ± 7.80%, as determined by DSA.

3.1.2. Immediate Angiographic and 30-Day Outcomes. All 105 stents met the technical success criteria, resulting in a 100% success rate, and postoperative stenosis averaged 27.31 ± 8.89% (Table 1). Within 30 days after stent placement, 7 (6.73%) patients developed stroke or died, 4 (3.81%) patients experienced an ischemic stroke, and 3 (2.88%) patients developed a hemorrhagic stroke. One patient with a hemorrhagic stroke died, yielding a total mortality rate of 0.95%. One patient with a right MCA stenosis experienced hyperperfusion cerebral hemorrhage on the second day after stent placement and died, despite immediate symptomatic treatment. One patient with stenosis at the end of the left ICA developed a subarachnoid hemorrhage 12 hours after the stent was implanted. This patient subsequently underwent decompressive craniectomy, gradually achieved full recovery, and exhibited a mRS score of 3 on day 30 after the procedure. One patient with cerebellar hemorrhage did not present any visible symptoms but scored 1 on the mRS on day 30 following the procedure. Three patients with BA stenosis and one patient with MCA stenosis developed a perforating infarction within 30 days after the procedure, but the symptoms were not severe. After receiving antiplatelet therapy, their symptoms improved, and their mRS scores were 0-2 at the 30-day telephone follow-up interview.

3.2. Systematical Review

3.2.1. Search Results. The literature selection process is shown in Figure 1. The initial database search identified 351 citations. Fifty-two duplicates were excluded, and 291 articles were excluded after reading the titles and abstracts, leaving eight articles. Two articles presented overlapping data, and we chose to include the article with the longest study duration and the largest number of cases. One additional study was excluded for including only patients with complete occlusion of the cerebral artery. Therefore, seven studies, including the institutional series, were included in the systematic review.

3.2.2. Characteristics of Included Studies. The baseline information for all studies is shown in Table 2. Studies were published between 2012 and 2019. All included studies were retrospective observational case studies that lacked comparisons to other treatments as control groups. Due to these characteristics, all selected studies had a high risk of bias, as assessed by the NOS scale (Table S2). Five studies were conducted in East Asia, while the other two studies were conducted in Germany and Turkey.

A total of 557 patients underwent Enterprise stent implantation for 588 ICAS lesions. The average age ranged from 56.8 to 64.0, and the pretreatment mean stenosis ranged from 65.4% to 92.0%. All studies reported some within 30 days after Enterprise implantation. Five studies, including 343 lesions, reported angiographic follow-up examinations, with the mean time ranging from 6 to 22 months. Five studies, including 370 lesions, reported results from clinical follow-up examinations, with the mean time ranging from 6.2 to 25.6 months.

3.2.3. Immediate Angiographic and 30-Day Outcomes. The summary of adverse events after Enterprise implantation is shown in Table 3, and the forest diagram of the results is shown in Figure 2. The technical success rate ranged from 98.5% to 100%, with only one procedure that did not achieve technical success. Posttreatment stenosis was reported for

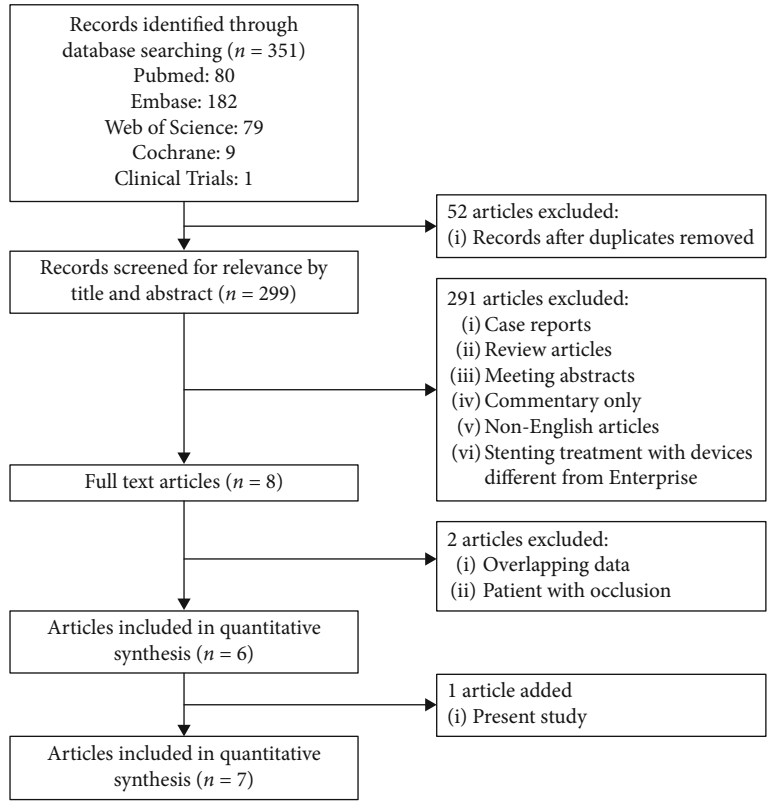

Figure 1: Flowchart shows study selection procedure. 7 studies were included in this systematic review.

474 lesions in five studies, ranging from 12 ± 10% to 27.31 ± 8.89% (Table 2). Within 30 days following PTAS, the pooled incidence of adverse events was as follows: stroke or death, 7.4% (95% CI 5.5%–10.1%); hemorrhagic stroke, 3.1% (95% CI, 1.9%–5.0%); ischemic stroke, 4.5% (95% CI, 3.0%–6.73%); and mortality, 1.2% (95% CI, 0.5%–2.6%). The pooled incidence of intraprocedural complications was 2.2% (95% CI, 1.2%–4.0%), including vasospasm, hematoma in the groin, and asymptomatic dissection of the stented segment. These results were not heterogeneous ($I^2 = 0$), and no apparent publication bias was observed in the funnel chart (Figure S2). We conducted a subgroup analysis of complications that occurred within 30 days by separating patients with lesions into AC and PC subgroups. The complication rate of patients with AC lesions was 6.7% (95% CI, 3.6%–12.3%), and for patients with PC lesions was 8.1% (95% CI, 4.9%–13.4%). There was no significant statistical difference between the two subgroups (Figure S3).

3.2.4. Imaging and Clinical Follow-Up. Five studies, including 370 lesions, reported outcomes observed at clinical follow-up examinations. The pooled incidence of ischemic stroke or TIA in the territory of the qualifying artery beyond 30 days was 3.2% (95% CI, 1.1%–9.5%) (Figure 2). Since $I^2 = 56$, we chose the analysis result obtained from the random-effects model. Through sensitivity analysis, we determined that the heterogeneity primarily resulted from the study by Wang et al. [15]. No deaths were reported during the follow-up examinations. Five studies, including 343 lesions, reported imaging follow-up results. The pooled incidence of ISR was 10.1% (95% CI, 4.6%–22.2%), and the pooled incidence of symptomatic ISR was 4.9% (95% CI, 2.9%–8.5%). The results of ISR were highly heterogeneous ($I^2 = 75$). Using sensitivity analysis, we established that the heterogeneity principally resulted from the study by Vajda et al. [17]. We speculated that the heterogeneity might be caused by differences in the length of follow-up times. Based on the asymmetry of the funnel chart, we believe that the three results described above presented some degree of publication bias (Figure S2).

4. Discussion

We summarized our experience in a high-volume center and all published studies before May 2020 on the treatment of ICAS with the Enterprise stent and evaluated the safety and efficacy of the Enterprise stent. An analysis of 588 lesions in 557 patients revealed that the incidence of stroke or mortality within 30 days after the procedure was 7.4% (95% CI 5.5%–10.1%), and all but one procedure obtained technical success. In the SAMMPRIS and VISSIT trials, the incidence of adverse events within 30 days of PTAS with non-Enterprise stents was 14.7% and 24.1%, respectively, which are higher than the rates reported in this study. The long-term effect of treatment, as assessed by the incidence of ischemic stroke or TIA in the territory of the qualifying artery beyond 30 days, was 3.2% (95% CI, 1.1%–9.5%). Thus, our findings provided evidence to support the safety and effectiveness of Enterprise stent placement in the treatment of ICAS.

Table 2: Baseline characteristics of the patients and the lesions.

Study name	Period	Location	Design	No. of patients/lesions	Male/female ratio	Age (yr) (mean ± SD)	Stroke/TIA ratio	Lesion site AC/PC	Prestent stenosis rate (%) (mean ± SD)	Poststent stenosis rate (%) (mean ± SD)	Mean clinical or angiographic follow-up (months)
Vajda 2012	2007-2011	Germany	R	189/209	132/57	64	100/89	89/120	65.4 ± 0.8	25.1 ± 1.0	6.9
Feng 2015	2009-2013	China	R	44/44	32/12	60.45 ± 9.07	26/18	25/19	79.32 ± 8.18	NA	25.6
Lee 2016	2013-2014	South Korea	R	24/30	20/4	61.8 ± 10.3	NA	20/10	81 ± 11.3	18 ± 6.8	15.8
Wang 2016	2012-2014	China	R	60/62	42/18	56.8 ± 8.0	22/38	14/48	NA	22.8 ± 4.8	6.3
Huang 2019	2014-2018	China	R	68/70	46/22	59.43 ± 9.74	65/3	54/16	NA	NA	NA
Salik 2019	2012-2017	Turkey	R	68/68	56/12	62 ± 7	61/7	29/39	92 ± 6	12 ± 10	22
Present	2017-2020	China	R	104/105	60/44	58.61 ± 9.32	83/21	47/58	87.13 ± 7.80	27.31 ± 8.89	NA

yr: year; SD: standard deviation; R: retrospective study; NA: not available; TIA: transient ischemic attack; AC: anterior circulation; PC: posterior circulation.

Table 3: Summary of adverse events after Enterprise implantation.

Study	Intraprocedural complications	Any stroke or death within 30 days				Ischemic stroke or TIA in the territory of the qualifying artery beyond 30 days	Mortality beyond 30 days	ISR	
		Stoke		Nonfatal stroke	Death			Asymptomatic	Symptomatic
		Hemorrhagic	Ischemic						
Vajda 2012	4/209	8/189	10/189	16/189	2/189	4	0/174	39/174	4/44
Feng 2015	0/44	1/44	3/44	4/44	0/44	0	0/44	1/44	2/44
Lee 2016	0/30	1/24	2/24	2/24	1/24	0	0/24	1/20	0/20
Wang 2016	3/62	0/60	2/60	2/60	0/60	5	0/60	1/45	5/45
Huang 2019	0/70	2/68	1/68	3/68	0/68	NA	NA	NA	NA
Salik 2019	1/68	0/68	0/68	1/68	0/68	0	0/68	2/60	0/60
Present	0/105	3/104	4/104	6/104	1/104	NA	NA	NA	NA

NA: not available.

The endovascular procedure emerged as a novel ICAS treatment in the 1980s. Although technology and equipment have undergone constant innovation and improvement, the procedure has never become the predominant treatment for ICAS [26, 27]. Results of the WAISD and SAMMPRIS trials confirmed the safety of AMT [5]. However, for patients with high-grade stenosis, the rate of stroke recurrence after AMT was close to 20% per year [11]. For many patients with severe ICAS (stricture > 70%), PTAS treatment is still an important alternative treatment. Additionally, the results of the SAMMPRIS trial have been criticized by some experts due to limitations in stent selection, patient inclusion, and technical aspects of the procedures [28]. Therefore, exploring optimal treatments for ICAS is still a worthy endeavor.

After minimizing the limitations of the SAMMPRIS trial, an RCT in China, China Angioplasty and Stenting for Symptomatic Intracranial Severe Stenosis (CASSISS) [29], was initiated and is ongoing. Early reports from the CASSISS trial differed from the SAMMPRIS study results, including the observation that the incidence of 30-day adverse events in patients with high-grade ICAS treated by PTAS was only 4.3%. This result increased the confidence of practitioners to use PTAS for ICAS treatment in China. The extensive use of Wingspan stents in the SAMMPRIS trial also has been widely criticized [12]. Some experts believed that the rigidity and high radial force of the Wingspan stent were related to the high incidence of perioperative complications [30]. Recently, the Wingspan Stent System Post Market Surveillance Study (WEAVE) trial [31] and the Wingspan One-year Vascular Events and Neurologic Outcomes (WOVEN) trial [32] reported acceptable results. As postmarket surveillance studies, the WEAVE and WOVEN trials strictly enrolled patients treated on-label with the Wingspan stent and reported that 2.67% of patients had died or developed stroke within 72 hours, and 8.5% of patients had died or developed stroke at the one-year follow-up. These results suggest that when assessing the use of PTAS for ICAS treatment, the choice of an appropriate patient group is critical.

Following the failure of the SAMMPRIS and VISSIT trials, studies on the feasibility and effectiveness of using other alternative stents to treat symptomatic ICAS have been continuing [9, 13–20]. Among the many stent options, the self-expanding Enterprise stent has been used frequently for ICAS treatment, especially in our center. The Enterprise stent, which was specifically developed to treat wide-necked intracranial cerebral aneurysms, has a closed-cell design, special carrier system, and lower radial force compared with the Wingspan stent [15]. It has a diameter of 4.5 mm and has four lengths of 14, 22, 28, and 37 mm, so it is suitable for intracranial blood vessels with a diameter of 2.5-4.0 mm. The release rate of the Enterprise stent is less than 70%, and it is recyclable. More importantly, the Enterprise stent is exceptionally malleable, and its delivery catheter tip is soft and flexible, making it easier to reach the lesion area than more rigid stents [13]. Due to the wide application of the Enterprise stent to treat aneurysm embolization [33], it has been reported that it could reach areas inaccessible by other types of stents, such as the Neuroform EZ and Solitaire stents [34]. Interestingly, Vajda et al. proposed that the Enterprise stent could be delivered to any part of the circle of Willis with the aid of microcatheters [13].

Several previous studies reported low perioperative complication rates when using the Enterprise stent to treat ICAS that ranged from 1.47% to 12.50% [9, 13–17]. The results of this study agree with previous reports, as only 7.4% (95% CI 5.5%–10.1%) of patients experienced stroke or death within 30 days after Enterprise stent implantation. More adverse events were caused by ischemic events, 4.5% (95% CI 3.0%–6.7%), and although the incidence of hemorrhagic events was slightly lower, 3.1% (95% CI 1.9%–5.0%), death was always related to hemorrhagic stroke. Additionally, we conducted a subgroup analysis based on the AC/PC lesion location, and the complication rate was not significantly different between the two subgroups.

Several studies reported additional complications related to the procedure, such as vasospasm and stent migration [9, 13]. The periprocedural complication rates of the current study were undoubtedly better than the stent group of the SAMMPRIS trial but slightly higher than the WEAVE trial, the early results of the CASSISS trial, and the AMT group of the SAMMPRIS trial. These results could be related to patient selection, operator experience, and characteristics of individual PTAS. As the complication rate within 30 days after PTAS in the VISSIT trial was as high as 24.1%, the trial

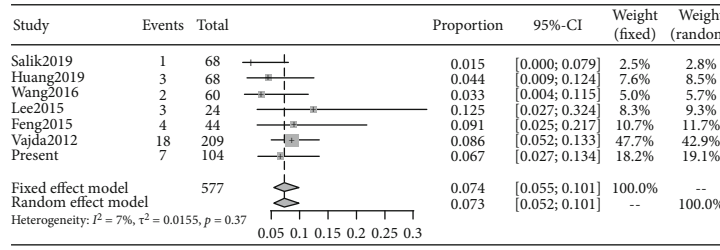

(a)

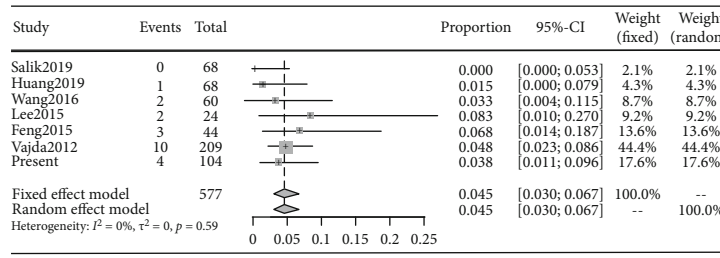

(b)

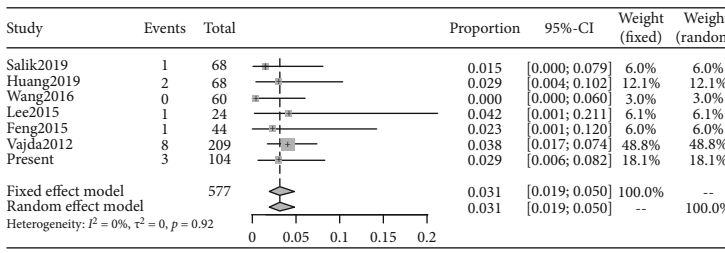

(c)

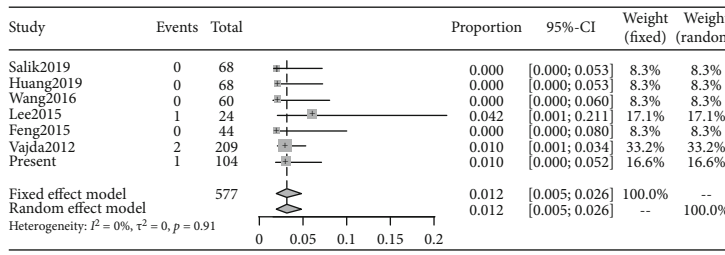

(d)

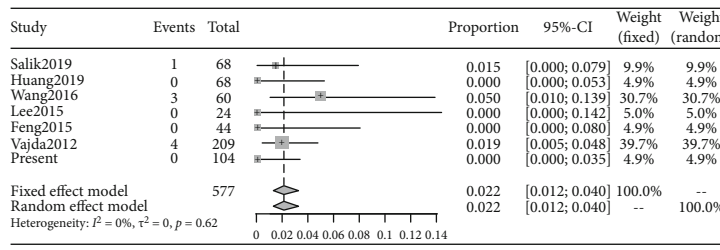

(e)

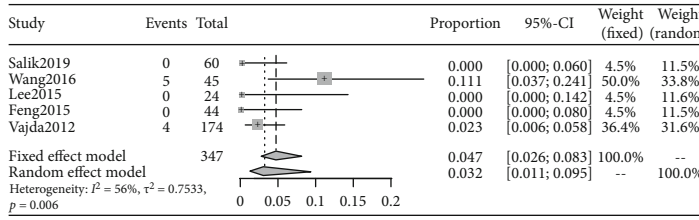

(f)

Figure 2: Continued.

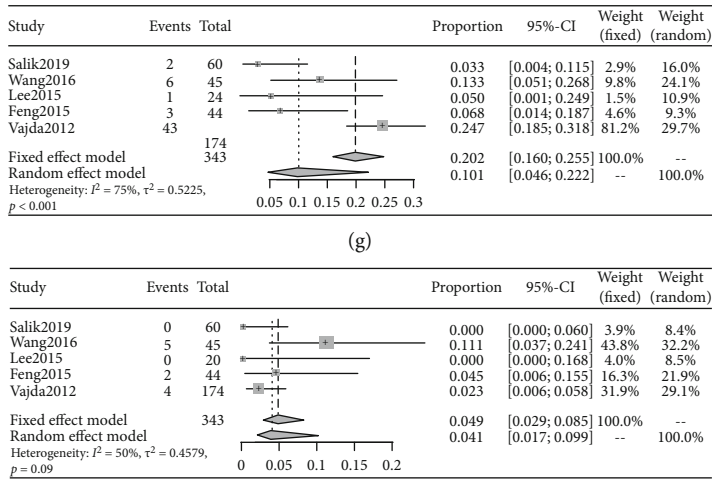

Figure 2: Pooled analysis outcome. (a) Any stroke or death within 30 days. (b) Ischemic stroke within 30 days. (c) Hemorrhage stroke within 30 days. (d) Mortality within 30 days. (e) Intraprocedure complication. (f) Ischemic stroke or TIA in the territory of the qualifying artery beyond 30 days. (g) In-stent restenosis during imaging follow-up. (h) Symptomatic in-stent restenosis during imaging follow-up.

was terminated early. It is generally considered that the balloon-expandable stent is more rigid and less flexible than self-expanding stents and may be difficult to navigate along curved blood vessels [24]. Some experts believed that PTAS complications were related to the morphological classification of lesions, as proposed by Mori et al. [9, 14, 35], and the complication rates of type B and type C lesions were higher. Recently, a multicenter, single-arm study involving 159 patients explored the application of balloon-expandable stents in the treatment of ICAS. The complication rate at 72 hours after surgery was 0%, but the study included more Mori A (33.3%) and Mori B (52.2%) lesions, so the therapeutic effect of balloon-expandable stents for Mori C lesions is still worth exploring [36].

There are relatively few studies on other types of stents, so it is challenging to draw broad conclusions [18, 19]. A single-center study involving 76 patients explored the effect of a new generation of closed-cell self-expandable stents, the Acclino® flex stent, in the treatment of ICAS. The incidence of stroke or death within 30 days after PTAS was 6.5%, which is similar to the results of this study [19]. Also, another study reported that using the Neuroform EZ stent to treat ICAS has the possibility of reducing complication risks. That study included 71 consecutive patients, and no stroke or death was observed within 30 days after surgery. The open-cell design of the Neuroform EZ stent was thought to be associated with this result [18]. However, the exact risk factors for these perioperative complications after PTAS with the Enterprise stent are still uncertain, and further research is needed [37]. In particular, for high-grade stenosis, the low complication rate in our study supported the safety of Enterprise stent implantation in ICAS treatment.

For the follow-up results of the systematic review, the incidence of stroke, TIA, or death over 30 days after PTAS was 3.2% (95% CI, 1.1%–9.5%). This result was better than the AMT (6.4%) and stent groups (5.3%) in the SAMMPRIS trial and lower than the AMT (5.7%) and stent groups (12.1%) in the VISSIT trial. These results indicated that the long-term stroke prevention of the Enterprise stent was relatively good. Long-term complications are often associated with ISR, and the high incidence of ISR after stent implantation for ICAS has long been a major disadvantage of placing stents [38]. ISR is common in the first year after PTAS and an important cause of nonsurgical ischemic events after stent placement [10]. Importantly, we found that the ISR rate during the follow-up period after Enterprise stent implantation was 10.1% (95% CI 4.6%–22.2%), and the incidence of symptomatic ISR was 4.9% (95% CI 2.9%–8.5%). These results are in line with results from a previous meta-analysis of PTAS for ICAS treatment [39]. The Wingspan stent had an ISR rate between 6% and 42.8% [9], and the ISR rate was as high as 26.5% in the VISSIT trial using the balloon-expandable stent. The ISR rate in the study by Vajda et al. was 24.71%, which potentially could be related to the patient inclusion criteria and follow-up times, as numerous patients with a stenosis rate of 50%-70% were included and followed for a long time until ISR was detected [17].

Recently, a meta-analysis demonstrated that drug-eluting stents performed better in preventing ISR, with an ISR incidence of only 4.1% and an asymptomatic ISR incidence of 3.0% [20]. However, the risk of low-grade chronic inflammation leading to late stent thrombosis limits the application of drug-eluting stents. Moreover, drug-eluting stents are quite stiff, making it challenging to reach complex stenosis lesions, causing drug-eluting stents to be inferior to the Enterprise stent in terms of operability [20].

Several relevant studies have indicated that ISR may be related to lesion location, preoperative stenosis, use of a balloon, and the application of antiplatelet drugs [38]. However, few studies have focused on the mechanisms underlying ISR. A few studies have reported that the low radial force of Enterprise stents might play a role in reducing the ISR rate because it is related to intimal hyperplasia [33]. Currently, treatment for ISR includes medical therapy,

bypass surgery, and endovascular recanalization, but most of these treatments have unsatisfactory outcomes [38]. In our center, the use of antiplatelet agents was strictly regulated based on the WASID trial to better prevent the emergence of ISR.

5. Limitations

Limitations associated with a retrospective single-arm study were unavoidable in the institutional series. Despite the authenticity of medical records, recall bias and selection bias were common, and the lack of a control group limited the scope of the results. For the systematic review, all included studies were retrospective single-center studies and lacked appropriate control groups for comparison with other treatments. The follow-up times and imaging methods for each study were highly variable, which may have confounded the clinical and angiographic results. The small number of available studies limited the effectiveness of evaluating publication bias. Also, this study only included relevant studies that took place in the last ten years. Over time, stenting technologies have continuously improved. The complication rate has decreased, which might be partially responsible for the heterogeneity in the results when studies published across a long-time span were compared. According to the Grading of Recommendations, Assessment, Development, and Evaluation framework, we found that the heterogeneity and methodological limitations of the included studies negatively impacted data in this study [40–42]. Nevertheless, with 557 patients and 588 lesions, this systematic review was the most extensive study to date that investigated the use of the Enterprise stent for ICAS. This study provided useful data to evaluate the effects of the Enterprise stent in the treatment of ICAS.

6. Conclusion

The use of the Enterprise stent for intracranial angioplasty may be safe and effective in the treatment of ICAS. When used appropriately, the vast majority of ICAS patients receiving Enterprise stent implantation obtained good outcomes and excellent neurological performance during the follow-up period. However, considering the limitations associated with the level of evidence in this study, additional RCTs are needed to further verify the effects of Enterprise stents for ICAS. Furthermore, the results of this study might provide assistance in the selection of stents for endovascular treatment of symptomatic severe ICAS.

Data Availability

The statistical results of our single center, as well as the data of the system review and the results of the pooled analysis, can be obtained in the manuscript and supplementary materials.

Conflicts of Interest

The authors declare that there is no conflict of interest regarding the publication of this paper.

Authors' Contributions

BWS and CX have contributed equally to this paper. BWS did the search, screening, and quality assessment of the articles, coding articles, conducting the analysis, and writing and revising the manuscript. CX did the search, screening, and quality assessment of the articles, coding articles, conducting the analysis, and writing and revising the manuscript. PW monitored the data collection and analyzed the data. ML monitored the data collection and analyzed the data. SCX conducted the study of single-center case series and collected and analyzed the data. CLW conducted the study of single-center case series and collected and analyzed the data. XYL did the statistical analysis and editing of the manuscript. YPL did the statistical analysis and editing of the manuscript. HZS did the study designer, overall methodological supervision, checking the analysis, and main manuscript reviewer.

Acknowledgments

We thank EditSprings for the English revision. This study was funded by the National Nature Science Foundation of China (Grant nos. 82071309), Natural Science Foundation of Heilongjiang Province of China (Grant nos. YQ2019H015), and Natural Science Foundation of Heilongjiang Province of China (Grant nos. ZD2018018).

Supplementary Materials

Table S1: database search strategy. Table S2: a modified version of the Newcastle-Ottawa Quality Assessment Scale. Figure S1: screening flowchart of the institutional series. Figure S2: funnel chart for detecting publication bias. Figure S3: subgroup analysis based on the anterior and posterior circulation of cerebral artery. *(Supplementary Materials)*

References

[1] C. Banerjee and M. I. Chimowitz, "Stroke caused by atherosclerosis of the major intracranial arteries," *Circulation Research*, vol. 120, no. 3, pp. 502–513, 2017.

[2] R. V. Krishnamurthi, V. L. Feigin, M. H. Forouzanfar et al., "Global and regional burden of first-ever ischaemic and haemorrhagic stroke during 1990-2010: findings from the Global Burden of Disease Study 2010," *The Lancet Global Health*, vol. 1, no. 5, pp. e259–e281, 2013.

[3] Y. Wang, X. Zhao, L. Liu et al., "Prevalence and outcomes of symptomatic intracranial large artery stenoses and occlusions in China: the Chinese Intracranial Atherosclerosis (CICAS) Study," *Stroke*, vol. 45, no. 3, pp. 663–669, 2014.

[4] W. N. Kernan, B. Ovbiagele, H. R. Black et al., "Guidelines for the prevention of stroke in patients with stroke and transient ischemic attack," *Stroke*, vol. 45, no. 7, pp. 2160–2236, 2014.

[5] M. I. Chimowitz, M. J. Lynn, H. Howlett-Smith et al., "Comparison of warfarin and aspirin for symptomatic intracranial arterial stenosis," *The New England Journal of Medicine*, vol. 352, no. 13, pp. 1305–1316, 2005.

[6] A. Wabnitz and M. Chimowitz, "Angioplasty, stenting and other potential treatments of atherosclerotic stenosis of the intracranial arteries: past, present and future," *Stroke*, vol. 19, no. 3, pp. 271–276, 2017.

[7] C. P. Derdeyn, M. I. Chimowitz, M. J. Lynn et al., "Aggressive medical treatment with or without stenting in high-risk patients with intracranial artery stenosis (SAMMPRIS): the final results of a randomised trial," *Lancet*, vol. 383, no. 9914, pp. 333–341, 2014.

[8] O. O. Zaidat, B. F. Fitzsimmons, B. K. Woodward et al., "Effect of a balloon-expandable intracranial stent vs medical therapy on risk of stroke in patients with symptomatic intracranial stenosis: the VISSIT randomized clinical trial," *Journal of the American Medical Association*, vol. 313, no. 12, pp. 1240–1248, 2015.

[9] Z. Feng, G. Duan, P. Zhang et al., "Enterprise stent for the treatment of symptomatic intracranial atherosclerotic stenosis: an initial experience of 44 patients," *BMC Neurology*, vol. 15, no. 1, p. 187, 2015.

[10] C. P. Derdeyn, D. Fiorella, M. J. Lynn et al., "Nonprocedural symptomatic infarction and in-stent restenosis after intracranial angioplasty and stenting in the SAMMPRIS trial (stenting and aggressive medical management for the prevention of recurrent stroke in intracranial stenosis)," *Stroke*, vol. 48, no. 6, pp. 1501–1506, 2017.

[11] P. Gao, D. Wang, Z. Zhao et al., "Multicenter prospective trial of stent placement in patients with symptomatic high-grade intracranial stenosis," *AJNR. American Journal of Neuroradiology*, vol. 37, no. 7, pp. 1275–1280, 2016.

[12] M. Fujimoto, Y. Shobayashi, K. Takemoto, S. Tateshima, and F. Viñuela, "Structural analysis for Wingspan stent in a perforator model," *Interventional Neuroradiology*, vol. 19, no. 3, pp. 271–275, 2013.

[13] A. E. Salik, H. H. Selcuk, H. Zalov, F. Kilinc, M. Cirak, and B. Kara, "Medium-term results of undersized angioplasty and stenting for symptomatic high-grade intracranial atherosclerotic stenosis with Enterprise," *Interventional Neuroradiology*, vol. 25, no. 5, pp. 484–490, 2019.

[14] C. M. Huang, Y. F. Hong, S. H. Xing et al., "Thirty-day outcomes of the Enterprise stent in treating hypoperfusion of symptomatic intracranial stenosis," *World Neurosurgery*, vol. 129, pp. e429–e435, 2019.

[15] X. Wang, Z. Wang, C. Wang, Y. Ji, X. Ding, and Y. Zang, "Application of the Enterprise stent in atherosclerotic intracranial arterial stenosis: a series of 60 cases," *Turkish Neurosurgery*, vol. 26, no. 1, pp. 69–76, 2016.

[16] K. Y. Lee, D. Y. Chen, H. L. Hsu, C. J. Chen, and Y. C. Tseng, "Undersized angioplasty and stenting of symptomatic intracranial tight stenosis with Enterprise: evaluation of clinical and vascular outcome," *Interventional Neuroradiology*, vol. 22, no. 2, pp. 187–195, 2016.

[17] Z. Vajda, E. Schmid, T. Güthe et al., "The modified Bose method for the endovascular treatment of intracranial atherosclerotic arterial stenoses using the Enterprise stent," *Neurosurgery*, vol. 70, no. 1, pp. 91–101, 2012.

[18] H. Xu, T. Quan, O. O. Zaidat et al., "Neuroform EZ stenting for symptomatic intracranial artery stenosis: 30 days outcomes in a high-volume stroke center," *Frontiers in Neurology*, vol. 10, p. 428, 2019.

[19] L. Meyer, H. Leischner, G. Thomalla et al., "Stenting with Acclino® (flex) for symptomatic intracranial stenosis as secondary stroke prevention," *Journal of Neurointerventional Surgery*, vol. 12, no. 11, pp. 1127–1131, 2020.

[20] G. Ye, X. Yin, X. Yang et al., "Efficacy and safety of drug-eluting stent for the intracranial atherosclerotic disease: a systematic review and meta-analysis," *Journal of Clinical Neuroscience*, vol. 59, pp. 112–118, 2019.

[21] R. A. Agha, C. Sohrabi, G. Mathew et al., "The PROCESS 2020 guideline: updating consensus Preferred Reporting of CasE series in surgery (PROCESS) guidelines," *International Journal of Surgery*, vol. 84, pp. 231–235, 2020.

[22] D. Moher, A. Liberati, J. Tetzlaff, D. G. Altman, and for the PRISMA Group, "Preferred reporting items for systematic reviews and meta-analyses: the PRISMA statement," *BMJ*, vol. 339, no. jul21 1, article b2535, 2009.

[23] A. Stang, "Critical evaluation of the Newcastle-Ottawa scale for the assessment of the quality of nonrandomized studies in meta-analyses," *European Journal of Epidemiology*, vol. 25, no. 9, pp. 603–605, 2010.

[24] R. Der Simonian and N. Laird, "Meta-analysis in clinical trials," *Controlled Clinical Trials*, vol. 7, no. 3, pp. 177–188, 1986.

[25] J. P. Higgins, S. G. Thompson, J. J. Deeks, and D. G. Altman, "Measuring inconsistency in meta-analyses," *BMJ*, vol. 327, no. 7414, pp. 557–560, 2003.

[26] C. J. Eskey, P. M. Meyers, T. N. Nguyen et al., "Indications for the performance of intracranial endovascular neurointerventional procedures: a scientific statement from the American Heart Association," *Circulation*, vol. 137, no. 21, pp. e661–e689, 2018.

[27] T. Wang, K. Yang, J. Luo et al., "Outcomes after stenting for symptomatic intracranial arterial stenosis: a systematic review and meta-analysis," *Journal of Neurology*, vol. 267, no. 3, pp. 581–590, 2020.

[28] C. P. Derdeyn, D. Fiorella, M. J. Lynn et al., "Mechanisms of stroke after intracranial angioplasty and stenting in the SAMMPRIS trial," *Neurosurgery*, vol. 72, no. 5, pp. 777–795, 2013.

[29] P. Gao, Z. Zhao, D. Wang et al., "China angioplasty and stenting for symptomatic intracranial severe stenosis (CASSISS): a new, prospective, multicenter, randomized controlled trial in China," *Interventional Neuroradiology*, vol. 21, no. 2, pp. 196–204, 2015.

[30] Y. Zhu, H. Zhang, Y. Zhang et al., "Endovascular metal devices for the treatment of cerebrovascular diseases," *Advanced Materials*, vol. 31, no. 8, article e1805452, 2019.

[31] M. J. Alexander, A. Zauner, J. C. Chaloupka et al., "WEAVE trial: final results in 152 on-label patients," *Stroke*, vol. 50, no. 4, pp. 889–894, 2019.

[32] M. J. Alexander, A. Zauner, R. Gupta et al., "The WOVEN trial: Wingspan one-year vascular events and neurologic outcomes," *Journal of Neurointerventional Surgery*, vol. 13, no. 4, pp. 307–310, 2021.

[33] D. Xu, C. Zhang, T. Wang et al., "Evaluation of enterprise stent-assisted coiling and telescoping stent technique as treatment of supraclinoid blister aneurysms of the internal carotid artery," *World Neurosurgery*, vol. 110, pp. e890–e896, 2018.

[34] S. Rohde, J. Seckinger, S. Hähnel, P. A. Ringleb, M. Bendszus, and M. Hartmann, "Stent design lowers angiographic but not clinical adverse events in stenting of symptomatic intracranial stenosis-results of a single center study with 100 consecutive patients," *International Journal of Stroke*, vol. 8, no. 2, pp. 87–94, 2013.

[35] T. Mori, M. Fukuoka, K. Kazita, and K. Mori, "Follow-up study after intracranial percutaneous transluminal cerebral balloon angioplasty," *AJNR. American Journal of Neuroradiology*, vol. 19, no. 8, pp. 1525–1533, 1998.

[36] K. Kang, Y. Zhang, J. Shuai et al., "Balloon-mounted stenting for ICAS in a multicenter registry study in China: a comparison with the WEAVE/WOVEN trial," *Journal of NeuroInterventional Surgery*, 2020.

[37] S. Yaghi, P. Khatri, A. de Havenon et al., "Peri-procedural stroke or death in stenting of symptomatic severe intracranial stenosis," *Journal of Neurointerventional Surgery*, vol. 12, no. 4, pp. 374–379, 2020.

[38] K. Kang, F. Gao, D. Mo et al., "Outcome of endovascular recanalization for intracranial in-stent restenosis," *Journal of Neurointerventional Surgery*, vol. 12, no. 11, pp. 1094–1098, 2020.

[39] F. Siddiq, M. Z. Memon, G. Vazquez, A. Safdar, and A. I. Qureshi, "Comparison between primary angioplasty and stent placement for symptomatic intracranial atherosclerotic disease: meta-analysis of case series," *Neurosurgery*, vol. 65, no. 6, pp. 1024–1034, 2009.

[40] H. Balshem, M. Helfand, H. J. Schünemann et al., "GRADE guidelines: 3. Rating the quality of evidence," *Journal of Clinical Epidemiology*, vol. 64, no. 4, pp. 401–406, 2011.

[41] G. H. Guyatt, A. D. Oxman, R. Kunz et al., "GRADE guidelines 6. Rating the quality of evidence–imprecision," *Journal of Clinical Epidemiology*, vol. 64, no. 12, pp. 1283–1293, 2011.

[42] M. H. Murad, B. A. Swiglo, A. N. Sidawy, E. Ascher, and V. M. Montori, "Methodology for clinical practice guidelines for the management of arteriovenous access," *Journal of Vascular Surgery*, vol. 48, no. 5, pp. S26–S30, 2008.

Hindawi
BioMed Research International
Volume 2021, Article ID 5575173, 5 pages
https://doi.org/10.1155/2021/5575173

Research Article

Endovascular Double-Layer Bare Stent Placement in the Treatment of Posttraumatic Pseudoaneurysm

Wenle Tan[1], **Shubin Dou**[2], **Jijin Yang**[3], **Jiang Xiong**[4], **Xiquan Zhang**[2] and **Feng Duan**[1]

[1]*Department of Interventional Radiology, The General Hospital of Chinese People's Liberation Army, Beijing 100853, China*
[2]*Traumatic Interventional Department, The 960th Hospital of Chinese People's Liberation Army, Zibo, Shandong Province 255300, China*
[3]*Department of Interventional Radiology, Changhai Hospital, Shanghai 200433, China*
[4]*Department of Vascular Surgery, The General Hospital of Chinese People's Liberation Army, Beijing 100853, China*

Correspondence should be addressed to Xiquan Zhang; jrkzxq@163.com and Feng Duan; duanfeng@vip.sina.com

Received 7 January 2021; Revised 19 February 2021; Accepted 3 March 2021; Published 11 March 2021

Academic Editor: Xing Chen

Objective. To investigate the efficacy and safety of endovascular double-layer bare stent placement for the treatment of traumatic false aneurysm (TFA). *Methods*. This is a retrospective review of five patients with TFA undergone double-layer bare stent placement in our center between February 2011 and August 2020. There are 2 males and 3 females aged 29-65 years, with an average age of 43 years. One case suffered from common carotid artery pseudoaneurysm, and four cases suffered superficial femoral artery pseudoaneurysm. *Results*. The endovascular interventional treatment was successful in all 5 patients, and the pseudoaneurysms disappeared after treatment. No TFA recurrence and no complications such as instent stenosis, stent migration, stent fracture, endoleak, and infection were observed during the 3-99-month follow-up period. *Conclusion*. For the treatment of TFA, endovascular interventional therapy with double-layer bare stent was minimally invasive, safe, and effective with fewer complications. It could preserve all branches of parent artery and had the advantage of lower cost. It can be used in the treatment of TFA in selected cases. However, further clinical researches with larger cohorts are needed before its long-term efficacy can be completely clarified.

1. Introduction

Traumatic false aneurysm (TFA) refers to peripheral hematoma caused by the partial rupture of the arterial vascular wall after injury. Since the vascular lumen is connected to the hematoma, a tumor-like expansion of the hematoma cavity may occur under the high arterial blood pressure. The lesion is known as a pseudoaneurysm because there is no normal three-layer structure of arteries [1]. Pseudoaneurysm can, if left untreated, become a life-threatening situation by thrombosis, rupture, or distal embolization [2]. Thus, proper and timely treatment is very important.

Before the era of endovascular techniques, open surgical aneurysmectomy was the conventional treatment for TFA [3]. In recent years, with the advances of new tools and embolization materials, endovascular interventional therapy, a minimally invasive and safe method, has been applied by interventional radiologists to treat TFAs, giving satisfactory results [4]. Based on the locations, types, and collateral pathways of pseudoaneurysm, different individualized treatments should be adopted, including single or overlapped stent-assisted coiling and covered stents [5, 6]. Zhang et al. reported that multiple overlapping uncovered stents could be a feasible option in the endovascular management of complicated peripheral and visceral artery aneurysms where side branches need to be maintained [7]. There was no similar case in the literature using dual-bare stents for the treatment of TFA with a long-term follow-up for 99 months. This study

is aimed at evaluating the long-term clinical therapeutic effect of double-layer bare stent implantation for TFA.

2. Subjects and Methods

2.1. General Data. In this study, five TFA patients with an average age of 43 years (2 males and 3 females, aged 29-65 years) were admitted to our emergency department from February 2011 to August 2020. The causes of TFA included sharp injury in 1 case and traffic injuries in 4 cases. The TFA injury sites included common carotid artery ($n = 1$) and superficial femoral artery ($n = 4$). The clinical manifestations consisted of continuously enlarging pulsatile mass in the site of injury, palpable tremor, vascular murmur, and discomfort and pain in the limbs on the traumatic side. The diagnosis was confirmed by computed tomography angiography (CTA) before operation.

2.2. Treatment. All five patients underwent CTA before treatment to determine the exact location, diameter, morphology, and collateral circulation of TFA [8]. After preoperative and intraoperative examination and assessment, double-layer bare stent placement was performed in all patients.

2.2.1. Surgical Procedure. Five milliliters of 2% lidocaine hydrochloride was subcutaneously injected for local anesthesia. After intravenous administration of heparin sodium (0.6-0.8 mg/kg), the femoral artery was punctured using the standard Seldinger technique. With the help of supersmooth guide wire, the catheter was delivered to the proximal vessel of TFA. Digital subtraction angiography (DSA) was performed to determine the location, morphology and size of TFA, the diameters of the distal and proximal blood vessels, and the main branch vessels that maybe involved. The tip of the catheter was inserted into the normal blood vessel to establish a working channel for the guide wire. The stent was slowly released after accurate positioning with the aid of bony landmarks and DSA path diagram. Since the diseased segment involved important collateral circulation, overlapping bare stents were placed. At least 2 cm of anchoring area was required at the two ends of pseudoaneurysm. The bare stents (LifeStent, Bard Company, USA) were slowly placed across the neck of the pseudoaneurysm, and the therapeutic effect was evaluated by DSA. If there was no endoleak or if the blood flow into the hematoma cavity slowed down significantly, the implantation of bare stents was stopped; if there was still contrast agent filling in the hematoma cavity, another bare stent was implanted [9].

2.2.2. Criteria for Successful Treatment of TFA with Endovascular Stent Implantation. The final angiography showed good stent position and an immediate decrease of flow in the sac of pseudoaneurysm. All branches of the parent artery were preserved. The endovascular stents implantation was regarded as successful. After the operation, the femoral artery puncture point was sutured with a conventional vascular suture device to stop bleeding, followed by local compression for about 10 minutes. Subsequently, the femoral artery puncture point was compressed with elastic bandage for 24 hours.

2.3. Follow-Up. CTA or angiography was performed 3, 6, and 12 months after discharge and then annually to observe if there was recurrence of TFA, the blood flow of collateral vessels, and the possible migration, rupture, and stenosis of stents, endoleak, and infection.

3. Results

3.1. Therapeutic Efficacy. Double-layer bare stents (LifeStent, Bard Company, USA) were successfully implanted in all five patients. Postoperative angiography showed that the pseudoaneurysm was hardly visible, and no important collateral vessels were occluded. All patients experienced local mass shrinkage and pain relief, and the pulsation and arterial murmur disappeared. The ischemic symptoms were improved. No wound infection was found, and there was no interventional therapy-associated complication. The overall therapeutic efficacy was satisfactory.

3.2. Follow-Up Outcome. The postoperative follow-up lasted 3 to 99 months (median: 24 months). All patients showed good outcome during the follow-up period, and no complications such as instent stenosis, migration, rupture, or endoleak were observed.

3.3. Typical Cases

(1) Case 1. A 29-year-old male patient with pseudoaneurysm of the right common carotid artery caused by head trauma (Figure 1)

(2) Case 2. A 36-year-old female patient presented with a pseudoaneurysm of the left superficial femoral artery due to a comminuted pelvic fracture (Figure 2)

4. Discussion

TFA is mostly caused by direct or indirect violence to the arteries. Since the pseudoaneurysm is composed of fibrous tissue, it cannot heal naturally. Most TFAs increase in size gradually with the impact of blood flow. TFA may rupture and bleed easily without proper and timely treatment. And once the thrombus on the inner wall of the blood vessel falls off, it may cause distal arterial embolism which compresses the veins and nerve adjacent and causes serious outcomes, even death [10]. The current therapy of TFA includes conservative treatment, surgical treatment, and endovascular treatment. With the development of interventional technology, endovascular minimally invasive treatment has largely replaced surgical treatment. It mainly includes endovascular covered stent-graft exclusion, implantation of multiple layer overlapping bare stents, and stent-assisted coil embolization [11, 12]. However, stent-assisted coiling has the risk of follow-up recurrence and rerupture [13]. The covered stent showed poor compliance and could lead to endoleak without complete apposition and occlude the arterial branches [14]. Aleksandar et al. reported a case of a giant hepatic artery aneurysm treated with dual layer stent placement as flow-diverting option. The hypothesis of preserving side branches that arise from the aneurysm or close to it may be an

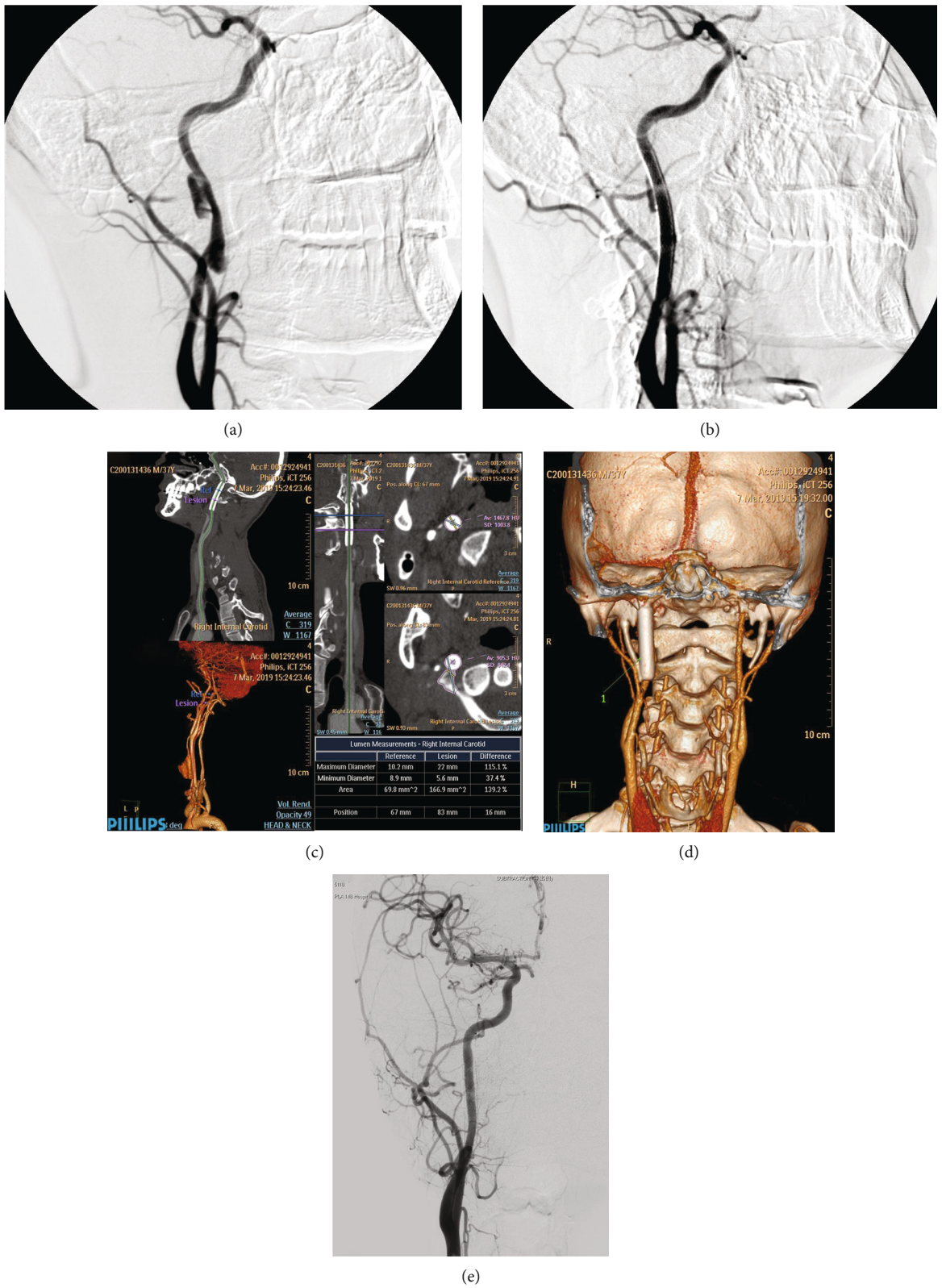

Figure 1: Pseudoaneurysm of the right common carotid artery caused by head trauma. (a) DSA before operation in February 2011 revealed a pseudoaneurysm of the right common carotid artery. (b) After double-layer bare stent placement, DSA showed that the hematoma cavity disappeared and no contrast extravasation. (c, d) CTA in Mar 2019 revealed that the blood flow in the stent lumen was smooth, and there was no stenosis in the lumen. (e) Angiography in May 2019 showed that the blood flow in the stent lumen was smooth, and there was no stenosis in the lumen.

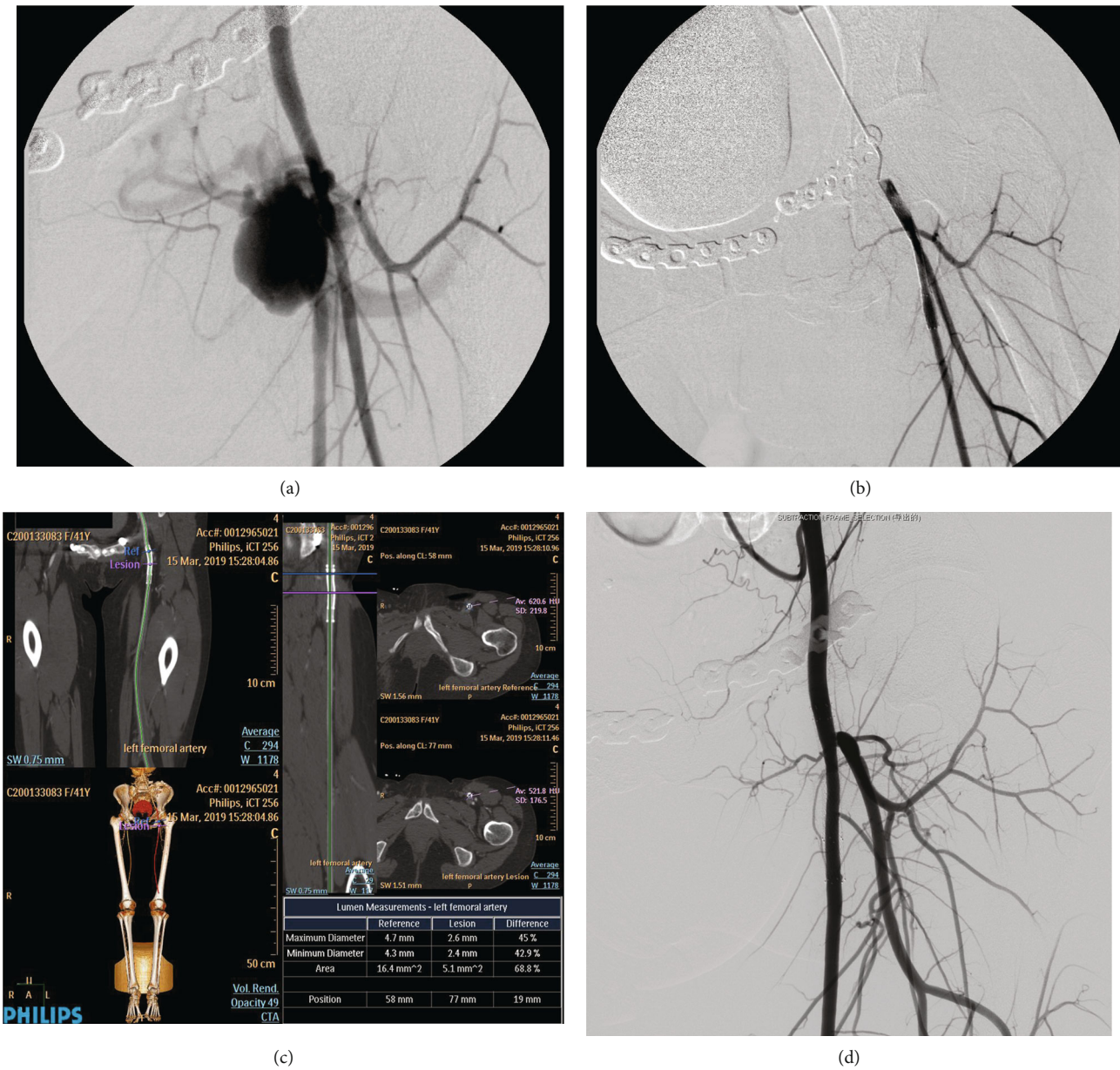

Figure 2: A pseudoaneurysm of the left superficial femoral artery due to a comminuted pelvic fracture. (a) DSA before the operation in March 2014 revealed a pseudoaneurysm at the root of the left superficial femoral artery with a 2.9 × 2.2 cm of maximum diameter. (b) After double-layer bare stent placement, DSA showed that the hematoma cavity disappeared and no contrast extravasation. (c) CTA in Mar 2019 revealed that the blood flow in the stent lumen was smooth, and there was no stenosis in the lumen. (d) Angiography in May 2019 revealed that the blood flow in the stent lumen was smooth, and there was no stenosis in the lumen.

additional potential advantage of dual layer stents over traditional stent grafts [15].

With regard to selection of stents for endovascular interventional therapy in TFA patients, multiple factors should be considered, such as long-term patency, risk of vascular rupture, coexisting thrombosis, and surrounding collateral arteries. Treatment should be individualized for different patients. The covered stent can directly cover the rupture or distal end of the pseudoaneurysm through a physical barrier, which separates the blood stream from the TFA cavity and thus prevent blood flow from impacting the hematoma cavity. As the pressure in the hematoma cavity decreases, emboli form inside the hematoma and gradually occlude the pseudoaneurysm [16]. However, the covered stent has disadvantages of affecting collateral occlusion and poor compliance. Multiple overlapping bare stents can keep important collateral vessels patent and thus are safe and effective in treating TFA [17], with relatively lower cost. In this study, all the five patients underwent double-layer bare stent implantation, and the clinical symptoms of these patients were significantly improved without obvious complications. During the long-term follow-up (up to 99 months), CTA revealed that the hematoma cavity disappeared, and the artery where the pseudoaneurysm was located had smooth blood flow. No obvious

stenosis in the stent was observed. Therefore, it is concluded that double-layer bare stent placement is one of the effective methods for TFA.

Our study was limited by its single-arm retrospective design and the small sample size. Thus, we cannot make the conclusion that double-layer bare stents can replace covered stents in the treatment of pseudoaneurysm. However, with the accumulation of cases and the extension of follow-up time, double-layer bare stent placement may become an alternative to covered stent, especially for cases with important collateral circulation. Further investigations are necessary to define the feasibility, safety, efficacy, and durability associated with this treatment option.

Data Availability

The data used to support the findings of this study are included within the article.

Conflicts of Interest

The author(s) declare(s) that they have no conflicts of interest.

Authors' Contributions

Wenle Tan and Shubin Dou contributed equally as first authors in this study.

References

[1] V. Etezadi, R. T. Gandhi, J. F. Benenati et al., "Endovascular treatment of visceral and renal artery aneurysms," *Journal of Vascular and Interventional Radiology*, vol. 22, no. 9, pp. 1246–1253, 2011.

[2] E. M. San Norberto, L. A. Fidalgo-Domingos, N. Cenizo, Á. Revilla, J. H. Taylor, and C. Vaquero, "Endovascular treatment of venous bypass graft pseudoaneurysm with the new Solaris self-expanding covered stent," *Case Reports in Vascular Medicine*, vol. 2020, Article ID 4871814, 4 pages, 2020.

[3] E. M. Marone, D. Mascia, A. Kahlberg, C. Brioschi, Y. Tshomba, and R. Chiesa, "Is open repair still the gold standard in visceral artery aneurysm management?," *Annals of Vascular Surgery*, vol. 25, no. 7, pp. 936–946, 2011.

[4] N. Tulsyan, V. S. Kashyap, R. K. Greenberg et al., "The endovascular management of visceral artery aneurysms and pseudoaneurysms," *Journal of Vascular Surgery*, vol. 45, no. 2, pp. 276–283, 2007, discussion 283.

[5] N. E. A. Saad, W. E. A. Saad, M. G. Davies, D. L. Waldman, P. J. Fultz, and D. J. Rubens, "Pseudoaneurysms and the role of minimally invasive techniques in their management," *Radiographics*, vol. 25, Supplement 1, pp. S173–S189, 2005.

[6] M. Venturini, P. Marra, M. Colombo et al., "Endovascular repair of 40 visceral artery aneurysms and pseudoaneurysms with the Viabahn stent-graft: technical aspects, clinical outcome and mid-term patency," *Cardiovascular and Interventional Radiology*, vol. 41, no. 3, pp. 385–397, 2018.

[7] Y. Zhang, Q. Lu, Z. Zhao et al., "Multiple overlapping uncovered stents as an alternative flow-diverting strategy in the management of peripheral and visceral aneurysms," *Journal of Vascular Surgery*, vol. 60, no. 5, pp. 1209–1217, 2014.

[8] S. Zbair, J. Dinari, A. Siwane, S. Lezar, and F. Essodegui, "Post traumatic pseudoaneurysm of the external carotid," *The Pan African Medical Journal*, vol. 28, p. 272, 2017.

[9] L. Zhang, C. P. Yin, H. Y. Li et al., "Multiple overlapping bare stents for endovascular visceral aneurysm repair: a potential alternative endovascular strategy to multilayer stents," *Annals of Vascular Surgery*, vol. 27, no. 5, pp. 606–612, 2013.

[10] N. Li, Q. S. Lu, J. Zhou, J. M. Bao, Z. Q. Zhao, and Z. P. Jing, "Endovascular stent placement for treatment of spontaneous isolated dissection of the superior mesenteric artery," *Annals of Vascular Surgery*, vol. 28, no. 2, pp. 445–451, 2014.

[11] K. Spanos, C. Karathanos, K. Stamoulis, and A. D. Giannoukas, "Endovascular treatment of traumatic internal carotid artery pseudoaneurysm," *Injury*, vol. 47, no. 2, pp. 307–312, 2016.

[12] J.-P. P. M. de Vries, "Treatment of complex thoracoabdominal or juxtarenal aortic aneurysms with a multilayer stent," *Journal of Endovascular Therapy*, vol. 19, no. 1, pp. 125–127, 2012.

[13] J. Steinberg, V. Cheung, G. Goel, J. S. Pannell, J. Nation, and A. Khalessi, "Vessel-preserving stent-assisted coil embolization of an extracranial internal carotid artery pseudoaneurysm that developed after tonsillectomy in a pediatric patient: initial case report," *Journal of Neurosurgery. Pediatrics*, vol. 19, no. 1, pp. 8–12, 2017.

[14] W. Wang, M. H. Li, Y. D. Li et al., "Treatment of traumatic internal carotid artery pseudoaneurysms with the Willis covered stent: a prospective study," *The Journal of Trauma*, vol. 70, no. 4, pp. 816–822, 2011.

[15] A. Gjoreski, F. Risteski, and G. Damjanoski, "Successful endovascular treatment of a giant hepatic artery aneurysm with dual layer stents placement as flow-diverting option: case report," *Open Access Macedonian Journal of Medical Sciences*, vol. 7, no. 3, pp. 403–406, 2019.

[16] B. Mohan, S. Singal, A. S. Bawa, P. Mahindra, and M. Yamin, "Endovascular management of traumatic pseudoaneurysm: short & long term outcomes," *Journal of Clinical Orthopaedics and Trauma*, vol. 8, no. 3, pp. 276–280, 2017.

[17] V. Stager, R. Gandhi, D. Stroman, C. Timaran, and H. Broker, "Traumatic internal carotid artery injury treated with overlapping bare metal stents under intravascular ultrasound guidance," *Journal of Vascular Surgery*, vol. 53, no. 2, pp. 483–486, 2011.

Hindawi
BioMed Research International
Volume 2021, Article ID 5543520, 15 pages
https://doi.org/10.1155/2021/5543520

Research Article

Advances in Endovascular Intervention Using Biomaterials: Study on Heat Efficiency of Scissor-Type Ultrasonic Catheter Device

Minoru Morita,[1] **Jingjing Yang**,[2] **and Zhongwei Jiang**[1]

[1]*Yamaguchi University, Tokiwadai 2-16-1, Ube, Yamaguchi, Japan*
[2]*Kunming University of Science and Technology, 727 South Jingming Road, Chenggong District, Kunming 650500, China*

Correspondence should be addressed to Minoru Morita; mmorita@yamaguchi-u.ac.jp

Received 5 January 2021; Revised 8 February 2021; Accepted 20 February 2021; Published 10 March 2021

Academic Editor: Xing Chen

To improve the performance of the ultrasonic device during the endovascular operation, a scissor-type ultrasonic catheter device with compound vibration was developed. The heat generated by friction between the target and the device affects its coagulation mechanism while the actuator contacts the tissue. The scissor-type ultrasonic catheter device proposed in this study is expected to improve heat generation performance because it has the action of rubbing the object when it is pushed by combined vibration. In addition, since it is constructed by simple notch processing, it can be miniaturized and can be expected to be introduced into catheters. However, the observation of ultrasonic vibration during frictional heating is difficult, which is an issue for device design. In this paper, a thermal-structure coupling analysis was done using the finite element method to calculate the heat generation efficiency and evaluate its coagulation performance.

1. Introduction

Vibration has been widely utilized for therapeutic purposes. Since the 1950s, many medical devices based on vibration have been invented and applied for therapy applications including tissue cutting, cataract phacoemulsification, fat emulsion, ultrasonography, bone fracture healing, cancer treatment, sonothrombolysis, and so on [1, 2]. These devices work based on mechanical vibration, and the effective vibration needs to be delivered to the tip directly in complicated environments with many restrictions. In this thesis, a new end-effector with the desired vibration mode at the end-effector tip was designed for catheter surgery applications. The proposed new structure of the end-effector can transmit the longitudinal elastic wave through a shaft and convert it into scissor-type vibration (compound longitudinal-transversal vibration) just at the end-effector tip.

The main research line of this thesis is to design an effective end-effector used in a microcatheter for hemostasis by coagulated proteins. In the coagulation of proteins by friction of an end-effector which is excited by mechanical vibration, the tip transversal vibration is needed for supplying friction heating function in narrow blood vessels. An ultrasonic catheter surgery device is a device that uses ultrasonically vibrating heat to denature the tissue protein and simultaneously performs hemostasis and cutting function at the incision. According to the reports on hemostasis by an ultrasonic device [3, 4], the essential hemostatic mechanism is that the coagulated proteins caused by the friction heat seal the bleeding vessels. For these devices, the heat generation efficiency depends on the state of contact between the tissue and the vibrating blade because the blood coagulation needs enough heat (the coagulated protein occurs at 63 degrees [5]). On the contrary, it will take a long time to interrupt the blood flow if the heat does not rise enough, which will lead to incision closure difficulties and other tissue damage. Therefore, we realized that the effective solution for stopping the bleeding quickly during surgery is to improve the heat generation efficiency at the incision.

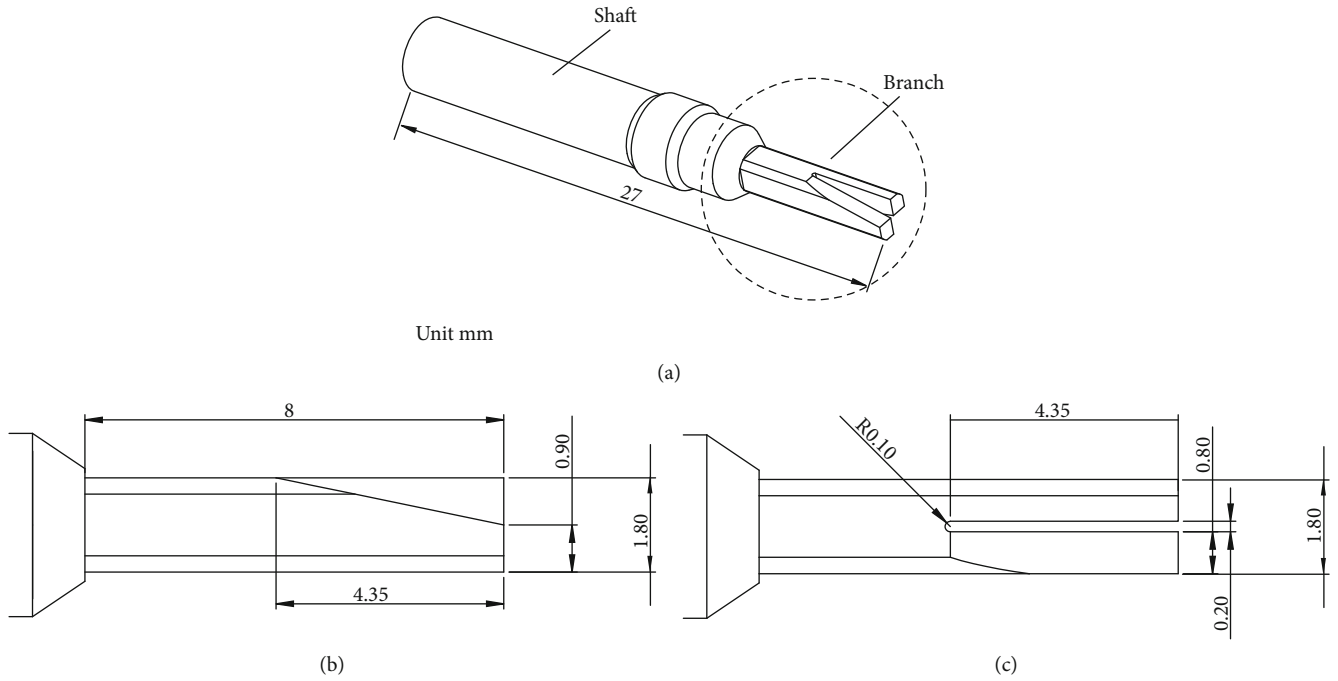

Figure 1: Schematic image of scissor-type ultrasonic device: (a) isometric view, (b) side view of branch, and (c) top view of branch.

In this study, we analysed an ultrasonic catheter surgery device with a novel structure to improve the heat generation efficiency by exciting the scissor-type compound vibration at the tip of the device and using the ultrasonic vibration of rubbing while pushing the blade against the tissue. To find the optimal design of this new ultrasonic catheter surgery device, it is necessary to evaluate the heat generation phenomenon and compare it with other models. It is difficult to observe small vibrations at a high sampling speed. Due to the individual differences of biomaterials, the reproducibility of the test and associated parameters which contribute to device performance are difficult to be ensured and evaluated, respectively. Therefore, we developed a finite element analysis model with heat-structural interaction to evaluate the device's coagulating characteristics, and the heat generation performances with different model shapes were simulated and compared in this paper.

2. Design and Modelling

2.1. Designed Method of Ultrasonic Device. The schematic image of the new proposed scissor-type actuator was designed in our previous research [6–9], as shown in Figure 1. This actuator consisted of a shaft and two small branches.

The two branches were connected to the shaft, and two inverse symmetrical slant planes are cut at the head end of the branches. Figure 2 presents the cutaway view of the scissor-type ultrasonic incision device. It works the following way. Firstly, a sinusoid voltage with the required frequency is applied to the transducer to generate the longitudinal elastic wave. Then, the longitudinal wave propagates through the shaft and reaches to the branch; the wave impinges on the slant plane with an oblique angle and excites a fluctuating motion of the branch due to the reflection and mode conversion caused by the wave reflection. Finally, swing the branches in the opposite direction between branches I and II like a scissor, as shown in Figure 2.

2.2. Mathematic Modelling of Structural-Heat Problem. The structural dynamics equation is as follows [10, 11].

$$[M]\{\ddot{u}\} + [D]\{\dot{u}\} + [K]\{u\} = \{F(t)\} + [P]. \quad (1)$$

Here, $[M]$, $[D]$, and $[K]$ are the mass matrix, damping matrix, and stiffness matrix, respectively; $\{F(t)\}$ is the time-varying load; $[P]$ is the contact pressure; and $\{u\}$, $\{\dot{u}\}$, and $\{\ddot{u}\}$ are the displacement, velocity, and acceleration, respectively. The penalty method was used to calculate the contact pressure $[P]$, and then Equation (1) was used to calculate the frictional stress and vibrational velocity of the actuator. The transient analysis was done to analyse the heat transfer between the actuator and tissue, as follows:

$$[C]\left\{\dot{h}\right\} + [K]\{h\} = \{Q(h)\}, \quad (2)$$

where $[C]$ is the specific heat matrix, $[K]$ is the thermal conductance matrix, $\{Q(t)\}$ is the heat flow matrix, and $\{h\}$ and $\{\dot{h}\}$ are the temperature and time derivative of temperature, respectively.

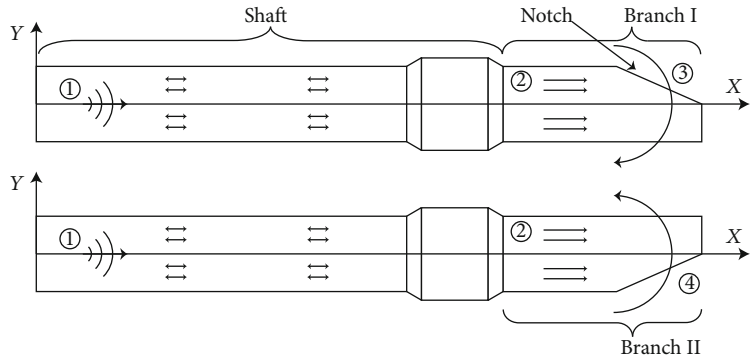

Figure 2: Cutaway of two inverse symmetry branches: ① input signal, ② longitudinal wave propagating to tip, ③ mode conversion and swing branch I, and ④ branch II swings the opposite direction from branch I.

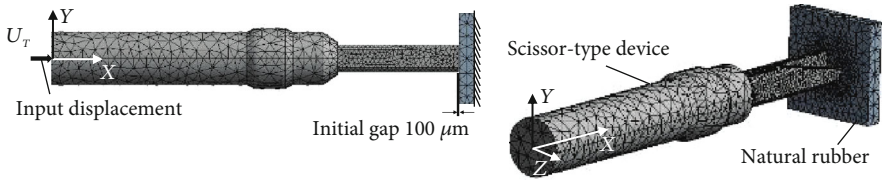

Figure 3: Three-dimensional view of FEM model for scissor-type device. Finite element mesh was generated using 10-node tetrahedral elements: (a) side view; (b) isometric view.

Table 1: Parameters of actuator and natural rubber.

Material property	Titanium	Natural rubber
Young's Modulus	96 GPa	17.6 MPa
Density	4620 kg/m^2	1200 kg/m^2
Poisson ratio	0.36	0.3
Thermal expansion	9.4×10^{-6}/°C	270×10^{-6}/°C
Thermal conductivity	21.9 W/m°C	0.2 W/m°C
Specific heat	522J/kg°C	150 J/kg°C
Frictional coefficient	0.2	
Initial temperature	22°C	

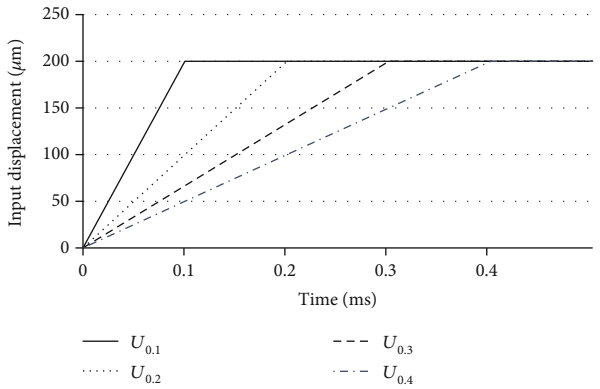

Figure 4: Input displacement signal.

2.3. Finite Element Method and Modelling. The finite element method (FEM) model used in this study was based on the previous research method, which has proposed an analysis method for friction stir welding [12–18]. The FEM model of the ultrasonic catheter surgery for structural-heat analysis was developed by ANSYS software, as shown in Figure 3. The material of the human tissue was used as the natural rubber to simplify simulation. As the mesh near the contact surface, 0.2 mm 10-node tetrahedral elements were used. The material parameters of the actuator and nature rubber are listed in Table 1. As the boundary condition, the bottom surface of the rectangular parallelepiped rubber target was fixed. From previous research, the shaft of the ultrasonic catheter used in this research has a structure to generate only longitudinal vibration [6, 9]. Therefore, only the X-direction displacement was inputted to the left end of the shaft as a boundary condition. The input signal was the displacement with 200 μm added on the left end of the shaft to press the shaft to the rubber target, and the phenomenon of heat generation during vibration of the actuator was recorded. As we know, resonance of the actuator by the input sinusoidal wave requires a relatively long analysis time to obtain enough amplitude, which leads to the problem of computational cost. In addition, the ultrasonic catheter device does not generate heat unless pressed against the

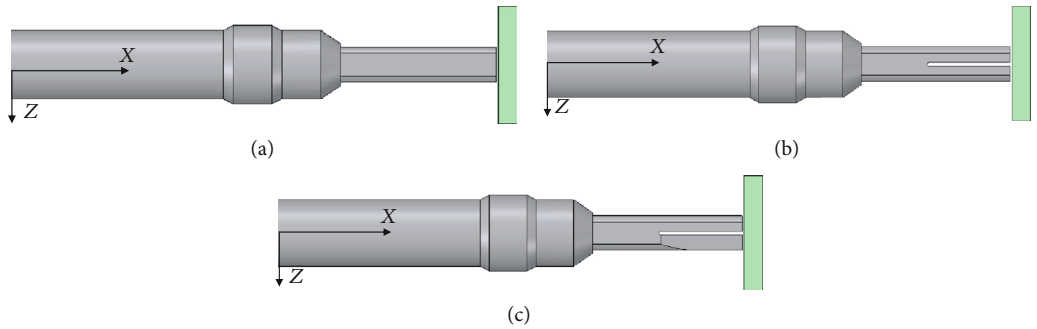

Figure 5: Model shapes of branches with different tips: (a) Model 1 (longitudinal), (b) Model 2 (longitudinal+slit), and (c) Model 3 (scissor).

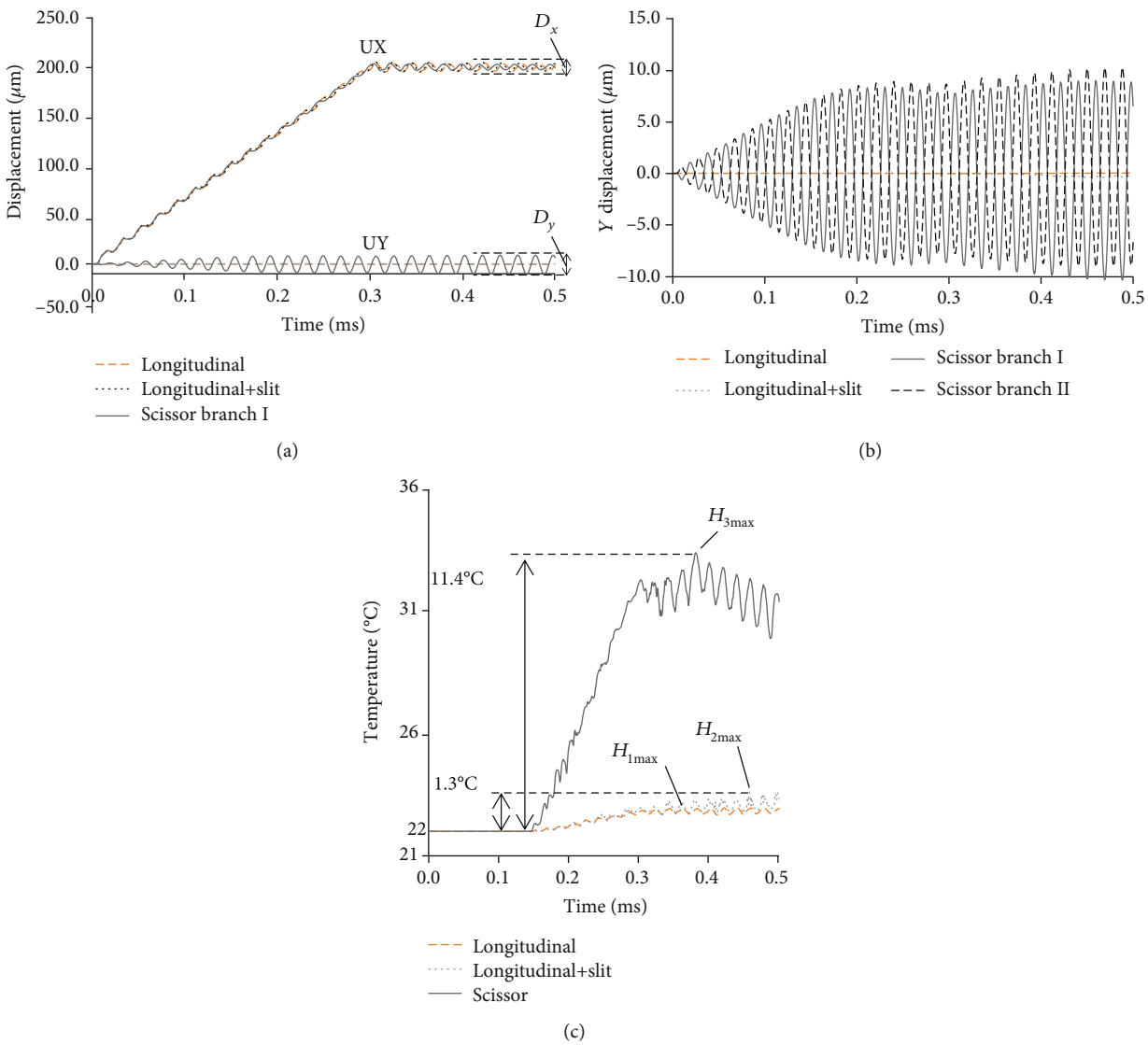

Figure 6: Time curve results of displacement and temperature about each branch model shape tip: (a) X- and Y-direction displacement-time curve, (b) Y-direction displacement-time curve, and (c) temperature-time curve.

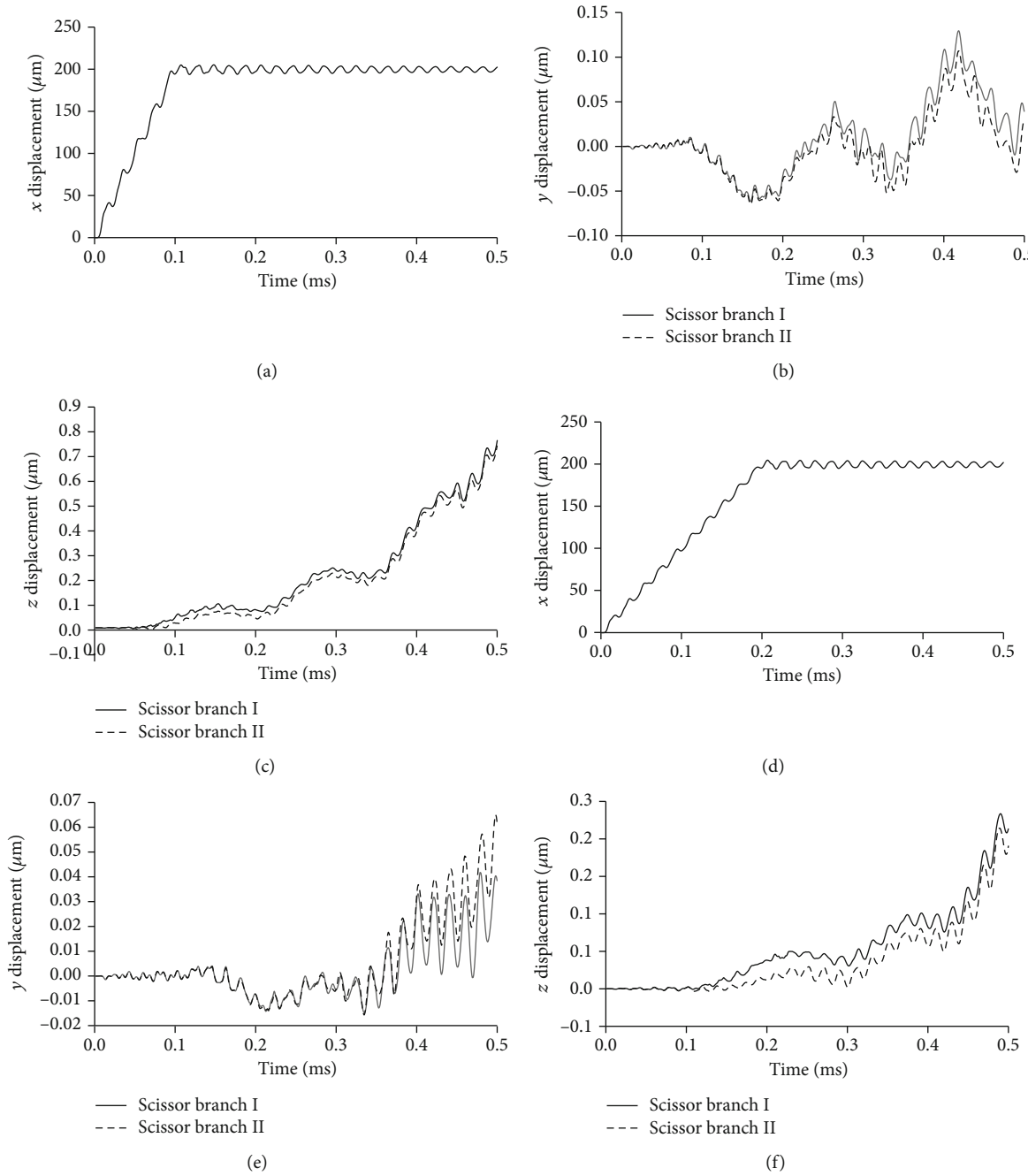

Figure 7: Continued.

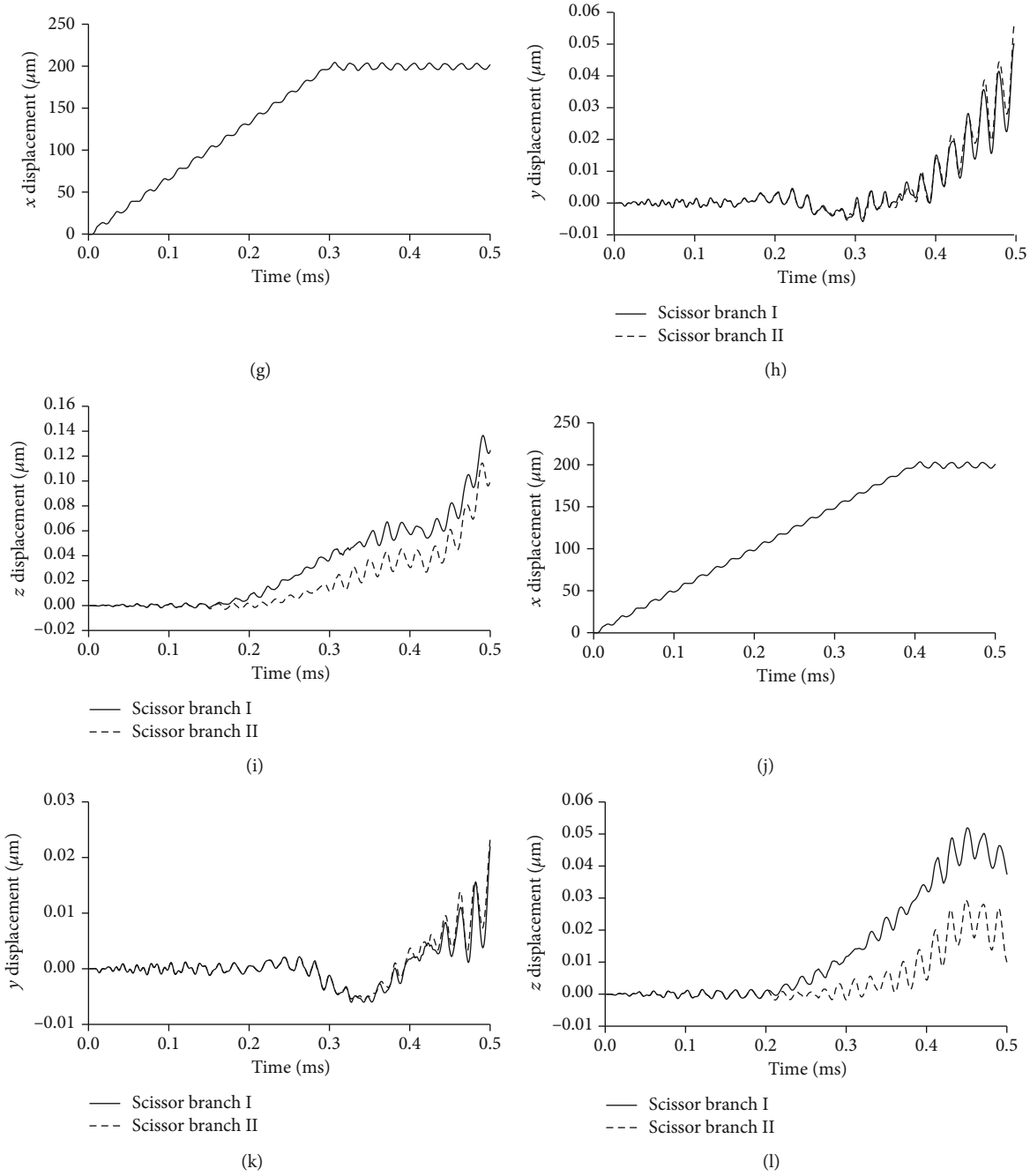

Figure 7: Continued.

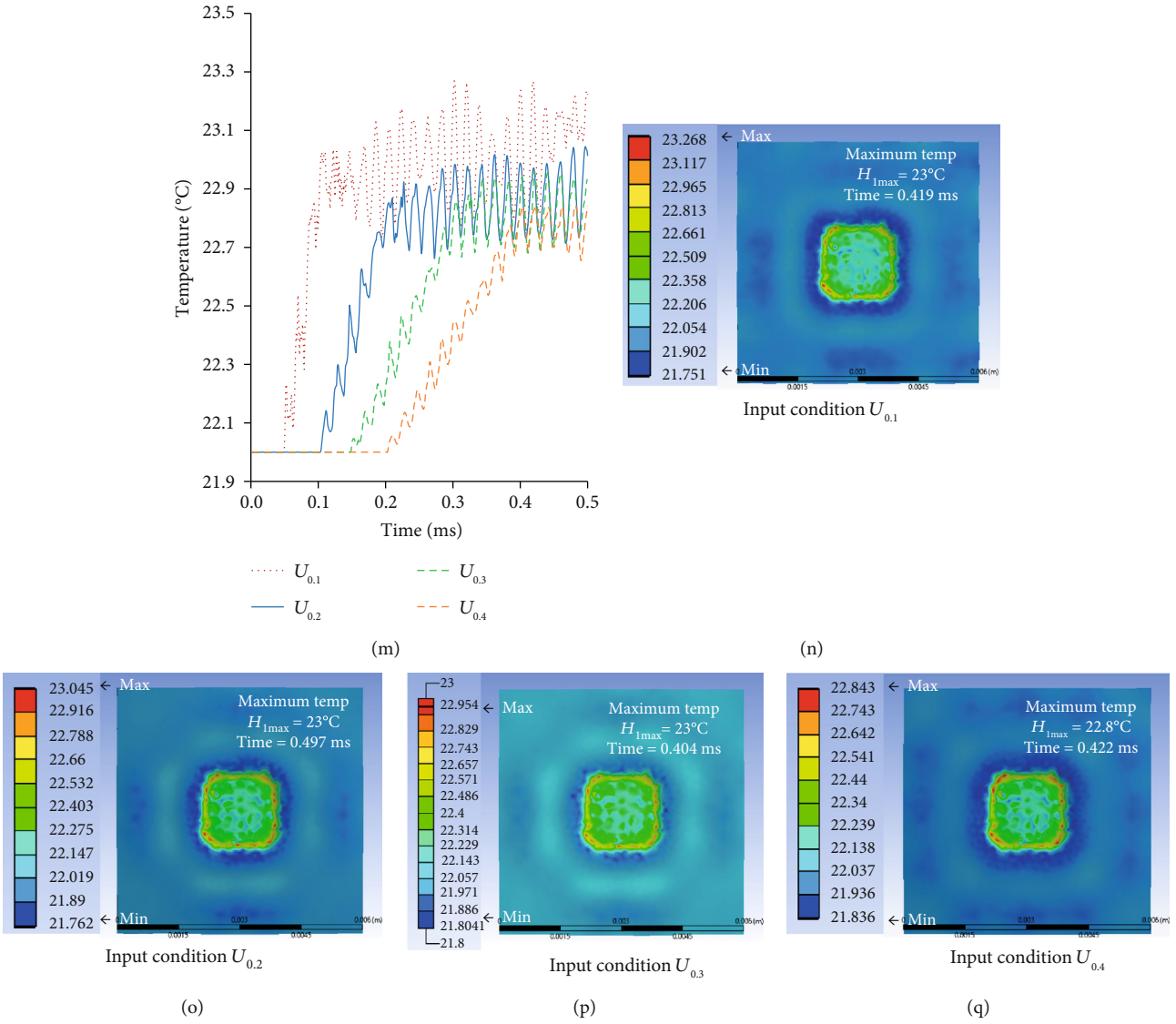

FIGURE 7: Analysis results of ultrasonic catheter device Model 1 (longitudinal). (a–c) Displacement-time curve of input condition $U_{0.1}$. (d–f) Displacement-time curve of input condition $U_{0.2}$. (g–i) Displacement-time curve of input condition $U_{0.3}$. (j–l) Displacement-time curve of input condition $U_{0.4}$. (m) Temperature-time curve. (n–q) Temperature contour map at peak value of input condition $U_{0.1}$~$U_{0.4}$.

target. Considering the above problems, in this study, the input displacement (U_T) was sliced by different time, as Equation (3) and Figure 4 show, and enough sinusoidal amplitude and can be obtained in a short analysis time. The initial gap between the catheter device tip and natural rubber was 100 μm.

$$U_T = \begin{cases} 200[\mu\text{m}] \bullet \dfrac{t}{T} \ (t \le T), \\ 200[\mu\text{m}] (t > T), \end{cases} \quad T = 0.1 \sim 0.4. \tag{3}$$

3. Results and Discussion

3.1. Effect of Branch Shape. To confirm the effect of the branch shape on the heat generation efficiency, three types of models with different structures were developed and analysed, as shown in Figure 5. Model 1 (longitudinal tip) has a simple branch with no slit and notches on the actuator tip, in which the longitudinal vibration mode was excited along the whole actuator. In Model 2 (longitudinal+slit), a slit was cut at the centre of the branch, and the longitudinal vibration mode same as Model 1 was excited. Compared with the above 2 models, Model 3 cut two inverse symmetrical slant planes at the branch tips, and a scissor-type vibration was excited successfully by the longitudinal input signal. Figure 6 shows the analysis results of the displacement in the X- and Y-directions and the friction heat temperature for each model. For the input displacement, the function at $T = 0.3$ ms in Equation (3) was used. As the results show, the displacements in the X-direction were the same for each model;

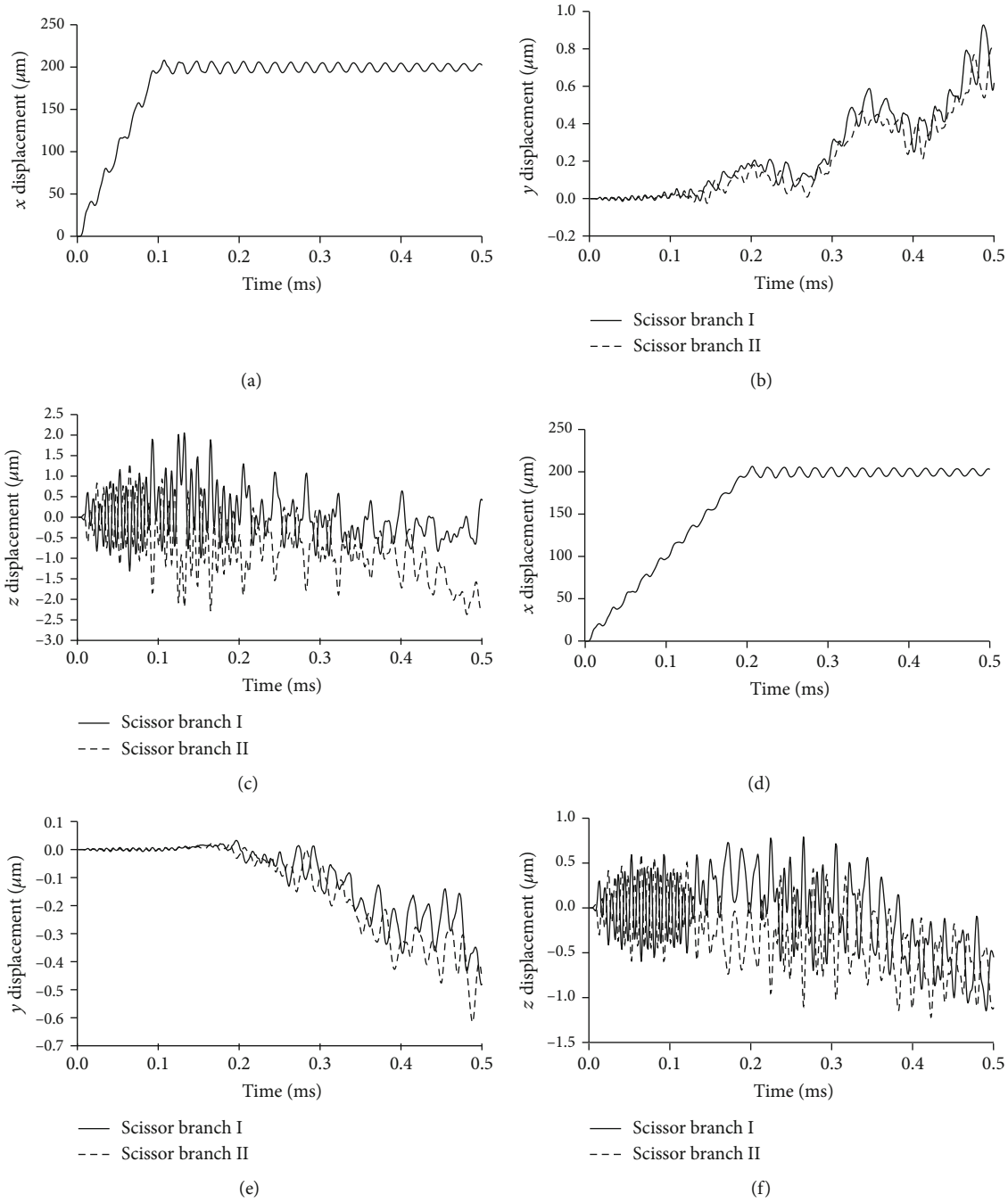

Figure 8: Continued.

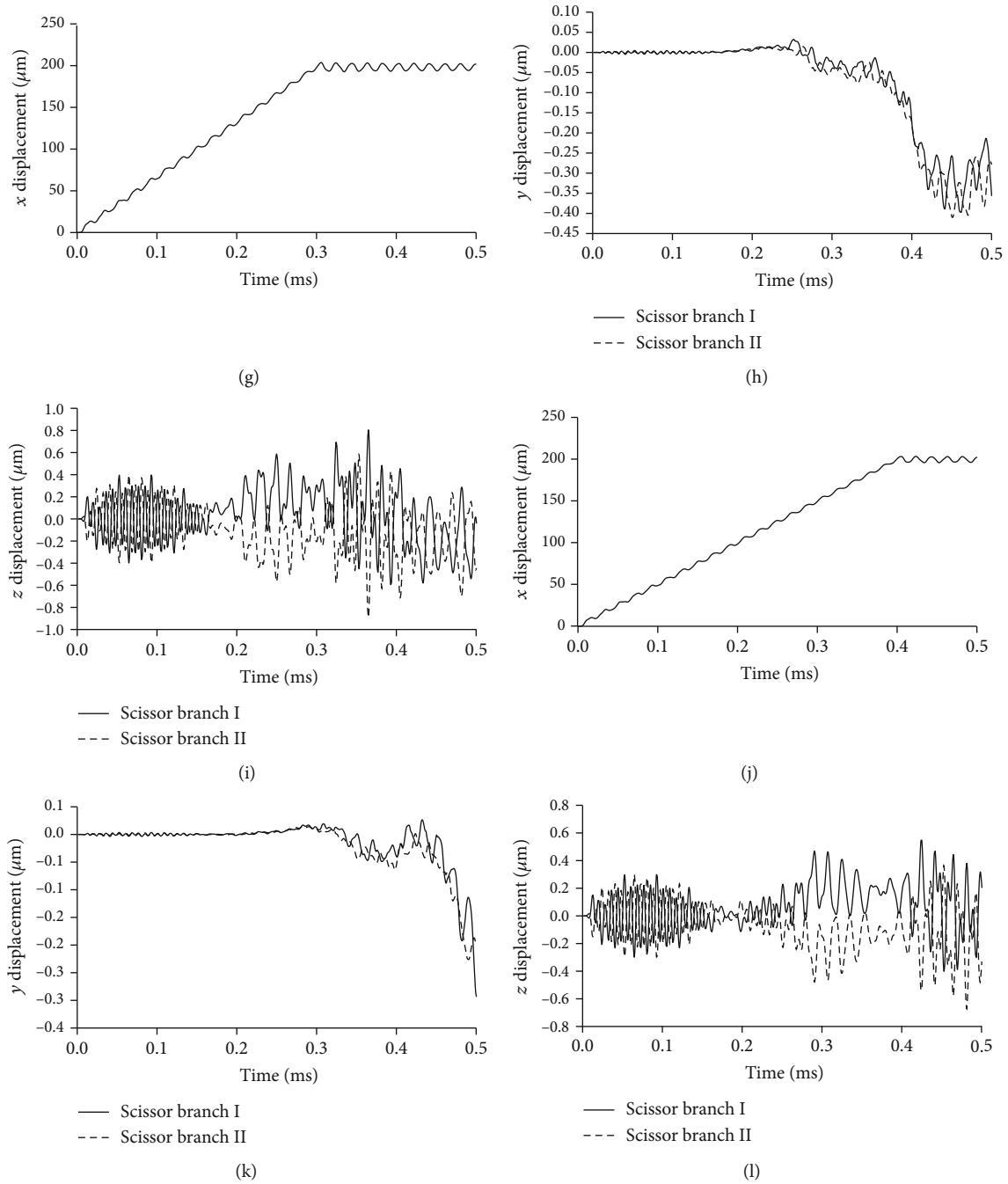

Figure 8: Continued.

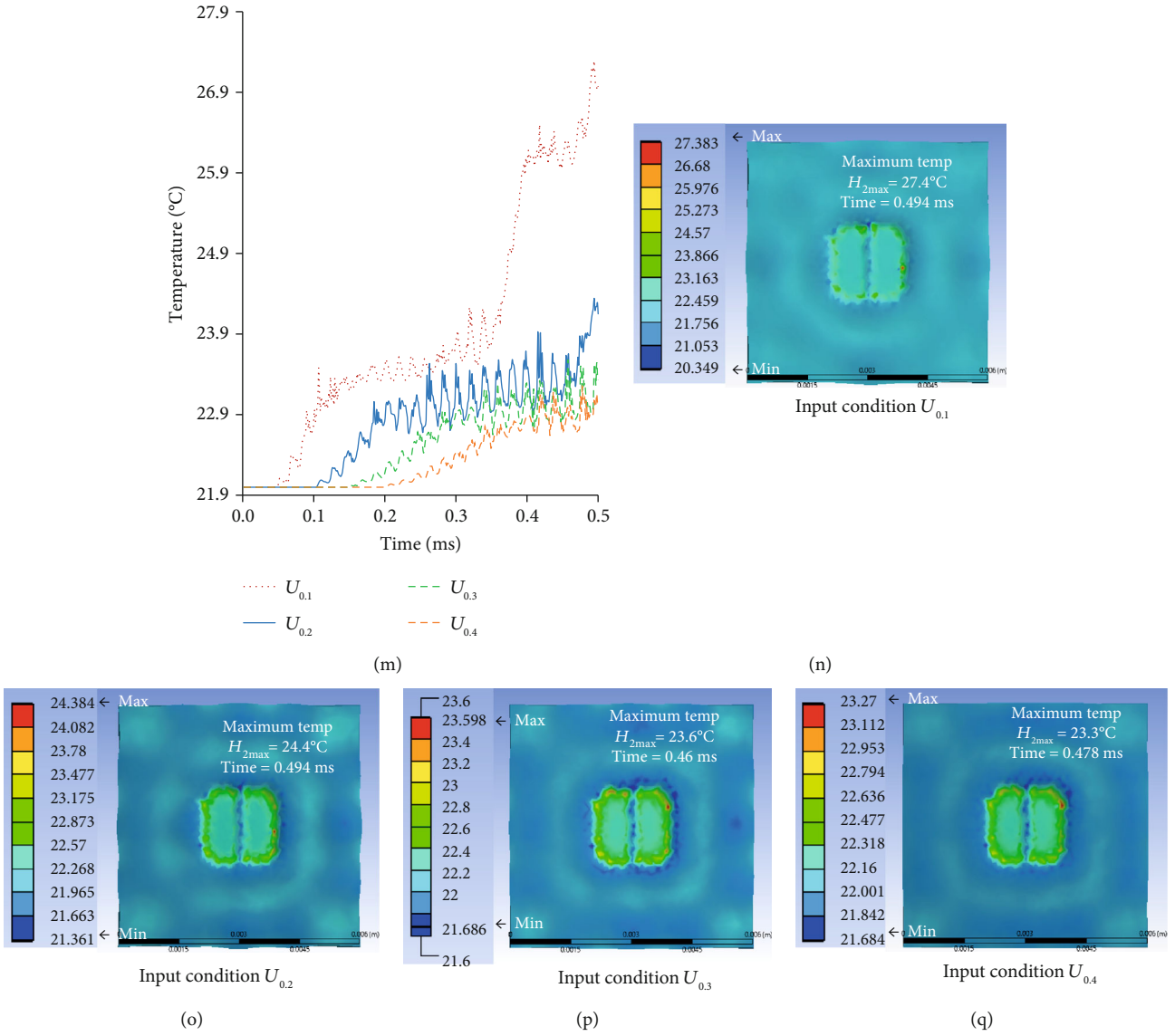

FIGURE 8: Analysis results of ultrasonic catheter device Model 2 (longitudinal+slit). (a–c) Displacement-time curve of input condition $U_{0.1}$. (d–f) Displacement-time curve of input condition $U_{0.2}$. (g–i) Displacement-time curve of input condition $U_{0.3}$. (j–l) Displacement-time curve of input condition $U_{0.4}$. (m) Temperature-time curve. (n–q) Temperature contour map at peak value of input condition $U_{0.1}$~$U_{0.4}$.

however, the displacements in the Y-direction were totally different. Under the same input longitudinal displacement, the longitudinal vibrations at the branch tips are almost the same, but the transverse vibration of Model 3 was clearly bigger than that of the other two models, which means Model 3 excited the transverse vibration successfully. The Y-direction displacements of branches I and II of Model 3 are recorded and shown in Figure 6(b). Obviously, the transverse vibrations of these two branches are reversed at the same time. It is confirmed that each branch vibrated in the opposite direction, which induces a scissor-type vibration at the actuator tip. The displacement in the Z-direction was about 10% of the X-direction; it is considered that the influence of the heat generation by the Z-direction displacement is small.

Comparing the maximum frictional heat temperature (H_{max}) of each model, Models 1 and 2 increased only 1.3°C from the initial temperature of 22°C in 0.5 ms, while Model 3 increased 11.4°C. The temperature increase rate of the scissor-type actuator is more than 10 times compared with that of the other two models. This indicates that the heating generation of Model 3 is higher than that of the other models. From these results, it is considered that generating the vibration amplitude in the Y-direction due to the swing in Figure 2, ③ and ④, contributed to the improvement of the heat generation performance of Model 3. To analyse the thermal distribution between the

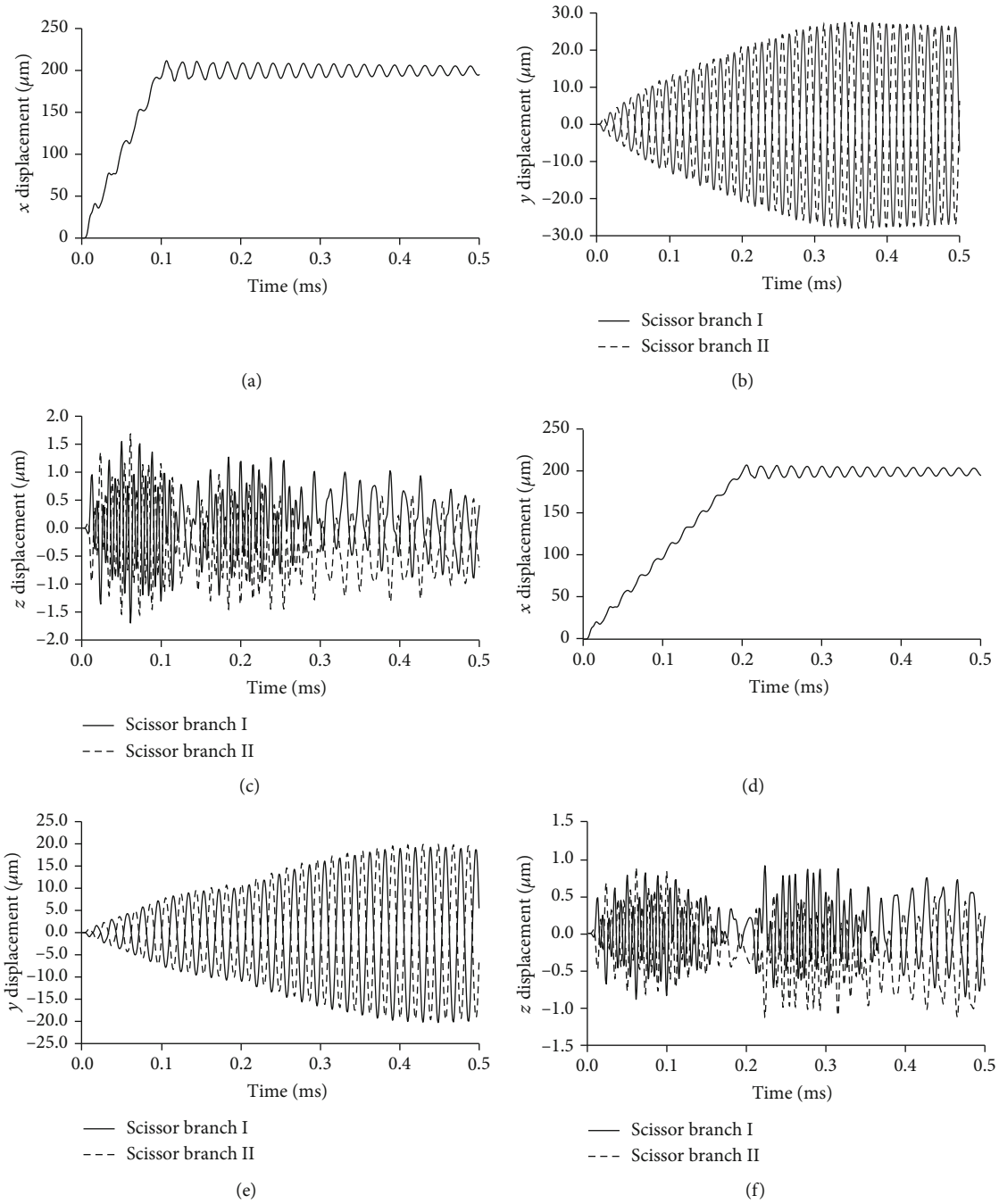

Figure 9: Continued.

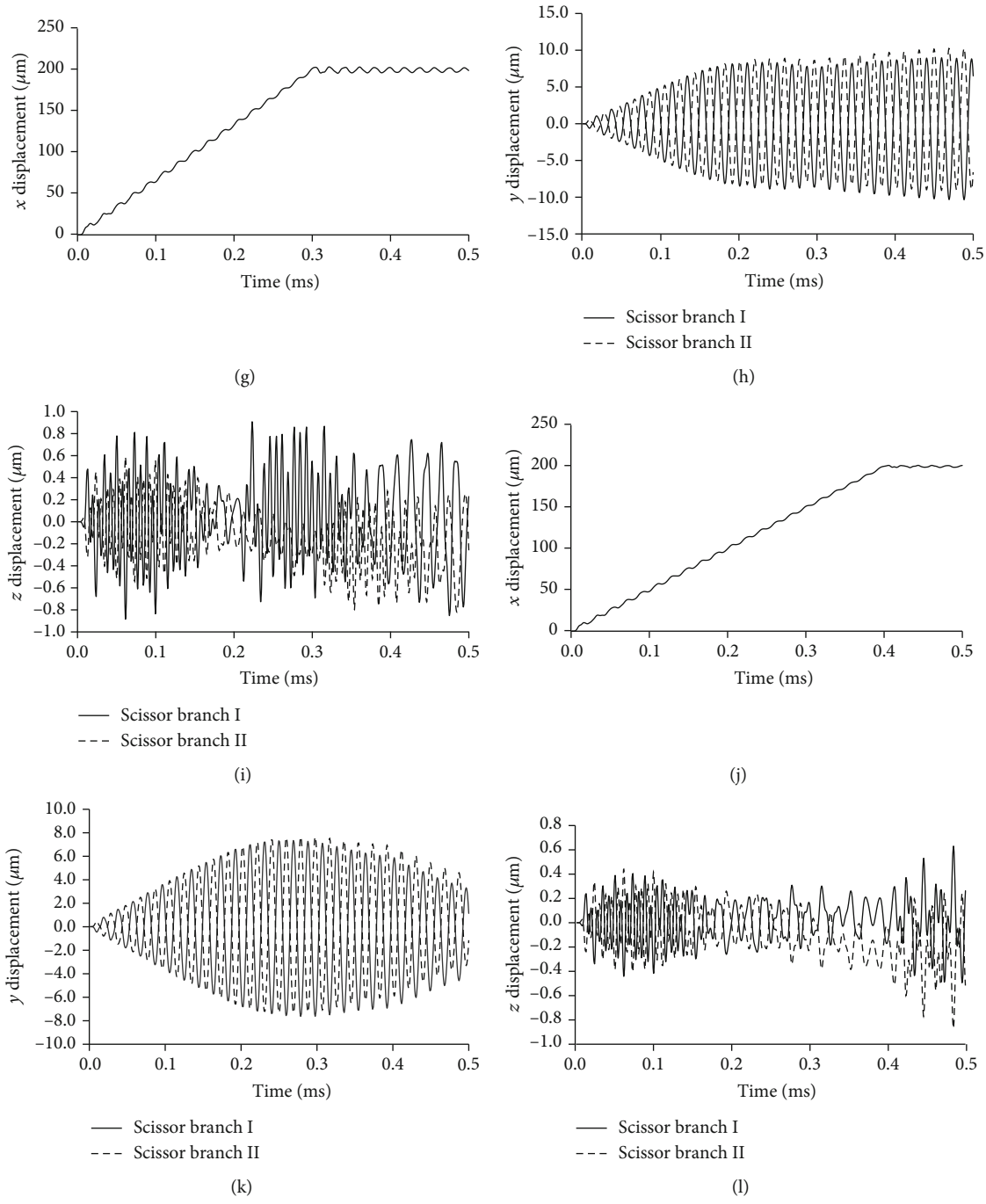

Figure 9: Continued.

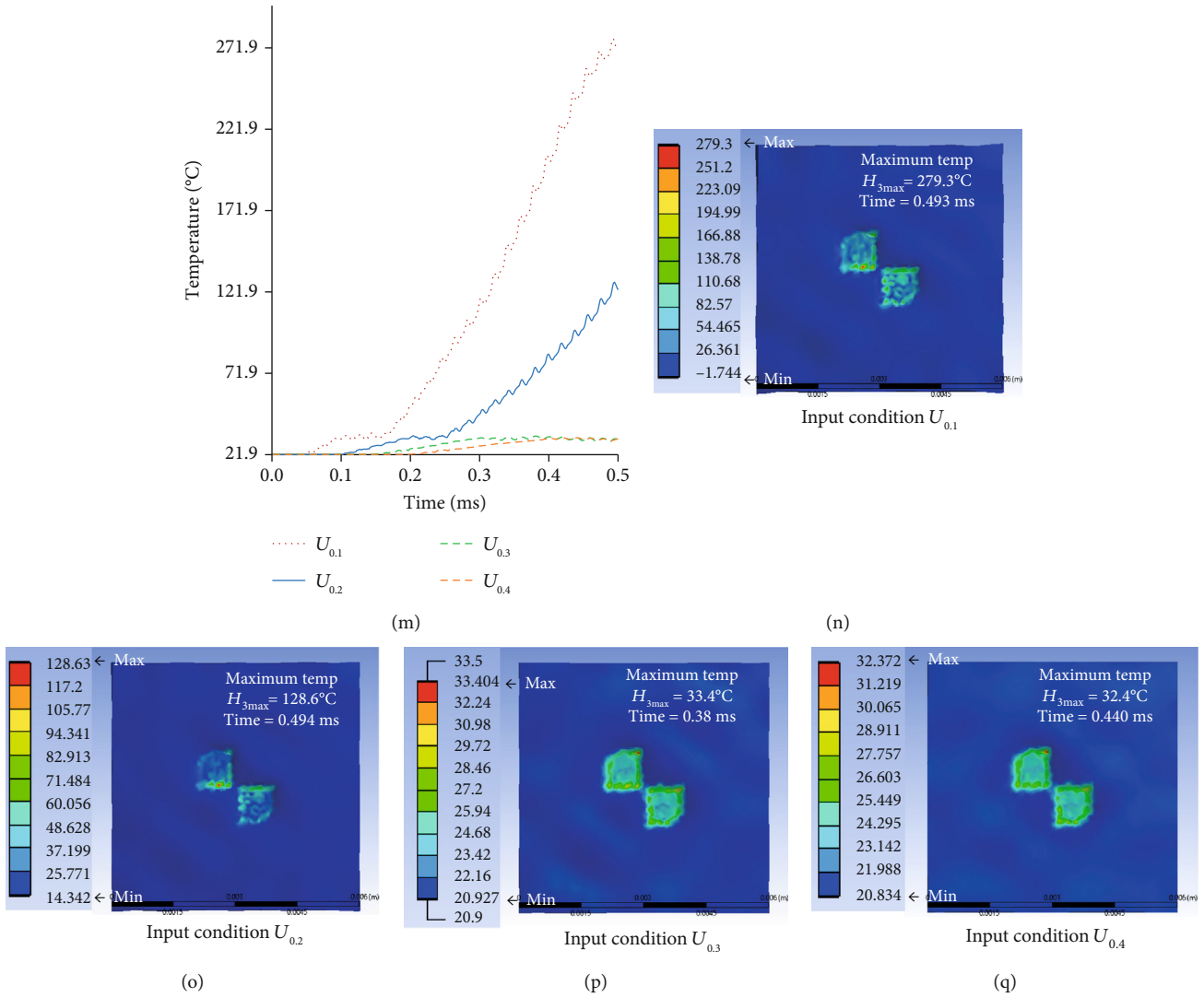

Figure 9: Analysis results of ultrasonic catheter device Model 3 (scissor). (a–c) Displacement-time curve of input condition $U_{0.1}$. (d–f) Displacement-time curve of input condition $U_{0.2}$. (g–i) Displacement-time curve of input condition $U_{0.3}$. (j–l) Displacement-time curve of input condition $U_{0.4}$. (m) Temperature-time curve. (n–q) Temperature contour map at peak value of input condition $U_{0.1}$~$U_{0.4}$.

actuator tip and rubber, the temperature contour maps of different models at the peak value time were recorded and shown in Figures 7–9. The heat generation tends to increase at the edge of the tip of the ultrasonic catheter device.

3.2. Effect of Input Velocity. Since this paper analyses by the input condition of Equation (3) and Figure 4, the input speed affects the results and the results may differ from the real operation. To evaluate the validity of the analysis model, the effect of changing the input velocity on displacement was discussed in this chapter. The velocity condition was changed by using the function at $T = 0.1$, 0.2, 0.3, and 0.4 ms in Equation (3). The measurement point was set as the catheter device tip. Figures 7–9 show the analysis results about the displacement-time curve, temperature-time curve, and temperature contour map of each model. Figures 10(a)–10(c) show the simulated results of peak-to-peak displacements in each direction (*Dx*, *Dy*, and *Dz*). The results show that the expected vibration modes are excited in each model. Figure 10(d) summarizes the analysis results of the maximum temperature of the target rubber. The displacement results were suggested to be valid because the displacement in each direction increased with the speed of the input displacement, and the *Y*-direction displacement of Model 3 has the opposite direction vibration in each branch. The temperature results were suggested to be valid because the heat generation starting time has become faster depending on the speed of the input displacement, and the temperature also increased with the speed. In Figure 10(a), the input velocity has a big influence on the output

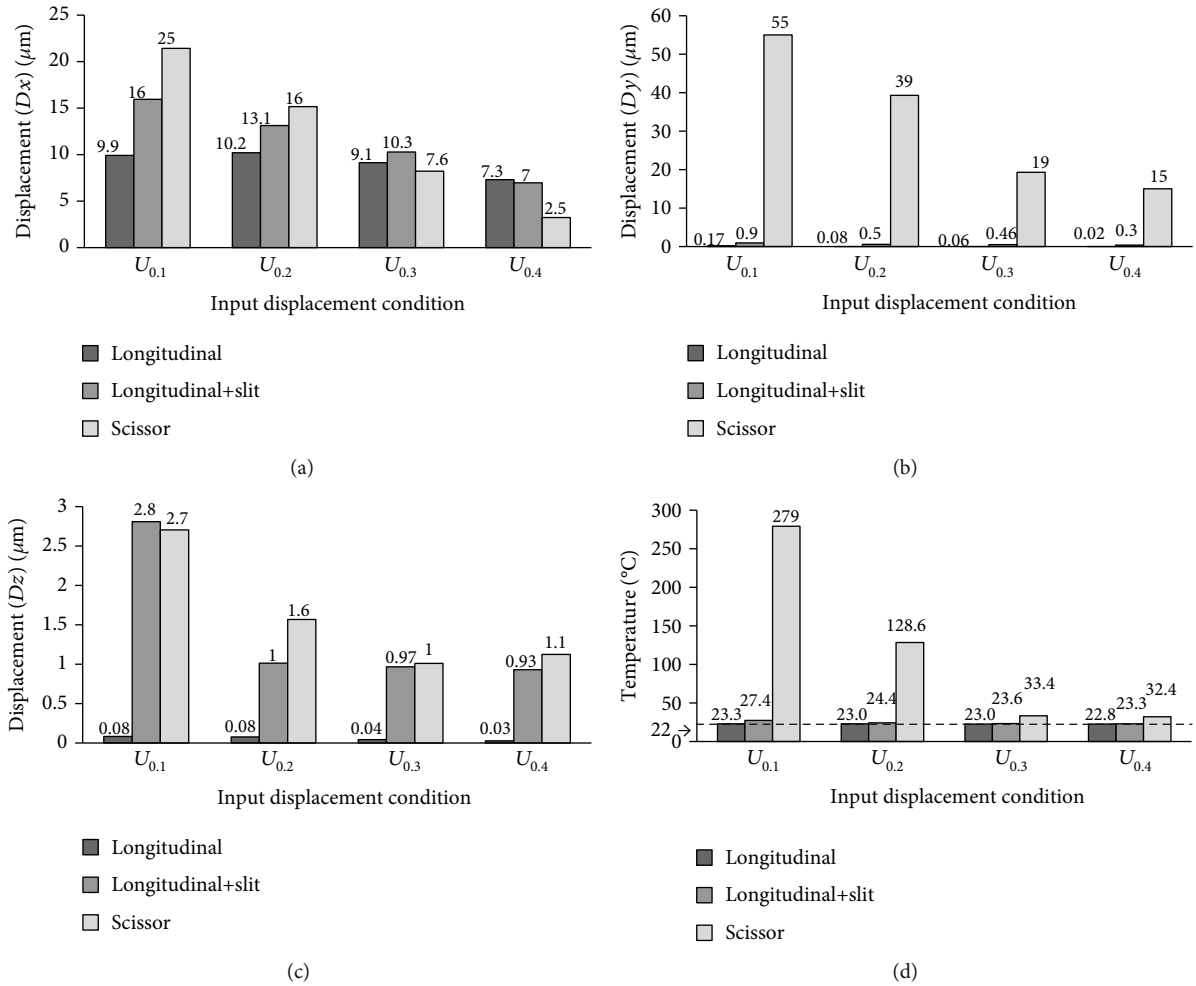

Figure 10: Peak-to-peak displacement and maximum template results of each branch model tip with different input velocities, (a) X-direction displacement (Dx), (b) Y-direction displacement (Dy), (c) Z-direction displacement (Dz), and (d) maximum temperature (H max).

displacement of the X-direction in Model 3 (scissor). It is considered that the bending vibration of the Y- and Z-directions can be affected by the amplitude of the X-direction. The dashed line of Figure 10(d) is drawn at the initial temperature of 22°C; the result of the temperature corresponds well to the result of the displacement in the Y-direction in Figure 10(b).

Moreover, the result of Model 3 (scissor) suggested that the Y-direction displacement has a large effect on the heat generation because the results are better under the input conditions of $U_{0.3}$ and $U_{0.4}$, even though the X-direction displacement is smaller than the other models. From these results, the amplitude increases in a direction parallel (Y- or Z-direction) to the surface of the target are conjectured to improve the heat generated performance. These results were explained in terms of the heating phenomenon by friction; the validity of the analytical model is considered to have been evaluated. This fact indicates that the scissor-type vibration mode contributes to the improvement of the heat generation performance because this mode vibrates parallel to the surface while pressing the target.

4. Conclusions

In this paper, the ultrasound catheter device was designed to generate a composite vibration like a scissor, and then the structural-heat interaction analysis was conducted by a series of finite element models to evaluate the heat generating performance. In the simulation, the results of improving the heat generation performance with our developed scissor-type ultrasonic catheter device were obtained. This fact indicates that the scissor-type vibration mode contributes to the improvement of the heat generation performance because this mode vibrates parallel to the surface while pressing the target. This indicates that the heating generation of our developed ultrasonic catheter device has higher friction heat performance than the other models. We plan in the near future to study the coagulation experiment of blood vessels using a scissor-type ultrasound catheter device.

Data Availability

The data that support the findings of this study are available from the corresponding author upon reasonable request.

Conflicts of Interest

The authors declare that they have no conflicts of interest.

Acknowledgments

This work was supported by JSPS KAKENHI Grant Number 18K12107 and National Natural Science Foundation of China Grant number 51865021.

References

[1] G. T. Harr, "Therapeutic ultrasound," *European Journal of Ultrasound*, vol. 9, no. 1, pp. 3–9, 1999.

[2] G. T. Harr, "Therapeutic applications of ultrasound," *Progress in Biophysics & Molecular biology*, vol. 93, no. 1-3, pp. 111–129, 2007.

[3] J. F. Amaral, "Ultrasonic dissection," *End. Surgery*, vol. 2, pp. 181–185, 1994.

[4] J. F. Amaral, "The experimental development of an ultrasonically activated scalpel for laparoscopic use," *Surgical Laparoscopy & Endoscopy*, vol. 4, no. 2, pp. 92–99, 1994.

[5] S.-A. M. Boddy, J. W. A. Ramsay, S. S. C. Carter, P. J. R. Webster, D. A. Levison, and H. N. Whitfield, "Tissue effects of an ultrasonic scalpel for clinical surgical use," *Urological Research*, vol. 15, no. 1, pp. 49–52, 1987.

[6] M. Ajoudanian, Z. W. Jiang, and M. Morita, "Study on a new type micro-stirrer excited by longitudinal elastic wave for thrombus dissolution," *International Journal of Applied Electromagnetics and Mechanics*, vol. 37, no. 1, pp. 67–77, 2011.

[7] M. Ajoudanian, Z. W. Jiang, and M. Morita, "Design of a novel type micro-stirrer excited by longitudinal elastic wave for thrombus dissolution," *Journal of Biomechanical Science and Engineering*, vol. 6, no. 4, pp. 262–269, 2011.

[8] M. Ajoudanian, Z. W. Jiang, and M. Morita, "Structural analysis and design of micro-stirrer driven at a requested frequency for thrombus dissolution," *International Journal of Applied Electromagnetics and Mechanics*, vol. 41, no. 3, pp. 217–225, 2013.

[9] J. Yang, M. Morita, and Z. Jiang, "Design of a novel scissoring micro-stirrer for blood clot dissolution," *Sensors and Actuators A: Physical*, vol. 248, pp. 130–137, 2016.

[10] *ANSYS workbench mechanical Dynamic analysis seminar text 19.0 (in Japanese) CYBERNET SYSTEMS CO.*, pp. 146–171, 2020.

[11] *ANSYS workbench mechanical Heat transfer Analysis Seminar Text 19.0 (in Japanese), CYBERNET SYSTEMS CO.*, pp. 94–105, 2020.

[12] Y. J. Chao, X. Qi, and W. Tang, "Heat transfer in friction stir welding—experimental and numerical studies," *Journal of manufacturing science and engineering*, vol. 125, no. 1, pp. 138–145, 2003.

[13] X. K. Zhu and Y. J. Chao, "Numerical simulation of transient temperature and residual stresses in friction stir welding of 304L stainless steel," *Journal of Materials Processing Technology*, vol. 146, no. 2, pp. 263–272, 2004.

[14] V. Soundararajan, S. Zekovic, and R. Kovacevic, "Thermo-mechanical model with adaptive boundary conditions for friction stir welding of Al 6061," *International Journal of Machine Tools and Manufacture*, vol. 45, no. 14, pp. 1577–1587, 2005.

[15] P. Prasanna, B. S. Rao, and G. K. M. Rao, "inite element modeling for maximum temperature in friction stir welding and its validation," *The International Journal of Advanced Manufacturing Technology*, vol. 51, no. 9-12, pp. 925–933, 2010.

[16] M. N. Balcı, B. Yıldırım, and S. Dag, "Analysis of frictional contacts with heat generation considering temperature dependent properties," *International Journal of Mechanical Sciences*, vol. 101, pp. 59–69, 2015.

[17] C. S. Zhang, F. Z. Feng, Q. X. Min, and J. Z. Zhu, "Effect of engagement force on vibration characteristics and frictional heating in sonic IR imaging," *NDT & E International*, vol. 76, pp. 52–60, 2015.

[18] G. Chen, Q. Ma, S. Zhang, J. Wu, G. Zhang, and Q. Shi, "Computational fluid dynamics simulation of friction stir welding: a comparative study on different frictional boundary conditions," *Journal of Materials Science & Technology*, vol. 34, no. 1, pp. 128–134, 2018.

Hindawi
BioMed Research International
Volume 2021, Article ID 6693784, 7 pages
https://doi.org/10.1155/2021/6693784

Research Article

Coronary Anomalies in 11,267 Southwest Chinese Patients Determined by Angiography

Xin Jiang,[1,2] **Ping Zhou**,[3] **Chunlan Wen**,[2] **Zhao Yin**,[2,4] **Tao Liu**,[2] **Meiling Xu**,[5] **Chengming Yang**,[2] **Hongyong Wang**,[2] **Wenxing Song**,[6] **Yuqiang Fang**,[2] **and Chunyu Zeng**[2]

[1]*Department of Cardiology, People's Hospital of Dadukou, Dadukou District, Chongqing 400080, China*
[2]*Department of Cardiology, Chongqing Institute of Cardiology, Daping Hospital, Army Medical University, Chongqing 400042, China*
[3]*Department of Cardiology, The First People's Hospital of Chongqing Liang Jiang New Area, Chongqing 401121, China*
[4]*Department of Cardiology, 306th Hospital of PLA, Beijing 100101, China*
[5]*Chongqing Emergency Medical Center, Chongqing University Central Hospital, Chongqing 400014, China*
[6]*Department of Cardiology, People's Hospital of Dazhu, Dazhu District, Chongqing 402360, China*

Correspondence should be addressed to Yuqiang Fang; yuqfang1024@163.com and Chunyu Zeng; zengchunyu02@163.com

Received 22 December 2020; Revised 29 January 2021; Accepted 8 February 2021; Published 19 February 2021

Academic Editor: Xing Chen

Background. The prevalence of coronary artery anomalies (CAAs) is rare and varies among different countries or areas. More importantly, the symptoms exhibited by some CAAs make the diagnosis of coronary artery disease (CAD) difficult and hamper the physician from making the right intervention for CAD patients. *Objective*. To investigate the prevalence of CAAs in 11,267 patients from three hospitals in Southwest China. *Methods*. 11,267 patients who have undergone coronary angiography from three Southwest China hospitals were investigated retrospectively. Dominance patterns, prevalence, and the location of each CAA were recorded and analyzed. *Results*. The presence of a dominant right coronary artery (RCA) was found in 60.58% of patients. CAAs were found in 11.12% (1258) patients, and 87.66% anomalies were located in the left anterior descending (LAD) artery and its branches. Most of CAAs were found to be myocardial bridges (MBs, 1060 cases, 9.41%). Other CAAs included anomalous coronary origin (43 cases, 0.38%), coronary artery fistulas (CAFs, 36 cases, 0.32%), and coronary artery aneurysm or ectasia (119 cases, 1.06%). It also noted that most anomalies were found with RCA originating from the left coronary sinus (79.07%), most CAFs were located in the LAD and its branches (58.33%), and most coronary artery ectasias were located in the RCA (43.25%). *Conclusions*. CAAs in patients from Southwest China were unique compared to other studies. Recognition of these CAAs is important for accurate diagnosis and treatment choice of patients with chest pain.

1. Introduction

Coronary angiography (CAG) [1] has traditionally been utilized to detail the coronary vasculature before intervention and surgery and remains the reference standard of imaging modality. Although it has some inherent disadvantages, the high accuracy and lower risk of CAG have made it a useful tool for the diagnosis of coronary artery disease (CAD). With the benefit of CAG, the number of patients who receive percutaneous coronary intervention (PCI) is increasing fast. In China, for example, the number of PCIs performed in 2011was 341,069 which increased to 454,505 in 2013 [2]. This showed an increase of 113,436 patients in 2 years. Therefore, it is important to distinguish a normal image from that of an anomaly of the coronary artery for accurate reference in physician clinics.

Traditionally, coronary arteries are anatomically categorized into 3 groups based on their anatomical features [3], i.e., normal coronary anatomy, anatomical variations of the coronary artery, and coronary artery anomaly (CAA). The frequency of coronary anomalies varied in different countries or regions. For example, the absence of the left main coronary artery was about 0.4%–8% of the total population in Turkey and Singapore [4, 5]; the frequency of coronary artery

anomaly was 2.34% in native Chinese Hans and 3.93% in native Chinese Uighurs [6].

It is known that, besides coronary stenosis, many diseases could lead to chest pain. The anomaly of the coronary artery is a major one, which includes severely compressed myocardial bridges, coronary fistulas, coronary aneurysm, and congenital absence of the main coronary artery. Although the prevalence of these anomalies is rare, CAAs could lead to severe complications, make the diagnosis of CAD difficult, and hamper the ability of the physician to perform the correct intervention for patients with CAD [7, 8]. As a representative city in Southwestern China, Chongqing is famous for its mountainous geography, diverse ethnic groups, and massive immigration from other areas of China. However, the prevalence of CAAs in Southwest China is not known. In this present study, we investigated these characteristics, including coronary dominance pattern and prevalence of CAAs, in patients from 3 hospitals in the southwestern region of China, who had undergone CAG, and compared our results with the reported data from different races or regions.

2. Methods

2.1. Patients. As we reported previously [9], 11,267 patients (4830 females, 6437 males) from Southwest China participated in this research, which lasted from January 2010 to November 2014. They were patients ranging in age from 22 to 92 years (63.4 ± 13.8 years), who were admitted to the 3 southwestern hospitals to undergo CAG. These patients exhibited chest pains, shortness of breath, palpitations, and arrhythmias and were suspected to have CAD. The baseline clinical characteristics of all these patients are shown in Table 1 [9]. The study protocol conforms to the ethical guidelines of the 1975 Declaration of Helsinki as reflected in an a priori approval by the institution's human research committee. Also, all patients have given their informed consent prior to their inclusion in the study.

2.2. Procedure of Selective Coronary Angiography. As shown in the literature [9, 10], standard transradial techniques were used for angiography. Lidocaine was used as the local anesthesia. The right radial artery was cannulated using a 21-gauge needle and a transradial kit with a 30-centimeter-(cm) long, 6-French (F) introducer (Terumo, Tokyo, Japan). With the introducer in place, 200 μg nitroglycerin and 2000 IU heparin were introduced into the side port of the sheath. If the operation lasted for more than 1 hour, another dose of heparin (1000 IU/h) was administered intravenously. A 5 F multipurpose catheter (Terumo, Tokyo, Japan) 130 cm long was alternatively used for selective angiography using standard techniques. Briefly, the catheter tip was placed on the orifice of the target artery (the left or the right coronary artery) and introduced with a 0.035″ hydrophilic guide wire (Terumo, Tokyo, Japan). We used iopromide 370 (Bayer, Bayer Schering Pharma, Germany) to take magnified angiography images at different angles. If the angiography failed when using the 5 F multipurpose catheter, the 6 F Judkins catheters (J6F, Cordis Corporation, USA) or 6 F pig catheters (Cordis Corporation, USA) would be used instead. If the radial artery was too small or too circuitous for catheters to manipulate, the femoral artery would be used instead.

Table 1: Demographic characteristics and clinical features among patients.

Clinic characteristics	No. of patients (%)
Male/female	6437/4830
Age(years)	22-92 (63.4 ± 13.8)
Clinical presentations	
Typical angina	6138 (54.47)
Atypical chest pain*	2094 (18.58)
Acute coronary syndrome	819 (7.27)
Syncope	372 (3.31)
Arrhythmia or palpitation	725 (6.43)
Recheck the stent	1523 (13.52)
Risk factors for CAD	
Hypertension	4893 (43.43)
Diabetes mellitus	4027 (35.74)
Smoking	3628 (32.2)
Hyperlipidemia	2937 (26.07)
Family history of CAD	4288 (38.06)

*Atypical chest pain: chest pain not caused by myocardial ischemia. CAD: coronary artery disease.

Table 2: Distribution of coronary dominance.

Coronary dominance	No. of patients (%)
RCA dominance	6825 (60.58)
Balanced type	3100 (27.51)
LCA dominance	1342 (11.91)

2.3. The Classification and Definition for Coronary Dominance and Coronary Artery Anomaly. Coronary dominance is defined as the artery whose branches supply the blood of the posterior ventricular wall. Traditionally, the classification of CAAs was based according to Angelini et al.'s methods [11], namely, (a) anomalous pulmonary origins of the coronary arteries, (b) anomalous aortic origins of the coronary arteries, (c) congenital atresia of coronary arteries, (d) myocardial bridging, (e) CAFs, (f) coronary artery aneurysms, and (g) coronary stenosis.

Myocardial bridge (MB) [12] refers to a small segment of the coronary artery tunneling under the myocardium rather than resting on top of it, which presents stenosis compressed by the myocardium during the systole period and presents a normal beat during the diastole period. In the present study, the compressed stenosis of the MB segment was divided into 3 levels: mild (<50%), middle (50-75%), and severe (≥75%). CAFs refer to the abnormal connection between the coronary artery and other structures, including the coronary vein, heart chamber, or pulmonary artery. According to Altin et al. [4], coronary artery ectasia is an abnormal dilatation of the coronary artery segment with the dilated segment 1.5 to 2 times of the adjacent segment, while coronary aneurysm

Table 3: Profile of CAAs among 11267 patients.

Coronary artery anomaly	LMCA	LAD and branches	LCX and branches	RCA and branches	Total case no. (no/11267 ∗ 100%)
MBs		1045	13	2	1060 (9.41)**
Origin anomaly	3		2	38	43 (0.38)
CAFs		21	3	12	36 (0.32)
Aneurysms or ectasias		42	27	50	119 (1.06)
Total case no (no/1258 ∗ 100%)	3 (0.24)	1108 (88.07)##	45 (3.58)	102 (8.11)	1258

** $P < 0.001$ compared with other CAA groups; ## $P < 0.001$ compared with other arteries. Total prevalence of CAAs was 11.22% (1258 cases) and MB took the majority (1060 cases, 9.41%). According to the modified classification [13], the prevalence of CAAs was 0.7% (79/11267) when myocardial bridges (MBs) and coronary artery aneurysms/ectasias were excluded. CAAs: coronary artery anomalies; MBs: myocardial bridges; CAFs: coronary artery fistulas; LMCA: left main coronary artery; LAD: left anterior descending; LCA: left coronary artery; LCX: left circumflex artery; RCA: right coronary artery.

Table 4: Distribution of myocardial bridges.

MB segment	LAD	LCX	RCA	Branch of LAD	Total no. (%)
Mild compressed (<50%)	772	13	1	1	787 (74.1)**
Middle compressed (50~75%)	185	0	1	1	187 (17.61)
Severely compressed (≥75%)	86	0	0	2	88 (8.29)
Total	1043 (98.21)##	13 (1.23)	2 (0.19)	4 (0.38)	1062

Table 5: Details of coronary origin anomaly.

	No. of cases	Prevalence of origin anomaly (%)
RCA originated from left coronary sinus	34	79.07*
RCA originated from ascending aorta	3	6.98
Right conus branch originated directly from right coronary sinus	1	2.32
LMCA absence	2	4.65
LMCA originated from right coronary sinus	1	2.32
LCX absence	1	2.32
LCX originated directly from left coronary sinus	1	2.32
Total	43	100

* $P < 0.01$ vs. other abnormal origins. RCA: right coronary artery; LMCA: left main coronary artery; LCX: left circumflex artery.

refers to the dilated segment that is more than 2 times of the adjacent segment.

2.4. Statistical Analysis. The angiography images of these patients were analyzed by 2 independent investigators. It is noted that those patients with CAAs that occur as a part of complex congenital heart diseases were excluded from this study.

Data and categorical variables were presented as counts or percentages. Statistical analysis was performed by using the two-tailed paired Student t-test and chi-square test. A P value < 0.05 was considered significant. Statistical analyses were performed using SPSS version 18.0 (SPSS Inc., USA).

3. Results

3.1. Distribution of Coronary Dominance. As shown in Table 1 [9], 11,267 (6437 males, 4830 females) patients were subjected to diagnostic coronary angiography with mean age of 63.4 ± 13.8 years. Most patients presented with RCA dominance (60.58%, $P < 0.001$), with about 27.51% patients being of the balanced type and only 11.91% patients were LCA dominant (Table 2).

3.2. Profile of Coronary Artery Anomalies. As shown in Table 3, the total prevalence of CAAs was 11.22% (1258 cases); MB took the majority of CAAs in Southwest Chinese patients (1060 cases, 9.41%). According to the modified classification [13], the prevalence of CAAs was 0.7% (79/11267) when MB and coronary artery aneurysms/ectasias were excluded. As to artery location, most CAAs were located in LAD and its branches (1108 cases, 88.07%). According to the modified classification with MBs and coronary artery aneurysms/ectasias excluded, the CAAs in the RCA were the main prevalence (50 cases), and the majority of CAAs were of coronary origin anomaly (43 cases, 0.38%).

3.3. The Distribution of Myocardial Bridges. There were 1060 patients (9.41%) with MB segments, each patient having 1 MB, except for 2 patients who had 2 MB segments in LAD. The distribution of MBs is shown in Table 4. Most MBs were located in LAD (1043 segments, 98.21%), the left circumflex artery (LCX) had about 1.23% (13 segments), the branch of

Table 6: Distribution of coronary artery fistulas.

Fistulas	LAD-	LCX-	RCA-	Diagonal of LAD-	Total
Left atrium	8 (22.22)			4 (11.11)	12 (33.33)
Left ventricle				2 (5.55)	2 (5.55)
Right atrium			4 (11.11)		4 (11.11)
Right ventricle	1 (0.28)		6 (16.67)		7 (19.44)
Cardiac vein	1 (0.28)	2 (5.55)	2 (5.55)	2 (5.55)	7 (19.44)
Pulmonary artery	2 (5.55)	1 (0.28)			3 (8.33)
Aorta				1 (0.28)	1 (0.28)
Total	12 (33.33)	3 (8.33)	12 (33.33)	9 (25)	36 (100)

LAD: left anterior descending; LCX: left circumflex artery; RCA: right coronary artery.

LAD had about 0.38% (4 segments), and RCA had about 0.19% (2 segments). It was noted that most MB segments were mildly compressed (787 segments, 74.1%), middle compression was intermediate (187 segments, 17.61%), and severe compression (88 segments, 8.29%) was the least.

$^{\#\#}P < 0.001$ compared with other arteries; $^{**}P < 0.001$ compared with other compressed levels. MBs: myocardial bridges; LMCA: left main coronary artery; LAD: left anterior descending; LCX: left circumflex artery; RCA: right coronary artery.

3.4. The Distribution of Coronary Origin Anomaly. Forty-three cases (0.38%) of abnormal coronary origin were found in this study. As shown in Table 5, the most original anomaly is RCA, originating from the left coronary sinus (34 cases, 79.07%), while other original anomalies were RCA originating from the ascending aorta (3 cases, 6.98%) and absent left main coronary artery (LMCA) (2 cases, 4.65%). Only 1 case was found with the right conus branch originating directly from the right coronary sinus with an absent LCX. The LMCA originated from the right coronary sinus, with the LCX originating directly from the left coronary sinus.

3.5. The Distribution of Coronary Artery Fistulas. There were 36 patients (0.32%) with CAFs. As shown in Table 6, CAFs mainly occurred in 4 coronary arteries: LAD (12 cases, 33.33%), LCX (3 cases, 8.33%), RCA (12 cases, 33.33%), and the diagonal branch of LAD (9 cases, 25%). LAD and its branches were the major artery found with CAFs (21cases, 58.33%). The CAFs entered on the left atrium (12 cases, 33.33%), right ventricle (7 cases, 19.44%), cardiac veins (7 cases, 19.44%), right atrium (4 cases, 11.11%), pulmonary artery (3 cases, 8.33%), left ventricle (2 cases, 5.55%), or aorta (1 case, 0.28%).

3.6. The Distribution of Coronary Artery Aneurysms or Ectasias. There were 113 patients (1.00%) suffering from coronary artery ectasias, and only 6 patients (0.05%) were presented with coronary aneurysms. The coronary aneurysms were found in the LAD (4 cases) and the LCX (2 cases). As shown in Table 7, the coronary artery ectasias (CAEs) mainly affected 4 coronary arteries: RCA (50 cases, 43.25%), LAD (34cases, 33.33%), LCX (25 cases, 22.12%), and the diagonal branch of LAD (4 cases, 3.54%).

Table 7: Distribution of coronary artery ectasias.

	No. of patients	Prevalence of coronary ectasias (%)
RCA	50	44.25
LAD	34	30.09
LCX	25	22.12
Diagonal branch of LAD	4	3.54
Total	113	100

4. Discussion

In the present study, we investigated the CAAs in patients from Southwest China and found that the prevalence was 11.12%. According to the modified classification [13], after exclusion of MBs and coronary artery aneurysms/ectasias, the prevalence was reduced to 0.7% (79/11267). Among CAAs, the myocardial bridge was the most common, which is consistent with Cademartiri et al.'s report [14]. It is noted that our findings are not completely consistent with other reports (As shown in Table 8). For example, 60.58% of patients in our study had RCA dominance, while other reported studies indicated the prevalence at more than 80% [14]. After exclusion of MB and coronary ectasias according to the modified classification [13], the prevalence of CAAs was only 0.7%, which is lower than what was reported in Pan et al.'s study [6], which also showed that CAA frequency was 2.34% for the Chinese Han and 3.93% for the Chinese Uyghur people [6]. The reported prevalence of CAAs varied from 0.4% to 8.47% in different countries or areas [11, 14–19]. Moreover, the abnormal origination of the coronary artery varies among different populations. In our study and those from India, the most abnormal origin is from the RCA [19, 20], while in Turkey and the Netherlands, the most common is from the left main artery (LMA) [11, 14–16], from the LCX for Turkey [17], and from the LAD for Hungary [18].

The myocardial bridge was the major anomaly in our present study as well as in others [14]. We found that most MB segments are located in the LAD, with only a few located in the LCX, branch of the LAD and RCA. These results were similar to the other studies (0.83~11.9%) using coronary angiography [14, 21–24]. In Beijing, Ma et al. found that

Table 8: Prevalence distribution of coronary major artery anomalies in different countries.

Literature	Country	Sample size	Major artery (percentage)	Prevalence of CAAs except MB and ectasias, no. (%)	Major CAA (no. %, artery)
Present study	Southwest China	11,267	RCA (60.58)	79 (0.7)	MB (1,060, 9.41, LAD) Origin (43, 0.38, RCA)*
Pan et al. [6]	Xinjiang, Chinese Han, Chinese Uyghur	4746 1934		111 (2.34) 76 (3.93)	Origin (23, 0.48, RCA) Origin (19, 0.98, RCA)
Altin et al. [4]	Turkey	5548	RCA (81.6)	78 (1.4)	Origin (68, 1.2, LMA)
Cademartiri et al. [14]	Netherlands	543	RCA (86.6)	46 (8.47)	MB (59, 10.86, LAD) Origin (18, 3.3, LMA)*
Aydinlar et al. [15]	West Turkey	12,059		100 (0.8)	Origin (48, 0.40, LMA)
Safak et al. [16]	Izmir, Turkey	16,768		120 (0.7)	Origin (86, 0.51, LMA)
Göl et al. [17]	Turkey	58,023		257 (0.4)	Origin (203, 0.35, LCX)
Kardos et al. [18]	Hungary	7694		103 (1.3)	Origin (98, 1.27, LAD)
Garg et al. [19]	India	4100		39 (1.0)	Origin (35, 0.85, RCA)
Zheng et al. [20]	Nanjing, China	1879			Origin (24, 1.3, RCA)

*According to the modified classification [13], myocardial bridge and coronary ectasias were excluded.

the prevalence of MBs was 13.6% (336/2462) from the China-Japan Friendship Hospital [25]. In Northeast China, it was reported to be 10.53% (10/95) from Heilongjiang Province [26] and 24.14% (140/580) from Liaoning Province [27]. Our study showed that the frequency of Southwest China was lower as compared with Heilongjiang Province and Liaoning Province in Northeast China. It is known that there are different methods used to diagnose the presence of a myocardial bridge. Other than coronary angiography, coronary computed tomographic angiography is widely used due to its noninvasive characteristics. Of course, autopsy of the heart is the ultimate method for the diagnosis of CAAs. However, the prevalence of CAAs using these methods shows a big difference. For example, coronary computed tomographic angiography shows the frequency of MBs at 22.5% (39/350) in patients from Saudi Arabia [22], 10.86% (39/350) from the Netherlands [14], 44% (108/245) from New York [23], and 26% (39/350) from Israel [24]. Heart autopsy shows the frequency at 34.5% (69/200) in patients from Warsaw [28]. Although the reasons leading to the difference are complicated, the sensitivity of the method used and the different populations are the major ones. Due to its noninvasive nature, more and more people would prefer coronary CT angiography (CTA) examination, even in some patients without any obvious symptoms. In some areas, CTA is taken as a routine procedure during physical examination, although abuse of CTA has escalated in the past few years.

The abnormal origin of the coronary artery is another commonly observed CAA. Similar to the myocardial bridge, the results are different among countries or areas. In China and India [19, 20], the major abnormal origin of the coronary artery is the RCA, whose prevalence varies from 0.38% to 1.3%. In Europe and other countries, the major abnormal coronary artery origin is the left coronary artery (including the left main artery [11, 14–16], LCX [17], and LAD [18]) with a frequency of 0.4~3.3%. Abnormal origin of the coronary artery might elicit some symptoms, with the anomaly of the LMA or LAD showing more clinical symptoms than that of the LCX [22]. Although other abnormal origins of the coronary artery are rare, the consequences are serious, even leading to death during infancy [29–31]. For example, coronary artery originating from the pulmonary artery leads to almost 90% of patients dying during infancy. LMA is the most common, with the LAD and RCA being less common. For those who survive, this anomaly may eventually cause angina, myocardial infarction, and heart failure because of the retrograde blood flow and a left to right shunt, thus requiring the immediate need to be repaired by surgery [29]. In our present study, we did not find any severe abnormal origin of the coronary artery, which might be ascribed to the fact that most patients in our study were adults.

CAF is a fault in the connection between the coronary artery and another vessel or chamber, and the frequency of CAFs is 1/50,000 at birth and 1/500 after cardiac catheterization [13, 17]. Previous studies reported that more than half of the CAFs involved the RCA [13, 17]. However, in the present study, we found the most CAFs involved the LAD and its branches. Moreover, inconsistent with previous reports showing that most of CAFs shunt into the right ventricle and right atrium [15], our present study showed a scattering of the CAF shunt into the left atrium (13 cases, 33.33%), right ventricle (7 cases, 19.44%), cardiac veins (7 cases, 19.44%), right atrium (4 cases, 11.11%), pulmonary artery (3 cases, 8.33%), left ventricle (2 cases, 5.55%), and aorta (1 case, 0.28%). Although the CAF in our study is small and asymptomatic, some reported CAFs are large and may result in pulmonary hypertension, congestive heart failure, bacterial endocarditis, rupture, or myocardial ischemia [17].

Coronary artery ectasia and aneurysm are another rare form of anomaly. They may be associated with inflammatory, connective tissue and some other congenital diseases [11, 32–34]. They were usually considered to be variants of coronary atherosclerosis [15]. In the present study, the frequency of coronary ectasia was 1.00% and coronary aneurysm was 0.05%, which are lower than those found in other studies

[11, 32]. Because of the similar prognosis as with atherosclerosis, it was recommended to treat these patients as those with CAD [11, 32–34].

5. Conclusion

This study is the first to investigate a relatively large scale of patients in Southwest China and thus shows valuable information. The prevalence of the four CAAs is as follows: MB (9.41, 1060 cases), origin anomaly (0.38, 43 cases), CAFs (0.32, 36 cases), and aneurysms or ectasias (1.06, 119 cases), and most CAA anomalies were located in the LAD artery and its branches. The limitation of this work is that only three hospitals in Southwest China were involved; more hospitals with a larger scale of patients are needed to affirm the finding of this investigation in the future.

Data Availability

The data used to support the findings of this study are included within the article.

Consent

All procedures followed were in accordance with the ethical standards of the responsible committee on human experimentation (institutional and national) and with the Helsinki Declaration of 1975, as revised in 2000 (5). Informed consent was obtained from all patients for being included in the study.

Conflicts of Interest

All authors declare that there is no conflict of interest.

Authors' Contributions

Xin Jiang and Ping Zhou contributed equally in this work.

Acknowledgments

These studies were supported by grants from the National Science Foundation of China (81570312).

References

[1] A. S. Almeida, S. C. Fuchs, F. C. Fuchs et al., "Effectiveness of clinical, surgical and percutaneous treatment to prevent cardiovascular events in patients referred for elective coronary angiography: an observational study," *Vascular Health and Risk Management*, vol. 16, pp. 285–297, 2020.

[2] H. Li and J. Ge, "Cardiovascular diseases in China: current status and future perspectives," *Intternational Journal of Cardiology Heart Vascular*, vol. 6, pp. 25–31, 2015.

[3] A. Fathala and W. Hassan, "Coronary artery anomalies: a diagnostic challenge," *Journal of the Saudi Heart Association*, vol. 23, no. 1, pp. 37–39, 2011.

[4] C. Altin, S. Kanyilmaz, S. Koc et al., "Coronary anatomy, anatomic variations and anomalies: a retrospective coronary angiography study," *Singapore Medical Journal*, vol. 56, no. 6, pp. 339–345, 2015.

[5] H. Akkaya and E. E. Gunturk, "Coronary artery anomalies and dominance: data from 7,858 patients in a single center in Turkey," *Minerva Cardioangiologica*, 2020.

[6] C. Pan, G. Azhati, Y. Xing, Y. Wang, and W. Liu, "Comparison of congenital coronary artery anomalies between Uyghur and Han: a multi-slice computed tomography study in Xinjiang, China," *Chinese Medical Journal*, vol. 128, no. 1, pp. 15–19, 2015.

[7] R. Beecham, S. Prater, and J. Batlle, "Coronary artery anomalies," in *StatPearls*, StatPearls Publishing, Treasure Island, 2020.

[8] A. Kochar and T. Kiefer, "Coronary artery anomalies: when you need to worry," *Current Cardiology Reports*, vol. 19, no. 5, p. 39, 2017.

[9] Z. Yin, C. Zeng, X. Zhang et al., "The characteristics of coronary stenosis in 11,267 patients from Southwest China: a retrospective study," *Journal of Thrombosis and Thrombolysis*, vol. 45, no. 1, pp. 142–150, 2018.

[10] Y. Fang, C. Yang, X. Wang, L. Zhou, H. Wang, and C. Zeng, "Feasibility and application of single 5F multipurpose catheter in coronary and peripheral angiography via a transradial approach," *International Journal of Cardiology*, vol. 151, no. 2, pp. 182–186, 2011.

[11] P. Angelini, S. Villason, and A. V. Chan, "Normal and anomalous coronary arteries in humans," in *Coronary artery anomalies: a comprehensive approach*, P. Angelini, Ed., pp. 27–150, Lippincott Williams & Wilkins, Philadelphia, 1999.

[12] R. Nakanishi, R. Rajani, Y. Ishikawa, T. Ishii, and D. S. Berman, "Myocardial bridging on coronary CTA: an innocent bystander or a culprit in myocardial infarction?," *Journal of Cardiovascular Computed Tomography*, vol. 6, no. 1, pp. 3–13, 2012.

[13] U. Guntekin, E. Saglam, M. Tuncer, Y. Gunes, and H. Gumrukcuoglu, "Incidence of coronary artery anomalies in applied coronary angiography at our clinic," *MN Kardiyoloji*, vol. 16, pp. 19–24, 2009.

[14] F. Cademartiri, L. la Grutta, R. Malagò et al., "Prevalence of anatomical variants and coronary anomalies in 543 consecutive patients studied with 64-slice CT coronary angiography," *European Radiology*, vol. 18, no. 4, pp. 781–791, 2008.

[15] A. Aydinlar, D. Çiçek, T. Sentürk et al., "Primary congenital anomalies of the coronary arteries," *International Heart Journal*, vol. 46, no. 1, pp. 97–103, 2005.

[16] O. Safak, E. Gursul, M. Yesil et al., "Prevalence of coronary artery anomalies in patients undergoing coronary artery angiography: a review of 16768 patients. A retrospective, single-center study," *Minerva Cardioangiologica*, vol. 63, no. 2, pp. 113–120, 2015.

[17] M. K. Göl, M. A. Ozatik, A. Kunt et al., "Coronary artery anomalies in adult patients," *Medical Science Monitor*, vol. 8, no. 9, pp. CR636–CR641, 2002.

[18] A. Kardos, L. Babai, L. Rudas et al., "Epidemiology of congenital coronary artery anomalies: a coronary arteriography study on a central European population," *Catheterization and Cardiovascular Diagnosis*, vol. 42, no. 3, pp. 270–275, 1997.

[19] N. Garg, S. Tewari, A. Kapoor, D. K. Gupta, and N. Sinha, "Primary congenital anomalies of the coronary arteries: a coronary arteriographic study," *International Journal of Cardiology*, vol. 74, no. 1, pp. 39–46, 2000.

[20] L. Zheng, Z. D. du, L. Z. Jin et al., "Evaluation of coronary artery diameter in normal children by echocardiography and its clinical significance," *Zhonghua Er Ke Za Zhi*, vol. 51, no. 5, pp. 371–376, 2013.

[21] D. Wang, J. P. Sun, A. P. Lee et al., "Evaluation of left ventricular function by three-dimensional speckle-tracking echocardiography in patients with myocardial bridging of the left anterior descending coronary artery," *Journal of the American Society of Echocardiography*, vol. 28, no. 6, pp. 674–682, 2015.

[22] R. H. Donkol and Z. Saad, "Myocardial bridging analysis by coronary computed tomographic angiography in a Saudi population," *World Journal of Cardiology*, vol. 5, no. 11, pp. 434–441, 2013.

[23] L. Lubarsky, M. P. Gupta, and H. S. Hecht, "Evaluation of myocardial bridging of the left anterior descending coronary artery by 64-slice multidetector computed tomographic angiography," *The American Journal of Cardiology*, vol. 100, no. 7, pp. 1081-1082, 2007.

[24] A. R. Zeina, M. Odeh, J. Blinder, U. Rosenschein, and E. Barmeir, "Myocardial bridge: evaluation on MDCT," *American Journal of Roentgenology*, vol. 188, no. 4, pp. 1069–1073, 2007.

[25] E. S. Ma, G. L. Ma, H. W. Yu, W. Wu, and K. Li, "Assessment of myocardial bridge and mural coronary artery using ECG-gated 256-slice CT angiography: a retrospective study," *The Scientific World Journal*, vol. 2013, Article ID 947876, 6 pages, 2013.

[26] L. Cheng, S. Jing, and Y. Zhang, "A comparison study between CT angiography with 64-multislice spiral computed tomography and selective X-ray coronary angiography," *Experimental and Therapeutic Medicine*, vol. 5, no. 3, pp. 969–971, 2013.

[27] Y. J. Niu, X. L. Zhang, A. D. Cao, and B. Leng, "Clinical value of the correlations of mural coronary artery compression extent with myocardial bridge length and thickness evaluated by 128-slice CT," *Experimental and Therapeutic Medicine*, vol. 5, no. 3, pp. 848–852, 2013.

[28] M. Loukas, B. Curry, M. Bowers et al., "The relationship of myocardial bridges to coronary artery dominance in the adult human heart," *Journal of Anatomy*, vol. 209, no. 1, pp. 43–50, 2006.

[29] Y. Xiao, M. Jin, L. Han et al., "Two congenital coronary abnormalities affecting heart function: anomalous origin of the left coronary artery from the pulmonary artery and congenital left main coronary artery atresia," *Chinese Medical Journal*, vol. 127, no. 21, pp. 3724–3731, 2014.

[30] F. Ghaderi, A. Gholoobi, and A. Moeinipour, "Unique echocardiographic markers of anomalous origin of the left coronary artery from the pulmonary artery (ALCAPA) in the adult," *Echocardiography*, vol. 31, no. 1, pp. E13–E15, 2014.

[31] C. Alva, F. D. Gómez, S. Jiménez-Arteaga et al., "Anomalous origin of the left coronary artery from the pulmonary artery. Echocardiographic diagnosis," *Archivos de Cardiología de México*, vol. 79, no. 4, pp. 274–278, 2009.

[32] T. Ebina, Y. Ishikawa, K. Uchida et al., "A case of giant coronary artery aneurysm and literature review," *Journal of Cardiology*, vol. 53, no. 2, pp. 293–300, 2009.

[33] J. Roncalli, M. A. Marachet, H. Rousseau, and J. M. Fauvel, "Left-circumflex coronary artery to right atrium fistula with saccular aneurysm and its endovascular treatment," *Cardiovascular Revascularization Medicine*, vol. 8, no. 2, pp. 114-115, 2007.

[34] A. Luz, J. Silveira, H. Carvalho, and L. Gomes, "Right coronary artery aneurysm," *International Journal of Cardiology*, vol. 114, no. 3, pp. E122–E123, 2007.

Hindawi
BioMed Research International
Volume 2021, Article ID 6656926, 7 pages
https://doi.org/10.1155/2021/6656926

Research Article

The Preference, Effect, and Prognosis of Intra-Aortic Balloon Counterpulsation in Acute Myocardial Infarction Complicated by Cardiogenic Shock Patients: A Retrospective Cohort Study

Wenjun Wang,[1,2,3] Feifei Yang,[1,2,3] Xixiang Lin,[1,2,3] Qin Zhong,[1,2,3] Zongren Li,[1,2,3] Xu Chen,[1,2,3] Junfeng Wang,[4] and Kunlun He[1,2,3]

[1]*Key Laboratory of Ministry of Industry and Information Technology of Biomedical Engineering and Translational Medicine, Chinese PLA General Hospital, Beijing 100853, China*
[2]*Translational Medical Research Center, Chinese PLA General Hospital, Beijing 100853, China*
[3]*Medical Artificial Intelligence Research Center, Chinese PLA General Hospital, Beijing 100853, China*
[4]*Julius Center for Health Sciences and Primary Care, University Medical Center Utrecht, 3584 CG Utrecht, Netherlands*

Correspondence should be addressed to Junfeng Wang; wangjunfeng7@gmail.com and Kunlun He; kunlunhe@plagh.org

Received 1 December 2020; Revised 4 January 2021; Accepted 8 January 2021; Published 20 January 2021

Academic Editor: Xing Chen

Backgrounds. Intra-aortic balloon counterpulsation is increasingly used in acute myocardial infarction complicated by cardiogenic shock. The aim of this study was to explore the preference, effect, and prognosis of intra-aortic balloon counterpulsation in acute myocardial infarction complicated by cardiogenic shock patients. *Methods*. Data of acute myocardial infarction complicated by cardiogenic shock patients at the Fourth Medical Center of PLA General Hospital were collected retrospectively. A propensity score was calculated with a logistic regression which contained clinically meaningful variables and variables selected by Lasso and then used to match the control group. The cumulative incidence curve and Gray's test were employed to analyse the effect and prognosis of intra-aortic balloon counterpulsation on mortality. *Results*. A total of 1962 acute myocardial infarction cases admitted between May 2015 and November 2018 were identified, and 223 cases with acute myocardial infarction complicated by cardiogenic shock were included as the study cohort, which contained 34 cases that received IABP and 189 cases that did not receive IABP. Patients with higher alanine aminotransferase (OR = 1.93, 95% CI 1.29-2.98), higher triglyceride (OR = 3.71, 95% CI 1.87-7.95), and higher blood glucose (OR = 1.08, 95% CI 0.99-1.18) had a higher probability of receiving intra-aortic balloon counterpulsation. In the propensity score matching analysis, 34 cases received intra-aortic balloon counterpulsation and 102 matched controls were included in the comparison. By comparing the cumulative incidence of in-hospital mortality, there was no statistically significant difference between the intra-aortic balloon counterpulsation group and matched control group ($P = 0.454$). *Conclusion*. The use of intra-aortic balloon counterpulsation may not improve the prognosis of the acute myocardial infarction complicated by cardiogenic shock patients.

1. Introduction

At present, despite marked advances in medical treatment and revascularization techniques, acute myocardial infarction complicated by cardiogenic shock (AMI-cardiogenic shock) has still higher mortality [1–4]. In this urgent clinical treatment situation, one therapeutic selection is intra-aortic balloon pump counterpulsation (IABP), which is the most commonly used intervention for AMI-cardiogenic shock [2, 5–8]. From a pathophysiological point of view, the contributions of IABP treatment include increasing diastolic coronary perfusion and decreasing left ventricular aortic systolic pressure (afterload) and myocardial oxygen consumption [8–15]. Therefore, by reducing the cardiac workload, improving blood flow and cardiac output, IABP is considered a clinical treatment of AMI-cardiogenic shock patients [11]. Some observational studies indicated that the prognosis of patients receiving IABP was better than that of patients not receiving

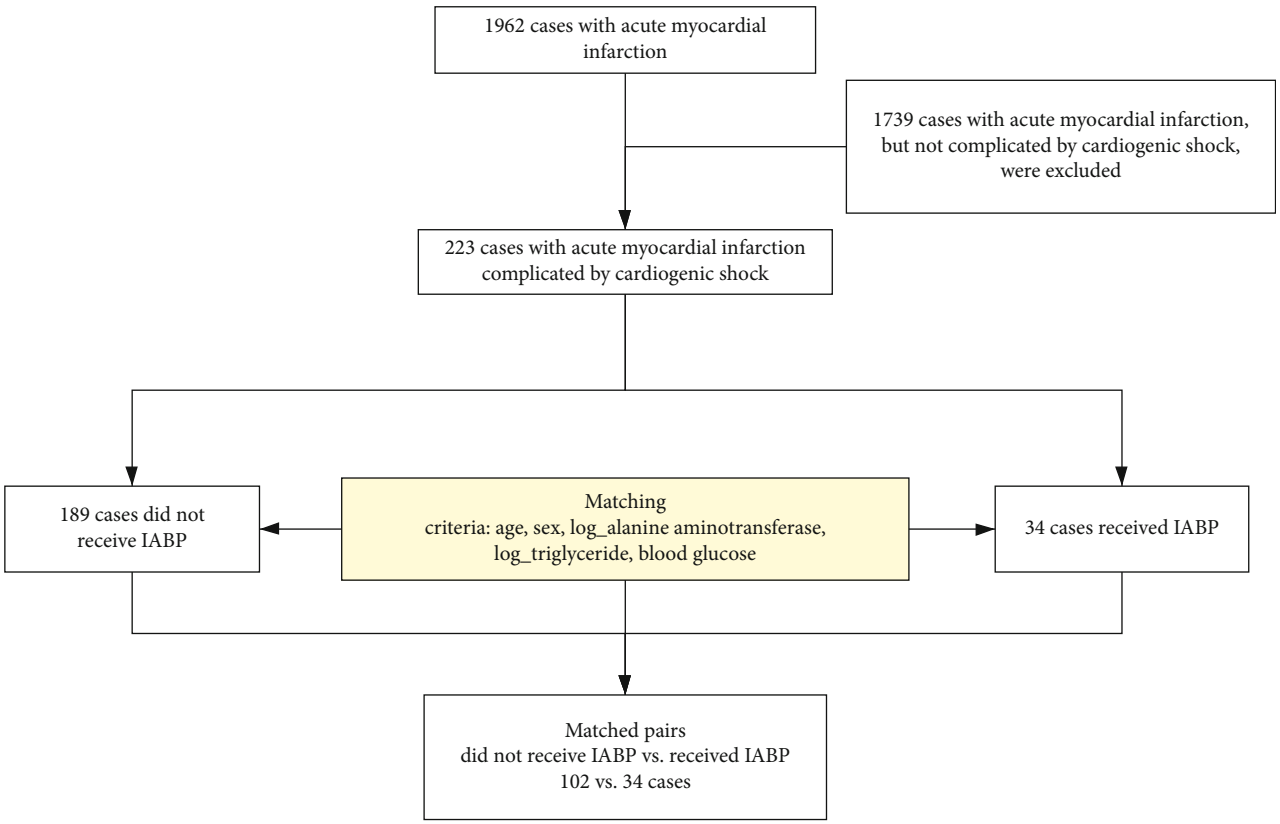

Figure 1: Flowchart of patient inclusion and the matching procedure. From a total of 1962 acute myocardial infarction cases in the Fourth Medical Center of PLA General Hospital, 223 cases met the acute myocardial infarction complicated by cardiogenic shock inclusion and exclusion criteria. Thirty-four cases received IABP, and 102 cases of matched pairs did not receive IABP.

it. The American College of Cardiology and American Heart Association (ACC/AHA) and also the European Society of Cardiology (ESC) strongly recommend the use of IABP in patients with AMI-cardiogenic shock. However, some observational studies and new randomized controlled trials (RCTs) revealed that the use of IABP was not found to improve mortality among AMI patients with cardiogenic shock [5, 12, 14, 16, 17].

Therefore, the use of IABP supports hemodynamics, but evidence on improving the prognosis of AMI-cardiogenic shock patients was still controversial. We established a retrospective cohort study from a single center, to explore the impact of IABP on the mortality of patients with AMI-cardiogenic shock. By matching patients who have received IABP and patients who have not received IABP, we explored the mortality of patients with AMI-cardiogenic shock in the hospital. In addition, we explored the prognostic factors for mortality in AMI-cardiogenic shock patients receiving IABP. Recommendations are given clinically in order to better assist the treatment of AMI-cardiogenic shock and improve the survival rate of patients.

2. Methods

2.1. Data. A retrospective cohort was established to investigate mortality associated with IABP for acute myocardial infarction complicated by cardiogenic shock. Patients admitted in the Fourth Medical Center of PLA General Hospital between May 2015 and November 2018 with a diagnosis of acute myocardial infarction were identified from the electronic medical records. The exclusion criterion was acute myocardial infarction not complicated by cardiogenic shock.

Demographic, clinical, laboratory, and clinical outcome data were obtained from the hospital's electronic clinical medical records. At the first clinical consultation, demographic, clinical, and laboratory data were collected within 24 hours after admission. The outcome of interest was in-hospital death, with discharge as the competing risk event, and event time was defined as the time from admission to either event whichever came first.

2.2. Statistical Analysis. Continuous variables were presented as median and interquartile range (IQR), and categorical variables were presented as number and its corresponding percentage. Variables with a right-skewed distribution were log-transformed before being included in the analysis. Missing values were imputed with single imputation. Univariate logistic regression was used to explore the risk factors of receiving IABP in AMI-cardiogenic shock patients, and a cause-specific Cox model was used to explore the prognostic factors of mortality in AMI-cardiogenic shock patients receiving IABP.

To ensure the assumption of positivity (i.e., each patient has a nonzero probability of being assigned to either

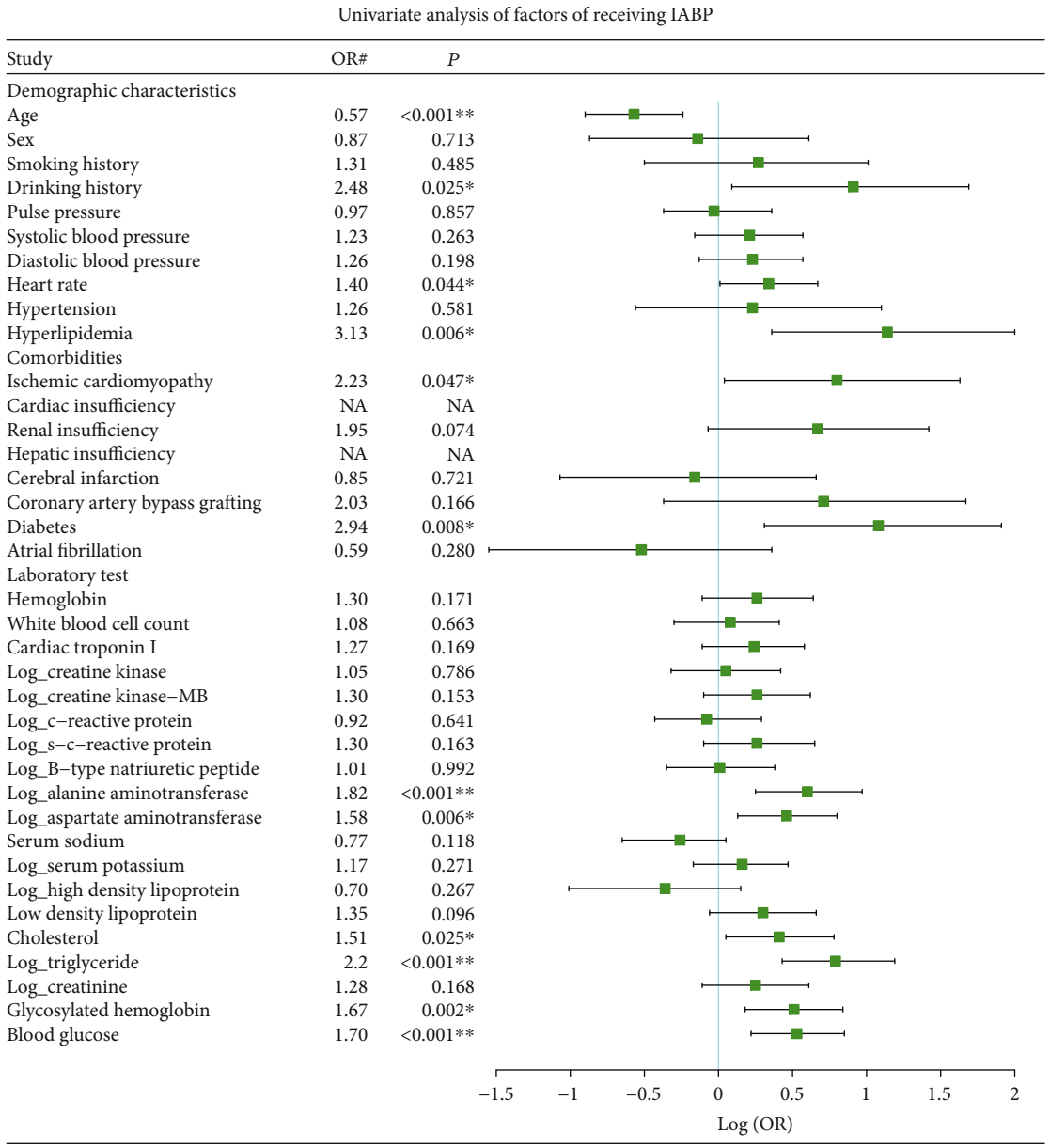

Figure 2: Univariate analysis of factors for receiving IABP in the AMI-cardiogenic shock patients. *The P value is between 0.05 and 0.001. **The P value is <0.001. #Standardized OR, OR per SD increase for continuous variables, and OR compared to the reference group for categorical variables. NA: (quasi-) complete separation variables, where OR is not applicable.

Table 1: Multivariate logistic regression for receiving IABP in the AMI-cardiogenic shock patients.

Variable	OR (95% CI)	P
Log (alanine aminotransferase)	1.93 (1.29, 2.98)	<0.001**
Log (triglyceride)	3.71 (1.87, 7.95)	0.001*
Blood glucose	1.08 (0.99, 1.18)	0.085

*The P value is between 0.05 and 0.001. **The P value is <0.001.

treatment group) is met in the propensity score analysis, we used a two-step approach in exploring the predictors of receiving IABP and matching IABP patients with controls.

In the first step, variables that led to (quasi-) complete separation were automatically identified as predictors (with an OR being infinite), and a deterministic matching based on these variables was performed (i.e., patients in the group with zero probability of receiving IABP were excluded from further analyses). In step two, we used Lasso for variable selection to determine other predictors of receiving IABP, after excluding those predictors already identified in step one. The selected variables were used as matching variables (in addition to age and sex) in the propensity score matching analysis (with a ratio of 3 : 1). The number of variables selected by Lasso was determined with the 1-in-10 rule of thumb: number of selected variables = max (1, number of cases/10). The cumulative incidence curve and Gray's test

Table 2: Clinical characteristics of the matched patients (the IABP group and the matched control group) in the Fourth Medical Center of PLA General Hospital.

Variable[#]	IABP group ($N = 34$)	Matched control group ($N = 102$)
Age	66.00 (62.00, 82.25)	77.00 (67.75, 81.00)
Sex (male)	19 (55.90%)	57 (55.90%)
Log (alanine aminotransferase)	3.71 (2.69, 4.24)	3.18 (2.76, 3.91)
Log (triglyceride)	0.47 (0.02, 0.91)	0.16 (-0.07, 0.37)
Blood glucose	8.78 (5.96, 15.55)	7.41 (5.32, 9.96)

[#]Continuous variable (median, IQR); categorical variable (N, percent).

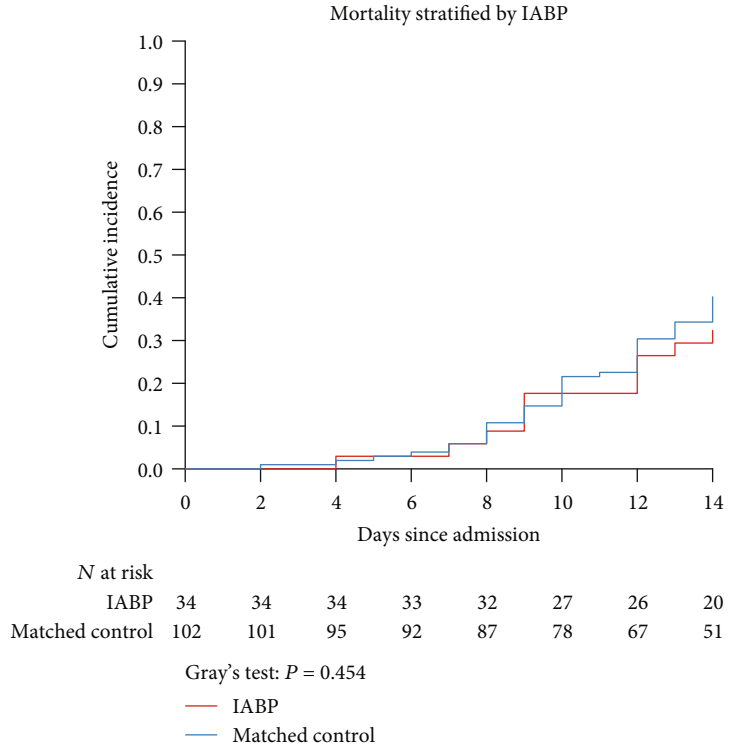

Figure 3: Cumulative incidence curves for in-hospital mortality stratified by IABP. The cumulative incidence was used to assess the primary end point of mortality for the IABP group (red line) and the matched control group (blue line).

were used to compare the in-hospital mortality of patients receiving IABP and matched controls. Statistical analyses were conducted using R software (version 3.6.1) and packages dplyr, mice, glmnet, Hmisc, AUC, survival, cmprsk, descry, and forestplot.

3. Results

3.1. Patients. A total of 1962 acute myocardial infarction cases admitted between May 2015 and November 2018 were identified. After excluding 1739 cases not complicated by cardiogenic shock, 223 cases with AMI-cardiogenic shock were included as the study cohort, which contained 34 (15.25%) cases that received IABP and 189 cases that did not receive IABP (Figure 1).

3.2. Factors Associated with Receiving IABP. Univariate logistic regression revealed that patients with higher drinking history, heart rate, hyperlipidemia, ischemic cardiomyopathy, diabetes, alanine aminotransferase, aspartate aminotransferase, cholesterol, triglyceride, glycosylated hemoglobin, and blood glucose and younger age had a higher probability of receiving IABP (Figure 2). All IABP patients were from cardiac insufficiency and nonhepatic insufficiency groups; thus, these two factors were considered predictive variables for receiving IABP. Next, based on the rule of thumb, three most important variables (34/10) were selected by Lasso: alanine aminotransferase, triglyceride, and blood glucose, and the effect sizes were estimated with a multivariable logistic regression model. Patients with higher alanine aminotransferase (OR = 1.93, 95% CI 1.29-2.98), higher triglyceride (OR = 3.71, 95% CI 1.87-7.95), and higher blood glucose (OR = 1.08, 95% CI 0.99-1.18) had a higher probability of receiving IABP (Table 1).

3.3. Effect of IABP. After excluding non-IABP patients in cardiac insufficiency and nonhepatic insufficiency groups, each

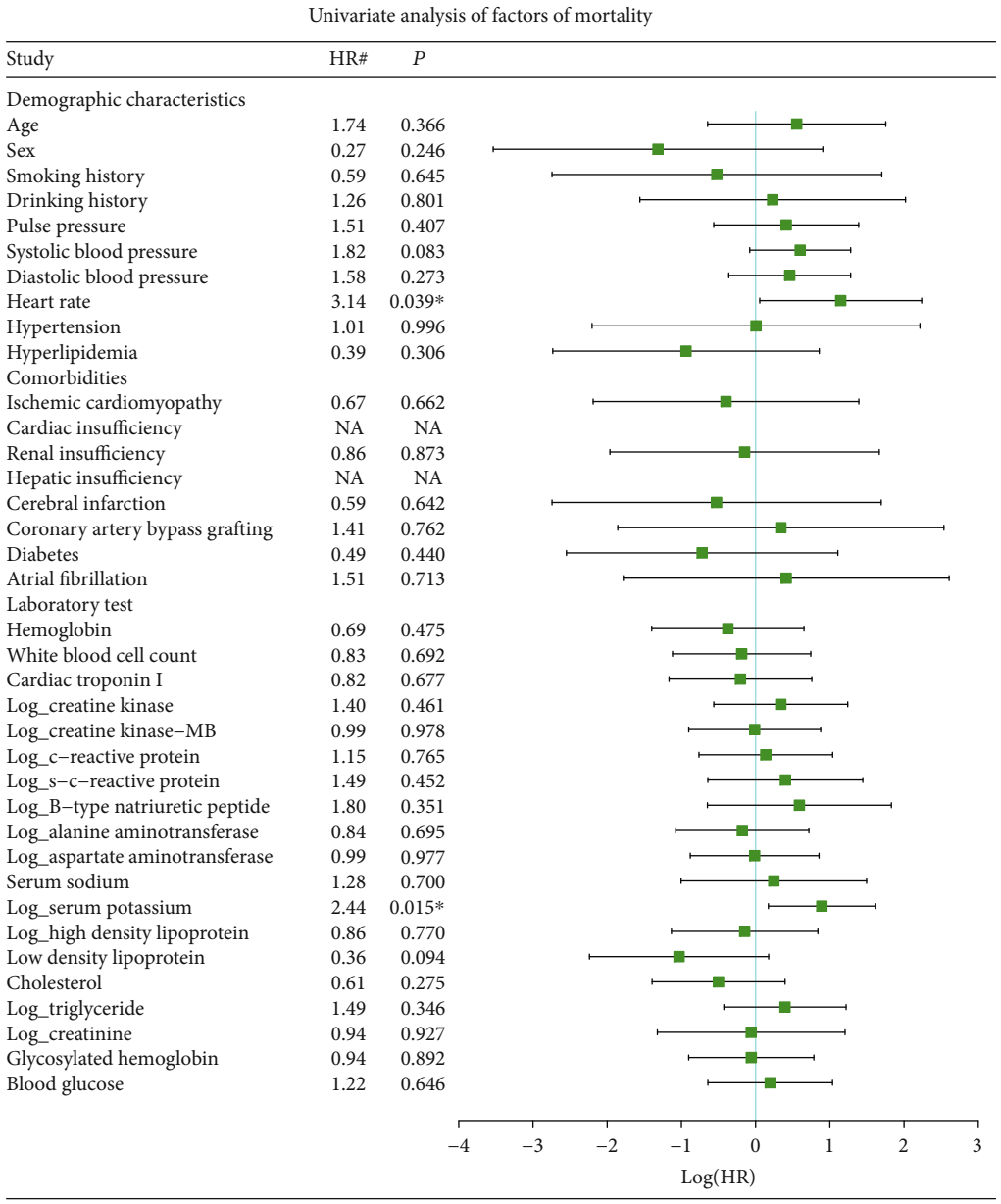

Figure 4: Univariate analysis of factors for mortality in the AMI-cardiogenic shock patients receiving IABP. *The P value is between 0.05 and 0.001. **The P value is <0.001; #Standardized HR, HR per SD increase for continuous variables, and HR compared to the reference group for categorical variables. NA: (quasi-) complete separation variables, where HR is not applicable.

IABP patient was matched with three controls by the propensity score calculated based on age, sex, alanine aminotransferase, triglyceride, and blood glucose. Finally, 102 patients not receiving IABP were selected as the control group (Figure 1). The distributions of these matching variables were comparable between IABP and matched non-IABP groups (Table 2). The model performance of the propensity score model was good with a C-index of 0.80. Therefore, the model including age, sex, alanine aminotransferase, triglyceride, and blood glucose can provide a reliable prediction on the probability of getting treated with IABP.

When comparing the cumulative incidence of in-hospital mortality, there was no statistically significant difference between the IABP group and the matched control group ($P = 0.454$; Figure 3). The cumulative incidence of mortality at days 7 and 14 was 0.06 (0.00, 0.14) and 0.32 (0.17, 0.24) in patients with IABP, respectively.

3.4. Factors Associated with the Mortality in AMI-Cardiogenic Shock Patients Receiving IABP. Univariate Cox regression revealed that patients receiving IABP with a higher heart rate and serum potassium had a higher probability of death (Figure 4).

4. Discussion

This retrospective cohort study revealed that the use of IABP cannot improve the mortality of AMI-cardiogenic shock

patients. Despite the fact that there are still great controversies about the use of IABP that can improve the prognosis of AMI-cardiogenic shock patients and some observational studies revealed a trend toward lower mortality for patients if they received IABP, these findings may result from the clear inequality of baseline risk factors [18, 19]. In our study, we used Lasso regression to identify the most important factors of receiving IABP and used them as the matching parameters (in addition to age and sex) to balance the baseline risk factors. From the cumulative incidence curve of AMI-cardiogenic shock mortality stratified by IABP use, there was no statistically significant difference in 14-day mortality between the IABP group and matched control group. Our study result is consistent with the conclusions of some observational and RCT studies [12, 13, 20–23]. Therefore, IABP may not improve the prognosis of AMI-cardiogenic shock patients.

From a pathophysiological point of view, the main feature of death in AMI-cardiogenic shock is unstable hemodynamics with reduced systolic and mean arterial pressures that lead to reduced oxygen supply to vital organs [9], while the IABP can give hemodynamic support to these hemodynamically unstable patients by increasing blood flow to the heart and decreasing the cardiac workload [2]. However, the reason why the mortality of AMI-cardiogenic shock patients was not sufficiently reduced may be because the effects on cardiac output are modest [24]. Therefore, we speculate that the therapeutic effects seem to be limited in improving hemodynamics, which apparently could not be converted into an improved prognosis of AMI-cardiogenic shock patients.

Our results revealed that higher heart rate and serum potassium may lead to higher mortality in AMI-cardiogenic shock patients receiving IABP. A previous study revealed that serum potassium and heart rate can increase the risk of mortality of patients with AMI [25]. Therefore, heart rate and serum potassium need to be closely monitored for AMI-cardiogenic shock patients receiving IABP.

Our study has several limitations. First, the sample size of our study is not large enough. Therefore, the research may not have good statistical power, which may be one of the reasons why statistically significant result was not observed. Therefore, a larger cohort is needed to further study the effect of IABP on the mortality of patients with acute myocardial infarction complicated by cardiogenic shock. Second, this is a retrospective single-center study, and some laboratory tests were not taken within the first day after admission. We used an imputation method to deal with these missing values; however, a single imputation may lead to uncertainty in results. A prospective cohort will provide stronger evidence.

In conclusion, the use of intra-aortic balloon counterpulsation may not improve the prognosis of the acute myocardial infarction complicated by cardiogenic shock patients.

Data Availability

The research data used to support the findings of this study are available from the corresponding authors upon request.

Conflicts of Interest

All authors declared that there were no conflicts of interests.

Authors' Contributions

Wenjun Wang and Feifei Yang contributed equally to this work. Junfeng Wang and Kunlun He contributed equally to the supervision of this work.

Acknowledgments

We thank all medical staff, researchers, and patients who participated in this study. In addition, we especially thank Beijing BioMind Technology Company, Mrs. Peifang Zhang, Mr. Zhenzhou Wu, Mr. Yanlong Hu, and Mr. Jinzhu Ding for participating. This work was supported by the National Key Research and Development Program of China (No. 2017YFC0114001).

Supplementary Materials

Supplemental Table 1: clinical characteristics of the AMI-cardiogenic shock patients. *(Supplementary Materials)*

References

[1] K. Thygesen, J. S. Alpert, A. S. Jaffe et al., "Fourth universal definition of myocardial infarction (2018) – ScienceDirect," *Journal of the American College of Cardiology*, vol. 72, no. 18, pp. 2231–2264, 2018.

[2] S. Unverzagt, R. Prondzinsky, M. Buerke, K. Werdan, J. Haerting, and H. Thiele, "Intra-aortic balloon pump counterpulsation (IABP) for myocardial infarction complicated by cardiogenic shock," *Cochrane Database of Systematic Reviews*, vol. 7, article Cd007398, 2011.

[3] L. Lu, M. Liu, R. R. Sun, Y. Zheng, and P. Zhang, "Myocardial infarction: symptoms and treatments," *Cell Biochemistry and Biophysics*, vol. 72, no. 3, pp. 865–867, 2015.

[4] R. J. Goldberg, F. A. Spencer, J. M. Gore, D. Lessard, and J. Yarzebski, "Thirty-year trends (1975 to 2005) in the magnitude of, management of, and hospital death rates associated with cardiogenic shock in patients with acute myocardial infarction: a population-based perspective," *Circulation*, vol. 119, no. 9, pp. 1211–1219, 2009.

[5] Y. Ahmad, S. Sen, M. J. Shun-Shin et al., "Intra-aortic balloon pump therapy for acute myocardial infarction," *JAMA Internal Medicine*, vol. 175, no. 6, pp. 931–939, 2015.

[6] X. R. Zhang, L. Su, S. J. Chen, X. G. Zhang, and Y. H. Ying, "A meta-analysis on efficacy of intra-aortic balloon pump therapy in patients with acute myocardial infarction," *Zhonghua Xin Xue Guan Bing Za Zhi*, vol. 41, no. 5, pp. 432–437, 2013.

[7] H. Thiele, B. Allam, G. Chatellier, G. Schuler, and A. Lafont, "Shock in acute myocardial infarction: the Cape Horn for trials?," *European Heart Journal*, vol. 31, no. 15, pp. 1828–1835, 2010.

[8] T. G. Papaioannou and C. Stefanadis, "Basic principles of the intraaortic balloon pump and mechanisms affecting its performance," *ASAIO Journal*, vol. 51, no. 3, pp. 296–300, 2005.

[9] L. X. van Nunen, M. van't Veer, S. Schampaert et al., "Intra-aortic balloon counterpulsation in acute myocardial infarction:

old and emerging indications," *Netherlands Heart Journal*, vol. 21, no. 12, pp. 554–560, 2013.

[10] A. Kantrowitz, S. Tjonneland, P. S. Freed, S. J. Phillips, A. N. Butner, and J. L. Sherman Jr., "Initial clinical experience with intraaortic balloon pumping in cardiogenic shock," *JAMA*, vol. 203, no. 2, pp. 113–118, 1968.

[11] S. S. Dhruva, J. S. Ross, B. J. Mortazavi et al., "Association of use of an intravascular microaxial left ventricular assist device vs intra-aortic balloon pump with in-hospital mortality and major bleeding among patients with acute myocardial infarction complicated by cardiogenic shock," *JAMA*, vol. 323, no. 8, pp. 734–745, 2020.

[12] H. Thiele, U. Zeymer, N. Thelemann et al., "Intraaortic balloon pump in cardiogenic shock complicating acute myocardial infarction: long-term 6-year outcome of the randomized IABP-SHOCK II trial," *Circulation*, vol. 139, no. 3, pp. 395–403, 2018.

[13] H. Thiele, U. Zeymer, F. J. Neumann et al., "Intra-aortic balloon counterpulsation in acute myocardial infarction complicated by cardiogenic shock (IABP-SHOCK II): final 12 month results of a randomised, open-label trial," *The Lancet*, vol. 382, no. 9905, pp. 1638–1645, 2013.

[14] J. Cao, W. Liu, J. Zhu, and H. Zhao, "Risk factors and clinical characteristics of in-hospital death in acute myocardial infarction with IABP support," *International Journal of Clinical and Experimental Medicine*, vol. 8, no. 5, pp. 8032–8041, 2015.

[15] J. D. Talley, E. M. Ohman, D. B. Mark et al., "Economic implications of the prophylactic use of intraaortic balloon counterpulsation in the setting of acute myocardial infarction. The Randomized IABP Study Group. Intraaortic balloon pump," *The American Journal of Cardiology*, vol. 79, no. 5, pp. 590–594, 1997.

[16] Z. Dahdouh, V. Roule, T. Lognoné, R. Sabatier, and G. Grollier, "Left main coronary artery transradial rescue percutaneous coronary intervention for acute myocardial infarction complicated by cardiogenic shock with Impella ventricular mechanical support," *Cardiovascular Revascularization Medicine*, vol. 13, no. 2, pp. 142.e1–142.e4, 2012.

[17] T. Bochaton, L. Huot, M. Elbaz et al., "Mechanical circulatory support with the Impella® LP5.0 pump and an intra-aortic balloon pump for cardiogenic shock in acute myocardial infarction: the IMPELLA-STIC randomized study," *Archives of Cardiovascular Diseases*, vol. 113, no. 4, pp. 237–243, 2020.

[18] P. J. Kovack, M. A. Rasak, E. R. Bates, E. M. Ohman, and R. J. Stomel, "Thrombolysis plus aortic counterpulsation: improved survival in patients who present to community hospitals with cardiogenic shock," *Journal of the American College of Cardiology*, vol. 29, no. 7, pp. 1454–1458, 1997.

[19] E. M. Ohman, J. Nanas, R. J. Stomel et al., "Thrombolysis and counterpulsation to improve survival in myocardial infarction complicated by hypotension and suspected cardiogenic shock or heart failure: results of the TACTICS trial," *Journal of Thrombosis and Thrombolysis*, vol. 19, no. 1, pp. 33–39, 2005.

[20] M. Droppa, M. Vaduganathan, R. V. Venkateswaran et al., "Cangrelor in cardiogenic shock and after cardiopulmonary resuscitation: a global, multicenter, matched pair analysis with oral P2Y12 inhibition from the IABP-SHOCK II trial," *Resuscitation*, vol. 137, pp. 205–212, 2019.

[21] M. Seyfarth, D. Sibbing, I. Bauer et al., "A randomized clinical trial to evaluate the safety and efficacy of a percutaneous left ventricular assist device versus intra-aortic balloon pumping for treatment of cardiogenic shock caused by myocardial infarction," *Journal of the American College of Cardiology*, vol. 52, no. 19, pp. 1584–1588, 2008.

[22] K. Fengler, G. Fuernau, S. Desch et al., "Gender differences in patients with cardiogenic shock complicating myocardial infarction: a substudy of the IABP-SHOCK II-trial," *Clinical Research in Cardiology*, vol. 104, no. 1, pp. 71–78, 2015.

[23] G. D. Dangas, A. S. Kini, S. K. Sharma et al., "Impact of hemodynamic support with Impella 2.5 versus intra-aortic balloon pump on prognostically important clinical outcomes in patients undergoing high-risk percutaneous coronary intervention (from the PROTECT II randomized trial)," *The American Journal of Cardiology*, vol. 113, no. 2, pp. 222–228, 2014.

[24] S. Scheidt, G. Wilner, H. Mueller et al., "Intra-aortic balloon counterpulsation in cardiogenic shock," *The New England Journal of Medicine*, vol. 288, no. 19, pp. 979–984, 1973.

[25] H. Xi, R.-H. Yu, N. Wang, X.-Z. Chen, W.-C. Zhang, and T. Hong, "Serum potassium levels and mortality of patients with acute myocardial infarction: a systematic review and meta-analysis of cohort studies," *European Journal of Preventive Cardiology*, vol. 26, pp. 145–156, 2019.

Hindawi
BioMed Research International
Volume 2021, Article ID 6653967, 13 pages
https://doi.org/10.1155/2021/6653967

Review Article

Application of 3D Printing in Implantable Medical Devices

Zhenzhen Wang and Yan Yang

College of Mechanical Engineering, Chongqing University of Technology, Chongqing, China

Correspondence should be addressed to Yan Yang; yangyan@cqut.edu.cn

Received 5 November 2020; Revised 29 December 2020; Accepted 4 January 2021; Published 13 January 2021

Academic Editor: Xing Chen

3D printing technology is widely used in the field of implantable medical device in recent decades because of its advantages in high precision, complex structure, and high material utilization. Based on the characteristics of 3D printing technology, this paper reviews the manufacturing process, materials, and some typical products of 3D printing implantable medical devices and analyzes and summarizes the development trend of 3D printed implantable medical devices.

1. Introduction

With the continuous improvement of people's health awareness, implantable medical devices to improve patients' life quality have also been widely used [1]. When the shape of the implantable medical devices is complex, it is often difficult to process and even unable to process. 3D printing technology can produce implantable medical devices with any complex shape, without having to consider processing problems, and solve the design and manufacturing problems of complex implantable medical devices. 3D printing technology plays an increasingly important role in implantable medical devices by virtue of its ability to print and shape most materials [2], its precision, personalized and other customized requirements [3], and its high material utilization rate in the printing process. This article briefly describes the application of 3D printing in implantable medical devices.

2. 3D Printing Manufacturing Process

3D printing is also known as additive manufacturing; it is done through layer-by-layer stacking techniques, and according to the designed 3D model, complex and diverse physical entities can be manufactured [4]. Common manufacturing processes for 3D printing include Stereo Lithography Apparatus (SLA) [5], Laminated Object Manufacturing (LOM) [6], Selective laser Sintering (SLS) [7], Fused Deposition Modeling (FDM) [8], and Three-Dimensional Printing (3DP) [9].

2.1. Stereo Lithography Apparatus. Stereo Lithography Apparatus is the earliest practical rapid prototyping technology in 3D printing technology. As early as 1984, it was proposed by Charles W. Hull in the United States and patented in 1986. In 1986, Charles W. Hull established 3D systems in and released the world's first commercial 3D printer SLA-250 in 1988. The working principle of Stereo Lithography Apparatus (Figure 1): a layer of powder material is laid flat on the upper surface of the formed part, then heated to a temperature exactly below the unsintered point of the powder. The control system controls the laser beam scanning on the powder layer in order the cross-section outline of the layer, making the powder temperature rise to the melting point, sintering and bonding with the formed part below. After the first layer is completed, the workbench lowers the thickness of one layer, spreads a layer of uniform and dense powder on it, and sinters the section of the new layer until the entire model is completed. Its basic composition is shown in Figure 1, including ultraviolet laser, lifting platform, scraper, liquid horizon, and photosensitive resin. This technology is widely used in orthopedic repair and tissue engineering and can be used to print skull and hip bones.

Stereo Lithography Apparatus has high molding efficiency and stable operation; the printed parts have high

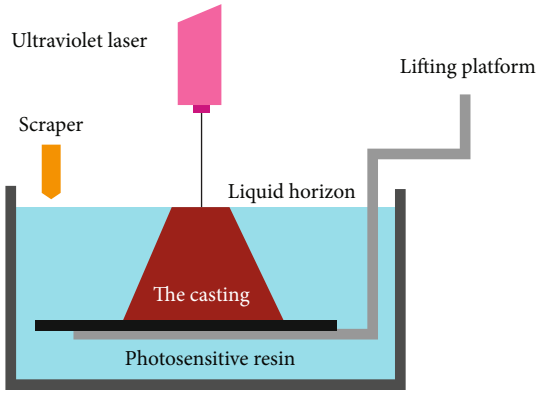

Figure 1: The working principle of Stereo Lithography Apparatus [10].

precision and high finish. But the equipment is relatively large, and there are still problems in the size of optical pixels, which limits the microstructure in the plane [10].

Due to the low penetration depth of ultraviolet light, the application of SLA technology exited by ultraviolet light sources is limited. So, a novel and cost-effective 3D printing technology has emerged: NaYF4:Yb3+/Tm3+ up-conversion microcrystals to produce internal deep ultraviolet (UV) light centers as a light curing source in the polymer matrix by near infrared light excitation. Excellent up-conversion emission from NaYF4:Yb3+/Tm3+ microcrystals is demonstrated by using microcrystals as gain medium to realize up-conversion lasing emission centered at 291,346 and 364 nm. This 3D printing technique, in which a low cost semiconductor laser is used, is potential to print large structures at high printing efficiency.

2.2. Laminated Object Manufacturing. Laminated Object Manufacturing was first developed by the Helisys Company in 1986 and has been developed rapidly since it came out in 1991. Laminated Object Manufacturing is one of the most mature 3D printing technologies. The working principle of Laminated Object Manufacturing (Figure 2): Laminated Object Manufacturing (LOM) uses thin materials such as paper and plastic film. The surface of the sheet is coated with a layer of hot melt adhesive in advance. In the process of machining parts, the sheet is hot-pressed and radiated to bond it with the formed workpiece below is the first step, with CO_2 laser on the new layer of adhesive cut out parts of section contour and the workpiece frame, and the cross section profile between the frame and the excess of aligned to carve up and down in the area of the grid; after the laser cutting is completed, the worktable drives the formed workpiece down and separates from the strip-shaped sheet (material belt); then, the feeding mechanism rotates the receiving shaft and the feeding shaft, to drive the material belt to move the new layer to the processing area, and the worktable rises to the processing plane; finally, the hot-pressing rod is used for hot-pressing; the number of layers of the workpiece is increased by one layer, so the height of the workpiece is increased by one layer, and then, the cross-section profile is cut on the new layer. This is repeated until all the cross-sections of the part are bonded and cut, and a layered manufacturing solid part is obtained. The general process of layered solid manufacturing technology molding is roughly graphics processing, substrate production, prototype production, residual material removal, and postprocessing. LOM including laser, heated roller, material supply roll, layered part and support material, platform, waste take-up roll, and part layer outline and crosshatch. The technique can be applied to orthopedics such as temporal bone, dental jaw, and mandible.

Since the materials processed by the layered solid molding process are easy to obtain, the raw material cost of the process is low, and the precision of the manufactured workpieces is relatively ideal, which is suitable for the molding of large-sized workpieces. However, the mechanical properties of the workpiece produced by this technology are relatively low, and compared with other printing technologies, the efficiency of the layered solid molding process is poor [11].

2.3. Selective Laser Sintering. The selective laser sintering process was first developed by DTM in 1987 and was patented in 1988 by C.R. Dechard of the University of Texas at Austin. In 1992, C.R. Dechard released sinter station, a commercial 3D printer based on selective laser sintering technology in the DTM Company, which was founded by C.R. Dechard. The selective laser sintering usual laser utilized is CO_2 due to the absorption by the polymers being much more efficient at this wavelength. Working principle of selective laser sintering process (Figure 3): in a closed molding chamber install two cylinder piston mechanism, one of the cylinders for powder, the other for molding. Before the forming process begins, the powder material is heated to a temperature just below the sintering point using an infrared plate. At the beginning of forming, the piston in the powder-feeding cylinder moves up for a certain amount, the powder laying drum evenly spreads the powder on the processing surface of the forming cylinder, and the laser beam scans the first layer of information at a given speed and energy under the control of the computer. Where the laser beam sweeps the powder is sintered and solidified into a sheet of a given thickness. The unsintered powder is used as a support so that the first layer of the part is made. At this time, as soon as the molding cylinder piston moves down, the feed rainbow piston moves up, and the powder is laid and rolled again; then, the laser beam is scanned according to the second layer of information, and the second layer formed is also sintered and solidified on the first layer. In this way, a 3D solid part is produced by stacking layer by layer [12]. This process is basically the same as the Stereo Lithography Apparatus (SLA), except the SLA's liquid resin is replaced with a powder material that can be sintered under laser light; the roller is optimized by a temperature control unit to smooth the material to ensure the fluidity of the powder, and the heat of the working chamber is controlled to make the powder bond firmly. By melting the polymer in the powder, the metal powder with high melting point is bonded together. After forming, the binder is removed by degreasing process, leaving a large number of honeycomb holes in the material, which is extremely conducive to the preparation of porous materials. This technology can be used to make scaffolds to promote bone regeneration.

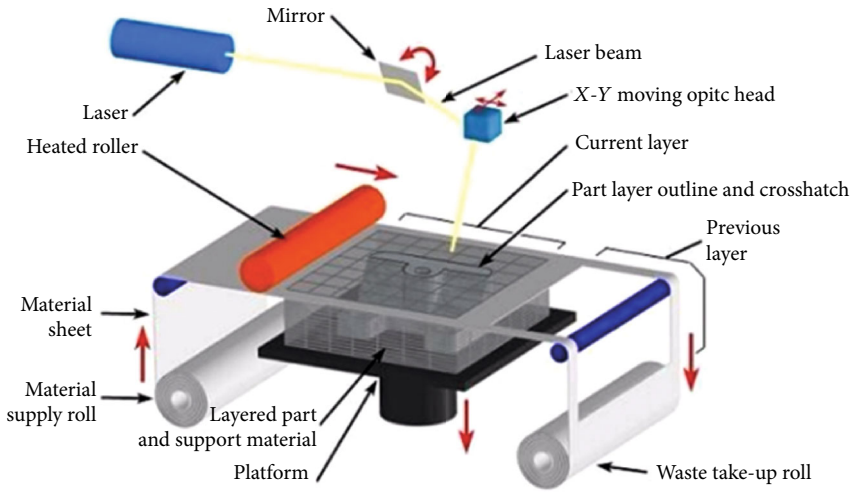

Figure 2: Laminated Object Manufacturing.

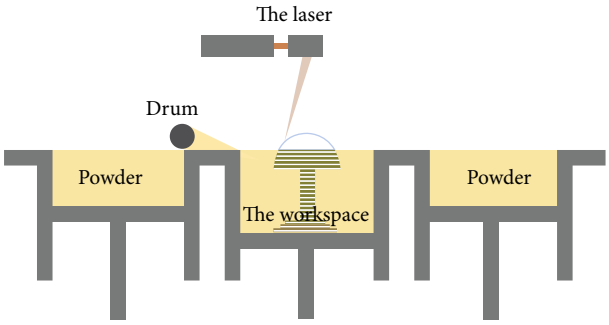

Figure 3: Working principle of selective laser sintering process.

The most prominent advantages of selective laser sintering are the variety of materials that can be processed and the short production cycle. The disadvantages of this technology are the low strength and poor surface quality of manufactured parts [13].

2.4. Fused Deposition Modeling. Fused deposition manufacturing was first invented by Scott Crump in 1988. In 1992, Stratasys was granted a 3D printing technology patent for fused deposition manufacturing technology. In the same year, Stratasys launched the world's first 3D printer based on fused deposition manufacturing technology—"3D Modeler." Fused deposition manufacturing is mainly used to mold thermoplastic polymer materials. The main principle (Figure 4) is the thermoplastic polymer wire is transported to a heating extruder via a feed unit, under the action of the heater above the nozzle based on the set process temperature, after heating to molten state, uniform extrusion, layer by layer on the forming platform and cooling solidification. When one layer of cross-section is completed, the worktable descends a certain height, and then, another layer is machined on the formed section, so as to repeat until the workpiece is manufactured [14], particularly widely used in bone engineering.

All of the fused deposition manufacturing technology can be widely used; the first of reasons is the fused deposition manufacturing technology does not use a laser, so compared with the laser-containing molding technology, its manufacturing cost is low. It can be machined with a variety of materials, high material utilization, to a large extent to reduce the cost of forming. However, the forming rate of this technology is low, and the surface of the workpiece has stripe sense, and the manufacturing precision is low [15].

2.5. Three-Dimensional Printing. In 1989, Emanuel M. Sach and John S. Haggerty of MIT applied for patents for 3D printing technology in the United States. After that, Emanuel M. Sachs and John S. Haggerty perfected the technology many times and eventually form a 3D printing process. The working principle of Three-Dimensional Printing (Figure 5): the powder material is laid flat in the working groove. Under the control of the computer, the nozzle sprays selectively based on the information of the cut workpiece, so that part of the powder is bonded and gradually forms a cross section. After the section is printed, the workbench drops a certain height, and then, the next layer is bonded until the workpiece is completely formed. The prototype bonded with a binder is of low strength and should be placed in a heating furnace for further curing or sintering. Cheekbones, mandibles, and skulls can all be printed by this technology.

The Three-Dimensional Printing process can process a wide variety of materials and has a fast forming speed, which can be used to print workpieces with complex structures. However, because it is only bonded by adhesive, the precision and surface quality of the printed workpiece are poor, and the strength of the prototype part is low, which requires subsequent treatment [16–18]. Due to its low cost, small size, fast molding speed, color printing can be realized and other advantages, this technology is getting more and more attention [19, 20].

In the 3D printing process, it is not easy to achieve both the large size and high precision of the formed part. At present, the working platform of powder spreading equipment on the market is generally not large. The main reason is that after the beam passes through the galvanometer, it can only precisely control the spot with uniform distribution of energy

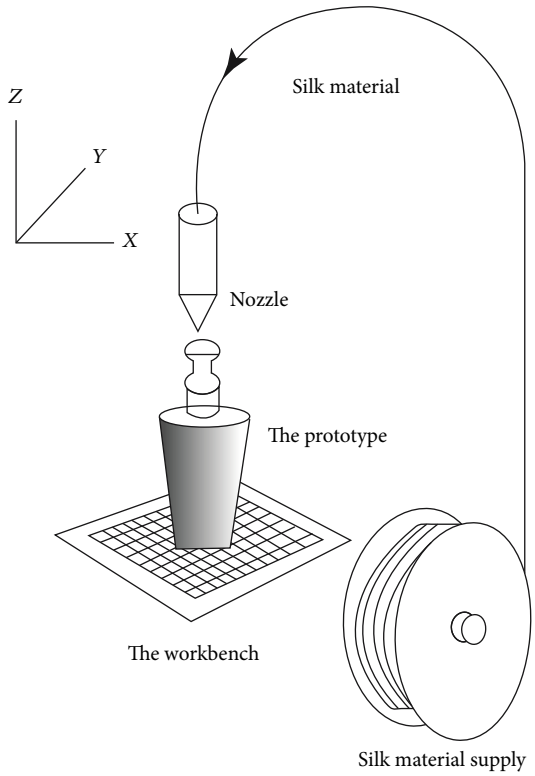

Figure 4: The working principle of fused deposition manufacturing [14].

density in a certain area. So, how to improve the accuracy of optical components or realize multiple beams synchronous control is a development direction. In addition, 3D printing manufacturing is different from the general coating technology. It is coating on top of coating, which can be called "recoating technology." The thickness, flatness of each layer, and the degree of layer-to-layer bonding directly affect the stability and accuracy of the formed part, which need to be improved by adjusting equipment and process parameters.

The above manufacturing processes are all printed layer by layer; free-style 3D printing technology not only overcomes the structural design limitations of traditional layer-by-layer printing but also helps to achieve 3D printing of low-viscosity or slow-curing materials. As an emerging printing method, development free-style 3D printing system represents a major advance in biomedical engineering, because most of the materials used in the biomedical field involve soft substances, such as biomaterials, living cells, biopolymers, and silicones; these materials were previously printed using traditional AM systems. The free-style 3D printing system enables researchers to print these low viscosity materials and explore a wider range of soft materials for various applications. With the growing popularity of free-style 3D printing systems, a growing number of publications in the field of tissue engineering, vascularization, microaids, 4D printing, and manufacturing of elastomer. As an emerging printing method, free-style 3D printing system has been developed and solves many biomedical applications unmet need for producing, in particular, of low-viscosity material or slow-curing requirements.

3. 3D Printing Materials for Implantable Medical Devices

The development of 3D printing implantable medical devices is closely related to the development of medical level and material science, especially the development of biomaterials. Biological materials are substances that can be used to diagnose, treat, repair, or replace tissues and organs in the body or enhance their functions. They can be natural, artificial, or a combination of both.

Biomaterials used in 3D printing implantable medical devices can be divided into biomedical polymer materials, biomedical metal materials, biomedical ceramic materials, biomedical composite materials, and derived materials according to their properties.

3.1. Biomedical Polymer Materials. Biomedical polymer materials are the earliest and most widely used materials in the field of biobiomedicine, and they have applications in all fields of medicine. Biomedical polymer materials can be divided into two categories: nondegradable and degradable on the basis of their properties. Nondegradable polymer materials include polyethylene, polypropylene [21], and polyformaldehyde. This type of material has good physical and mechanical properties, also can remain stable for a long time in a biological environment. Degradable biological materials include collagen [22, 23], cellulose [24], and chitin. The material is degraded under the action of the biological environment, and part of the degraded product is absorbed and partly eliminated with the normal metabolism of the human body. Biomedical polymer materials are widely used in the repair of cardiovascular stents, soft tissues, and hard tissues.

3.2. Biomedical Metal Materials. Biomedical metal materials refer to metals or alloys used in biomaterials, also known as metal materials for surgical implants. The clinically used biomedical metal materials mainly include stainless steel [25], titanium and titanium alloys [26, 27], cobalt-chromium-molybdenum alloys [28], and medical precious metals [29]. This type of material has high fatigue resistance and mechanical strength, good mechanical properties, corrosion resistance, and biocompatibility. It is widely used in bone and joint substitutes, spinal implants, cardiovascular implants, etc.

3.3. Biomedical Ceramic Materials. Biomedical ceramics have also become biomedical inorganic nonmetallic materials. They began as biomedical materials in the early eighteenth century and were clinically applied in China in the 1970s. Biomedical ceramics are divided into biologically inert ceramics, biologically active ceramics, and biodegradable ceramics. Bioinert ceramics include alumina, zirconia, and carbon. These materials have stable structure and high strength, good abrasion resistance, and stable chemical properties. Bioactive ceramics include bioglass [30, 31] and tricalcium phosphate [32, 33], which form strong chemical bonds with tissues through chemical reactions in the body. Biodegradable bioceramics can induce the growth of new bone

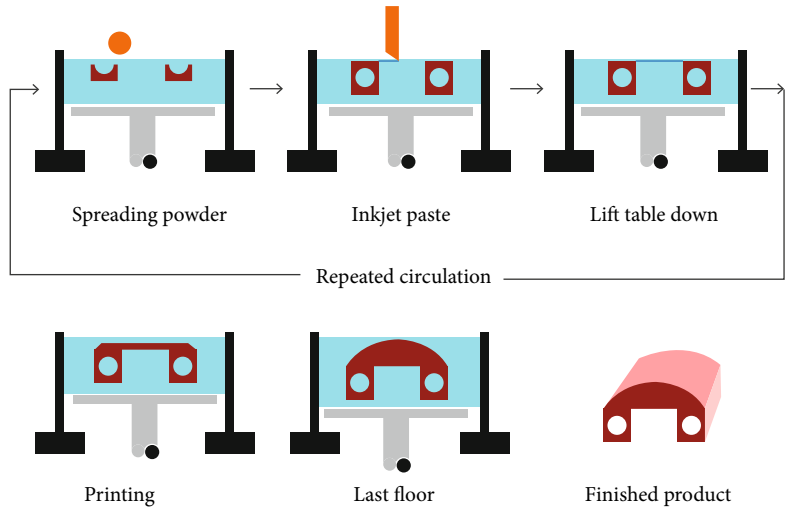

Figure 5: Three-Dimensional Printing.

since they can be absorbed in the living body, such as β-tricalcium phosphate bioceramics. Biomedical ceramics can be used to make artificial hip joints, artificial bones, valves, etc. The main problem of biomedical ceramics in clinical applications is poor strength and toughness.

3.4. Biomedical Composite Materials. Biomedical composite materials are composed of two or more different materials [34, 35]. Composite materials improve the performance of a certain material to a large extent, because it is a composite of different materials; the composite material will have new and unique properties that are different from the constituent materials. This new material property may be beneficial to the human body, or it may not be beneficial to the human body. Therefore, the composite material must not only have the expected physical and chemical properties but also must meet the requirements of biomechanical properties and biocompatibility. Biomedical composite materials include bone cement, coating materials, and nano-phosphoric lime. The biomedical composite material is widely used in repairing or replacing human tissues and organs or enhancing their functions and the manufacturing of artificial organs [36–38].

3.5. Derived Materials. Bioderived materials are also called biorenewable materials, which are formed from natural biological tissues through special processing. Since biological tissues have lost their vitality after special treatment, biologically derived materials are inanimate materials. Bioderived materials have similar configurations and functions to natural tissues, or because they have a composition similar to natural tissues, bioderived materials play a major role in the maintenance and replacement of human dynamic processes [39]. The biological material is widely used in artificial heart valves, skin masks, bone restorations, vascular restorations, etc.

For the moment, research on biomedical 3D printing technology is springing up. Many achievements have been made in medical 3D printing materials, especially in tissue engineering scaffold materials. However, biomedical 3D printing technology and its materials are still an emerging field, and various researches are still in the initial stage. To truly realize the clinical application of a long distance, there are still great challenges. Mechanical metamaterials such as superhard materials, auxiliary materials, hyperelastic materials, and self-assembled and programmable materials can be used in cartilage tissue engineering, bone tissue engineering, skin tissue engineering, vascularized tissue engineering, etc. Metamaterials begin with porous implants; these include biomimetic materials created from naturally derived buildings. Mechanical metamaterials also provide radical designs for functional tissue scaffolds; it has shown promising potential in bone tissue regeneration and orthopedic implants, with extreme rigid weight ratio, tunable hydraulic penetration, and even higher surface volume ratios; intelligent materials are a class of outstanding engineering materials due to their shape memory effect, Shape Memorty Materials (SMM) generally classified as Shape-Memory Polymers (SMP), Shape-Memory Ceramics (SMC), Shape Memory Alloys (SMA), and Shape-Memory Hydrogels (SMHs); out of which, SMP became a more notable and researchable class, intelligent materials to further open up the possibility more bone regeneration.

4. Typical 3D Printed Implantable Medical Devices

3D printed implantable medical devices are applied to various parts of the human body. Typical products include vascular stents, heart valve prostheses, orthopedic implants, and artificial joint prostheses.

4.1. Vascular Stents. Cardiovascular disease (CAD) is a disease that affects the myocardium, heart valves, or blood vessels, and its morbidity and mortality are gradually increasing. Around the world, cardiovascular disease kills a large number of people every year, and it is called the number one killer of health [40]. The treatment of cardiovascular disease has become the focus of research by relevant scholars in various

countries. The methods of treating cardiovascular diseases include drug treatment, external surgical treatment, and vascular stent interventional treatment [41–43]. The effect of drug treatment is not obvious, the recovery period after external surgery is long, and both of them may cause the patient to suffer secondary injury. As a minimally invasive surgery, vascular stents cause less pain, short operation time, less trauma, and quicker recovery after surgery. Therefore, vascular stent interventional therapy has become the main method for the treatment of cardiovascular diseases. Figure 6 is the process of preparing blood vessel stent by 3D printing technology.

Flege et al. [44] made use of selective laser melting (SLM) 3D printing technology to prepare the biodegradable vascular scaffolds for PLLA and PCL powder particles and then made the surface of the stent smooth by dip coating and spray treatment. The biodegradable stent is shown in Figure 7. The experimental results show that the method and the bioabsorbable scaffold prepared by the materials have good biocompatibility. Figure 7 is the vascular stent printed by SLM technology.

Kaesemeyer et al. [45] indicated the biodegradable vascular stent fabrication by the rapid vascular stent fabrication (RSF) system shown in Figure 8. The vascular stent is prepared from a copolymer of lactide, glycolide, ε-caprolactone, and lovastatin. The vascular stent not only has a supporting function but also releases drugs in the body that can be used to treat damaged endothelium and prevent thrombosis in the stent. Figure 8 shows the biodegradable stent prepared by RSF system.

Park et al. [46] prepared a spiral bioabsorbable PCL vascular stent (Figure 9). The drug coating of PLGA and PEG mixed with sirolimus was prepared by ultrasonic atomization and then implanted in the body for experiments. The release kinetics of Rolimus in the stent is a continuous curve, and the vascular intimal hyperplasia is reduced.

Van Lith et al. [47] used the 3D printing technology of microcontinuous liquid interface production to print a kind of curable biomaterial based on bioabsorbable citrate and prepared a bioabsorbable vascular stent with rapid, high-resolution, and customized design. Misra et al. used 3D printing technology to print the composite material doped with biodegradable polymer PCL and graphene nanoflakes, then prepared a vascular scaffold which can realize dual drug release.

From the domestic and foreign research status, 3D printing has a bright future in the application of vascular stent. However, the application of 3D printing technology in vascular stents is still in its initial state, and its application is still immature. At present, there are some problems in the application of 3D printing technology in vascular stents, such as vascular scaffolds made of biodegradable polymeric materials are deficient in mechanical properties due to the influence of material properties, and the positioning accuracy of vascular scaffolds is poor due to their expansion, which will affect the subsequent treatment.

4.2. Prosthetic Valve. The function of heart valves is to ensure that the blood in the heart flows in the correct direction. Heart valve disease will endanger human health and affect

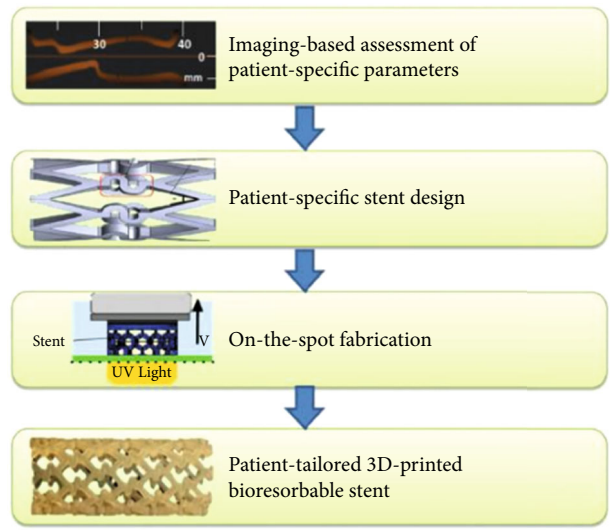

Figure 6: Process of preparing blood vessel stent by 3D printing technology [42].

the normal quality of life of humans. Myocardial infarction and senile valve disease due to aging are common in the elderly [48]. Hyperlipidemia, hypertension, and chronic kidney disease are common in modern adults, which can cause heart valve damage. Heart valve disease is a common heart disease in modern medicine. Valve lesions can hinder the normal flow of the blood and increase the burden of the heart, thus causing damage to heart function and leading to heart failure. There are three methods to treat heart valve disease: drug treatment, external surgical treatment, and interventional treatment. External surgical treatment refers to the use of artificial heart valve replacement or valvuloplasty for treatment, which is an effective treatment for high-risk patients, and it is also a radical cure for heart valve disease. The 3D printed heart valve can be customized based on different patients, so as to improve the accuracy and stability, reduce the rejection reaction of the patient's body, and improve the success rate of heart valve replacement [49]. Biological heart valve replacement and mechanical valve replacement are shown in Figures 10 and 11.

The development of artificial heart valves has gone through the stages of mechanical valves, biological valves, interventional valves, and tissue-engineered valves [51, 52]. Tissue valve is an active heart valve constructed by 3D printing technology.

In the 1960s, China began to study artificial heart valves. Professor Yongzhi Cai successfully performed mitral valve replacement with domestic cage valve [53]; the biomaterial artificial heart valve developed by the Beijing Fuwai Hospital has been successfully used in aortic valve replacement surgery; Kapetanovic et al. [54] used hyaluronic acid and methacrylate composite hydrogel to load human aortic valve interstitial cells, then increased the viscosity of the hydrogel by increasing the concentration of methacrylate, thereby promoting the transmission of information between cells and maintaining human fiber cell phenotype (Figure 12) and aortic valve model and printed entity.

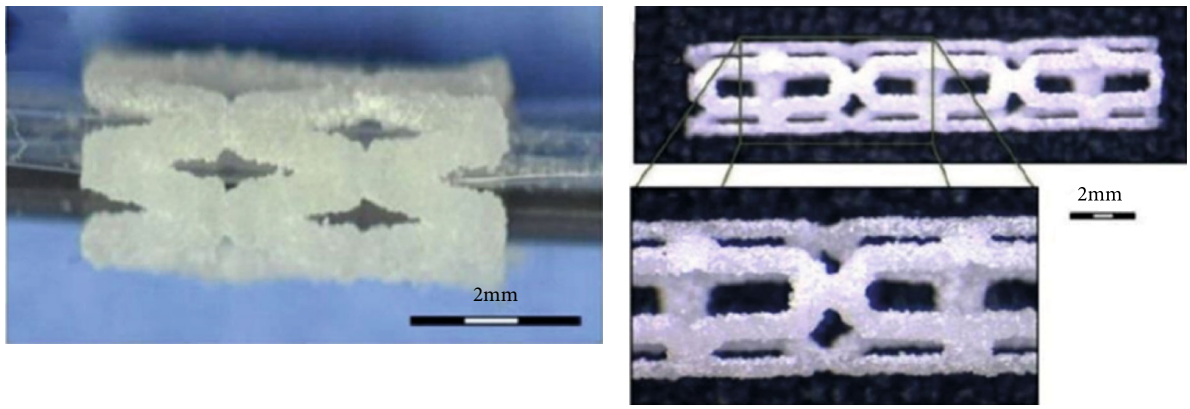

(a) PLC stents manufacturing (b) PLLA PLC stents manufacturing

Figure 7: Vascular stent printed by SLM technology [44].

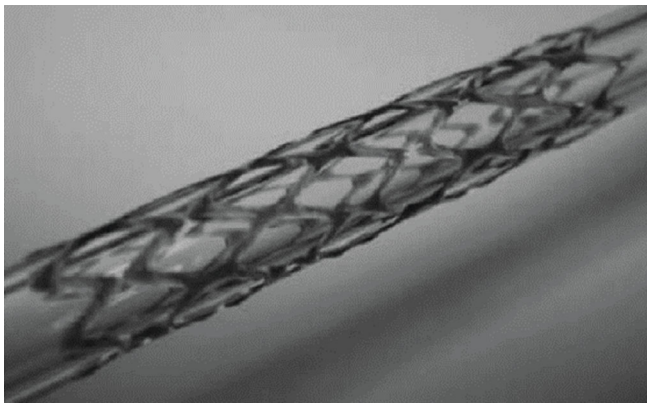

Figure 8: Biodegradable vascular stents prepared by RSF system [45].

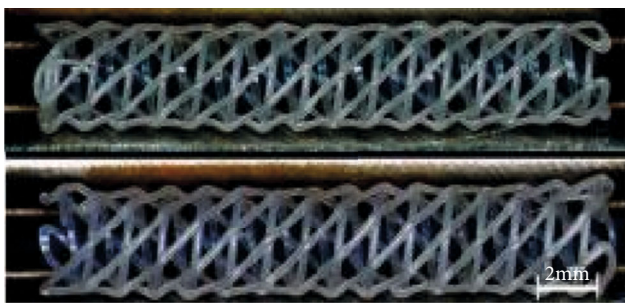

Figure 9: PCL spiral vascular stent [46].

There are still some deficiencies in the preparation of aortic valve in the world. There are some differences between the designed aortic valve and the natural aortic valve, and the non-Newtonian characteristics of the hydrogel are ignored in the printing process of the aortic valve. The phenomenon of swell will appear from the microneedle extrusion, which will affect the surface accuracy and dimensional accuracy of the aortic valve.

4.3. Orthopedic Implants. Bone tissue is an important part of the human body, as well as an important part of the bones. It plays an irreplaceable role in the human body. Bone tissue has a strong ability to regenerate bone and can repair and heal itself. However, when the bone defect reaches a certain degree, the bone tissue corresponding to the bone defect will not be able to repair itself [55, 56], and there will be some images in the defect site nonbone tissues like fibers grow; clinically, there are more and more bone defects caused by trauma, tumor resection, accidents, etc., so the demand for bone implants is increasing.

Methods for repairing bone defects include autografts, allografts [57, 58], and artificial bone substitute materials such as metal and polymer materials. Autologous bone transplantation requires two operations. The patient suffers a lot of pain, and the human body has a limited amount of autologous bone, which cannot provide unlimited bone sources [59]. The operations are not all successful [60]. However, due to different constitutions, allograft may cause immune rejection and carry the risk of infectious diseases from the donor [61]. Therefore, the research of artificial bone repair has become the focus of many related scholars [62].

Artificial bone scaffolds prepared by traditional methods such as gas foaming [63, 64], fiber bonding, freeze-drying, phase separation [65], and particle leaching cannot precisely control the cell pore shape and pore size of the artificial bone scaffold, which makes the artificial bone scaffold prepared biologically the performance does not meet the demand well. In recent years, 3D printing technology to manufacture artificial bone scaffold has become a preferred scheme, which has great potential in drilling.

In March 2014, the First Affiliated Hospital of the Fourth Military Medical University of Chinese PLA (Xijing Hospital) implemented 3D printing titanium alloy shoulder blade prosthesis, clavicular prosthesis, and pelvic prosthesis for three patients with bone tumors. The first two cases were the first in the world, and the last one was the first in Asia, which made a significant step in the application of 3D printing technology in bone tissue engineering [66]. Saijo et al. used 3D printing technology to prepare tricalcium phosphate powder into a personalized prosthesis and achieved satisfactory results in clinical applications; Dai Kerong and others used 3D printing technology to prepare metal materials into

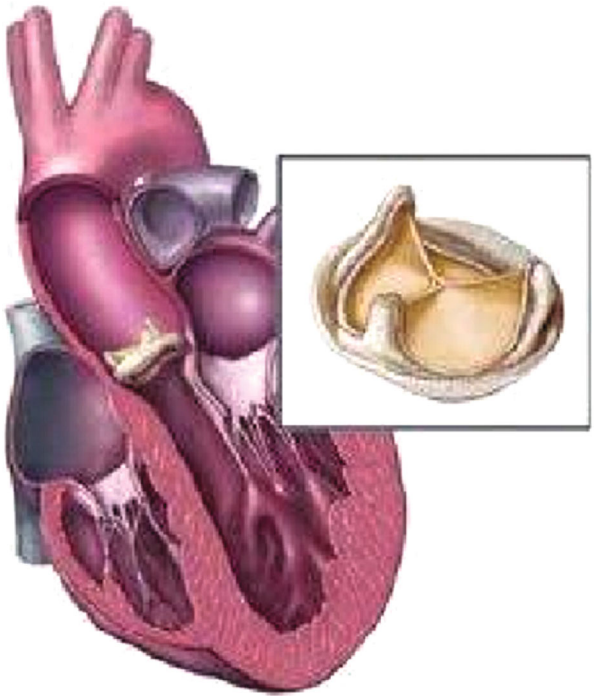

Figure 10: Biological heart valve replacement [50].

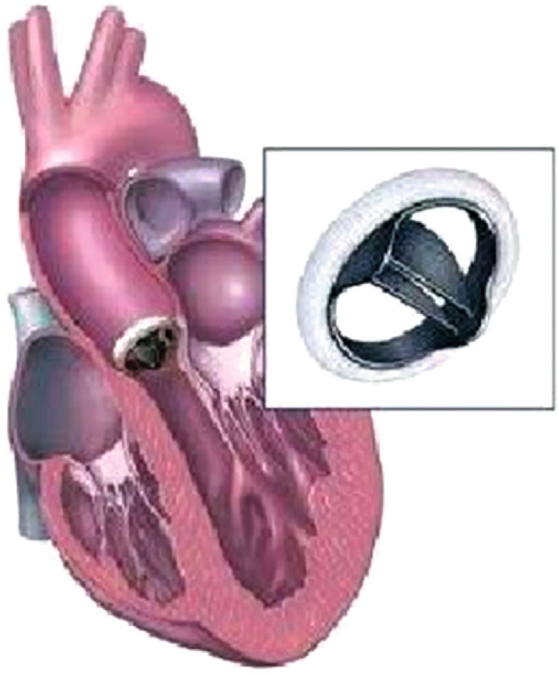

Figure 11: Mechanical heart valve replacement [50].

artificial pelvis, then successfully completed the replacement of the artificial pelvis and achieved satisfactory results in clinical practice. The titanium alloy clavicle and scapula prepared by Pei Yanjun and others using 3D printing technology were successfully implanted into the body of bone tumor patients, and the clinical effect was good.

With the development of society, 3D printing will be more and more widely used in orthopedics. However, the application of 3D printing technology in orthopedics is at the initial stage, and the technical materials are immature; there are still some problems: the 3D printed bone implant lacks large sample data and follow-up data; due to the high clinical requirements for implant materials, there are still some problems in material selection; the structure of human tissues and organs is complex, and the accuracy of printing still needs to be improved.

4.4. Artificial Joint Prostheses. Osteoarthritis (OA) is also known as degenerative arthritis. The disease damages articular cartilage and eventually leads to degenerative joint disease of the whole joint, which can lead to loss of normal joint movement and joint dysfunction. Joint replacement surgery, as a more difficult operation in the field of orthopedics, is used in clinical treatment of joint dysfunction, thereby restoring the shape and function of the joint.

Total hip arthroplasty (THA) is an operation in which artificial hip prosthesis is used to replace the dysfunctional hip joint [67, 68]. Hip joint prosthesis is suitable for the elderly with fresh or old femoral neck fractures and nonunion; middle-aged and elderly patients with severe degenerative osteoarthritis and avascular necrosis of the femoral head. Clinically, Cheng Wenjun and others performed artificial total hip replacement surgery for patients with femoral neck fractures, primary hip joints, and secondary osteoarthritis, which used traditional prostheses and 3D printed titanium alloy bones. There are two methods of trabecular metal cups. After the operation, it was found that the hip joint movement function of the two groups was greatly improved. However, the initial stability of the prosthesis of the 3D printed titanium alloy trabecular metal cups was better, and the initial stability of the bone in growth is better.

Total knee arthroplasty (TKA) is the most effective surgery for treating moderate to severe knee arthritis [69]. Knee joint prostheses refer to surgical implants used to replace the articular surfaces of the femur and tibia on both sides of the knee. The X-ray films of total knee arthroplasty were as shown in Figure 13.

Finger joint trauma is a common orthopedic disease in clinic. The important methods for the treatment of finger joint dysfunction are joint transplantation, arthroplasty, joint fusion, and artificial joint replacement. Artificial joint replacement is widely accepted for its advantages of finger function reconstruction and hand knuckle stability restoration. In 1940, Burman [71] carried out the alloy metacarpal head hemi-joint replacement technique, which is regarded as the prototype of the hand facet joint replacement technique. In 1959, the clinical application of total joint replacement prosthesis designed by Brannon and Klein [72] led to the widespread development of artificial joint replacement. In 1962, Swanson and Peltier [73] proposed a new concept of artificial finger joint prosthesis. In 1969, Niebauer et al. [74] and ChiaRi and Trieb [75] made improvements on the basis of Swanson. In the 1970s, the design of the prosthesis was more in line with the biomechanics and the application of the prosthesis that was close to the normal joint anatomy.

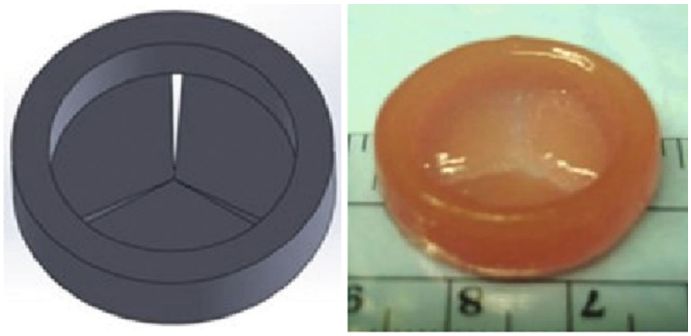

Figure 12: Aortic valve model and printed product [54].

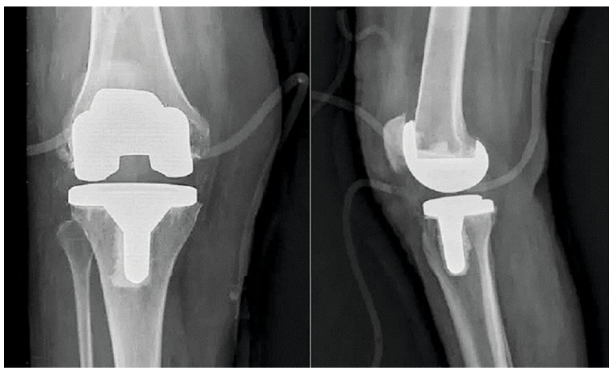

Figure 13: Total knee replacement X-ray [70].

At present, there are many types of human manual articular surface replacement prostheses used in clinical practice, including Linscheid et al. [76].

At present, 3D printing technology has been widely used in joint replacement surgery, but the innovation of the material and process of the prosthesis still needs to be enhanced to improve the stability and effectiveness of the prosthesis in the body.

4.5. Human Organs. 3D printing technology has a wide range of applications in the construction of functional tissue, including kidney, liver, multilayer skin [77], and other tissues or organs that can replace damaged or diseased tissues or organs.

Organ transplantation is the best treatment for end-stage renal disease (ESRD). However, the number of existing kidney donors is far less than the number of kidneys needed. For this reason, the use of 3D printing technology to print artificial kidneys has emerged to satisfy the donors required for surgery. Organovo used 3D printing technology to prepare the first whole-cell kidney tissue. King et al. [78] used 3D printing technology to prepare an in vitro model of three-dimensional proximal tubule tissue, which ushered in the dawn of organ transplantation and kidney regeneration. In 2011, Anthony Atala [79] of the Wake Forest University showed people 3D printing kidney technology; so far, 3D printing artificial organ technology has made great progress. The 3D printing technology of kidney organs is aimed at printing organs and tissues with organ functions. With the development of 3D printing technology and the continuous progress in the field of material science, it is expected that 3D printing artificial kidney can meet the needs of human body, improve the situation of kidney shortage, reduce people's pain, and improve people's life.

As one of the indispensable organs of human body, the structure of liver is complex. Compared with other organs, the liver has strong regeneration ability. But due to the small number of donors and the long regeneration cycle of its own liver, 3D printing of liver organs has become the core solution to solve the problem. In 2013, ZenI et al. [80] printed a translucent human liver model. Alkhouri and Zein [81] explored the use of 3D bioprinting technology to create miniature liver, which could be used to replace the pathological liver of end-stage liver failure. In 2013, Organovo printed a miniature liver with most functions of natural liver.

Skin transplantation is necessary for facial burns. If the burn area is too large, the amount of skin grafts required will increase, so that the supply exceeds demand. Using 3D printing technology to create artificial skin can not only meet the needs of skin transplantation but also reduce the pain of patients. Koch et al. [82] used 3D printing technology to print collagen, keratinocytes, and fibroblasts to prepare skin analogues. In 2013, Koch et al. [83] used 3D printing technology to print biological materials and prepared human skin tissues, which provided a reliable source for skin transplantation. Lee et al. [84] used 3D printing technology to print collagen, keratinocytes, and fibroblasts, respectively, to prepare skin tissue structure.

The emergence of 3D printing technology has given a solution to the problems faced by organ transplantation. But at present, 3D printing still needs to improve the resolution of 3D printing technology and the flexibility of biomaterials in the aspect of printing organs, so as to realize more complex and composite tissue or organ structures for clinical applications.

In general, with the development of materials science, technology, and imaging, 3D printing technology will be more and more widely used in cardiovascular and orthopedic fields. New 3D printing technologies such as in vivo direct printing, personalized generated heart implant device, and orthopedic implants will also greatly enrich the connotation of 3D printing technology and better benefit the cardiovascular patients and bone defect patients. But at present, the problems and challenges of 3D printing technology are also prominent. The first is the accuracy of printing, which involves imaging

mode and printing mode. The second is the material problem; it is a long-term task to find materials that meet the functional requirements, biological requirements, economic requirements, and technological requirements. The third problem is vascularization, the ability of 3D-printed tissues and organs to survive and function in the long term only based on stable vascularization. It is believed that 3D printing technology in cardiovascular and orthopedic applications will shine.

5. Conclusions

As a new type of digital printing technology, 3D printing has many advantages and huge applications in medicine, which makes every country invest more energy in the research and development of it. 3D printing technology has been applied in various fields of clinical medicine, especially in the application of implantable medical devices, which has been paid more attention by relevant scholars in various countries. Although 3D printing technology is currently in full swing, its technology still faces many challenges. For example, one of its challenges is how to develop various 3D printing raw materials. The second challenge is that 3D printing lacks industry standards for implantable medical devices. The third challenge is that the product technology chain has not yet been fully formed. As for the progress and development of 3D printing technology, the research on materials is the key. The biomaterials in the future should have the best mechanical properties, diffusion coefficient and biocompatibility, which are the basis and direction for 3D printing technology to advance in the future medical field. In addition, if the combination of biomaterials and printing technology can solve the problem of combining different types and functions of cells into a three-dimensional structure with complex functions and realize their basic functions. This technology will usher in a revolutionary change in 3D printing technology and biological tissue engineering, and the repair of human tissues and the transplantation of tissues and organs will be completely met by biological printing technology. In the future, independent 3D printing manufacturing centers for human organs can be built. This center can make corresponding implants in time according to the needs of the disease, so that the complex diseases encountered in clinical practice can be quickly solved, and patients' pain can be timely and effectively controlled.

The in situ 3D printing proposed for 3D printing is the implantation of original tissues in original body parts, avoiding foreign graft rejection and infection, for better recovery of the patient's body, and compared to bioprinted implants, in situ 3D printing is more accurate in size and shape, and it also overcomes the shortcomings of difficult implantation. One of the remaining challenges at the core of the further development of 3D printing in situ is the optimization and crosslinking of inks used in the process, Agostinacchio et al. [85] proposed the use of silk fibroin as an ink printing formula; different formulations of silk-based inks should be studied, characterized, and standardized, get shape fidelity, and at the same time, avoid the possible in vivo cytotoxic effects of photoinitiators during photopolymerization and expand the scale of manufacturing to be used in clinical practice. The emergence of smart materials or programmable materials, which can be converted by external stimuli, provides exciting new opportunities for 3D printing technology. This combination has led to a new field called 4D printing; the scale of 4D bioprinting to print bones has fascinating prospects. Compared with 3D printing, 5D printing saves 25% of materials in the printing process. 5D printing is a new branch of additive manufacturing. In this technology, the print head and the printable object have five degrees of freedom. Instead of the flat layer, it produces curved layers. In this process, the print part moves while the printer head is printing. So, printing undertakes the curve path of the part being printed rather than moving through a straight layer as in the case of 3D printers. The main advantage of this technology is to create a part with a curved layer with improved strength. A 5D printed model provides potential to fabricate artificial bone for surgery. Because human bones are not flat and having a curved surface, there is a requirement to manufacture artificial bones with 5D printing to provide excellent strength to these bone implants. This technology has great potential to fulfill this primary requirement. As the future of medical industry, 3D printing will become an important means of precision medicine and personalized medicine in the future. In the future, multidimensional printing will become a bright spot and vane in the medical field in the future and will promote the development of medical biology research in a country.

Conflicts of Interest

The authors declare that they have no conflicts of interest.

References

[1] W. Khan, E. Muntimadugu, M. Jaffe, and A. J. Domb, "Implantable medical devices," in *Focal Controlled Drug Delivery*, Advances in Delivery Science and Technology, A. Domb and W. Khan, Eds., pp. 33–59, Springer, Boston, MA, USA, 2014.

[2] K. K. VanKoevering, D. A. Zopf, and S. J. Hollister, "Tissue engineering and 3-dimensional modeling for facial reconstruction," *Facial Plastic Surgery Clinics of North America*, vol. 27, no. 1, pp. 151–161, 2019.

[3] X. Du, B. Yu, P. Pei, H. Ding, and Y. Zhu, "3D printing of pearl/CaSO4composite scaffolds for bone regeneration," *Journal of Materials Chemistry B*, vol. 6, no. 3, pp. 499–509, 2018.

[4] C. Wang, J. Lai, K. Li et al., "Cryogenic 3D printing of dual-delivery scaffolds for improved bone regeneration with enhanced vascularization," *Bioactive Materials*, vol. 6, no. 1, pp. 137–145, 2021.

[5] C. Sun and T. Liu, "The application of three dimensional printing technology in medicine," *Traditional Chinese Medicine*, vol. 8, no. 3, pp. 197–202, 2019.

[6] A. Pang, A. Joneja, D. C. C. Lam, and M. Yuen, "A CAD/CAM system for process planning and optimization in LOM (Laminated Object Manufacturing)," *IIE Transactions*, vol. 33, no. 4, pp. 345–355, 2001.

[7] C. Shuai, Z. Zeng, Y. Yang et al., "Graphene oxide assists polyvinylidene fluoride scaffold to reconstruct electrical

microenvironment of bone tissue," *Materials & Design*, vol. 190, article 108564, 2020.

[8] M. A. Cuiffo, J. Snyder, A. M. Elliott, N. Romero, S. Kannan, and G. P. Halada, "Impact of the fused deposition (FDM) printing process on polylactic acid (PLA) chemistry and structure," *Applied Sciences*, vol. 7, no. 6, p. 579, 2017.

[9] J. Yang, W. Yongkuan, C. Xian-lun, and H. Dazhi, "3D printing of ultra-high molecular weight polymer ethylene implants," *Electrical Processing and Mold*, vol. 1, pp. 52–55, 2019.

[10] A. G. Stevens, C. R. Oliver, M. Kirchmever et al., "Conformal robotic stereolithography," *3D Print Addit Manuf*, vol. 3, no. 4, pp. 226–235, 2016.

[11] D. Zheng, "Research status report on layered entity manufacturing technology," *Times Agricultural Machinery*, vol. 9, pp. 90-91, 2013.

[12] W. Zhu, C. Yan, Y. Shi, S. Wen, J. Liu, and Y. Shi, "Investigation into mechanical and microstructural properties of polypropylene manufactured by selective laser sintering in comparison with injection molding counterparts," *Materials and Design.*, vol. 82, pp. 37–45, 2015.

[13] Y. F. Pan, S. Yizhong, G. Dongdong, and X. Chengting, "Development status of selective laser sintering technology," *Tools and technology*, vol. 38, no. 6, pp. 3–7, 2004.

[14] T. Yin and W. Li, "Characteristics and development direction of rapid prototyping technology," *Modern Industrial Economy and Information Technology*, vol. 23, 2014.

[15] Z. Ping, J. Hua, and Z. Zhiting, "The principle and process of fused deposition rapid prototyping technology," *Machinery manufacturing and research.*, vol. 23, no. 5, pp. 17-18, 2003.

[16] C. Xuefei, S. Pengjie, Q. Yongjie, and Z. Ping, "Research and application of 3D printing bone tissue engineering scaffold," *Chinese Tissue Engineering Research*, vol. 25, pp. 4076–4080, 2015.

[17] Z. Difeng, Y. Jianming, H. Dazhi, C. Jinsong, and T. Yang, "The development and research status of 3DP three-dimensional printing technology," *Manufacturing Technology and Machine Tool*, vol. 3, pp. 38–43, 2017.

[18] J. Suwanprateeb and R. Chumnanklanc, "Three-dimensional printing of porous polyethylene structure using water-based binders," *Journal of Biomedical Materials Research, Part B: Applied Biomaterials*, vol. 78B, no. 1, pp. 138–145, 2006.

[19] N. W. Choi, M. Cabodi, B. Held, J. P. Gleghorn, L. J. Bonassar, and A. D. Stroock, "Microfluidic scaffolds for tissue engineering," *Nature Materials*, vol. 6, no. 11, pp. 908–915, 2007.

[20] J. Jang, J. Y. Park, G. Gao, and D. W. Cho, "Biomaterials-based 3D cell printing for next-generation therapeutics and diagnostics," *Biomaterials*, vol. 156, pp. 88–106, 2018.

[21] W. S. Tan, C. K. Chua, T. H. Chong, A. G. Fane, and A. Jia, "3D printing by selective laser sintering of polypropylene feed channel spacers for spiral wound membrane modules for the water industry," *Virtual and Physical Prototyping*, vol. 11, no. 3, pp. 151–158, 2016.

[22] X. Yang, Z. Lu, H. Wu, W. Li, L. Zheng, and J. Zhao, "Collagen-alginate as bioink for three-dimensional (3D) cell printing based cartilage tissue engineering," *Materials Science & Engineering. C, Materials for Biological Applications*, vol. 83, pp. 195–201, 2018.

[23] R. Shirazi, A. Shirazi-Adl, and M. Hurtig, "Role of cartilage collagen fibrils networks in knee joint biomechanics under compression," *Biomechanics*, vol. 41, no. 16, pp. 3340–3348, 2008.

[24] A. Awal, M. Rana, and M. Sain, "Thermorheological and mechanical properties of cellulose reinforced PLA bio- composites," *Mechanics of Materials*, vol. 80, pp. 87–95, 2015.

[25] R. Biodur, "108 Alloy (nickel-free high-nitrogen austenitic stainless steel alloy)," *Alloy Digest*, vol. 8, 1999.

[26] M. Niinomi, "Recent research and development in titanium alloys for biomedical applications and healthcare goods," *Science and Technology of Advanced Materials*, vol. 4, pp. 445–454, 2016.

[27] M. Niinomi, "Fatigue performance and cyto-toxicity of low rigidity titanium alloy, Ti–29Nb–13Ta–4.6Zr," *Biomaterials*, vol. 24, no. 16, pp. 2673–2683, 2003.

[28] R. Yibin and Y. Ke, "A new Ni-free drill-based alloy for vascular stent," *Rare Metal Materials and Engineering*, vol. 43, no. 1, pp. 101–104, 2014.

[29] C. Wigfield, J. Robertson, S. Gill, and R. Nelson, "Clinical experience with porous tantalum cervical interbody implants in a prospective randomized controlled trial," *British Journal of Neurosurgery*, vol. 17, no. 5, pp. 418–425, 2009.

[30] L. L. Hench, R. J. Splinter, W. C. Allen, and T. K. Greenlee, "Bonding mechanisms at the interface of ceramic prosthetic materials," *Journal of Biomedical Materials Research*, vol. 5, no. 6, pp. 117–141, 1971.

[31] I. D. Xynos, A. J. Edgar, L. D. K. Buttery, L. L. Hench, and J. M. Polak, "Gene-expression profiling of human osteoblasts following treatment with the ionic products of Bioglass® 45S5 dissolution," *Journal of Biomedical Materials Research*, vol. 55, no. 2, pp. 151–157, 2001.

[32] L. L. Hench, "Bioceramics: from concept to clinic," *Journal of the American Ceramic Society*, vol. 74, no. 7, pp. 1487–1510, 1991.

[33] H. Oonishi, "Orthopaedic applications of hydroxyapatite," *Biomaterials*, vol. 12, no. 2, pp. 171–178, 1991.

[34] H. Lu, K. Yu, S. Sun, Y. Liu, and J. Leng, "Mechanical and shape-memory behavior of shape-memory polymer composites with hybrid fillers," *Polymer International*, vol. 59, no. 6, pp. 766–771, 2010.

[35] X. Luo and P. T. Mather, "Conductive shape memory nanocomposites for high speed electrical actuation," *Soft Matter*, vol. 6, no. 10, pp. 2146–2149, 2010.

[36] J. K. Sherwood, S. L. Riley, R. Palazzolo et al., "A three-dimensional osteochondral composite scaffold for articular cartilage repair," *Biomaterials*, vol. 23, no. 24, pp. 4739–4751, 2002.

[37] W. Wang and K. W. K. Yeung, "Bone grafts and biomaterials substitutes for bone defect repair: a review," *Bioactive Materials*, vol. 2, no. 4, pp. 224–247, 2017.

[38] K. J. L. Burg, S. Porter, and J. F. Kellam, "Biomaterial developments for bone tissue engineering," *Biomaterials*, vol. 21, no. 23, pp. 2347–2359, 2000.

[39] F. R. de Gruijl, H. J. van Kranen, and L. H. F. Mullenders, "UV-induced DNA damage, repair, mutations and oncogenic pathways in skin cancer," *Journal of Photochemistry and Photobiology B: Biology*, vol. 63, no. 1-3, pp. 19–27, 2001.

[40] G. A. Roth, C. Johnson, A. Abajobir et al., "Global, regional, and national burden of cardiovascular diseases for 10 causes,1990 to 2015," *Journal of the American College of Cardiology*, vol. 70, no. 1, pp. 1–25, 2017.

[41] D. Qiushuang, "Analysis of combined medication regimen in the treatment of cardiovascular disease," *Chinese Medicine Guide*, vol. 15, no. 12, pp. 140-141, 2017.

[42] G. Wu, "Pay attention to the perioperative management of elderly general surgery patients," *Chinese Journal of Practical Surgery*, vol. 29, no. 2, pp. 109–111, 2009.

[43] S. Qian and X. Jianming, "The historical development and future prospects of coronary stents," *Advances in Cardiovascular Diseases*, vol. 37, no. 1, pp. 23–27, 2016.

[44] C. Flege, F. Vogt, S. Höges et al., "Development and characterization of a coronary polylactic acid stent prototype generated by selective laser melting," *Journal of Materials Science: Materials in Medicine*, vol. 24, no. 1, pp. 241–255, 2013.

[45] W. H. Kaesemeyer, K. G. Sprankle, J. N. Kremsky, W. Lau, M. N. Helmus, and G. S. Ghatnekar, "Bioresorbable polystatin fourth-generation stents," *Coronary Artery Disease*, vol. 24, no. 6, pp. 516–521, 2013.

[46] S. A. Park, S. J. Lee, K. S. Lim et al., "_In vivo_ evaluation and characterization of a bio-absorbable drug-coated stent fabricated using a 3D-printing system," *Materials Letters*, vol. 141, pp. 355–358, 2015.

[47] R. van Lith, E. Baker, H. Ware et al., "3D-printing strong high-resolution antioxidant bioresorbable vascular stents," *Advanced Materials Technologies*, vol. 1, no. 9, 2016.

[48] H. Fengyang, S. Jian, S. Lu, and G. Gao, "Development of artificial heart valves," *Medical Equipment*, vol. 30, no. 13, pp. 186–193, 2017.

[49] W. Z. Marx, S. Duanchao, X. Wang, and Z. Long, "Analysis of factors affecting the prognosis of patients with severe heart valve disease after artificial heart valve replacement," *China Medical Herald*, vol. 14, no. 26, pp. 64–67, 2017.

[50] W. Zhou, *Three Dimensional Printing of Cardiac Aortic Valve Based on Mold Extraction and Cell Damage Simulation[D]*, Dalian: Dalian University of Technology, 2019.

[51] S. P. Houstrop, A. Kadner, S. Melnitchouk et al., "Tissue engineering of function al trileaflet heart valves from human marrow stromal cells," *Circulation*, vol. 106, 12, Supplement 1, pp. 143–150, 2002.

[52] S. P. Hoerstrup, R. Sodian, S. Daebritz et al., "Functional living trileaflet heart valve grown in vitro," *Circulation*, vol. 102, Supplement 3, pp. 44–49, 2000.

[53] Z. Baoren and J. Zhu, *Artificial Heart Valve and Valve Replacement*, People's Medical Publishing House, Beijing, 1999.

[54] B. Duan, E. Kapetanovic, L. A. Hockaday, and J. T. Butcher, "Three-dimensional printed trileaflet valve conduits using biological hydrogels and human valve interstitial cells," *Acta Biomaterialia*, vol. 10, no. 5, pp. 1836–1846, 2014.

[55] S. Bose, S. Vahabzadeh, and A. Bandyopadhyay, "Bone tissue engineering using 3D printing," *Materials Today*, vol. 16, no. 12, pp. 496–504, 2013.

[56] E. Vorndran, C. Moseke, and U. Gbureck, "3D printing of ceramic implants," *MRS Bulletin*, vol. 40, no. 2, pp. 127–136, 2015.

[57] S. P. Pilipchuk, A. B. Plonka, T. Monje et al., "Tissue engineering for bone regeneration and osseointegration in the oral cavity," *Dental Materials*, vol. 31, no. 4, pp. 317–338, 2015.

[58] A. R. Amini, C. T. Laurencin, and S. P. Nukavarapu, "Bone tissue engineering: recent advances and challenges," *Critical Reviews in Biomedical Engineering*, vol. 40, no. 5, pp. 363–408, 2012.

[59] E. D. Arrington, W. J. Smith, H. G. Chambers, A. L. Bucknell, and N. A. Davino, "Complications of iliac crest bone graft harvesting," *Clinical Orthopaedics & Related Research*, vol. 329, no. 329, pp. 300–309, 1996.

[60] S. Stevenson, S. E. Emery, and V. M. Goldberg, "Factors affecting bone graft incorporation," *Clinical Orthopaedics & Related Research*, vol. 324, no. 324, pp. 66–74, 1996.

[61] Q. Wang, *Research on 3D Printing Sodium Alginate/Hydroxyapatite Hydrogel Composite Atsttrin Protein for Bone Defect Repair*, Zhejiang University, China, 2015.

[62] R. J. O'Keefe and J. Mao, "Bone tissue engineering and regeneration: from discovery to the clinic-an overview," *Tissue Engineering Part B: Reviews*, vol. 17, no. 6, pp. 389–392, 2011.

[63] L. Singh, V. Kumar, and B. D. Ratner, "Generation of porous microcellular 85/15 poly (DL-lactide-co-glycolide) foams for biomedical applications," *Biomaterials*, vol. 25, no. 13, pp. 2611–2617, 2004.

[64] Y. H. Lee, J. H. Lee, I. G. An et al., "Electrospun dual-porosity structure and biodegradation morphology of montmorillonite reinforced PLLA nanocomposite scaffolds," *Biomaterials*, vol. 26, no. 16, pp. 3165–3172, 2005.

[65] H. Fan, H. Tao, Y. Wu, Y. Hu, Y. Yan, and Z. Luo, "TGF-β3 immobilized PLGA-gelatin/chondroitin sulfate/hyaluronic acid hybrid scaffold for cartilage regeneration," *Journal of Biomedical Materials Research Part A*, vol. 95, no. 4, pp. 982–992, 2010.

[66] S. Tarafder, N. M. Davies, A. Bandyopadhyay, and S. Bose, "3D printed tricalcium phosphate bone tissue engineering scaffolds: effect of SrO and MgO doping on in vivo osteogenesis in a rat distal femoral defect model," *Biomaterials*, vol. 1, no. 12, pp. 1250–1259, 2013.

[67] H. Hosalkar, "CORR insights®: is age or surgical approach associated with osteonecrosis in patients with developmental dysplasia of the hip a meta-analysis," *Clinical Orthopaedics and Related Research*, vol. 474, no. 5, pp. 1178-1179, 2016.

[68] S. T. Mahan, J. N. Katz, and Y.-J. Kim, "To screen or not to screen? A decision analysis of the utility of screening for developmental dysplasia of the hip," *The Journal of Bone and Joint Surgery-American Volume*, vol. 91, no. 7, pp. 1705–1719, 2009.

[69] M. Fuchs, B. Effenberger, S. Märdian et al., "Mid-term survival of total knee arthroplasty in patients with postraumatic osteoarthritis arthritis," *Acta Chirurgiae Orthopaedicae et Traumatologiae Cecho-slovaca*, vol. 85, no. 5, pp. 319–324, 2018.

[70] W. Zhang, M. Wu, F.-j. Cui, and Y. Zhi-Xin, "Application of 3D printed osteotomy guide plate in total knee arthroplasty," *Chinese Journal of Bone and Joint Injury*, vol. 35, no. 8, pp. 835–837, 2020.

[71] M. S. Burman, "Vitalium cup arthroplasty of metararphalaneal joints of fingers," *Bulletin of the Hospital for Joint Diseases Orthopaedic Institute*, vol. 1, pp. 79–89, 1940.

[72] E. W. Brannon and G. Klein, "Experiences with a finger-joint prosthesis," *Plastic and Reconstructive Surgery*, vol. 24, no. 2, p. 224, 1959.

[73] A. B. Swanson and L. F. Peltier, "Silicone rubber implants for replacement of arthritic or destroyed joints in the hand," *Clinical Orthopaedics and Related Research*, vol. 342, pp. 4–10, 1997.

[74] J. J. Niebauer, J. L. Shaw, and W. W. Doren, "Silicone-dacron hinge prosthesis: design, evaluation, and application," *Annals of the Rheumatic Diseases*, vol. 28, Supplement 5, p. 56, 1969.

[75] C. CHIARI and K. TRIEB, "Metacarpophalangeal joint arthroplasty in rheumatoid arthritis," *The Journal of Bone and Joint Surgery. American Volume*, vol. 86, no. 8, pp. 1832-1833, 2004.

[76] R. L. Linscheid, P. M. Murray, M.-A. Vidal, and R. D. Beckenbaugh, "Development of a surface replacement arthroplasty for proximal interphalangeal joints," *The Journal of Hand Surgery*, vol. 22, no. 2, pp. 286–298, 1997.

[77] W.-C. Yan, P. Davoodi, S. Vijayavenkataraman et al., "3D bioprinting of skin tissue: from pre-processing to final product evaluation," *Advanced Drug Delivery Reviews*, vol. 132, pp. 270–295, 2018.

[78] G. Reint, A. Rak-Raszewska, and S. J. Vainio, "Kidney development and perspectives for organ engineering," *Cell and Tissue Research*, vol. 369, no. 1, pp. 171–183, 2017.

[79] H. N. Chia and B. M. Wu, "Recent advances in 3D printing of biomaterials," *Journal of Biological Engineering*, vol. 9, 2015.

[80] Y. Fan, Y. Yan-kun, and Z. Hong, "Application of 3D printing technology in the diagnosis and treatment of congenital heart disease," *Chinese Interventional Imaging and Therapy*, vol. 9, p. 630, 2014.

[81] N. Alkhouri and N. N. Zein, "Three-dimensional printing and pediatric liver disease," *Current Opinion in Pediatrics*, vol. 28, no. 5, pp. 626–630, 2016.

[82] L. Koch, A. Deiwick, S. Schlie et al., "Skin tissue generation by laser cell printing," *Biotechnology and Bioengineering*, vol. 109, no. 7, pp. 1855–1863, 2012.

[83] N. N. Zein, I. A. Hanouneh, P. D. Bishop et al., "Three-dimensional print of a liver for preoperative planning in living donor liver transplantation," *Liver Transplantation*, vol. 19, no. 12, pp. 1304–1310, 2013.

[84] V. Lee, G. Singh, J. P. Trasatti et al., "Design and fabrication of human skin by three-dimensional bioprinting," *Tissue Engineering. Part C, Methods*, vol. 20, no. 6, pp. 473–484, 2014.

[85] F. Agostinacchio, X. Mu, S. Dirè, A. Motta, and D. L. Kaplan, "In situ 3D printing: opportunities with silk inks," *Trends in Biotechnology*, 2020.

Hindawi
BioMed Research International
Volume 2020, Article ID 6622502, 6 pages
https://doi.org/10.1155/2020/6622502

Research Article

Combined Endovascular and Surgical Treatment of Chronic Carotid Artery Occlusion: Hybrid Operation

Long Yan[1], **Zhe Wang**[2], **Zhanchuan Liu**[3], **Haoyuan Yin**[4] and **Xuan Chen**[4]

[1]*Department of Interventional Neuroradiology, Beijing Tiantan Hospital, Capital Medical University, Beijing 100000, China*
[2]*Department of Gerontology, The First Hospital of Jilin University, Changchun, Jilin 130021, China*
[3]*Department of Neurosurgery, The Second Hospital of Jilin University, Changchun, Jilin 130041, China*
[4]*Department of Neurosurgery, The First Hospital of Jilin University, Changchun, Jilin 130021, China*

Correspondence should be addressed to Xuan Chen; chen_xuan@jlu.edu.cn

Received 12 October 2020; Revised 5 November 2020; Accepted 16 November 2020; Published 1 December 2020

Academic Editor: Weiluan Chen

Objectives. The optimal treatment choice of chronic carotid artery occlusion (CAO) remains inconclusive. This study was aimed at exploring the safety and effectiveness of hybrid surgery in the treatment of CAO and at determining predictors for successful recanalization. *Methods*. In this study, we enrolled 37 patients with CAO who underwent hybrid surgical treatment during the period 2016–2018. We extracted and analyzed patients' demographic data, disease characteristics, surgical success rates, perioperative complications, and prognosis. *Results*. A total of 37 patients with symptomatic CAO underwent hybrid surgical treatment. Thirty cases (81.1%) were successfully recanalized, while seven were not. Blood reflux after carotid endarterectomy occurred in 18 patients (60%) of the success group and 1 (14.3%) of the failure group (OR, 9.0; 95% CI, 0.95-54.5; $P = 0.042$). The rate of distal ICA reconstruction below the clinoid segment was 20 (66.7%) in the success group and 1 (14.3%) in the failure group (OR, 12.0; 95% CI, 1.3-113.7; $P = 0.029$). In patients with successful recanalization, no ischemic events occurred after surgery and during follow-up, but restenosis of >50% was found in one case. In the failure group, two patients experienced recurrent ischemic events during follow-up. Perfusion imaging in successful recanalization cases is significantly improved, preoperative I/C ratio was 1.44 (IQR 1.27-1.55), and postoperative 1.12 (IQR 1.05-1.23). National Institutes of Health Stroke Scale (NIHSS) score of successful recanalization cases was 5.35 (2.26) before surgery and 2.03 (1.40) at 6 months ($P < 0.01$). *Conclusion*. Hybrid surgery might be a safe and effective way to treat CAO. Distal internal carotid artery reconstruction to below the clinoid segment and blood reflux after carotid endarterectomy are predictors of successful recanalization.

1. Introduction

Chronic carotid artery occlusion (CAO) is an uncommon but important cause of ischemic stroke. The natural course of CAO varies greatly, and it can manifest as stroke, transient ischemic attack (TIA), or no symptoms at all. Territories of which blood supply is occluded rely on compensating collateral flow, but for some patients, these are not sufficient. Among patients with hemodynamic disorders, those with CAO have significantly higher rates of recurrent stroke and mortality [1]. Treatment of CAO is still controversial. Alternative treatments are as follows: conservative treatment including antiplatelets and anticoagulants, extracranial-intracranial (EC-IC) bypass, carotid endarterectomy (CEA), and endovascular recanalization.

Hybrid surgery refers to the combination of endovascular recanalization and CEA. Reaching the distal true lumen through the occluded segment is the key to successful recanalization in CAO. Hybrid surgery combines their advantages and overcomes their respective difficulties. CEA removes plaque, allowing the microcatheter and microguidewire to easily pass through to the distal true lumen. Some studies have reported the application of hybrid surgery in CAO [2–4], but the predictors of successful recanalization have not been

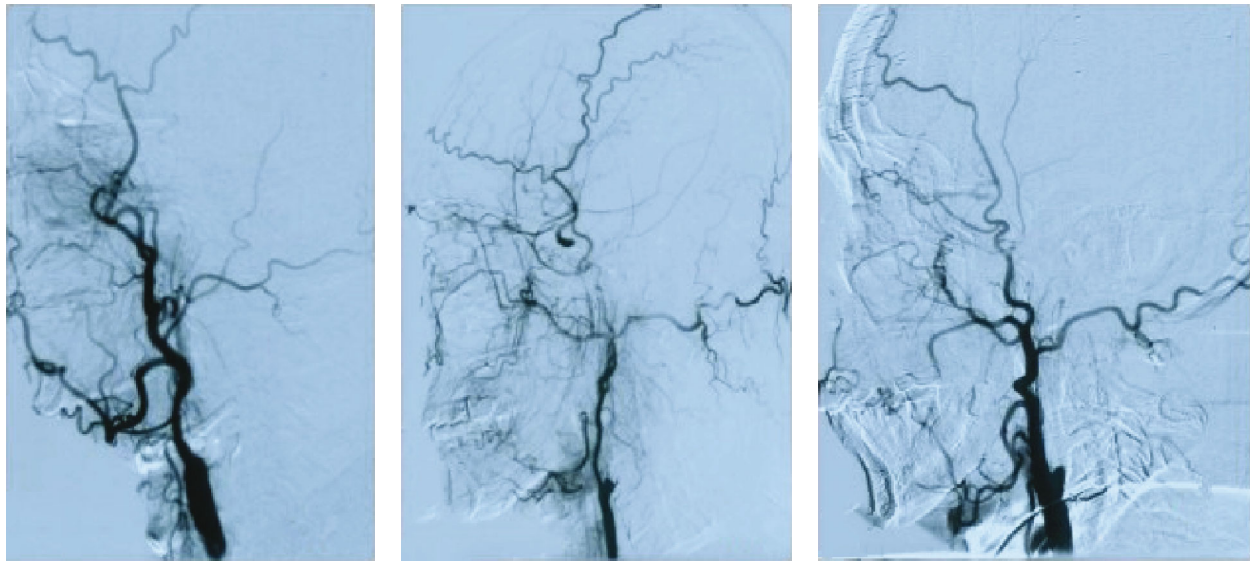

(a) (b) (c)

Figure 1: Stump condition: (a) no stump; (b) blunt stump; (c) tapered stump.

fully discussed. The purposes of the study are to explore the effectiveness and safety of hybrid surgery for CAO and the predictors of successful recanalization.

2. Materials and Methods

2.1. Patient Selection. This retrospective study was approved by the local institutional review board. We included symptomatic CAO patients who were hospitalized in the Department of Neurosurgery of the First Hospital of Jilin University (Changchun, China) from January 2016 to December 2018. CAO was defined as a duration of ≥4 weeks between diagnosis and treatment. Inclusion criteria were as follows: (1) 18–80 years old, (2) complete carotid artery occlusion as confirmed by digital-subtraction angiography (DSA), (3) TIA or stroke occurring in the occluded blood vessel supply area over the past 12 months, (4) computed tomography (CT) or magnetic resonance (MR) perfusion imaging confirming hypoperfusion on the occluded side, (5) CT or MR excluding extensive cerebral infarction, and (6) cases with complete clinical and imaging data to permit follow-up. Exclusion criteria were as follows: (1) severe diseases of the heart, liver, kidney, lung, or other vital organ, with estimated survival time < 3 months; (2) inability to tolerate general anesthesia for surgery; (3) allergy to contrast agents; (4) contraindication of, or resistance to, aspirin and/or clopidogrel; (5) other cerebrovascular diseases (intracranial aneurysms and cerebrovascular malformations) causing stroke; and (6) severe neurological dysfunction and impaired consciousness.

2.2. Data Collection. Baseline information included sex, age, diabetes, hypertension, smoking, drinking, and hyperlipidemia. NIHSS score on admission and duration from the last neurologic event to surgery was also collected. All imaging data are assessed individually by two neurosurgeons. All patients underwent CT perfusion imaging or MR perfusion imaging before and one week after surgery. Mean transit times (MTTs) of ipsilateral- (side of the occluded ICA-) to-contralateral (I/C) were calculated. The morphological description included the following: stump morphology: (1) blunt stump or no stump and (2) tapered stump (Figure 1). Compensatory vessels included the following: anterior communicating artery, posterior communicating artery, ipsilateral ophthalmic artery, and branches of other arteries. Reflux sites were categorized as follows: (1) below the clinoid segment (cavernous segment, petrous segment, and below) and (2) clinoid segment and above (clinoid segment, ophthalmic segment, or communicating segment). Surgical complications included hyperperfusion, ischemic events, hemorrhage events, carotid cavernous fistula, dissection, and so on.

2.3. Hybrid Surgical Procedure. After general anesthesia, patients were placed in the supine position with their heads tilted to the opposite side from the lesion. A straight incision was made at the front edge of the sternocleidomastoid muscle on the affected side to cut through the skin and platysma muscle after routine disinfection. We separated the skin and muscle along the front edge of the sternocleidomastoid muscle to the ICA sheath so that we could expose and cut the fascia of the ICA in order to lift that artery. The superior thyroid artery, external carotid artery, and distal end of the ICA were clamped in turn. Afterwards, we cut the common carotid artery (CCA) along the long axis to the distal end of the ICA. After stripping off the intima of the ICA containing the plaque and thrombus and then flushing and thoroughly stripping the lumen, we observed the distal end for blood reflux. After stitching up the vessel wall, an 8F catheter sheath was inserted into the right femoral artery to support the catheter to the bifurcation of the CCA. Via angiography, we observed the recanalization status of the distal blood vessels. If it remained occluded, we passed a microcatheter and microguidewire through to the occluded lumen in order to determine stenotic and occluded sites. Then, balloon-angioplasty was used to expand the blood vessel at the site

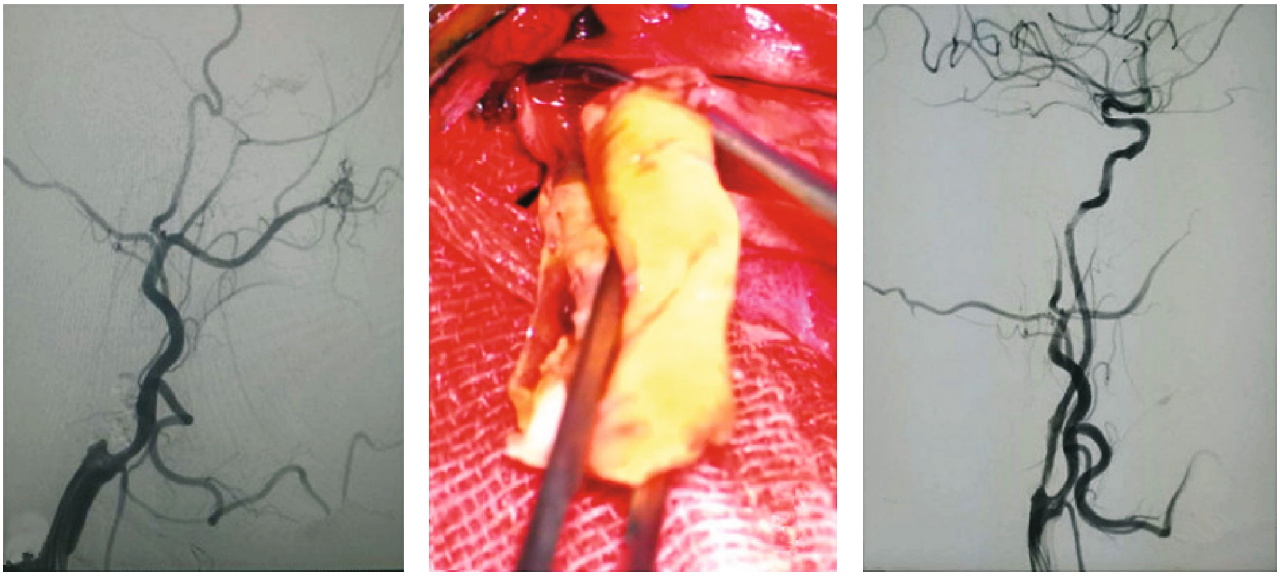

(a) (b) (c)

Figure 2: (a) Preoperative chronic carotid artery occlusion. (b) Remove carotid plaque. (c) Carotid artery recanalization after hybrid surgery.

of occlusion and stenosis, followed by insertion and release of the appropriate stent. A postsurgery blood flow reaching Thrombolysis in Cerebral Infarction (TICI) grade IIb or higher is defined as successful recanalizaiton (Figure 2).

2.4. Follow-Up. All patients were recommended for follow-up. Clinical follow-up content is as follows: all cases are recommended for outpatient or telephone follow-up and we record the patients' NIHSS score and record hemorrhage and ischemic events. Image follow-up content is as follows: color Doppler ultrasound at 1 month, CTA at 3 months, and DSA at 6 months to record whether the recanalized blood vessel is unobstructed, whether there is reocclusion or restenosis, and whether there are other vascular injuries, such as carotid artery dissection and pseudo aneurysm, and carotid cavernous fistula.

2.5. Statistical Analysis. We performed statistical analysis using SPSS software version 20.0 (IBM Corp., Armonk, New York, US). Normal distribution measurement data were expressed as means and standard deviations (SD), while skew distribution data were expressed as the median and interquartile range (IQR). Counting data were expressed in frequencies and percentages. We compared data between each group using Student's t test (normal distribution) or the Mann-Whitney U test (skewed distribution), the chi-square test, or Fisher's exact test according to the situation. $P < 0.05$ was considered a statistically significant difference.

3. Results and Discussion

3.1. Results. Of the 59 patients with symptomatic CAO who were admitted during the study period, a total of 37 patients were included in the study (Figure 3). Thirty cases (81.1%) were successfully recanalized and seven were not. Age, male sex, hypertension, diabetes, hyperlipidemia, smoking, and drinking did not differ significantly between the success and failure groups ($P > 0.05$). Male patients accounted for 89.1% of total cases, a significantly higher proportion than that of female patients. The majority of patients smoked (70.3%). Duration from last onset to surgery was 15.0 (IQR 14.0-33.75) days in cases of the success group and 60.0 (IQR 30.0-120.0) in those of the failure group ($P = 0.007$); therefore, disease last onset was longer in the failure group than in the success group (Table 1).

The lesion was on the left side in 18 cases and on the right side in 19. The occlusion was located in the CCA in 4 cases (10.8%), in the beginning of ICA in 27 cases (73.0%), and in other sites in 6 cases (16.2%). Most of the occlusions were located at the beginning of the ICA. Twenty cases had a tapered stump, and the other 17 cases had a blunt or no stump at all. After CEA, 19 cases showed blood reflux, with 18 successful recanalizations and 1 failure. The other 18 cases showed no blood reflux, with 12 successful recanalizations and 6 failures. ($P = 0.042$). In 16 cases of distal ICA reconstruction at the clinoid segment and above, 10 cases were successfully recanalized and 6 cases were not recanalized; 21 cases below the clinoid segment were successfully recanalized in 20 cases and 1 case was not recanalized ($P = 0.029$) (Table 2).

There were 2 cases of intracranial hemorrhage, 1 case died of sudden breathing, cardiac arrest, and cerebral hemorrhage on the second day after operation; 1 case died of intracranial hemorrhage caused by rupture of the blood vessel during operation. Two cases showed hyperperfusion, which was relieved after medication. There were no ischemic events in the success group after surgery or during follow-up, but restenosis of >50% was found in one case. Of the seven patients with failed recanalization, two had recurrent ischemic events during follow-up (Table 3).

Preoperative I/C ratio in success group cases was 1.44 (IQR 1.27-1.55); 1 week after surgery, the I/C ratio in these cases was 1.12 (IQR 1.05-1.23), $P < 0.01$. Cerebral perfusion

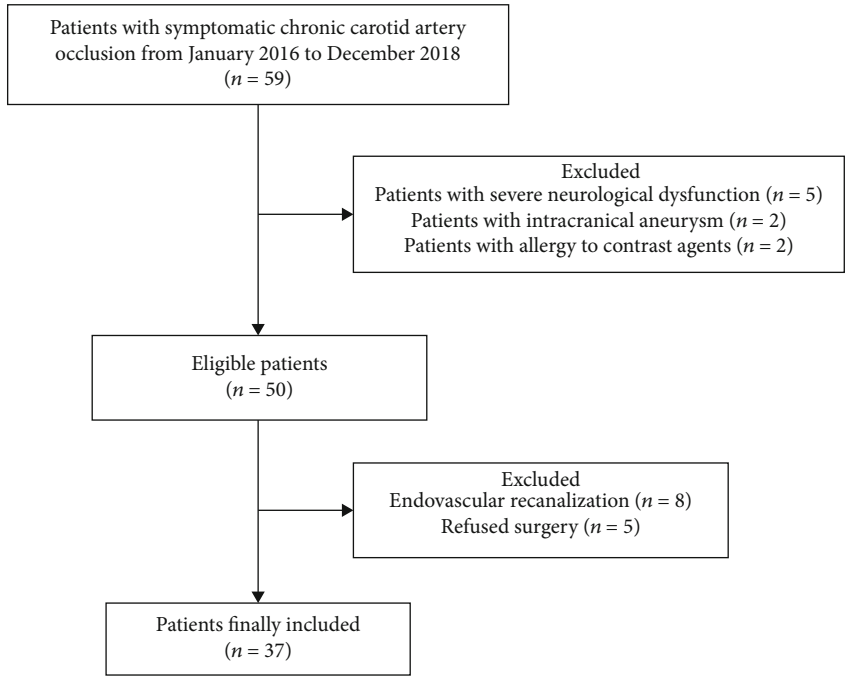

Figure 3: Selection of patients.

Table 1: Baseline characteristics of patients.

	Total ($n = 37$)	Success group ($n = 30$)	Failure group ($n = 7$)	P value
Age, mean (SD)	62.1 (6.4)	62.9 (6.4)	58.9 (6.1)	0.140
Male, *n* (%)	33 (89.1%)	27 (90.0%)	6 (85.7%)	1.000
Hypertension, *n* (%)	24 (64.9%)	21 (70.0%)	3 (42.9%)	0.213
Diabetes, *n* (%)	20 (54.1%)	16 (53.3%)	4 (57.1%)	1.000
Hyperlipidemia, *n* (%)	19 (51.4%)	15 (50.0%)	4 (57.1%)	1.000
Smoking, *n* (%)	26 (70.3%)	21 (70.0%)	5 (71.4%)	1.000
Drinking, *n* (%)	16 (43.2%)	14 (46.7%)	2 (28.6%)	0.674
Duration from last onset to surgery, median (IQR)	30.0 (14.5-47.5)	15.0 (14.0-33.75)	60.0 (30.0-120.0)	0.007

in success group cases was significantly improved. Preoperative NIHSS score in success group cases was 5.35 (2.26); at 6-month follow-up, NIHSS score in these cases was 2.03 (1.40), $P < 0.01$. Neurological function was significantly improved in postoperative patients (Table 4).

3.2. Discussion. Even with intensive drug treatment, the CAO annual stroke recurrence rate is 6% to 20% [1, 5]. It is necessary to establish an alternative treatment with an acceptable safety and efficacy profile. In this study, the recanalization rate of hybrid surgery was 81.1%, with a relatively low risk of complications. We found that distal ICA reconstruction to below the clinoid segment and blood reflux after carotid endarterectomy are predictors of successful recanalization.

Various treatment methods for CAO have developed gradually since the 1960s, including bypass surgery, CEA, and intravascular recanalization under interventional radiology. EC-IC bypass is not recommended duo to failing to reduce the risk of recurrent ipsilateral ischemic stroke within 2 years compared with medical therapy [6]. CEA, due to anatomical limitations, is applicable only for occlusion at the origin of the internal carotid artery (ICA). For long-segment occlusions that extend to the intracranial segment, pure CEA presents challenges to successful recanalization [7]. With the development of neurointerventional technology and materials, endovascular recanalization has been more frequently explored, and more studies have reported the improved possibility of successful endovascular recanalization [8–10]. In one study enrolling 138 patients who underwent endovascular recanalization surgeries, 85 of them (61.6%) were technically successful [11]. However, 6 patients experienced recurrent stroke, death, or intracranial hemorrhage, and 11 (8.0%) had intracranial carotid cavernous fistulae. Thus, the recanalization success rate is still unsatisfactory and the complication rate still high [12].

CEA for the treatment of CAO is limited to occlusion location at places that can be exposed during operation while no long-segment thrombosis exists in the distal blood vessels, which restrict its scope of application. As to endovascular treatment, it was first reported in 2013 for CAO patients [2]; all three patients were successfully recanalized. The cerebral-perfusion imaging showed significant improvement,

Table 2: Lesion characteristics of patients.

	Success group ($n = 30$)	Failure group ($n = 7$)	OR (95% CI)	P value
Left sided, n (%)	16 (53.3%)	2 (28.6%)	2.9 (0.5-17.1)	0.405
Occlusion site			—	0.085
CCA, n (%)	4 (13.3%)	0 (0.0%)		
Beginning of ICA, n (%)	23 (76.7%)	4 (57.1%)		
Other sites, n (%)	3 (10.0%)	3 (42.9%)		
Stump condition			0.9 (0.2-4.5)	1.000
Tapered, n (%)	16 (53.3%)	4 (57.1%)		
Blunt or no stump, n (%)	14 (46.7%)	3 (42.9%)		
Blood reflux after CEA, n (%)	18 (60.0%)	1 (14.3%)	9.0 (0.95-54.5)	0.042
Level of distal ICA reconstruction			12.0 (1.3-113.7)	0.029
Clinoid segment and beyond, n (%)	10 (33.3%)	6 (85.7%)		
Below clinoid segment, n (%)	20 (66.7%)	1 (14.3%)		

CCA: common carotid artery; ICA: internal carotid artery; CEA: carotid endarterectomy.

Table 3: Postoperative complications and follow up.

	Success group ($n = 30$)	Failure group ($n = 7$)
Hyperperfusion, n (%)	2 (6.7%)	0 (0.0%)
Ischemic stroke, n (%)	0 (0.0%)	2 (28.6%)
Hemorrhage, n (%)	1 (3.3%)	1 (14.3%)
Death, n (%)	1 (3.3%)	1 (14.3%)

Table 4: Imaging improvement and functional improvement.

	Success group		P
	Preoperative	Postoperative	
I/C, median (IQR)	1.44 (1.27-1.55)	1.12 (1.05-1.23)	<0.01
NIHSS, mean (SD)	5.35 (2.26)	2.03 (1.40)	<0.01

I/C: mean transit times ipsilateral-to-contralateral; NIHSS: National Institutes of Health Stroke Scale.

and no ischemic events occurred during the 6 months of follow-up. For the past few years, hybrid surgery, combining the CEA and endovascular treatment, has gradually developed to treat CAO. The occlusion site is more likely to locate at the beginning of the ICA for CAO. CEA removes the plaque at the origin ICA, allowing the microcatheter and microguidewire to easily pass through to the distal true lumen. This paves the way for endovascular interventional recanalization, which in turn treats the distal carotid artery lesion using balloons and stents. Theoretically, combing the advantages of the two surgical modalities may improve the success rate. Liu et al. reported [13] that of 21 patients who received hybrid surgical treatment, 15 (71.4%) were successfully recanalized without causing carotid dissections, intracranial hemorrhages, or new neurological deficits. In the current study, we enrolled a total of 37 patients and 30 (81.1%) were successfully recanalized. Therefore, it showed that hybrid surgery may be an effective surgical method for CAO.

Many studies reported the successful recanalization of CAO with hybrid surgery [2–4, 13], but few reported the predictors for successful recanalization. In this study, distal ICA reconstruction to below the clinoid segment and blood reflux after carotid CEA are predictors of successful recanalization. Both of these predictors indicate a shorter occlusion length. Hybrid surgery makes it possible to reach the distal true lumen through the occluded segment. The occlusion length may be another key factor of successful recanalization. We need more cases and more advanced inspection methods such as high resolution magnetic resonance imaging to verify.

The goal of treatment is to restore blood supply, improve hypoperfusion, and reduce the incidence of recurrent stroke. Studies have shown that hemodynamic damage in patients with CAO is significantly correlated with the incidence of stroke [14, 15]. CT/MR perfusion imaging has in fact been widely used in clinical practice for pre-and postevaluation of CAO cases. A study comparing CT perfusion imaging with positron emission tomography (PET) perfusion imaging in CAO patients showed that MTT parameters of CT perfusion imaging were significantly correlated with oxygen extraction fraction (OEF) as measured by PET [16]. Mukherjee et al. reported [17] that MR perfusion imaging in patients with CAO was linearly correlated with cerebral blood flow (CBF) as measured by PET. Due to the large differences in absolute-value measurement between different modalities, semiquantitative comparisons with the ipsilateral side of the lesion are mostly used at present, and their accuracy has been recognized [18]. All patients in this study underwent CT or MR perfusion before surgery and again 1 week after surgery. Successful cases had a preoperative I/C ratio of 1.44 (IQR 1.27-1.55) and a postoperative ratio I/C of 1.12 (IQR 1.05-1.23), which showed that perfusion was significantly improved before and after surgery.

There were some limitations to this study. First, it was a retrospective study and it is inevitable that the collection of relevant data will be biased; second, the number of cases in this study was small and could not be stratified in more detail based on the level of distal ICA reconstitution. Due to the small sample size, statistical methods used in this study were Student's t test (normal distribution) or Mann-Whitney U test (skewed distribution), the chi-square test,

or Fisher's exact test; univariate and multivariate analyses could not be performed.

4. Conclusions

Hybrid surgery may be a safe and effective method of treating CAO, with a higher success rate and fewer complications than traditional methods. Distal ICA reconstruction to below the clinoid segment and blood reflux after carotid endarterectomy are predictors of successful recanalization.

Data Availability

The data that support the findings of this study are available from the corresponding author upon reasonable request.

Conflicts of Interest

The authors declare that there is no conflict of interest regarding the publication of this paper.

Acknowledgments

We thank all of the patients and health care providers who participated in this study. We sincerely thank Professor Qi Luo (from the Department of Neurosurgery, the First Hospital of Jilin University, Changchun, Jilin, China) for guidance on the article.

Supplementary Materials

See table in the Supplementary Material for comprehensive data analysis. *(Supplementary Materials)*

References

[1] M. L. Flaherty, K. D. Flemming, R. McClelland, N. W. Jorgensen, and Brown RD Jr, "Population-based study of symptomatic internal carotid artery occlusion - incidence and long-term follow-up," *Stroke*, vol. 35, no. 8, pp. E349–e352, 2004.

[2] Y.-T. Shih, W. H. Chen, W. L. Lee, H. T. Lee, C. C. Shen, and Y. S. Tsuei, "Hybrid surgery for symptomatic chronic total occlusion of carotid artery: a technical note," *Neurosurgery*, vol. 73, suppl_1, pp. onsE117–onsE123, 2013.

[3] Y. Yang, X. Liu, R. Wang, Y. Zhang, D. Zhang, and J. Zhao, "A treatment option for symptomatic chronic complete internal carotid artery occlusion: hybrid surgery," *Frontiers in Neuroscience*, vol. 14, 2020.

[4] J. Li, C. Wang, S. Zou, Y. Liu, and L. Qu, "Hybrid surgery for nontaper or nonstump lesions in symptomatic subacute or chronic internal carotid occlusion: a better solution," *World Neurosurgery*, vol. 122, pp. E1416–e1425, 2019.

[5] C. J. M. Klijn, L. J. Kappelle, C. A. F. Tulleken, and J. van Gijn, "Symptomatic carotid artery occlusion," *Stroke*, vol. 28, no. 10, pp. 2084–2093, 1997.

[6] W. J. Powers, W. R. Clarke, R. L. Grubb et al., "Extracranial-intracranial bypass surgery for stroke prevention in hemodynamic cerebral ischemia the carotid occlusion surgery study randomized trial," *JAMA*, vol. 306, no. 18, pp. 1983–1992, 2011.

[7] J. E. Thompson, D. J. Austin, and R. D. Patman, "Carotid endarterectomy for cerebrovascular insufficiency: long-term results in 592 patients followed up to thirteen years," *Annals of Surgery*, vol. 172, no. 4, pp. 663–679, 1970.

[8] H.-L. Kao, M.-S. Lin, C.-S. Wang et al., "Feasibility of endovascular recanalization for symptomatic cervical internal carotid artery occlusion," *Journal of the American College of Cardiology*, vol. 49, no. 7, pp. 765–771, 2007.

[9] M. Shojima, S. Nemoto, A. Morita et al., "Protected endovascular revascularization of subacute and chronic total occlusion of the internal carotid artery," *American Journal of Neuroradiology*, vol. 31, no. 3, pp. 481–486, 2010.

[10] Y.-L. Fan, J. Q. Wan, Z. W. Zhou et al., "Neurocognitive improvement after carotid artery stenting in patients with chronic internal carotid artery occlusion," *Vascular and Endovascular Surgery*, vol. 48, no. 4, pp. 305–310, 2014.

[11] C. F. Yeh, Y. H. Chen, M. S. Lin et al., "Carotid-cavernous fistula after endovascular intervention for chronic carotid artery total occlusion," *Catheterization and Cardiovascular Interventions*, vol. 91, no. 4, pp. 735–741, 2018.

[12] Y.-H. Chen, W.-S. Leong, M.-S. Lin et al., "Predictors for successful endovascular intervention in chronic carotid artery total occlusion," *Jacc-Cardiovascular Interventions*, vol. 9, no. 17, pp. 1825–1832, 2016.

[13] B. Liu, W. Wei, Y. Wang, X. Yang, S. Yue, and J. Zhang, "Estimation and recanalization of chronic occluded internal carotid artery: hybrid operation by carotid endarterectomy and endovascular angioplasty," *World Neurosurgery*, vol. 120, pp. E457–e465, 2018.

[14] R. L. Grubb Jr., C. P. Derdeyn, S. M. Fritsch et al., "Importance of hemodynamic factors in the prognosis of symptomatic carotid occlusion," *JAMA*, vol. 280, no. 12, pp. 1055–1060, 1998.

[15] C. P. Derdeyn, K. D. Yundt, T. O. Videen, D. A. Carpenter, R. L. Grubb Jr., and W. J. Powers, "Increased oxygen extraction fraction is associated with prior ischemic events in patients with carotid occlusion," *Stroke*, vol. 29, no. 4, pp. 754–758, 1998.

[16] A. Kamath, W. S. Smith, W. J. Powers et al., "Perfusion CT compared to $H_2{}^{15}O/O^{15}O$ PET in patients with chronic cervical carotid artery occlusion," *Neuroradiology*, vol. 50, no. 9, pp. 745–751, 2008.

[17] P. Mukherjee, H. C. Kang, T. O. Videen, R. McKinstry, W. J. Powers, and C. P. Derdeyn, "Measurement of cerebral blood flow in chronic carotid occlusive disease: comparison of dynamic susceptibility contrast perfusion MR imaging with positron emission tomography," *American Journal of Neuroradiology*, vol. 24, no. 5, pp. 862–871, 2003.

[18] M. Koenig, M. Kraus, C. Theek, E. Klotz, W. Gehlen, and L. Heuser, "Quantitative assessment of the ischemic brain by means of perfusion-related parameters derived from perfusion CT," *Stroke*, vol. 32, no. 2, pp. 431–437, 2001.